DESIGNING OF NEW BIOCERAMIC MATERIALS FOR HARD TISSUE ENGINEERING

A THESIS PRESENTED BY

NIMMY MOHAN

TO
SREE CHITRA TIRUNAL INSTITUTE FOR MEDICAL SCIENCES AND TECHNOLOGY
THIRUVANANTHAPURAM
INDIA

IN PARTIAL FULFILMENT OF THE REQUIREMENTS
FOR THE AWARD OF

DOCTOR OF PHILOSOPHY

2019

CERTIFICATE

I, Nimmy Mohan, hereby certify that I had personally carried out the work depicted in the thesis entitled, *"Designing of New Bioceramic Materials for Hard Tissue Engineering"*, except where due acknowledgment has been made in the text. No part of the thesis has been submitted for the award of any other degree or diploma prior to this date.

Trivandrum — Nimmy Mohan

20 / 04/ 2019 — Reg. No: 2012/PhD/06

CERTIFICATE

Dr. P.R. Harikrishna Varma

Head, BMT Wing

This is to certify that Nimmy Mohan in the Division of Bioceramics, under the Department of Biomaterial Science and Technology of this Institute has fulfilled the requirements prescribed for the Ph.D. degree of Sree Chitra Tirunal Institute for Medical Sciences and Technology, Trivandrum.

The thesis entitled, *"Designing of New Bioceramic Materials for Hard Tissue Engineering",* was carried out under my direct supervision. No part of the thesis was submitted for the award of any degree or diploma prior to this date. Clearance was obtained from the Institutional Ethics Committee/ Institutional Animal Ethics for carrying out the study.

Trivandrum

20/ 04/ 2019

Dr. P.R. Harikrishna Varma

(Research Supervisor)

Office Seal

The thesis entitled

DESIGNING OF NEW BIOCERAMIC MATERIALS FOR HARD TISSUE ENGINEERING

Submitted by

Nimmy Mohan

for the degree of

Doctor of Philosophy

of

SREE CHITRA TIRUNAL INSTITUTE

FOR

MEDICAL SCIENCES AND TECHNOLOGY,

THIRUVANANTHAPURAM- 695011

Is evaluated and approved by

…… ……..

Dr. P.R. Harikrishna Varma
(Research Supervisor)

Examiner

Acknowledgements

I take this opportunity with pleasure to thank all who contributed in many ways for the success of this study. I am greatly indebted to my supervisor, Dr. P.R. Harikrishna Varma, for his valuable guidance, cheerful enthusiasm, freedom and encouragement during the entire course of this work. It was only due to his understanding, personal support and patience that I was able to complete my research work in a respectable manner. The Director, SCTIMST and The Head, BMT Wing are greatly acknowledged for the facilities provided in the campus for carrying out the research work. I express my sincere gratitude to The Registrar and The Deputy Registrar for all the academic assistance in this venture. Besides my supervisor, I thank my Doctoral Advisory Committee members, Dr. Prabha D Nair, Dr. Annie John, and Dr. P. V Mohanan, for their valuable time, support, suggestions and corrections in my work which helped to improve my thesis and presentation. I thank Dr. Manoj Komath, Head of the Department of Biomaterial Science and Technology for his motivation and support which helped me in my work and thesis writing. I offer my sincere thanks and gratitude to my lab members (former and present) Mr. Vijayan S, Dr. Suresh Babu S, and Mr. Sreekumar R whose expertise helped me in the analysis and my material characterisation studies. I am very much grateful to Dr. Rajesh P my senior colleague, best friend and well-wisher who taught me the basics of ceramic synthesis, characterisation and various analytical methods. He has rendered his immense support in carrying out the work and also helped me in the correction of manuscripts of my publications and thesis. I thank Mr. Sreekanth PJ, Mr. Nishad KV, Mr. Adarsh R.K, Mrs. Anchu R, Ms. Archana A, Dr. Sandhya. S, Dr. Padmaja P, Dr. Francis Bonafice Fernandez, Dr. Eva.C.Das, Dr. Remya K.R, Ms. Malini S, Ms. Gayathry G, Dr. Shanthi Krishna, Dr. Syama S for their valuable friendship and support during my work. I owe my sincere thanks to Dr. P.R Umashankar, Dr. Sachin Shenoy and all members of Division of In Vivo Models and Testing (DIMT) for conducting the in vivo experiments. Dr. P. V. Mohanan & Dr. Gayathri

V. Eshwar are greatly acknowledged for cell culture training provided at the Toxicology Division. I express my thanks to Dr. P. R Anilkumar and Mrs. Deepa for Confocal imaging and cytotoxicity studies at the Division of Tissue Culture. Dr. Sabareeswaran, Mrs. Sulekha Baby and all staffs of Histopathology Division are gratefully acknowledged for their help in sample preparation and imaging of histopathology slides. I express my sincere thanks to Dr. Kalliyana Krishnan V, Dr. Vibha, Mrs. Lakshmi, Mrs. Dhanya, and all members of Dental Products Laboratory for Micro CT imaging. I am thankful to Dr. Roy Joseph, Mrs Jincy and Mrs

Lakshmi of Division of Polymeric Medical Devices for mechanical testing facilities provided. The help given by Mr. Ramesh Babu, Mr. Reji and all staff of Precision Fabrication Facility are acknowledged for fabrication of moulds for ceramic casting for various studies. I sincerely thank Prof. Jorgen Kjems, (Director) Interdisciplinary Nanoscience Centre (i NANO),Aarhus University Denmark for giving me the opportunity to work in his lab as part of the student exchange programme in the Indo Danish Collaborative Project. The support and help given by my friends, staff and students of BMT wing of SCTIMST are greatly acknowledged. I am greatly indebted to the Department of Biotechnology, Government of India for the providing me the fellowship under the Indo Danish Collaborative Programme.

I thank my parents, my brother, my maternal uncle, my husband, my son and all my family members who supported me throughout my PhD programme to make it a reality and dream come true. I thank the Almighty for blessing me with the opportunity to do research, for giving me the health, courage, and inner strength which kept me moving in all the ups and downs during the entire study period.

This thesis is specially dedicated to my beloved parents, who always supported me in all my endeavours, giving me strength, moral support and encouragement to follow my dreams and attain my goals.

Nimmy Mohan

Contents

LIST OF FIGURES

LIST OF TABLES

Abbreviations

α-TCP	α-Tricalcium phosphate
β-TCP	β-Tricalcium phosphate
AP	Ammonium dihydrogen orthophosphate
CN	Calcium nitrate tetrahydrate
CH	Calcium hydroxide
CHA	Carbonate derived hydroxyapatite
THA	Tricalcium phosphate derived hydroxyapatite
BG	Bioactive glass
BCP	Biphasic calcium phosphate
CLSM	Confocal laser scanning microscope
EDS	Energy dispersive X-ray spectroscopy
ESEM	Environmental scanning electron microscope
FTIR	Fourier Transform Infrared Spectroscopy
HA	Hydroxyapatite
ICP-OES	Inductively coupled plasma - optical emission spectroscopy
IR	Infrared
MSCs	Mesenchymal stem cells
ADMSCs	Adipose derived mesenchymal stem cells
PBS	Phosphate buffered solution
RT	Room temperature
SBF	Simulated body fluid
SEM	Scanning electron microscope
TEM	Transmission electron microscope
TCP	Tricalcium phosphate
XRD	X-ray diffraction

SYNOPSIS

Bone substitutes are essential in the treatment of non-union fractures, infectious bone diseases such as osteomyelitis, excision of malignant tumours, spinal, joint reconstruction procedures, dental fractures etc. They are also extensively used as bone void fillers in orthopaedics and dentistry. Among the bioactive ceramics used in bone grafting, hydroxyapatite (HA) has gained sustained interest because of its similarity with the bone mineral constitution along with its biocompatibility and osteoconductive properties. However, the use of sintered hydroxyapatite ceramics is limited due to their poor degradation rates and lack of osteoinductive properties. Different methods have been sought for in order to resolve these problems - (i) substituting the hydroxyapatite lattice with different dopant elements such as silicon, strontium, fluorine etc. to improve the biocompatibility, degradation rate and radio opacity, (ii) Designing of composite materials containing HA and tri calcium phosphate (TCP) to improve the resorption rates, (iii) tailor the ceramics in such a way to minimise/avoid the conventional high temperature sintering processes, enabling faster dissolution for the material compared to the sintered ceramics. Nevertheless, synthesis of hydroxyapatite through a non-sintered ceramic processing route has not been explored in detail.

The thesis presents a detailed study on the development of hydroxyapatite based ceramic materials from various precursor matrices through hydrothermal exchange reactions. Hydrothermal method is one of the most ideal and feasible solution to prepare well-crystallized, homogeneous hydroxyapatite crystals with controlled morphology, composition and purity without the agglomeration of crystals at low temperature. Various precursor materials based on different calcium salts such as calcium oxide, calcium carbonate, bioactive glasses and lower calcium phosphates were chosen as starting materials. Finally, two systems one from a lower calcium phosphate (TCP) origin and another from a synthetic calcium carbonate

(Calcite) origin as a stable precursor source were optimised. These materials were converted to hydroxyapatite via hydrothermal exchange reactions in appropriate reaction medium of ammonium dihydrogen phosphate, calcium nitrate tetrahydrate and calcium hydroxide to supplement for the calcium and phosphate ions. The hypothesis developed is that the formation of hydroxyapatite is due to dissolution/precipitation reaction, where in calcium / phosphate ions from the precursor source gets dissolved from the surface and reacts with the phosphate ions/calcium ions from solution (reaction medium). Posner clusters which are precursors of hydroxyapatite nucleation are generated which then grew and matured as hydroxyapatite nano-crystals on active surface sites of the material. This growth was identified to have a preferred orientation of crystals either on the ab- plane (c-axis) or c-plane (a-axis) resulting in an axial or radial growth of hydroxyapatite. The precursors and the developed materials were characterised by physicochemical methods to ensure the phase purity, elemental composition, functional groups, porosity and surface morphological features. Biocompatibility evaluations by various *in vitro* and *in vivo* tests such as bioactivity studies in simulated body fluid, degradation tests via dissolution studies, cytocompatibility tests such as cytotoxicity and cell-material interaction studies; and functional assay by ALP (alkaline phosphatase) activity were done. *In vivo* implantation tests were performed using the newly developed fast resorbing materials, namely carbonate derived hydroxyapatite (CHA) and tricalcium phosphate derived hydroxyapatite (THA) as a dental extraction socket filler in rabbit model. Resorption of the test materials (CHA) and (THA) were compared with hydroxyapatite sintered granules as control materials.

The thesis is divided into eight chapters. Chapter 1 - An introduction to the work done as an overall summary. Chapter 2 - Literature review on biomaterials and its use for various applications in medicine. Further it explains the biology of bone and the need for ceramic materials for various clinical problems. It is followed by the preparation and processing of

bioceramic materials for bone grafting. Hydrothermal method of ceramic preparation is detailed in this section which is the experimental method used in the work. The chapter also explains the crystal growth mechanisms under hydrothermal conditions. Literature survey on the use of resorbable bone filler materials for dental extraction socket filling has also been illustrated in the last section of this chapter. Chapter 3 - divided into three sections- (i) Materials and methods used in the fabrication process of precursor matrices, which is the initial phase of the study. The experimental setup and the optimisation of reaction parameters for the material synthesis are also explained here. (ii) Materials and methods used for the preparation of hydroxyapatite scaffolds from calcium carbonate precursors (CHA), its characterisation, the methods used for the biocompatibility evaluation of the developed hydroxyapatite scaffolds and an application perspective of the developed CHA material as a promising drug carrier, (iii) Materials and methods used for the preparation of hydroxyapatite scaffolds from tricalcium phosphate precursors (THA), characterisation of the developed scaffolds and the cytocompatibility evaluation. Chapter 4 - Results obtained in the conversion of the precursor scaffolds (initial phase) for the optimisation of the reaction parameters and the physicochemical characterisation of the materials. Chapter 5 - Results obtained for the CHA scaffold prepared and their *in vitro* evaluation. Chapter 6 - Results obtained for the THA scaffolds prepared and their *in vitro* evaluation. Chapter 7 - the *in vivo* experimental results obtained in the safety and efficacy testing of the newly developed CHA and THA materials in comparison to the control hydroxyapatite granules. This chapter is followed by a discussion on the results obtained as a separate unit. Chapter 8 - Summary of the work which provides a conclusion based on the overall work carried out. Lastly, perspectives of future opportunity in relation to novel avenues opened up by this work are described. Citation of references, list of publications in journals, patents applied and papers presented at conferences are also included.

CHAPTER - 1

INTRODUCTION

Summary

Slow resorption is one of the significant problems encountered in using sintered hydroxyapatite as a synthetic bone substitute in the repair and regeneration of the bone tissue. An ideal bone substitute material (bone scaffold) integrates with the surrounding bone tissue and gets resorbed into the body in the same rate as the healing of the bone defect. The need for bone substitutes is essential in non-union fractures, infectious bone diseases such as osteomyelitis, excision of malignant tumours etc. They are also extensively used as bone void fillers in orthopaedics and dentistry.

Bone grafting is one of the most commonly used surgical methods to augment bone regeneration in orthopaedic procedures (Dimitriou et al., 2011). Autogenous bone grafts (harvested from the same patient) are considered as the gold standard in bone tissue repair with a success rate of about 80 to 90% but require an additional surgery for the patient causing pain and morbidity and is limited in supply. It has increased chances of secondary infections and inflammations to the patient (Bauer and Muschler, 2000). Another alternative is the use of allograft that involves the bone from a donor or a cadaver, but has complications such as the transfer of blood borne diseases and other compatibility issues (Gitelis and Cole, 2002). As the amount of available natural bone grafts cannot meet the demand of impending global pandemic of aging and obesity, other alternatives such as synthetic bone substitutes (A. Alex Jahangir, 2008) have been sought.

Further, people explored the use of natural or synthetic bone grafts along with healthy progenitor cells and adequate growth factors to promote faster healing at the injured site using the principles of tissue engineering. Tissue engineering is an interdisciplinary approach where materials science, biology and engineering mechanics are employed for an effective treatment in the repair and regeneration of tissues.

Tissue engineering uses scaffolds (metals, polymers, ceramics or composites), cells (differentiated or undifferentiated stem cells) and growth factors: bone morphogenetic proteins (BMP)/platelet-derived growth factor (PDGF/ transforming growth factor β (TGF-β)/ insulin-like growth factor (IGF) etc. to promote effective bone healing (Vehof et al., 2002, Jansen et al., 2005).

An ideal scaffold used for bone tissue engineering should mimic bone morphology, structure and function to integrate into the surrounding tissue. It should also possess adequate porosity with interconnected nature, which allows proper cellular attachment, growth, exchange of nutrients & oxygen and favour extracellular matrix production (Hulbert et al., 1972). Another important criterion is the degradation rate of the scaffolds. The degradation rate of the scaffold should match with the growth rate of neo-tissue, so that as the injury is healed, the new bone is regenerated and the scaffold is totally degraded (Salgado et al., 2004).

Some of the most common materials used as bone grafts include calcium phosphate based ceramics such as tricalcium phosphate and their lower analogues, hydroxyapatite, coralline (hydroxyapatite derived from marine corals), bioactive glasses and their composite systems. Among the different materials used in bone

grafting, hydroxyapatite bioactive ceramics has gained sustained interest because of its similarity with the natural bone mineral constitution along with its biocompatibility and osteoconductive properties (Hench, 1993). Despite the chemical constitution, the use of hydroxyapatite sintered ceramics are limited due to its poor degradation rates and osteoinductive properties. Hence, various methods are sought, in order to resolve these problems. Substitution of the hydroxyapatite lattice with different dopants such as Silicon, Strontium, Fluorine atoms helped to improve the biocompatibility, degradation rate and radio opacity (Carlisle, 1980, Reffitt et al., 2003). Combination of TCP and HA to form composite materials with a better degradation profile *in vivo* can be another alternative for faster resorption.

Non-sintered ceramic processing can be a promising solution to obtain fast resorbing ceramics *in vivo*, as it improves the porosity and dissolution rate of the material by suitable ion exchanges with the surrounding body fluids. The dissolution of sintered ceramics is slow since sintering creates shrinkage, reduction in porosity and grain growth which in turn affects the resorption process *in vivo*. Synthesis of hydroxyapatite materials through a non-sintered ceramic processing route has not been studied in detail as yet and hence its worth investigating.

In this thesis, we developed hydroxyapatite ceramic materials from various precursor matrices by hydrothermal exchange reactions. Hydrothermal reactions are reactions that are conducted above the ambient conditions such as above room temperature (25 °C) and one atmosphere pressure in a closed apparatus known as a hydrothermal reaction vessel/reactor or sometimes known as an autoclave. Hydrothermal method is one of the suitable methods to prepare well-crystallized, homogeneous

hydroxyapatite crystals with controlled morphology, composition and phase purity (Suchanek, 1998, Yoshimura and Suchanek, 1997).

Our aim was to develop large scaffolds of hydroxyapatite having various shapes such as blocks, spheres, cylinders, cones etc suitable for various bone filling applications. In order to achieve this, different calcium salts were used as precursor materials. The conversion efficiency and the precursor stability were first optimised. Based on the results obtained, two systems - one from a lower calcium phosphate (TCP) origin and another from a calcium carbonate (Calcite) origin were chosen as stable precursors. These materials were converted to hydroxyapatite via hydrothermal exchange reactions in appropriate solutions to supplement the adequate phosphate and calcium ions. The formation of hydroxyapatite is hypothesized to be due to dissolution/precipitation reactions and exchange reaction mechanisms. The ions from the precursor source gets dissolved from the surface of the material and reacts with the phosphate ions/calcium ions from the reaction medium to form HA nuclei and grow as apatite crystals on active surface sites of the material. In the case of calcite precursors, an exchange of ions takes place such that the phosphate ions from the supplemented medium is substituted in the calcite lattice. Physicochemical characterisation of the materials were carried out before and after the conversion reactions to ensure the phase purity, elemental composition, presence of functional groups, porosity and surface morphological features. The materials were also tested for biocompatibility evaluations by various *in vitro* and *in vivo* tests such as bioactivity studies in simulated body fluid, dissolution studies, cytotoxicity evaluations, cell material interaction studies and ALP (alkaline phosphatase) activity. *In vivo* implantation tests were performed using the newly developed fast resorbing

material as a dental extraction socket filler. Resorption of the test materials were compared with hydroxyapatite sintered granules as control materials.

The thesis is divided into eight chapters. Chapter 1 - An introduction which summarises the overall work. Chapter 2 - details the literature review on biomaterials and its use for various applications in medicine. It explains the biology of bone and the need for ceramic materials for various clinical problems. Further it explains the preparation and processing of bioceramic materials for bone grafting. Hydrothermal method of ceramic preparation is described which is the experimental method used in this work. Since the application perspective of the material is for a dental extraction socket filler, literature survey on the use of resorbable bone filler materials for dental extraction socket filling is also included. Chapter 3 - Divided into three sections: (i) Materials and methods used in the fabrication process of precursor matrices including the experimental setup and the optimisation of reaction parameters for the material synthesis. (ii) Materials and methods used for the preparation of hydroxyapatite scaffolds from calcium carbonate precursors (CHA), its characterisation, the methods used for the biocompatibility evaluation of the developed hydroxyapatite scaffolds and an application perspective of the developed CHA material as a promising drug carrier. (iii) Materials and methods used for the preparation of hydroxyapatite scaffolds from tricalcium phosphate precursors (THA), characterisation of the developed scaffolds and the cytocompatibility evaluation. Chapter 4 - Results obtained in the conversion of the precursor scaffolds, optimisation studies and the physicochemical characterisation of the materials. Chapter 5 - Results obtained for the CHA scaffold prepared and their *in vitro* evaluation. Chapter 6 - Results obtained for the THA scaffolds prepared and their *in*

vitro evaluation. Chapter 7 - the *in vivo* experimental results obtained in the safety and efficacy testing of the newly developed CHA and THA materials in comparison to the control hydroxyapatite granules. This chapter is followed by a discussion on the results obtained as a separate unit. Chapter 8 – Summary of the work which provides a conclusion based on the overall work carried out. Future perspectives of the work are described. Citation of references, list of publications in journals, patents applied and papers presented at conferences are also included.

CHAPTER - 2

LITERATURE REVIEW

Biomaterials

Biomaterials are materials that are made to interact with the living system for therapy (treat, augment, repair, or replace a tissue of the body) or for diagnosis (Buddy D. Ratner, 2004). A biomaterial replaces a part or a function of the body in a safe, reliable, economic and physiologically acceptable manner. They are intended to function in contact with tissue, blood and biological fluids, and could be used in prosthetic, diagnostic, therapeutic, and storage applications without adversely affecting the living organism and its components (Joon Park, 2007). Evolution of biomaterials science and technology dates back to 1950's to its origin of the first generation of bio-inert materials which later improvised to the second generation during 1980's with the aim of bioactive materials, and finally the third generation evolved since 2000 with the goal of regeneration of functional tissues. Biomaterials science combines biology, medicine, chemistry, cell biology, engineering and material science (Buddy D. Ratner, 2004) under one umbrella.

Biomaterials are classified into metals, polymers and ceramics and their composites. Metallic biomaterials mainly consist of Stainless steel (316L), Co-Cr alloys, Au-Ag-Cu-Pd alloys and titanium based materials. They are mostly used for orthopaedic and dental implants in load bearing applications. Bioceramics of clinical use includes hydroxyapatite, tricalcium phosphate, bioactive glass, lower calcium phosphates and their composites. They also include bioinert ceramics such as zirconia and alumina that are used for load bearing applications. Polymeric biomaterials include poly

methyl methacrylate (PMMA), poly lactic acid/ poly glycolic acid (PLA/PGA), poly ethylene (PE), poly propylene (PP), polyamides (PA), poly tetra fluoro ethylene or Teflon (PTFE), poly urethanes (PU), and silicones. The properties of these biomaterials are dependent on their atomic structure and bonding (Wong and Bronzino, 2007).

In metals we find single or multiple elements arranged in geometric lattices that are linked by metallic bonds. Due to the availability of free electrons, metals are good conductors of heat and electricity. Conduction of valance electrons in metals can cause corrosion. Body fluids may give an aggressive environment to metallic implants since they contain all the reactive elements such as oxygen, H protons, and ionic salts and hence corrosion of alloys or metals is considered a serious issue during long term performance of permanently implanted metallic materials.

Ionic or rigid covalent bonds are seen in ceramics. Here the covalent bonds between identical atoms are non-polar and electrically uniform while those between unlike atoms are polar. The bonding effects are classified by localised valence electrons and lack of tolerance to lattice deformation is responsible for the characteristic behaviour of ceramics. Ceramics are electrical and thermal insulators because of the absence of electrons in the conduction band. Due to the presence of strong covalent/ionic bonding (high bonding energy and high melting point) they work at high temperatures when compared to metals and alloys. Ceramics show rigidity and hardness yet they are brittle than metals. They exhibit good strength in compression but low tensile or bending strength.

Polymers have rotational covalent bonds between atoms producing flexible long chain molecules. They are relatively inert materials and are unreactive due to lack of free electrons; they have low electrical conductivity and non-magnetic property. When the neighbouring polymer chains have physical tangling or very weak secondary chemical bonding, they can be extremely ductile and pliable, such that it can be formed into complex shapes. Crosslinking of covalently bound polymeric chains produces either elastic rubbers or rigid polymers depending on the degree of crosslinks. Low degree of crosslinking produces flexible rubber and high degree of crosslinking produce hard and rigid polymers. Major drawback of polymers is that they decompose at modest temperatures or degrade via oxidation/hydrolysis (Qizhi Chen, 2018).

In order to accept a material as a biomaterial it has to be biocompatible. Biocompatibility refers to the ability of a biomaterial to perform with an appropriate host response in a specific application (Williams, 2008). Biocompatibility of biomaterials is identified based on their cytotoxicity (cell/tissue death), mutagenicity (damage to genes), carcinogenicity (cancer formation), thrombogenicity (blood clotting), pyrogenicity and allergenicity (immune responses). Taking all the factors into account FDA had approved the definition of biocompatibility as a material that does no harm to the host body (Recum, 1998).

When designing a new biomaterial, various factors have to be taken under consideration from the materials science aspect which includes mechanical properties, degradation rates, porosity, moldability, surface morphology and shaping requirements for specific applications. In terms of biology and medicine a material

should possess bioactivity, inhibit immune responses and foreign body reactions, provide growth factor requirements and enable vascularisation with the existing tissue.

Bone Biology

Bone is a well-organised, complex specialised connective tissue with remarkable toughness, resilience, characteristic growth mechanism and regenerative capacity. It is appropriate to understand the biology and anatomy of the bone tissue in detail in order to construct the appropriate bone substitute for a clinical use.

The human skeleton is the internal framework of the body. The major function of the skeletal system includes the support for soft tissue and provides attachment for skeletal muscles. It protects the internal organs, assists in movement along with skeletal muscles, stores and releases minerals. They contain red bone marrow, which produces blood cells and yellow bone marrow, which stores triglycerides (fats).

The bones in the human body are classified according to different shapes as: Long Bones (Clavicle, Humerus, Radius, Ulna, Femur, Tibia, Fibula, Metatarsals and Metacarpals); Short Bones (Carpals and Tarsals); Flat Bones (Ribs, Parietal bone from skull, Sternum and Scapula). Sesamoid Bones (Patella); and Irregular Bones (Skull, Pelvis, and Vertebrae).

Bone is classified according to the microstructure as cortical and cancellous bone and based on the organization of collagen fibers they are classified as woven bone and lamellar bone.

Structure of Bone

A fully developed bone tissue in the adult skeleton has two architectural forms:

1. Trabecular or cancellous or spongy bone (around 20% of the total skeleton) and
2. Cortical or compact bone (around 80% of the total skeleton)

Compact Bone Tissue

Compact bone is the strongest form of bone tissue with minimal spaces and is located beneath the periosteum of all bones. Compact bone tissue provides protection and mechanical function. The components of compact bone tissue are arranged in repeating structural units called osteons or haversian systems. Each osteon consists of a central (haversian) canal with its concentrically arranged lamellae, lacunae, osteocytes, and canaliculi. The areas between osteons contain interstitial lamellae, which also have lacunae with osteocytes and canaliculi. Interstitial lamellae are fragments of older osteons that have been partially destroyed during bone rebuilding or growth. Lamellae that encircle the bone just beneath the periosteum or encircle the medullary cavity is known as circumferential lamellae. Blood vessels, lymphatic vessels, and nerves from the periosteum penetrate compact bone through transverse perforating or Volkmann's canals. Neighbouring osteocytes communicate via gap junctions. The canaliculi connect lacunae with one another and with the central canals, forming an intricate, miniature system of interconnected canals throughout the bone. This helps in the exchange of nutrients and oxygen to the osteocytes and aids the removal of wastes.

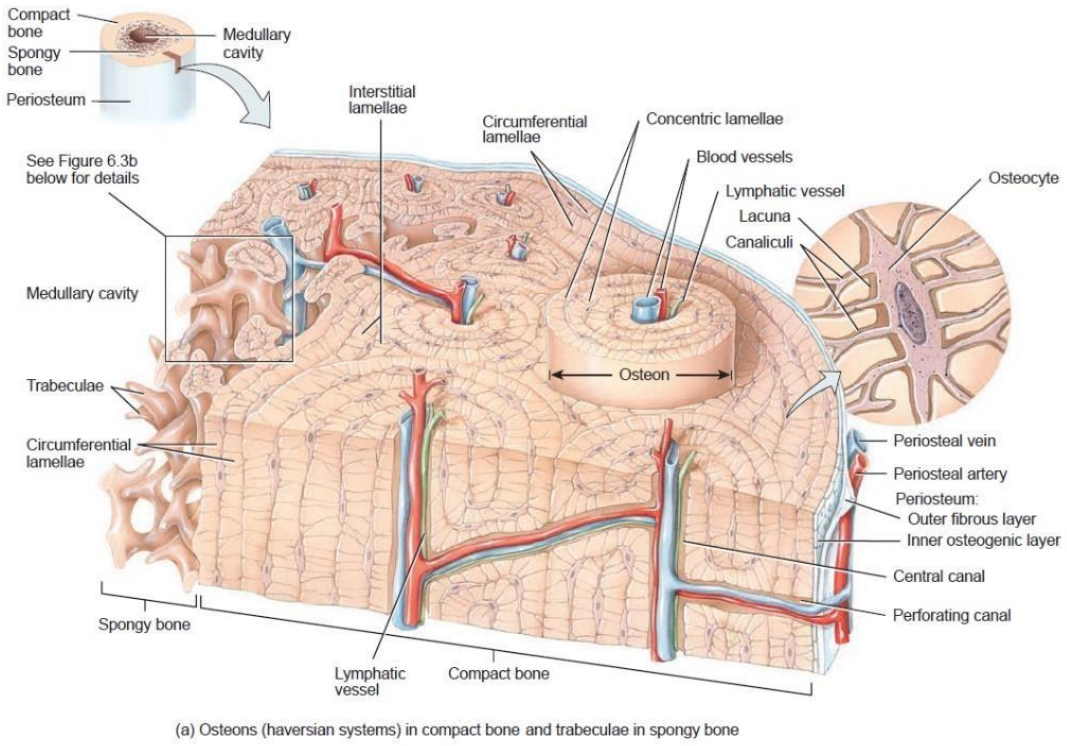

Figure 2.1. Pictorial representation of compact bone structure (Anatomy and Physiology)

Spongy bone tissue

Spongy bone consists of lamellae arranged in an irregular pattern forming trabeculae. Trabecular bone is porous, light and has spaces between them to incorporate bone marrow where hemopoiesis (blood cell production) occurs in adults. Each trabecula contains lacunae with osteocytes. Canaliculi radiate outward from the lacunae. Osteocytes receive nourishment from the blood circulating through the blood vessels in the spaces between trabeculae. Spongy bone is found in the interior of short, flat, and irregularly shaped bones, and most of the epiphyses of long bones. A layer of compact bone always covers spongy bone for protection.

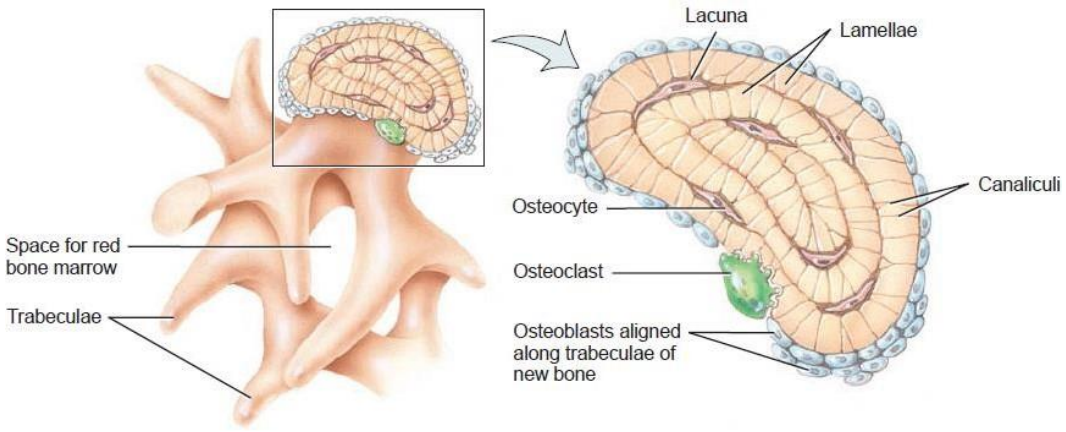

Figure 2.2 Pictorial representation of cancellous bone structure (Anatomy and Physiology)

Bone histology

The histology of bone shows four types of cells namely osteogenic cell (which develops into an osteoblast), osteoblast (bone forming cells), osteoclasts (bone resorbing cells) and osteocyte (cells that maintains the bone tissue).

Osteogenic cell: Osteogenic cells also known as osteoprogenitor cells or pre osteoblasts are mainly found in the inner layer of the periosteum. They are undifferentiated cells with high mitotic activity and are the only bone cells that divide. These cells differentiate and develop into osteoblasts to form new bones. Immature osteogenic cells remain in the deep layers of the periosteum and the marrow.

Osteoblasts: Osteoblasts are bone-forming cells that are normally found at the surface of bones. Some osteoblasts get transformed to osteocytes and lie embedded within the ECM. These osteocytes help in the maintenance of the bone tissue. It is the major cellular component of the bone. During bone formation, the surface layer of osteoblasts consists of cuboidal cells, called active osteoblasts. When the bone-

forming unit is not actively synthesizing bone, the osteoblasts are flattened and become inactive.

Osteoclasts: Osteoclasts are large multinucleated cells, which is responsible for the dissolution of the bone in the bone remodelling process. They are found inside small depressions in the bone surface called the Howship lacunae. Osteoclasts are formed by the fusion of many cells derived from circulating monocytes in the blood. They have ruffled borders with their microvilli in contact with the surface of the bone tissue. Osteoclasts secrete number of enzymes which dissolve the organic (collagen) and the inorganic (calcium and phosphorus) of the bone. Mineralized bone is first broken into fragments; the osteoclast then engulfs the fragments and digests them within cytoplasmic vacuoles. Calcium and phosphorus liberated by the breakdown of the mineralized bone are released into the bloodstream. Unmineralized bone (osteoid) is protected against osteoclastic resorption.

Osteocyte: Osteocytes lie within the bone matrix and are responsible for the maintenance of the bone tissue. Osteocytes are the most abundant type of cells in mature bone tissue. They also are long-lived, surviving as long as the bone they occupy exists. Osteocytes are derived from osteoblasts, the bone-forming cells. By means of these canaliculi, nutrients and waste products are exchanged to maintain the activity of the osteocytes (Vacanti, 2013).

Biochemistry of Bone Tissue

Bone is a composite material with an organic matrix (30-35% dry weight) and inorganic matrix of calcium phosphate (hydroxyapatite) around 65-70%. The organic matrix is made of Type 1 collagen (90%) whereas 10% is of non-collagenous

proteins such as osteocalcin, matrix Gla protein, bone sialoprotein (BSP), osteopontin, osteonectin and alkaline phosphatase (ALP). The non-collagenous proteins are synthesised at different stages of osteoblastic differentiation. Expression of ALP and collagen 1 peaks during initial phase whereas osteopontin and osteocalcin are expressed during later stages (DA, 1972).

The inorganic component of the bone is particularly composed of carbonated hydroxyapatite (bone mineral) with the chemical formula of $(Ca_{10}[PO_4]_6[OH]_2$ whose calcium to phosphorus ratio varies between 1.8 to 3.2 (Fountos et al., 1997). The collagenous and non-collagenous proteins initiate the nucleation and deposition of the bone mineral. They also regulate the orientation, size and growth rate of apatite crystals. Once the nucleation is initiated, amorphous calcium phosphate, gets precipitated first which is then converted to octa calcium phosphate and finally matures to form hydroxyapatite crystals (Tzaphlidou and Zaichick, 2003).

Need for Bone Graft Substitutes

The clinical need for natural and synthetic substitutes arises when bone tissue is injured and cannot heal by itself in certain cases. Some typical examples can be open fractures with tissue devascularisation & bone loss, delayed unions and non-unions leading to morbidity, bone tumours & related surgical defects (challenge - radiation/chemotherapy hazards), spine fusions & arthrodesis of joints, bone loss with failed hip and knee replacements, diseases like osteoporosis, osteogenesis and osteomyelitis. Grafting of bone is a major reconstructive challenge for surgeons and the choice of material selection remains difficult. Autografts in the form of

cancellous, cortical, or corticocancellous grafts from donor sites such as iliac crest and distal radius are always considered as the gold standard (Bhatt and Rozental, 2012) in grafting.

An ideal bone graft is expected to provide the required structural integrity, osteoinduction, osteoconduction, support the osteogenesis of cells and finally have the osteointegrative ability to bond to the host tissue. The bone grafts must provide the required mechanical strength at the site of application with adequate compressive strength, torsional and shear resistance properties. Osteoinduction is the environment provided by the grafting material in the presence of growth proteins to induce osteogenic differentiation of host progenitor cells to osteoblasts. Osteoconduction is provided from a bioactive matrix that provides the framework for bone ingrowth. This matrix has to support and facilitate fibrovascular ingrowth, host progenitor cell migration into the scaffold, osteoblast attachment, and eventually lead to new bone formation.

With the possession of osteoconductive, osteoinductive and osteogenic properties, an autologous bone graft can integrate into the host bone completely and hence is regarded as the gold standard in treating bone defects (V.M. Goldberg, 2005). The major issue related to the harvesting process of autografts include donor site complication and pain, increased blood loss, increased operative time, potential for donor site infection and the limited volume of material available (Chiarello et al., 2013, JM., 2011).

Considering the limitation of autologous bone grafts, allografts were considered as an alternative. Here the grafting material is harvested from one individual and

transplanted to a genetically different individual of the same species. Allografts were used in patients having poor healing potential, established non-union, and extensive comminution after fractures (V.M. Goldberg, 2005). Allografts are machined and customized, therefore available in various forms such as cortical, cancellous and highly processed bone derivatives (demineralized bone matrix) (Roberts and Rosenbaum, 2012). In comparison to autografts, allografts were found to be immunogenic and demonstrate a higher failure rate due to activation of major histocompatibility complex (MHC) antigens (Stevenson and Horowitz, 1992). The initial osteoinduction phase would be destroyed by immune response followed by inflammatory cells causing necrosis of osteo-progenitor cells (Stevenson, 1987, Stevenson et al., 1991).

Demineralized bone matrix (DBM) is a processed allograft derivative with 40% of the mineral content of the bone matrix, which is removed by mild acid treatment, while collagens, non-collagenous proteins and growth factors remain unaffected (Boyce et al., 1999). Due to its inferior mechanical properties and poor structural integrity it is mainly used for bone filling applications (Finkemeier, 2002).

Synthetic Bone grafts

Due to the limited availability of natural bone grafts, which cannot meet the needs of aging population, the dire need for synthetic substitutes became apparent. Accordingly, various biomaterials were developed mostly based on ceramics and polymers and composites. Some of the common synthetic grafts include calcium sulphate, calcium phosphate (CaP) ceramics, CaP cements, bioactive glass or

combinations (Zwingenberger et al., 2012). Bone graft substitutes could reduce donor site morbidity, immunogenicity and disease transmission.

Calcium Sulphate

Calcium sulphate, also known as plaster of Paris, is an osteoconductive and biodegradable material used in bone filling applications since 1892 (Wang and Yeung, 2017). It is prepared by heating gypsum having an alpha hemihydrate crystal structure. It can be made in different forms such as hard pellets or injectable viscous fluids that harden *in vivo*. Calcium sulphate has rapid resorption rate and weak internal strength, and hence can only be used to fill small bone defects with rigid internal fixation, the ingrowth of vascular and new bone happens in conjunction with the resorption of the graft. It is reported that calcium sulphate was unable to achieve an optimal fusion rate in spinal arthrodesis, mainly because of faster degradation in early phase of bone regeneration than actual bone deposition. However, being less expensive, calcium sulphate is a widely used material. It can be used in combination with hydroxyapatite to improve its properties. The material is also used to deliver antibiotics like gentamycin or vancomycin in the treatment of infectious bone diseases like osteomyelitis (Carson and Bostrom, 2007).

Calcium Phosphate Ceramics

Calcium phosphate ceramics are a class of materials classified based on their difference in constitution of calcium to phosphate (Ca:P) ions in their crystal lattice. This greatly affects its mechanical properties and absorption rate. Biphasic calcium phosphate, tricalcium phosphate and hydroxyapatite are commonly used synthetic grafts for hard tissue applications. Furthermore, porous, non-porous and granular

forms are in commercial use too. The synthesised green bodies undergo high temperature processing in order to obtain stability. Hydroxyapatite is the popular material under this category owing to its similar chemical composition with respect to the mineral phase of the bone (Oonishi et al., 1997, C. Schwartz, 2005, Nich and Sedel, 2006, Gaasbeek et al., 2005, Scheer and Adolfsson, 2009).

Hydroxyapatite (HA)

Hydroxyapatite is the mineral found in the bones and teeth of humans and most of the mammals. It has a chemical composition $Ca_{10}(PO_4)_6(OH)_2$ (Ca:P ratio = 1.67) is well known for its osteoconductive and osteointergrative properties. Porous hydroxyapatite grafts (macropores > 100 μm) facilitates the adhesion, proliferation and differentiation of osteoprogenitor cells (Le Huec et al., 1995). It also allows proper revascularisation and bone ingrowth. Having high Ca:P ratio and crystallinity, the resorption rates of the material is greatly affected (Wenisch et al., 2003). When porous TCP grafts showed 80 % resorption in a 6 month study in rabbit cancellous bone, HA showed only 5 % resorption (Eggli et al., 1988). This drawback is overcome by introducing nanocrystalline HA with large surface to volume ratio. This significantly reduced the sintering temperature and thereby increased the resorption rate of the material (Kattimani et al., 2016).

Tricalcium phosphate (TCP)

β-TCP with the chemical formula $Ca_3(PO_4)_2$ (Ca: P ratio1.5) and rhombohedral crystal structure is widely used for bone grafting since 1920s (Albee, 1920). It is reported to have higher degradation and absorption rates than HA. Porous TCP materials provide vascularisation and bone replacement like that of HA. As a result

of the physiological pH (7.3 - 7.4), which is not suitable for TCP, it gets converted to HA after implantation (Buchanan, 2008) . Even though the material degrades within 6-24 months they have an unpredictable degradation profile, hindering the mechanical property of the material which limits its usage in bone grafting. Recent studies indicate that TCP promotes better angiogenesis when compared to HA and composites of HA and TCP (Chen et al., 2015b, Malhotra and Habibovic, 2016).

Biphasic Calcium Phosphate (BCP)

Biphasic calcium phosphate is a combination of hydroxyapatite and tricalcium phosphate in various ratios so that the benefits from both the materials can be utilized. By adjusting their proportions, the mechanical properties and the resorption rates can be controlled to make an effective grafting substrate.

Calcium Phosphate Cements (CPC)

Calcium phosphate cements were first used as bone grafting materials in 1980s (Brown, 1983). It was developed for the purpose of extending the adaptability and mouldability of bone grafts. CPCs are formulated by the acid-base setting reaction between dicalcium phosphate and tetra calcium phosphate to result in the formation of brushite or carbonated hydroxyapatite (dahllite). Apatitic CPC has better mechanical properties, but low degradation rates and injectability than brushitic CPC. Mechanical and biological properties of CPCs are improvised by preparing nanostructured formulations (Alivisatos, 2000, Tang et al., 2004, Olszta et al., 2007, Kim et al., 2010). CPCs are preferred for bone replacement in percutaneous vertebroplasty and kyphoplasty (Verron et al., 2014, Zaryanov et al., 2014).

Coralline HA

Coralline HA is derived from marine corals by removing the organic content and treatment of calcium carbonate backbone. Hence naturally occurring coralline HA can be termed as sterilised calcium carbonate. Calcium carbonate skeleton is converted to hydroxyapatite by treating with ammonium phosphate solution. It resembles a trabecular bone structure and is a resorbable material. It is available in the form of granules and blocks for clinical requirements. Interpore and Pro-osteon are the two commercially available products from coral, marketed by USA (Interpore International, Inc., Irvine, CA (Mercer, 2004)).

Bioactive Glasses

Bioactive glass or Bioglass® is a class of silicate based ceramics formulated in 1970's with the major content being silicon dioxide SiO_2 (45-52 wt %) and other constituent oxides include sodium oxide Na_2O, calcium oxide CaO, and phosphorus pentoxide P_2O_5 . The formulation of bioglass was later modified by the addition of potassium oxide K_2O, magnesium oxide MgO and boric oxide B_2O to improve the stability. Bioactive glass could form a strong physical bond to the host bone by the action of silicon ions on the bone surface. This interaction of Si ions subsequently resulted in the formation of a hydroxyapatite layer on the surface of bioglass. This layer of apatite favours the absorption of proteins and osteoprogenitor cells to the site. During a long term implantation of the material the apatitic layer was partially replaced by bone through a creep substitution process (Hench et al., 1971, Hench and Paschall, 1973, Välimäki and Aro, 2006, Neo et al., 1994).

Preparation of Bioceramic Materials for Bone Tissue Repair

Bioceramics are used for repair and replacement of diseased and damaged parts of musculoskeletal systems. They are classified according to their chemical compositions as bioactive ceramics (Calcium Phosphates), bio-inert ceramics (Zirconia, Alumina) and Glass-Ceramics (Silicate & Phosphate families of glasses and crystallised glasses). Based on the clinical applications and requirements these bioceramic materials are processed into various shapes such as blocks, rods, spheres, pellets, thin films and nano-sized powders. For defects that are not always exposed to high stress and loading, porous hydroxyapatite, β-tri calcium phosphate and their mixtures are used whereas highly dense zirconia and alumina ceramics are applied to load bearing applications such as hip joint balls and cups. Thin films of hydroxyapatite are also used as coating on metallic implants such as plates and screws for better osteointegration (Tanaka Y, 2008).

Bioactive ceramic preparation starts from the powder synthesis followed by the consolidation of powders into various shapes and size with or without porosity as per the clinical requirement. It is then densified by sintering to obtain the strength. Bioactive glass ceramics are prepared through sol-gel technique. Some of the important steps in bioceramic powder preparation and processing are discussed below with hydroxyapatite as an example: Ceramic powder preparation is mainly done by three methods:

1. Dry chemical method 2. Wet chemical method 3. Hydrothermal method

Dry Chemical Method

In dry chemical method, solid state chemical reactions takes place at high temperature which enhances the diffusion process of ions. It is a relatively simple procedure for HA preparation. Precursors for the solid state reactions are usually inorganic salts containing calcium and phosphate ions or a previously prepared calcium phosphate salt (Pramanik et al., 2007). In a typical example, Hydroxyapatite (HA) powders are prepared by the solid state chemical reactions between pyro calcium phosphate and calcium carbonate powders in the presence of water vapour. The reacted powders are then crushed by ball milling to remove the agglomeration and further high temperature treatment is given. Reactions at high temperatures lead to the formation of coarse-grained reaction products attributed to sintering and grain growth. Rapid solid state reaction also hinders the successful synthesis of thermodynamically metastable phases. The efficiency of solid state reactions is improved by increasing the area of contact between reacting solids. Reagents with large surface area are found to be effective reactants of solid state chemical reactions (Martinolich and Neilson, 2017). Reactivity can also be improved by pelletizing the powders so that contact between the crystallites increase. It is found that different parts of the crystal have different reactivities. The rate of diffusion of the solid particles is increased by increasing the temperature of the reaction. It can also be done by introducing defects in the lattice by using reagents such as carbonates and nitrates that decompose prior to or during reaction. The rate of nucleation of the product phase is maximised by using reactants with crystal structures similar to that of the product which is seen in topotactic & epitactic reactions. Inhomogeneity, phase impurity, agglomeration, and slow reaction rates are some of the problems

related to solid state synthesis (J.B. Goodenough, 1972, West, 2003, A. K. Cheetham, 1987, Mohan et al., 2016).

Hence, more feasible reaction methodologies are adopted in powder synthesis such as wet precipitation.

Wet Chemical Method

Wet chemical precipitation method is the most widely used method to synthesize crystalline bioceramics with high compositional homogeneity at low temperatures. Here liquid state precursors are used, hence the elements are mixed well in the atomic levels itself which helps in effective precipitation reactions.

Wet chemical precipitation method has two steps:

1) Crystal nucleation from a supersaturated solution

2) Crystal growth by the transport and kinetics of crystal sources from the environment onto the crystal nuclei.

The rate of the reaction is controlled by factors such as solvent, solutes, additives, degree of super saturation, pH, temperature, pressure, stirring conditions etc. Morphological control of the crystal is determined by the combination of all these factors. Wet chemical synthesis allows the formation of inorganic particles, oxides or metals, multi-component phases with controlled size and shape, high physico-chemical reactivity and very high purity control. Wet precipitation is usually conducted at pH values higher than 4.2 and temperatures ranging from 25 °C to <100 °C (Kim et al., 2010, Catros et al., 2010). HA powders are prepared from their calcium and phosphate salt solutions such as calcium nitrate $Ca(NO_3)_2$, calcium

hydroxide $Ca(OH)_2$, calcium chloride $CaCl_2$, ammonium phosphate $(NH_4)_2HPO_4$ or orthophosphoric acid H_3PO_4. Drop wise addition of the calcium solution to phosphate solution maintaining the molar ratio of (Ca/P) at 1.67 is performed under continuous stirring for HA precipitation. The pH of the solutions must be kept above 10 to avoid precipitation of other phases. Once the precipitation is completed the resultant suspension is kept for aging under atmospheric pressure. The precipitate then undergoes Ostwald's ripening to get matured HA crystallites. Ostwald ripening causes the change of an inhomogeneous structure over time, causing the small crystals or sol particles to dissolve, and redeposit into larger crystals. It is then filtered, dried and crushed into a powder. Two methods of CaP precipitation developed by Rathje in 1939 and Hayek and Newesely in 1963 (W. Rathje, 1939, E. Hayek, 1963). In Rathje's method dropwise addition of phosphoric acid to a stirring suspension of calcium hydroxide was employed. The reaction took place as follows:

$$10\ Ca(OH)_2 + 6\ H_3PO_4 \rightarrow Ca_{10}(PO_4)_6(OH)_2 + 18H_2O$$

Hayek and Newesely's method consisted of reaction between calcium nitrate and ammonium phosphate with added ammonium hydroxide according to the reaction:

$$10\ Ca\ (NO_3)_2 + 6(NH_4)_2HPO_4 + 8NH_4OH \rightarrow Ca_{10}(PO_4)_6(OH)_2 + 20NH_4NO_3 + 6H_2O$$

The jelly like precipitate obtained consist of fine grains with high specific surface value (80-90 m^2/g) having a high purity - single phase hydroxyapatite. The ceramic powder so obtained is further processed by milling to reduce the agglomeration and crush down to smaller size and then dried. Fine powders with superior quality can also be produced in large scale by a technique known as spray drying. Here the atomizing solution with precipitated powders (slurry) is passed through a nozzle at

controlled rate into a heated chamber. The solvent immediately evaporates when the solution is sprayed into the chamber and produces powders with particle size below the size of sprayed droplets. The use of cyclone makes this drying process more effective to collect the dried powders (Aoki, 1991).

Hydrothermal Synthesis

The term hydrothermal usually refers to any heterogeneous reaction in the presence of aqueous solvents or mineralizers under high pressure and temperature conditions to dissolve and recrystallize materials that are relatively insoluble under ordinary conditions. Hydrothermal method refers to wet chemical reactions carried out at high pressure (above 1 atm) and temperature (above 100 °C). Basic requirement for a hydrothermal reaction is a sealed pressure vessel capable of working at high pressure and temperature. Solvothermal is a word more preferably used by scientists since the chemical reaction occurs in the presence of a solvent in supercritical or near supercritical conditions. It is effective in the crystallization of poorly soluble compounds. It is useful for the synthesis of HA whiskers and small sized single crystals, which is hard to obtain via dry and wet precipitation at ordinary temperatures and pressures (Riman, 1993).

Sol-Gel Process

Sol-gel method is used for the manufacturing of oxide ceramics via hydrolysis of metal salts or peptization of metal oxides with subsequent coagulation of the product colloids (colloidal gels). Alternatively, it involves the hydrolysis of alcoholic solutions of metal alkoxides, formates, acetates or acetylacetonates forming polymeric gels. The formation of colloidal gels is preceded by the formation of a sol,

whereby the suspended colloidal particles are in either electrostatic or steric interaction by means of surface-active or polymer substances. Destabilization of the sol particles, causes coagulation and forms a 3-D gel. The hydrolysis of metal alkoxides dissolved in alcohol leads to condensation reactions and ensuing formation of inorganic polymers with metal-oxide-metal (M-O-M) framework as a structural unit. This reaction is driven towards completion by removal of the product water. Both linear and cross-linked polymers can result from partial hydrolysis, depending on the stoichiometric ratio of water and alkoxide, and the concentration of the added acid or base catalyst. Progressive poly-condensation gradually leads to gel formation and thereafter the wet gel is transformed to a xerogel by the extraction of the solvent (drying process). The conversion of the M-O-M containing polymer or gel into metal oxide (which can be considered as a macromolecule) is accomplished via heat treatment by calcination steps (Vioux, 1997).

Processing of Ceramics

Forming of green bodies

The ceramic powders are consolidated to various shapes according to the clinical requirement by pressing, foaming or moulding techniques into discs, cylinders, or rods with or without binders or deflocculants. Pressing of the powders are done mainly by three methods such as uniaxial pressing, cold isostatic pressing and hot isostatic pressing. During consolidation by pressing, the ceramic powders are subjected to high pressure with different holding and releasing time. In cold isostatic pressing (CIP) high pressure is applied from multiple directions through a liquid (water-oil mixture) or gaseous (argon) medium at room temperature whereas in hot

isostatic pressing (HIP), pressure is applied through nitrogen or argon medium along with high temperature treatment. This helps to produce materials with high density and strength (Burtrand Lee, 2005).

Sintering

Sintering is a thermal treatment applied to the ceramic green bodies, for the densification and consolidation of the construct. The synthesized ceramic powders are moulded into the required shapes in dense or porous forms as per the clinical needs. These entities are known as green bodies and needs further heat treatment for stability and strength. Sintering is performed at high temperatures in furnaces, below the melting point of the material. During sintering the constituent atoms or ions are driven to move to compensate for the surface energy differences among their convex and concave surfaces of the powder particles. The fusion of the particles takes place by the formation of bottlenecks and results in the development of strong chemical bonds. Lattice defects also create pathways for ions and atoms to move through the lattice structures. Ionic transport occurs exponentially with the rise in temperature. The diffusion of ions across the boundaries takes place as per the equation $D = A \exp(-Ea/RT)$; D is diffusion coefficient of ions A, Ea and R are the pre exponential term, activation energy, and gas constant at temperature T respectively. Grain size/crystallite size (Δd) increases in proportion with root of sintering time (t): $\Delta d \alpha \sqrt{t}$. Hence shorter time is required to sinter fine grained ceramic bodies. Densely sintered bodies with fine grains are tougher and stronger than porous ones with larger grains. The mechanical property of a ceramic is strongly dependant on its microstructure. Sintering temperature depends on the composition and crystalline

phase of bioceramics. Sintering is enhanced if a liquid phase takes part in the process; this process is known as vitrification. Thus, sintering produces polycrystalline ceramics consisting of numerous enlarged and coagulated grains of random orientation. The sintering of calcium hydroxyapatite occurs in the temperature range 1200 °C – 1250 °C, where the highest shrinkage of ~ 25 % takes place. Micro porosity is formed by the spaces that are left between the particles once they are sintered (Klawitter and Hulbert, 1971, Klawitter and Weinstein, 1974). Compact apatitic materials are sintered below 1300 °C whose average compressive strength varies from 50 to 150 MPa (W. David Kingery, 1976).

Machining

Shaping is necessary for fine designing of ceramics. Cutting tools for metals cannot be used for ceramics due to their fragility. Hence grinding and polishing are the methods used for the machining of ceramic bodies. Whetstones with polishing fluid and cloth, glass or metal are usually used for grinding and polishing of ceramics. Whetstones are mainly diamond, alumina, silicon carbide, boron nitride & silica.

Ceramic Coatings over metallic implants

Bioceramic coatings help in improvement of the biocompatibility of the metallic implants with the body. Coatings of hydroxyapatite are often applied to metallic implants (most commonly titanium/titanium alloys and stainless steels) to alter the surface properties. Several methods are used to coat the metallic implants with bioceramic powders such as Electrophoretic deposition, Laser coating, Plasma Spraying and Sputtering.

Material of Choice for Study - Hydroxyapatite

Bioactive ceramics are the most preferred biomaterial after autografts owing to its characteristics to form biologically active carbonated apatite layer on the surface of the material upon implantation, thus providing better integration of the material to the host tissue (Wang, 2003). Bioceramic materials based on hydroxyapatite are considered as ideal substitutes due to its similarity in chemical composition to the bone mineral. Synthetic stoichiometric HA has been extensively utilized as a skeletal replacement material (Hench, 1993). Since the material of our interest is also hydroxyapatite, the preparation processing and the structure of this mineral is discussed in detail.

Crystal structure of hydroxyapatite

Hydroxyapatite (HA) is chemically $Ca_{10}(PO_4)_6(OH)_2$ with a theoretical composition of 39.68 wt% Ca, 18.45 wt% P, Ca / P wt ratio of 2.151 and Ca / P molar ratio of 1.667. It crystallizes into hexagonal Bravais lattice in $P6_3/m$ space group with cell dimensions of a = b=9.432 Å and c = 6.881 Å. The density of hydroxyapatite is 3.219 g/cm^3 (Posner et al., 1958, Aoki, 1991). HA possess excellent biocompatibility and osteoconductivity which has been related to their propensity to nucleate hydroxyl carbonated apatite (HCA) crystals. When placed in bone tissue, a gradual change on the ceramic surface occurs that leads to the dissolution of calcium and phosphate ions from HA.

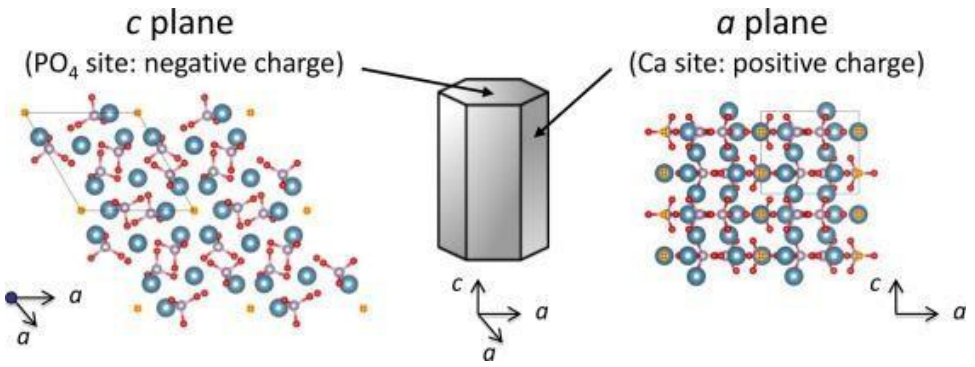

Figure 2.3. Hexagonal lattice of hydroxyapatite (Masahiro Okada, 2015)

Stoichiometric hydroxyapatite belongs to hexagonal crystal system with two major crystal planes a-plane (rich in calcium ions and positively charged) and the c-plane (rich in phosphate and hydroxide ions and negatively charged). Various hard tissues exhibit various morphologies of apatite crystals. In the surface of bone tissues, a-planes are more exposed, as the c-axis of the crystallites are parallel to the extending collagen fibres. Whereas in the case of tooth enamel larger crystallites are responsible for enamel prism formation where the c planes are more exposed at the surface (Weiner and Wagner, 1998, Daculsi et al., 1984). Hydroxyapatite nanoparticles (nano powders, nano crystals etc.) enhances the property of the material by increasing the surface to volume ratio and provides improved properties when compared to conventional ceramic powders, are produced by altering the synthesis methods. Two factors are involved in the surface activity of hydroxyapatite crystals - one is the surface area of the crystal expressed in m^2/g and the other is the physical and chemical properties of the crystal. With the combination of these factors bone mineral becomes metabolically active and the crystals have very large interface with extracellular fluids. The formation of the hydroxyapatite crystal progresses as it interacts with various ions such as calcium, phosphorus, sodium, carbonate and

magnesium in the presence of water from the bone matrix. If the water is low, the ions cannot diffuse through the milieu and hence affects the degree of mineralisation greatly. Hence younger bone tissues with higher water content are found to be more metabolically active than older matured bones.

Crystal growth of hydroxyapatite

Crystal maturation and growth of hydroxyapatite results from ionic exchanges from the solution phase to the solid phase. Mineral dissolution is linked to net ionic exchanges from the solid phase to the solution phase.

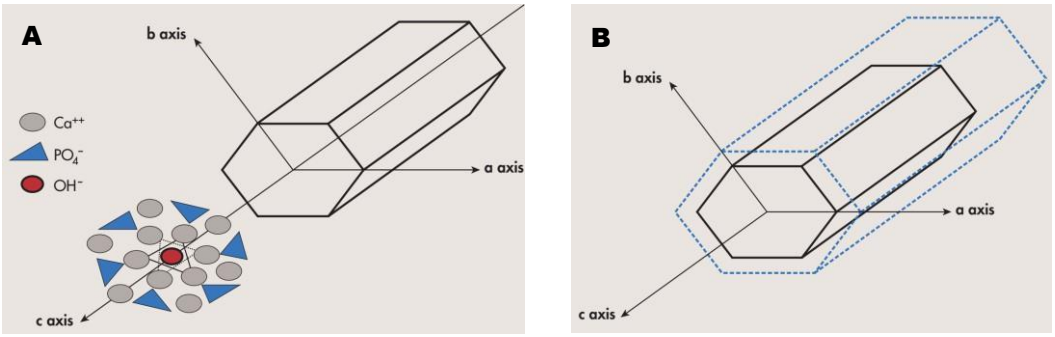

Figure 2.4. (A) Schematic illustration of the unit cell from a crystal of hydroxyapatite constituting bone mineral and (B) Schematic illustration showing the growth of a crystal of hydroxyapatite. Increase in length (c axis) increase in width and thickness (a and b axis) (Boivin, 2007).

However, ionic exchange also happens when there is an equilibrium (where no exchange effectively takes place) between solid and liquid phases. As the formation of the crystal proceeds, the ions constituting the crystal lattice can be replaced by other ions, either by ionic substitutions or by the exchange of surface ions. The increase in length of the apatite crystal is seen as c- axial growth (200 and 300 plane) whereas increase in the width of the crystal occurs along the a and b axis (002 plane) (Boivin, 2007).

During the synthesis of calcium hydroxyapatite, it is necessary to avoid the presence of magnesium ions because the presence of these ions may stabilise the secondary phases involved during the precipitation process and which may lead to the formation of β - whitlockite along with hydroxyapatite. If carbonate $(CO_3)^{-2}$ and bicarbonate HCO^{-3} ions are present in the solution or if carbon dioxide is present in the atmosphere it can lead to the formation of carbonated apatites. The substitution of $(CO_3)^{-2}$ ions may occur at the hydroxyl or the phosphate ion site of the lattice which is commonly known as A site substitutions and B type substitutions respectively. This brings about rearrangement of atoms in the crystal lattice resulting in the formation of apatitic carbonates. Synthetic carbonated apatites have reduced crystallinity whereas biological apatites are more crystalline and this crystallinity increases as the carbonate content increases (Posner A.S, 1984). The hydroxyl ions may also get replaced by chlorine or fluorine ions to produce chlorapatite or fluorapatite, the latter being very stable and is found in nature. When the hydroxyl ion site is substituted by larger groups such as carbonate, the neighbouring atoms are forced to rearrange due to steric reasons. The highest structural order is achievable by placing the hydrogen atom of hydroxyl group along the side of the oxygen atom of the next hydroxyl group, and thereby taking advantage of the polarisation effects of the oxygen and hydrogen atoms. In the aforementioned arrangement an ordered row of (OH^-) ions all in the same direction (-OH…-OH…-OH…) are obtained. When fluorine ions are substituted in the lattice they are more tightly bound to the lattice due to stronger hydrogen bonding effect. Thus, even a very small substitution of fluoride ions enhances the stability and orientation giving rise to well oriented apatite structure. In the case of chloride substitution this effect is less pronounced

since the electronegativity and the binding effects are less in the case for H and Cl ions. By introducing fluoride ions to the apatite lattice the sintering properties of the material is also improved.

Hydroxyapatite Crystal Morphology

Morphology control of hydroxyapatite particles depends on various synthesis parameters such as concentration of the reactants, ionic strength, pH, temperature, mixing of components so that the particle morphology is tuneable with the exposure of a - planes or c - planes respectively by controlling the crystallisation. This can help in modifying the anisotropic properties of the crystal which enhances the ability of adsorption of biomolecules.

Solid state reactions between $CaHPO_4$ and CaO powders produced well crystallised hydroxyapatite (HA) but require high temperatures and long treatment time. They had to be milled further to obtain powders of nano dimensions of the order of 10-40 nm. Other methods to synthesise nano powders by solid state reactions without milling was reported by Omori *et al.* where a mixture of HA and CaO matrix was prepared under non-stoichiometric conditions. Later the CaO was removed by washing to obtain well dispersible HA nanoparticles (Omori et al., 2014).

Wet precipitation methods require relatively lower synthesis temperature for nanoparticle preparation. This method is commonly opted because of their simplicity such that reactions usually involve the mixing of two aqueous salt solutions of calcium and orthophosphate at a pH > 7 which would yield highly supersaturated solutions of hydroxyapatite which induces rapid production of nanoparticles. Urea is sometimes added to control the growth of HA by making use of its thermal

decomposition. HA nanorods in the size range of 80-750 nm is reported to have synthesized by urea assisted method. The thermal decomposition of urea forms ammonia which increases the pH and degree of supersaturation of the solution and thereby leading to the formation of HA particles (Arce et al., 2004).

Hydrothermal treatment of homogeneous calcium phosphate solution where the calcium ions are dissolved by chelating ions such as EDTA or citric acid forms HA particles as a result of the thermal dissociation of calcium chelates in phosphate solutions. Other methods include micelle templated precipitation and emulsion methods. In micelle templated precipitation the surfactant micelles act as nanostructured templates. Micelles are formed when the surfactant molecules are higher in concentration than the critical micelle concentration (CMC). Different shapes such as spheres, cylinders, lamellas are possible for micelles which are controlled by surfactant molecular geometry and solution conditions such as concentration, temperature and ionic strength. Emulsion method is another technique that is used to synthesise nanoparticles with different morphologies like spheres, needles, platelets etc. Emulsion method involves the precipitation in a restricted space which forms small aqueous drops stabilised in an oil phase with surfactant molecules which minimises the agglomeration of particles. Better morphology control is achieved by restricting the crystal growth.

Hydrothermal Method of Hydroxyapatite Synthesis: *for better morphology control and cellular activity*

As discussed in section 2.5.3, hydrothermal reaction is a heterogeneous reaction in the presence of aqueous solvents or mineralizers under high pressure and temperature

which solubilise and recrystallize materials that are not possible under ordinary pressure and temperature conditions. The reaction is carried out under wet chemical conditions at high pressure and temperature (above 100 °C and 1 atm pressure). Upper limits of hydrothermal synthesis extend to over 1000 °C and 500 MPa pressure (Roy, 1994, Suchanek, 1998). Practical temperature and pressure restrictions for material synthesis fall around 350 °C and 100 MPa (saturated vapor pressure of water at this temperature is 16 MPa) below which reaction conditions are considered mild and above which conditions are considered severe. This transition from mild to severe conditions is determined mostly by corrosion and strength limits of the materials of construction that comprise the hydrothermal reaction vessels. Intensive research led to a better understanding of hydrothermal chemistry, which has significantly reduced the reaction time, temperature, and pressure for hydrothermal crystallization of materials ($T < 200$ ºC, $P < 1.5$ MPa). This breakthrough has made hydrothermal synthesis more economical, cost-effective and effective in the field of engineering and chemistry (Roy, 1994, Gersten et al., 2002, Oshimura M, 2000).

Even though hydrothermal research was initiated in the middle of the 19th century by geologists, this method was later seen to be useful for material scientists in hydrometallurgy and single crystal growth (K Byrappa, 2001). Early reports on hydrothermal synthesis dates back to marine coral conversions by D.M Roy *et al.* where aragonitic calcium carbonate was converted to hydroxyapatite preserving its strength and porosity. From there on natural sources like sea shells, egg shells, exoskeletons of many fishes were used as sources of precursor materials for these exchange processes (Roy and Linnehan, 1974). Hydroxyapatite which is formed by

the conversion of aragonitic calcium carbonate is found to be stronger than the original marine organism. Coralline HA (derived from corals) has been reported as biocompatible, osteoconductive and osteogenic bone graft ceramic which showed evidences of bone remodelling during neo tissue formation (Holmes et al., 1984, Elsinger and Leal, 1996, Vago et al., 2002). Sea shells (conch and clam) varieties, sea urchin spines, egg shells, crab shells, cuttlefish bones, abalone shells, bovine bone were other natural materials used as precursors for the hydrothermal exchange reactions. Coral, Cuttlefish, Sea urchin spine have interconnected porous structures with pore size 20-100 μm making it a prospective scaffold whereas seashells possess lamellar structures providing high mechanical strength and toughness (Sivakumar et al., 1996, Vecchio et al., 2007, Kim et al., 2012).

Both conch and clam shells are reported to give better osteointegration and new bone formation under i*n vivo* conditions when used as cylindrical implants in rat distal femur defect model – 6 week study (Zhang and Vecchio, 2006). Abalone and corbicula shells were also effectively converted to hydroxyapatite by hydrothermal exchange reactions in basic phosphate solutions (Chen et al., 2015a, Onoda and Yamazaki, 2016).

Egg shells were treated with hydrogen peroxide to remove the organic content followed by heating at 700 °C to obtain $CaHPO_4$ (monetite) and CaO (calcium oxide). The monetite and calcium oxide thus obtained from egg shells are then hydrothermally converted to hydroxyapatite under hydrothermal conditions at a temperature of 170 °C for 48 h (Castaño, 2012).

Calcium carbonate from the crab shells were transformed into hydroxyapatite by a hydrothermal process. Here, a biomorphic mineralization synthesis, is used to obtain hydroxyapatite-chitosan composite materials by the preservation of the natural structure of the original crab shells. By retaining the micro-structure as the crab shells, materials of high tensile modulus were prepared (Ge et al., 2010). Dicalcium phosphate dehydrate (DCPD) and anhydrous di calcium phosphate (DCPA) derived from bovine bone were used as starting materials of hydrothermal synthesis of hydroxyapatite at 160 °C and 200 °C under vapour pressure of 1-2 MPa. During the reaction the Ca/P ratio was adjusted with $Ca(OH)_2$. It was seen that whiskers of apatite were obtained with varying crystallinity (Jinawath et al., 2002b). With the advancement of research in this area, the idea of using synthetic precursor materials came to light. Calcium salts such as phosphates, oxides and carbonates in various phases were explored as starting materials to hydrothermal reactions.

The synthetic precursor materials for the preparation of hydroxyapatite by hydrothermal method are mainly $CaHPO_4$ (monetite), $CaHPO_4.2H_2O$ (brushite), ACP (amorphous calcium phosphate), fluorapatite, chlorapatite, tri calcium phosphates and sparingly soluble calcium salts such as calcium carbonates and calcium sulphates (Ishikawa and Eanes, 1993, Onuma, 2006, Suzuki et al., 2006, Jinawath et al., 2002a, Sunouchi et al., 2012, Furuta et al., 1998, Ishikawa, 2010). Organic acids such as citric acid, oxalic acid, ethylenediaminetetraacetic acid (EDTA) are added into the reaction medium to mask growth in particular planes and to make directional growth in preferred planes possible.

Synthesis of polymer and ceramic composite materials by hydrothermal exchange reactions were carried out by Yokogawa *et al.* in preparing a precursor slurry of apatite and agitating a mixture of $CaCO_3$ and $CaHPO_4.2H_2O$ with 3 kinds of polymeric fibres. The mixture was treated under hydrothermal conditions at 180 °C for 5 h to obtain thick coatings of hydroxyapatite on the polymer fibres. Spherical apatite particles of sub-micrometre size were observed on the fibres when the pH value was 6.5-10. At pH value of 4, the products on the fibres were rod-like apatite, 20-50 μm long, and seemed to have developed in the same direction (Yoshiyuki Yokogawa). HA nanorods have been successfully synthesized by a simple and mild hydrothermal treatment of calcium nitrate and sodium phosphate reagents in the presence of poly vinyl pyrrolidone (PVP) (Du et al., 2009). The oriented attachment and the effect of PVP were vital for regulation of the nucleation and crystal growth of rod-like HA crystal. The reaction temperature, molar ratio of Ca^{2+} to HPO_4^{2-}, and hydrothermal treatment time are also critical towards obtaining controlled morphology and grain size of HA crystals. S. Manafi *et al.* has reported the synthesis of HA nanorods aligned with ultrahigh crystallinity and high-yield through a hydrothermal approach. They used a mixture of cetyl trimethyl ammonium bromide (CTAB) $CH_3(CH_2)_{15}N^+(CH_3)_3Br^-$, $Ca(NO_3)_2$, $(NH_4)_2HPO_4$, NaOH and distilled water under hydrothermal condition, to synthesize single crystal HA nanorods with diameter of 20 ± 10 nm and length of 80 ± 20 nm (S. Manafi, 2008). The oriented hierarchical architecture of hydroxyapatite (HA) showed excellent performance in multiple functions in human hard tissues such as bone and teeth. Ethanol was used to control the growth of hydroxyapatite crystals and the increase in the quantity of ethanol inhibited the growth rate of apatite crystals whereas ethanol addition in small

quantities changed the morphology of the apatite crystals from rod to plate form (Goto T, 2011). In addition to fine HA powders, the hydrothermal technique allows synthesis of larger HA crystals, such as micron-sized HA whiskers. The HA whiskers were synthesised from aqueous solutions containing various concentrations of $Ca(OH)_2$, H_3PO_4, and lactic acid at 200 ºC for 5 h under a pressure of about 2 MPa, under moderate stirring (Suchanek et al., 1996). Here the Ca ions are chelated by the lactic acid, preventing precipitation of amorphous calcium phosphate at ambient temperatures and hence precipitation at elevated temperatures yields large HA crystals. By increasing the concentration of the lactic acid in the starting solution, whisker diameters increased and aspect ratios decreased while lengths remained almost unchanged. The Ca/P molar ratios of the HA whiskers obtained were in the range of 1.59 - 1.62, as compared with 1.67 for stoichiometric HA. Biphasic powders with HA and β-TCP phases have been successfully synthesized by a simple hydrothermal route using β-TCP powder. Rod shaped HA were yielded in this study (Sunarso 2013). Morphological control on hydroxyapatite crystals has attractive prospects such that they have promising effects of crystal planes on biological performance. The difference in the morphology and crystal growth of the HA was governed by reactivity of each crystal face of the precursor material and the crystal plane exposed to the surrounding solution, which was studied by Kim *et al*. They reported the reactivities of various faces of calcite single crystals and found that rod-shaped hydroxyapatite crystals with micron dimensions were formed on the (100) face of calcite after treatment at 160 °C for 3 to 24 h while nano dimensions of hydroxyapatite crystals were formed on the (111) plane. As the duration of the reaction increased, the morphology of the crystals also changed. An orientation effect

of rod shaped apatite was seen on (100) planes while such orientation was not observed on the (111) plane after the treatment. The (100) plane of calcite showed a higher reactivity than that of the (111) plane, which results in rapid crystal growth of hydroxyapatite (Kim, 2012). The same group has also studied the effects of solubility of the starting materials on the formation of hydroxyapatite. For this they have studied the dissolution precipitation reactions of single crystals of calcite, fluorite, calcium tartrate tetrahydrate with different solubilities. The observations was that calcium tartrate formed aggregation of nano hydroxyapatite, whereas fluorite formed plate like and calcite formed needle-like apatite all under hydrothermal conditions at 160 °C for 24 h. Hydroxyapatite formation results from the surface of the starting materials under hydrothermal conditions. The calcium ions on the surface of the precursor materials react with the phosphate ions from the medium to give the conversion reaction to form hydroxyapatite with different morphologies. Hydroxyapatite with different morphologies were synthesised which nano and micro rods, flowery patterns as well as plate morphologies were formed by the hydrothermal conversion of α-TCP powders without additives or surfactants (Liu et al., 2011). The Ca/P ratio was adjusted using calcium nitrate tetra hydrate in the reaction mixture (Ca $(NO_3)_2$. $4H_2O$) and reaction time was varied between 6 to 72 h and temperature of 90 – 180 °C. The findings were that aggregation of HA nanorods which grew along the c-axis were the reason for the formation of different microstructures and morphologies. The possible mechanism of growth here is explained based on a cluster growth model where calcium and phosphate ions dissolved into water to form Posner clusters ($Ca_9(PO_4)_6$) which were positively charged on the surface and is considered to be the growth unit of HA crystal. The

Posner clusters were seen attached to c-axis mostly leading to more and more growth along the c direction. But in the case where c surfaces are less predominant it leads to the aggregation of ab- planes and HA plates with smooth surfaces are obtained. The process of crystal growth is enhanced by Ostwald's ripening process and hence HA rods grew upto micrometre scale.

Design of Hydrothermal Experiments

Majority of the hydrothermal works has been carried out in the past by Edisonian trial and error methods for process development. This experimental approach suffers from its time-consuming nature and suffers the inability to clearly discern between processes that are controlled by either thermodynamics or kinetics. Thermodynamic modelling can be used to design a process which is thermodynamically favoured using the fundamental principles instead of the Edisonian methods (R. E. Riman, 2002, W. L. Suchanek, 2004). In order to optimise this for a given precursor system, the effects of thermodynamic variables such as concentration, temperature and pressure are modelled to define the processing variable space over which the phase of interest is stable. Different types of precursor systems can be compared and experiments can be designed to make materials that have never been previously prepared in hydrothermal solution. Hence the number of experiments required can be minimised in comparison to the Edisonian methods. Having found a well-defined thermodynamic variable set for a particular system a range of other conditions for control of reaction and crystallization kinetics can be explored for the purpose of ceramic powder preparation such as particle size, morphology, aggregation level etc.

Thermodynamic processing variables, such as temperature, pH, concentrations of reactants and additives, determine not only the processing space for a given material but also influence both reaction and crystallization kinetics. Morphology control is attained by the overall nucleation and growth rates, which control crystal size, and the competitive growth rates along principal crystallographic directions that control morphology. Size of the crystals can be controlled by varying temperature and concentration. It can also be controlled by the addition of surfactants, which can adsorb on specific crystallographic faces and solvents and regulate solubility.

Non-thermodynamic variables are also extremely important when operating in thermodynamically limited processing variable space. Stirring during crystal growth leads to an increase in the probability of spontaneous nucleation, a decrease in supersaturation inhomogeneities and an increase of the growth rate (R. E. Riman, 2002, W. L. Suchanek, 2004). The final size of the crystals is determined by a balance between the nucleation and growth rates. For instance, changing the stirring speed during powder synthesis can change the particle size (Suchanek et al., 2005). 3D porous structures with surface topographies to enhance bioactivity and osteoinductive ability are considered to be always a challenge in the scaffold design for bone tissue engineering applications. Bioceramic scaffolds with various surface morphologies could be an innovative method of scaffold design so as to study the effects of cell material interactions such as cellular attachment, proliferation and osteogenic differentiation of cells. Xia et al. reported the conversion of α - TCP precursor scaffolds by hydrothermal conditions and evaluated the effects *in vitro* and *in vivo* (Xia et al., 2013). It was seen that the nano topographical features were beneficial for cellular attachment and proliferation. It was seen that the *in vivo*

performance of the material also improved when compared to the control hydroxyapatite scaffolds. However, not much research has been done in this area and it is worth investigating as to how hydrothermally derived apatitic scaffolds act as an ideal material in bone tissue regeneration.

Merits of Hydrothermal Synthesis

The merits of hydrothermal synthesis for powder preparation when compared to other powder processing techniques is that powders are formed directly from solution which regulates the rate and uniformity of nucleation, growth and aging. This results in an improved control of crystallite size and morphology, significantly reduces the aggregation of particles, not possible with other synthesis processes (Riman, 1993). The nature of the powders can be anhydrous, crystalline or amorphous depending on the hydrothermal temperature. Precise control of powder morphology can also be significant. Powders with crystallites having well-developed shapes corresponding to particular crystallographic directions, such as whiskers, plates, or cubes, can be oriented to form materials with single crystal-like properties, or textured ceramic-ceramic composites with anisotropic properties (Shandilya et al., 2016). Another important advantage of the hydrothermal synthesis is that the purity of hydrothermally synthesized powders significantly exceeds the purity of the starting materials. It is because the hydrothermal crystallization is a self-purifying process, during which the growing crystals/crystallites tend to reject impurities present in the growth environment. The impurities are subsequently removed from the system together with the crystallizing solution, which does not take place during other synthesis routes, such as high temperature calcination. Particle size, shape, chemical

composition, stoichiometry are some of the unique properties of powders prepared via hydrothermal reactions. Hydrothermal processing can take place in a wide variety of combinations of aqueous and solvent mixture-based systems. When compared to solid state processes, liquids give a possibility for acceleration of diffusion, adsorption, reaction rate and crystallization, especially under hydrothermal conditions (Oshimura M, 2000). During crystal growth, stirring of the solution increases the probability of spontaneous reaction, decreases the rate of inhomogeneities, and increases the growth rate (R. E. Riman, 2002, W. L. Suchanek, 2004). Hydrothermal methods are more environmentally benign than many other synthesis methods, which can be attributed in part to energy conserving low processing temperatures, absence of milling, ability to recycle waste, and safe and convenient disposal of waste that cannot be recycled (Oshimura M, 2000). The low reaction temperatures also avoid other problems encountered with high temperature processes, for example poor stoichiometry control due to volatilization of components. Materials synthesized under hydrothermal conditions often exhibit differences in point defects when compared to materials prepared by high temperature synthesis methods. Hybrid hydrothermal techniques is used to enhance the reaction kinetics and efficiency of the reaction, this is done by combining microwaves, electrochemistry, ultrasound, mechanochemistry, or optical radiation to hydrothermal methods.

Demerits of Hydrothermal Synthesis

One of the main demerits of hydrothermal synthesis is the need for expensive autoclaves. It is impossible for observing the crystal as it grows, also there arises safety issues for high pressure reactions.

Application of bioceramic materials as dental extraction socket fillers

Dental Extraction Socket filling is one of the major areas where ceramic materials are used in the shape of tooth roots and such implants are known as 'root form implants'. These tooth root implants prevents the alveolar crest from disappearing which is commonly seen after tooth extractions or the vestibular curve of the ring from collapsing (Denissen and Groot, 1979). The implantation of tooth roots are performed using conical shaped ceramic samples usually of (30 x 10 x 10) mm size. The conical shape of the implant enables easiness to manufacture and highly suitable for dental roots. The synthetic roots are placed 2 mm below the crest and influence of lower and upper teeth is also checked in order to avoid failure due to mechanical loading. Root cones require very low flexural and torsional strength. The post clinical evaluation is done two years after the implantation procedure is done. Radiographs provide qualitative data to evaluate the healing process and to analyse the tissue binding to the material. Alveolar bone is seen to adhere to the implants three months after the surgical procedure. It usually seen that these implants give no clinical rejection such as inflammation, formation of fistulae, ulceration or pain and hence the experiments success rate is seen to be high. Reports show that only 3 % of the cases gave flaking as a result of inflammation of the surrounding natural mucous tissue causing detachment of the implant from the site. This site is further improvised

by applying a commercial crown above the root cones and thus providing a material support for the crown fixation. The attachment of the crown is performed after the calcium phosphate material has been stably fixed to the tissue which is ensured after thorough clinical evaluations. The crown helps in taking up immediate impact as a result of the mechanical loading forces from chewing of food and other localised stresses which is hard to overcome by the ceramic alone (de Groot, 1993). Durapatite (a compact polycrystalline form of hydroxyapatite) without fine porosity and no secondary crystal phase is an effective material for root grafts since it has adequate mechanical properties (tensile and compressive strength) and shows no inflammatory effects even after prolonged contact with bone and soft tissue.

Development of Hypothesis

The aim of this study was to propose a novel scaffolding method via hydrothermal routes to obtain large scaffolds for bone and dental filler applications. Since sintered hydroxyapatite has poor degradation their removal from the body is not in pace with the new bone formation. Hydroxyapatite scaffolds prepared via hydrothermal route is expected to improve the resorption rate of the material. The scaffolds are designed with interconnected open porosity to help in vascularisation and bone matrix deposition. Synthetic precursors from different calcium salt sources such as calcium carbonate, calcium oxide, lower calcium phosphates etc. are to be transformed to hydroxyapatite scaffolds. The precursor preparation and the reaction conditions involve low temperature processing. The strength of the scaffolds is expected to be sufficient for bone or dental filler applications which is achieved by the entanglement

of crystals which are developed during these exchange processes. The efficacy of the developed material will be ensured via *in vitro* and *in vivo* testing and evaluation.

Objectives of the research project

Objectives of the project can be outlined as:

- To experiment new scaffolding techniques for bone tissue engineering.
- To prepare various preforms of calcium salts and their composites for hydrothermal conversions.
- To achieve well oriented macro-crystal growth patterns.
- To analyze the nature of the crystals formed, their entanglements, structure, phase etc. To attain the strength of scaffolds and architecture via crystal growth
- To evaluate the *in vitro* performance of the material by assessing the cell viability of the materials, cytocompatibility, bioactivity to ensure *in vivo* performance, degradation to assess the resorption pattern and ALP activity tests to study the osteogenic differentiation potential of the stem cells to the osteoblastic lineage.
- To evaluate the *in vivo* safety and efficacy of the material as a dental filler application prior to clinical studies.

Work Plan

The study was divided into three phases

Phase I Material Synthesis and Characterization

(A) Precursor material preparation with good handling properties and stability under hydrothermal conditions

- Optimisation of reaction parameters.
- Physicochemical characterisation of the developed materials before and after the exchange reactions

(B) Material Preparation of Carbonate derived hydroxyapatite (CHA) and Tricalcium phosphate derived hydroxyapatite (THA)

- Physicochemical characterisation of the developed materials before and after the exchange reactions
- Degradation studies
- Drug elution studies of CHA

Phase II *In vitro* studies

- Bioactivity studies
- Cytotoxicity and viability studies
- Isolation and characterisation of rabbit adipose stem cells
- Cell material interaction studies
- Evaluation of osteogenic differentiation of human mesenchymal cell lines on the material by ALP activity

Phase III *In vivo* studies

- Safety and efficacy of CHA and THA as Dental extraction socket filler in Rabbit Model

CHAPTER - 3

MATERIALS AND METHODS

This chapter details the materials, instruments, and methods used to carry out the research work. Materials used for the work includes: Materials from natural origin – shells obtained from backwaters and sea shells; Materials synthesised in lab: Di Calcium Phosphate (DCP), Tri Calcium Phosphate (TCP) and bioactive glass; Materials Purchased: Commercially available powders of calcium oxide (portlandite), calcium carbonate (calcite).

Material Preparation

Materials of Natural Origin

Materials of natural origin were corbicula shells obtained from the freshwater bodies in the neighbourhood. They were first cleaned using mild detergents to remove the dirt and then sonicated in deionised water for 30 minutes. It is then oven dried at 80 degree Celsius for 5 h. These shells were then calcined at 600 °C at high temperature open hearth furnace for 6 h to remove the presence of the organic components. The obtained powders were then used as precursor materials for the exchange reactions. Using these powders, the hydrothermal exchange reactions were studied to optimise the reaction parameters for effective conversion reactions. Physicochemical characterisation of the powders were carried out before and after the hydrothermal process in order to analyse the phase conversion.

Materials of Synthetic Origin- Commercial powders

Commercially available powders of calcium oxide (extra pure grade 95% assay having molecular weight 56.08 and calcium carbonate (AR grade) molecular weight 100.09 and assay 99.5% from Finar Chemicals were used for the study. These powders were used for the preparation of porous matrices. The reaction parameters (variables) such as temperature, pressure, concentration, pH, and duration of reaction were optimised by various trials to obtain effective conversion of the powders to apatite phase. With respect to the obtained results from the powder conversions, the study was extrapolated to conversion towards large scaffolds. Porous preforms of calcium oxide and calcium carbonate powders were formulated by mixing them with naphthalene (porogen) and powdered to 125-micron size along with polyvinyl alcohol (PVA) as binders. Various ratios of these systems were formulated to obtain stable precursor bodies in the shape of spheres (10 mm) diameter and blocks of dimensions (10 mm × 10 mm × 10 mm). These materials were characterised before the exchange reactions for phase analysis by X-ray diffraction, functional group identification by FTIR, and surface morphology evaluation by scanning electron microscopy. They were then hydrothermally converted to apatite phase by treating with basic ammonium phosphate solution of 1 M concentration for different time periods. The time was adjusted in such a way as to obtain maximum possible conversion to hydroxyapatite phase. The materials were then washed by dipping in deionised water and oven dried prior to its physicochemical characterisation. It was further heated to 300 °C in the high temperature furnace to remove the presence of binders and porogens used during the preform fabrication.

Preparation of di calcium phosphate powders (in house developed method)

Solvent exchange method was used for the synthesis of DCP powders. A 20% (w/v) of orthophosphoric acid solution was prepared by diluting concentrated acid (Ranbaxy; Assay 88%, Specific gravity 1.75) in de-ionized water. Stoichiometric amount of calcium nitrate tetrahydrate (Ranbaxy; Assay 99%) was added and dissolved in the phosphoric acid solution to obtain a calcium to phosphate molar ratio of 1.00. The resulting clear solution was added drop wise into isopropyl alcohol (IPA, Merck) kept in a beaker mounted on a magnetic stirrer (IKA), under stirring. The pH of the solution was maintained it at 3.5 ± 0.1 by simultaneously adding ammonia solution (5%, obtained by diluting 25% NH_3, Ranbaxy) and monitored using a pH meter (Accumet) during the addition process. The addition rate was so adjusted that it could be completed within 15-20 minutes. Addition of ammonia and stirring continued for another 5 minutes and then kept an hour for maturation. The precipitate is separated by centrifugation at 3500 rpm in a centrifuge (MEGFUGE) and washed to remove the nitrate ion. Further they are vacuum dried at 40 °C to obtain the dicalcium phosphate powders.

The obtained powdered are confirmed for their phase purity before precursor fabrication. The powders are then mixed with binders such as starch and polyvinyl alcohol in a composition suitable for injectability (in house developed method) and then they are dropped into a hydrophobic bed to obtain spherical beads. It is then left to dry and then heated to 600 °C to remove the binders and to obtain good precursor stability. These beads were then hydrothermally converted to hydroxyapatite phase by exchange reaction in calcium hydroxide (1 M) at 150 °C for 12 h. It is then

removed from the pressure vessel, washed using deionized water and oven dried prior to physicochemical characterizations.

Preparation of hydroxyapatite porous scaffold from calcium carbonate (Calcite) source

Calcite powders (Finar Chemicals; 99.5% assay) was used for the study. The porous preforms were fabricated by a three step process which includes-

i. Preparation of the setting solution
ii. Mixing of calcite powders with the setting solution and casting
iii. Hydrothermal exchange reactions to obtain the hydroxyapatite phase

i. Preparation of the setting solution

The setting solution is made by making a cocktail mixture of orthophosphoric acid and sodium hydroxide to form a viscous solution with a final pH around 3.5 which is used to form the porous calcite precursor bodies. For this 14.8 M orthophosphoric acid (H_3PO_4) (S D Fine-Chem Limited, India) and 10 M sodium hydroxide (Merck Limited, India) were used to prepare the setting solution. Concentrated sodium hydroxide solution was added drop wise to the orthophosphoric acid with a constant stirring rate of 150 rpm in 50 ml portions with constant stirring in order to avoid excess heating and the change of pH is observed from 0.4 to 4.0. The solution is then cooled to room temperature and then it is transferred and made upto 250 ml in a standard flask using de ionised water. Further it is transferred to air tight storage bottles for use, this solution has a shelf life of 2-3 years. One millilitre of this solution contains 0.0059 mol of phosphate.

ii. Mixing of calcite powders with the setting solution and casting the slurry

Calcium carbonate powders (Rankem chemicals, India) 99.5% assay and 100.09 molecular weight were used for the study. It is mixed with the phosphoric acid based setting solution prepared in such a way as to obtain a material having adequate strength and good handling properties. For obtaining a stable calcite body the optimal powder to wetting liquid ratio was 1:2 (gm/ml). The mixing was done for 1 min and the thick frothy paste was cast into the required size and shape using stainless steel moulds. The setting process is complete around 5 to 10 min after which they are removed from the moulds and allowed to dry at room temperature for the next 48 h. Further it is washed with deionised water and dried in an air oven for 6 h at 80 °C prior to hydrothermal reactions.

iii. Hydrothermal Exchange Reactions for calcite conversions

The precursor materials prepared by this casting method can be made in various shapes and dimensions such as spheres, cones, cylinders, pellets, and blocks as intended for the clinical use. The preform scaffolds prepared by this method are suspended into a hydrothermal reaction vessel which is a Teflon lined stainless steel high pressure hydrothermal reactor (Amar Equipments, India). 1 M basic ammonium dihydrogen phosphate (Rankem chemicals, India) solution of pH 10.5 is used as the reaction medium. The reaction time is adjusted in such a way as to obtain maximum possible conversions. Reactions are conducted for different time periods such as 1 h, 4 h, and 8 h at 150 °C and a pressure of 10 – 15 bars. Once the reaction is complete the reaction vessel is allowed to cool to room temperature, the products were collected, washed with de ionised water and oven dried at 60 – 70 °C for 24 h prior

to further studies. The materials prepared from carbonate origin are termed as CHA (carbonate derived hydroxyapatite) hereafter.

Preparation of β- Tri Calcium Phosphate powders (TCP) (in house developed method)

A wet chemical precipitation method was employed to synthesise the β- tri calcium phosphate powders. The precipitation of TCP is based on the chemical reaction between salts of calcium nitrate tetra hydrate $Ca(NO_3)_2$. $4H_2O$ (Rankem Chemicals, India; 98% assay) and ammonium dihydrogen phosphate $NH_4H_2PO_4$ (Rankem Chemicals, India; 99% assay). The reagents are taken in such a way as to obtain the calcium to phosphorus ratio as 1.5 for the precipitation of TCP phase. The precipitation reaction is carried out at 60 °C at a constant stirring for 1 h and maintain the pH between 6 - 7 in order to avoid the precipitation of other phases. Once the reaction is complete the precipitate is allowed to settle down and then it is filtered before the ageing. It is then washed with deionised water and dried in hot air oven. The dried powders are then calcined at 300 °C in high temperature furnaces to remove the impurities, if any present. The calcined powders are then collected and then ball milled using zirconia balls to reduce the particle size down to micron levels. They are then sieved using 125 µ sieves in a sieve shaker (Retsch, AS 200 basic, Germany).

Preparation of porous preforms using β- TCP powders

The graded β- TCP powders prepared were mixed with 125 µ sized naphthalene as porogen in the powder to porogen ratio (4:1). This mixed powders were pelletised using pellet press (X Press 3630, NJ, USA) using a 13 mm die. Cylindrical shape

was formulated in a cylindrical die of 8 mm diameter and 30 mm length. The pellets prepared were used for *in vitro* studies and the cylinders were used for mechanical testing as well as for implantation studies. These compacted bodies were heat treated at 900 °C in a raising hearth electric furnace (Okey Model No: 45R5Y, India) to obtain better compaction and precursor stability required for the hydrothermal exchange reactions.

3.1.6.1 Hydrothermal Exchange reactions for β- TCP conversions

The β- TCP preforms prepared are then hydrothermally converted to apatite phase in the Teflon lined stainless steel high pressure hydrothermal reactor from (Amar Equipment's, India). The conversion reactions are studied in three different reaction mediums namely 1M basic ammonium di hydrogen phosphate (pH 10.5), 1 M calcium nitrate (pH 4.2) and 1M calcium hydroxide (pH 12) solutions. Since calcium hydroxide is sparingly soluble it is heated to 70 °C for 1 h with constant stirring and the supernatant solution is filtered out which is used as the reaction medium. The temperature range of the reactions were from 140 - 170 °C and the pressure developed was in the range of 5 - 15 bars. Basic pH conditions and the temperature used were effective in producing maximum conversions to the apatite phase. Physicochemical characterisations were carried out before and after the conversion reactions to ensure phase purity, functional group identification, and to study the surface microstructural changes. The materials of this class will be hereafter named as THA (TCP derived hydroxyapatite).

Preparation of sintered hydroxyapatite granules

Hydroxyapatite powders were synthesised by wet precipitation technique by the reaction between calcium nitrate and ammonium dihydrogen phosphate (Rankem, India) in Ca/P stoichiometric proportions of 1.67 at a pH 11 and at a temperature of 80^0 C. The precipitate obtained was then kept for aging for 24h for the complete maturation of hydroxyapatite phase. It was then washed with distilled water to remove soluble nitrates and ammonium ions. It was then followed by filtration, freeze drying and calcination at 300^0 C for 2 h. The obtained HA powder was pulverized and sieved to achieve a particle size less than 125 μm. The chemical reaction can be written as in equation given below. HA powder was prepared in batches of 75g.

$$10\,Ca(NO_3)_2.4H_2O + 6\,NH_4H_2PO_4 + 14\,NH_4OH \rightarrow Ca_{10}(PO_4)_6(OH)_2 + 20\,(NH_4NO_3) + 12\,H_2O$$

The free flowing powders were then mixed with pore formers, sintered and granulated to get porous HA granules. 1mm sized granules were used as control materials for extraction socket filling in the *in vivo* experiments.

Hydrothermal Reaction Vessel

The hydrothermal reaction vessel we use is a custom made design from Amar Equipment's, Mumbai, India. It has a Teflon lined vessel of 1litre capacity and a heating unit at the bottom and an upper unit with a lid comprising a pressure gauge, temperature sensor probe, an inlet and outlet valve, a pressure inlet valve and safety valve and a cooling system with a water inlet. The complete unit is made of stainless

steel 316L. It works upto a maximum temperature of 200 °C and a pressure of 200 bars. There is a pressure gauge to monitor the pressure changes inside the vessel and a temperature sensor probe which is introduced into the reaction chamber to track the changes in the temperature. It also has an inlet and outlet valve in the upper unit which is used to introduce reagents into the reaction vessel in between a reaction if needed or to take the products out in a molten stage or in between a reaction. There is a water cooling system which can be used to pass water to cool the system to reduce the temperature in between or to bring down the temperature when the reaction is complete. There is an online pressure and temperature monitoring system which is connected to a computer to monitor the reaction parameters. A safety valve is provided such that if any overshoots of pressure occurs, the rupture disc breaks and the pressure is released. Apart from this the experimental set up there is an external control unit which is used to set the temperature and pressure which is fed to the inputs of the device which is the user interface.

Figure 3.1. Hydrothermal Reaction Vessel

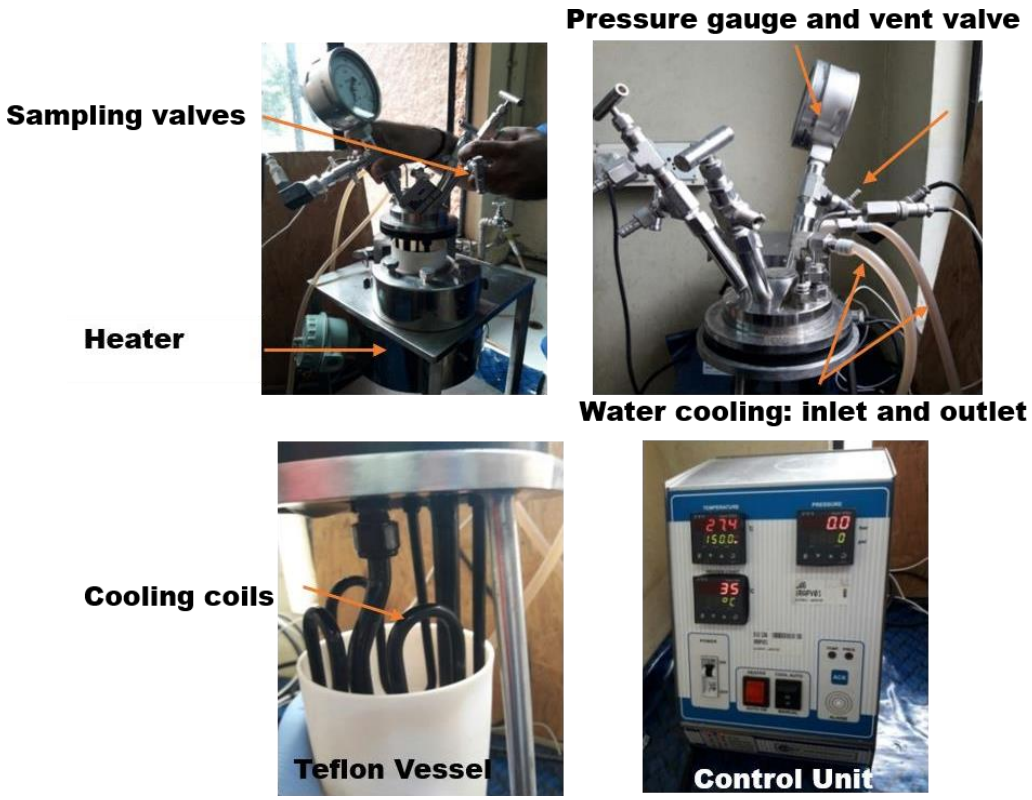

Figure 3.2. Hydrothermal Reactor Parts

Methods used for the analysis of the synthesised materials

Phase Analysis - X Ray Diffraction (XRD)

The precursor powder materials as well as their fabricated preforms were analysed for their phase purity before the conversion reactions and the converted scaffolds were analysed for their phase confirmation, crystallinity, orientation effect analysis and phase purity studies using X-ray diffraction technique (XRD). The X Ray Diffractometer works from a source of Cu Kα1 radiation having a wavelength of (λ=1.5418 A°) produced from a Cu target. The diffractometer (Bruker D8 Advance, Germany) works at an operating voltage of 40 kV and 30 mA with a scan range from

2θ range 20 – 50° and a scanning rate of 1° per minute employing a step size increments of 0.01°.

Generation of X -Rays

X-Rays are produced as a result of bombardment of electrons moving with very high velocity onto a metal target. In a X - Ray diffractometer the source of electrons is a heated tungsten (W) filament which acts as the cathode. The anode is usually a metal target of (Cu, Al, Mo, or Mg) usually Cu is used, which is kept in cooling water supply. When a high accelerating voltage is applied between the anode and cathode, electrons from cathode move with a high velocity towards the anode and collides with a K-shell electron, the electron in the K-shell is ejected leaving behind a 'hole'. An outer shell electron fills this hole (from the L-shell, M-shell, etc.) with an emission of a single X-ray whose energy is equivalent to the energy level difference between the outer and inner shell electron involved in the transition. When an electron falls from the L-shell to the K-shell, the X-ray emitted is called a K-α radiation which is used in the XRD instrument.

X-ray diffraction analysis

The method of X-ray diffraction depends upon the wave character of X-rays and the regular spacing of planes in a crystal. Although diffraction methods can be used for quantitative analysis, they are most widely used for qualitative identification of crystalline phases. Every atom in a crystal scatters an X-ray beam incident upon it in all directions. Because even the smallest crystal contains a very large number of atoms, the chance that these scattered waves would constructively interfere would be

almost zero except for the fact that the atoms in crystals are arranged in a regular, repetitive manner.

The condition for diffraction of a beam of X-rays from a crystal is given by Bragg equation (Cullity, 1956):

$$n\lambda = 2d \sin\theta$$

where, n is the order of reflection, λ is the wavelength of x-ray used, d the interplanar spacing and the magnitude of the distance between two adjacent parallel planes of atoms. Theta (θ) is the grazing angle between the lattice planes. Atoms located exactly on the crystal planes intensifies the diffracted beam whereas atoms exactly half way between the planes exert maximum destructive interference. When atoms are at some intermediate location it can interfere constructively or destructively depending on their exact location but with less effect. The position of the diffraction beam from a crystal depends only upon the size and shape of the repetitive unit of a crystal and the wavelength of the incident X-ray beam. But the intensities of the diffracted beam depend upon the type of atoms in the crystal and the locations of the atoms in the fundamental repetitive unit, the unit cell. No two substances therefore have absolutely identical diffraction patterns when one considers both the direction and intensity of all the diffracted beams; however, some similar, complex organic compounds may have almost identical patterns. The diffraction pattern is thus a "finger print" of a crystalline compound and the crystalline components of a mixture can be identified individually (Williard, 1986). The sharpness of the diffracted beam is a measure of the crystallinity of the sample. Phase identification using XRD is based on the unique pattern produced by every crystalline phase. The composition of

a sample can therefore be determined by comparing the diffraction pattern with the compilation of standard patterns that have been developed for most known compounds by the Joint Committee on Powder Diffraction Standards, (JCPDS) or recently termed the international centre for diffraction data (ICDD). XRD analysis can be used to compare the crystallite size bioceramics using the Debye-Scherrer equation (Cullity, 1956). This equation uses the half-height width of the diffraction peak of XRD pattern. The Scherrer equation is,

$$t = (K \times \lambda)/(B \times \cos \theta_B)$$

where *t* = thickness of crystallite; K = constant dependent on crystallite shape (0.89); λ = X-ray wavelength; B = FWHM (full width at half maximum) or integral breadth and θ_B= Bragg Angle

The crystallite size of hydroxyapatite was calculated with reference to the most intense 211 peak and by approximating the β value to be the measured peak width at half peak height in radians. The XRD pattern given below gives an overall idea about the information that can be gained from a XRD spectra.

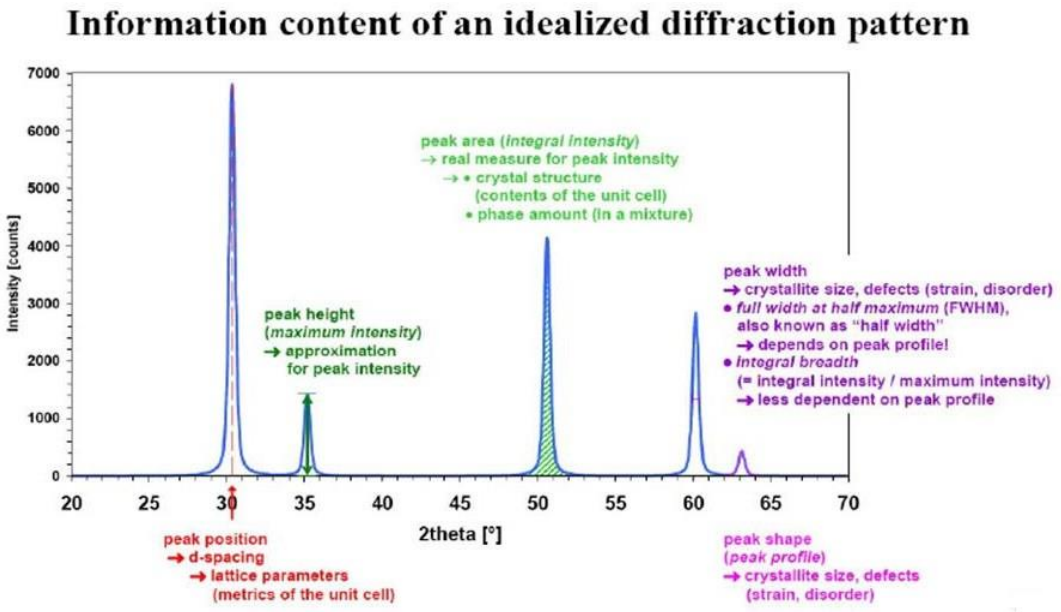

Figure 3.3. Information from an idealised diffraction pattern.

Preferred Orientation

When there is a stronger tendency for the crystallites in a powder or a texture to be oriented in one or more ways apart from the normal alignment pattern it is said to have a preferred orientation along a particular plane. Crystal morphology causes preferred orientation of particles in polycrystalline specimens. Needle shaped or plate shaped structures have preferred orientations. When the shapes of the crystallites are anisotropic (needle-like, plate-like etc.) there occurs non- random crystallite orientations due to natural preferences in the packing of anisotropic particles. This non-random particle orientation is called the preferred orientation and this may lead to considerable distortions of the scattered intensity. The intensity of the diffracted peak depends on the shape of the crystallites. Hence we observe some intensities to be stronger than expected whereas some others will be weaker than expected from random orientation.

When the powder particles have thin platelet -like shape they tend to agglomerate aligning their flat surfaces nearly parallel to one another. As a result, the orientations of the platelets are randomised via rotations about a common axis normal to their largest faces and such samples are expected to have a uniaxial preferred orientation or texture. When the particles are in the form of thin needles the orientations of the axes of the needles maybe nearly random in the plane of the sample. Furthermore, each needle has an additional rotational degree of freedom about its longest axis and such materials are expected to have an additional in-plane preferred orientation. Even more complex preferred orientation effects are seen when the elongated particles are flat (ribbon-like) since alignment occurs along the axis of the ribbon and also perpendicular to the flat surface (Zhuang et al., 2012, Pavel Fejdi, 2001).

Sample preparation to study preferred orientation effects.

The hydroxyapatite crystals formed as a result of the hydrothermal exchange reactions of tricalcium phosphate and calcium carbonate are analysed in detail in order to see if there are any preferred orientation effects. For this the crystals of apatite formed after the conversion reactions were isolated by mild sonication in isopropanol solvent. It was then dropped on a zero background sample holder so that there are no stray radiations. Once the solvent has vaporised the orientation of the crystals were analysed from their diffraction patterns.

Functional group identification by Fourier Transform Infrared Spectroscopy (FTIR)

FTIR spectral analysis was performed using Nicolet 5700 (Thermo Electron Corporation; Madison, USA) spectrometer and the spectra were collected in diffuse

reflectance (DRIFT) mode to determine the presence of functional groups. The samples before and after the hydrothermal reactions were powered and mixed with optical grade KBr powder. The spectra were recorded at a resolution of 4 cm^{-1} and scanned in the range 400 to 4000 cm^{-1} with an average of 64 scans. KBr powder was used as the background and diluent for the sample. Diffuse reflectance spectroscopy is a widely used technique in FTIR analysis. In diffuse reflectance spectroscopy, the sample is mixed with an infrared transmitting powder such as KBr. The DRIFT cell reflects radiation to the powder and collects the energy reflected back over a wide angle. Diffused scattered light can be collected directly from a sample or by using an abrasive sampling pad. The technique is particularly suitable for sampling powders or fibres. The spectrum obtained cannot be used directly for quantitative analysis. Kubelka and Munk developed an expression which relates the sample concentration to the scattered radiation intensity (Mendham J, 2002):

$$\frac{(1- R\infty)^2}{2R\infty} = \frac{c}{k}$$

where R∞ is the absolute reflectance of the layer, c is the concentration and k is the molar absorptivity.

Sample Preparation: The sample to be analysed is diluted in a transmitting matrix. The sample is finely ground using a mortar and pestle provided and KBr powder is added to the sample. Using the pestle, the sample along with the KBr powder is mixed so that the sample particles are small and evenly dispersed. The percentage of transmission of the strongest band in the resulting spectrum should ideally be in the range from 10-50%. A background spectrum of the KBr alone is collected. Then the

spectrum of the sample mixed with KBr is collected. The background is subtracted to produce a transmittance spectrum of the sample alone which is converted to an absorbance spectrum by performing a Kubelka-Munk mathematical transform on the data (Mendham J, 2002).

Surface Microstructural Analysis- Scanning Electron Microscopy (SEM) In this study an Environmental Scanning Electron Microscopy ESEM (ESEM, FEI Quanta 200, The Netherlands) is used for the surface structural analysis. The images of the material surface alone were captured without any coating. However, for the study of cell morphology, normal procedure is adopted for the SEM view which includes dehydration, critical point drying and gold coating (Hanke, 2001).

Scanning electron microscopy (SEM) is a method for high-resolution imaging of surface of materials. The SEM uses electrons for imaging, like a light microscope uses visible light. It offers a higher magnification (>100,000 X) and greater depth of field up to 100 times that of light microscopy. Qualitative and quantitative chemical analysis of the material is also obtained using an attachment of energy dispersive x-ray spectrometer (EDS) with the SEM. The SEM generates a beam of incident electrons by a thermal emission source, such as a heated tungsten filament, or by a field emission cathode. The energy of the incident electrons can be as low as 100 eV or as high as 30 keV depending on the evaluation objectives. The electrons are focused into a small beam by a series of electromagnetic lenses in the SEM column. Scanning coils near the end of the column direct and position the focused beam onto the sample surface. The electron beam is scanned in a raster pattern over the surface

for imaging. The beam can also be focused at a single point or scanned along a line for X-ray analysis.

Variable Pressure SEM: SEM imaging can be performed on a nonconductive sample when the chamber pressure is maintained at a level where most of the electrons reach the sample surface, but there are enough gas molecules to ionize and neutralize charging. Variable pressure SEM is used for samples that are not compatible with high vacuum such as the studies of cells, tissues, etc. The environmental scanning electron microscopy (ESEM) is such a technique where the sample can be viewed at different modes such as high vacuum, low vacuum and ESEM mode depending on the sample type.

Crystal Analysis- Transmission Electron Microscope (TEM)

High resolution transmission electron microscope was used to study the features of the crystals in detail. It was performed using an FEI, TECNAI S Twin microscope with an accelerating voltage of 100kV. For this the crystals were isolated by mild sonication and was suspended in isopropyl alcohol. This suspension was then dropped onto a Formar®- coated copper TEM grid and dried in vacuum at room temperature before observation and imaging.

3.3.4.1 Principle of TEM

TEM is a microscopic technique which is used to image thin solid specimens to study the finer details and internal structure of materials using high energy electrons. A thin solid specimen (≤ 200 nm) is bombarded in vacuum with a highly focussed monoenergetic beam of electrons. The beam will have sufficient energy to propagate through the specimen. A series of electromagnetic lenses magnifies this transmitted

electron signal. Diffracted electrons are observed in the form of a diffraction pattern beneath the specimen; this information is used to determine the atomic structure of the material in the sample. Transmitted electrons form images from small regions of the sample that contain contrast due to scattering with interactions between electrons and atomic constituents of the sample. Analysis of transmitted electron images gives information on the atomic structure and defects present in the material. These microscopes are capable of imaging at higher resolutions than light microscopes as a result of the smaller de Broglie wavelength of electrons. This enables the instrument to capture fine details as a single column of atoms, which is thousands of times smaller than a resolvable object seen in a light microscope. Transmission electron microscopy is a major analytical method in the physical, chemical and biological sciences.

Elemental analysis by inductively coupled plasma-optical emission spectroscopy (ICP-OES)

Inductively coupled plasma-optical emission spectroscopy (ICP-OES; OPTIMA 5300 DV, Perkin Elmer, USA) was used for the elemental analysis of the hydrothermally prepared ceramics, bioactivity studies, dissolution studies and to analyse if there are any depositions of calcium and phosphate ions in the tissues (heart, lungs liver, kidney, and spleen) collected from the animal after autopsy.

Protocol for tissue processing

The organs collected were dried at 60 °C overnight. The samples were weighed (0.5 g) each, into a boiling tube. 3 ml each of concentrated nitric acid (HNO_3- ICP grade) was added to the samples and kept in sand bath for tissue digestion. When the

volume of the solution in the boiling tube decreases it is further supplemented with 2 ml of con. HNO_3 and the process is continued with caution to avoid charring while the digestion process takes place. Finally, 1 ml of con HNO_3 and 2 ml of perchloric acid ($HClO_4$) is added and heated to get a clear solution without any tissue remnants or organic matter. This clear solution is transferred to an ICP vial and made upto 50 ml using HPLC grade water. This solution is then analysed with ICP-OES system.

Elemental Composition Determination

To study the elemental composition of the material, the samples were analysed for their calcium and phosphate contents before and after the exchange processes. For this a definite quantity of the material (precursor & converted samples) was weighed and dissolved in 1ml concentrated HNO_3 (ICP grade) and 9 ml of deionised water. 1ml of the above mixture is pipetted out and made upto 100 ml in a standard flask. Of this made up solution, 5.5 ml is used for the analysis of the ions.

Principle of ICP-OES

Plasma emission spectroscopy is an analytical technique used for the detection of trace elements. This technique uses inductively coupled plasma to produce excited atoms and ions that emit electromagnetic radiation at wavelengths characteristic of a particular element. The intensity of this emission is indicative of the concentration of the element within the sample. The ICP-OES is composed of two parts: the ICP and the optical spectrometer. The ICP torch comprises of three concentric quartz glass tubes. The output or "work" coil of the radio frequency (RF) generator surrounds part of this quartz torch. Argon gas is typically used to create the plasma. When the torch is turned on, an intense electromagnetic field is created within the coil by the high

power radio frequency signal flowing in the coil. This RF signal is created by the RF generator which is, effectively, a high power radio transmitter driving the "work coil" the same way a typical radio transmitter drives a transmitting antenna. The argon gas flowing through the torch is ignited with a Tesla unit that creates a brief discharge arc through the argon flow to initiate the ionization process. Once the plasma is "ignited", the Tesla unit is turned off. The argon gas is ionized in the intense electromagnetic field and flows in a particular rotationally symmetrical pattern towards the magnetic field of the RF coil. A stable, high temperature plasma of about 7000 K is then generated as the result of the inelastic collisions created between the neutral argon atoms and the charged particles. A peristaltic pump delivers an aqueous or organic sample into an analytical nebulizer where it is changed into mist and introduced directly inside the plasma flame. The sample immediately collides with the electrons and charged ions in the plasma and is itself broken down into charged ions. The various molecules break up into their respective atoms which then lose electrons and recombine repeatedly in the plasma, giving off radiation at the characteristic wavelengths of the elements involved (Mendham J, 2002, Hanke, 2001).

Micro-CT Analysis

Micro- CT was used to study the porosity of the scaffolds as well as to get a 3D image of the implanted material in the site. Microcomputed tomography is an X-ray based imaging method that provides an easy reliable and inexpensive access to the 3D micro architecture. This imaging technique is based on a finely focused X-ray source that illuminates the object and a planar detector that collects the magnified

projection images. Hundreds of angular views are acquired while the object of interest rotates. From these views, a computer processes a stack of virtual cross-sections, interpolating sections along different planes, to inspect the internal structure of the object. Based on this data, the computer can reconstruct a realistic 3D image which is cut into slices to produce 2D images. Micro-CT analysis is a powerful tool for the evaluation of bone tissue as it provides a 3D microarchitecture of the bone. Both *in vivo* and *ex vivo* imaging can be done using this method (Kallai et al., 2011, Hildebrand et al., 1999).

Micro- CT helps in the quantitative assessment of the bone's macrostructural characteristics such as geometry, microstructural features, relative mineralized bone volume (BV), bone thickness and connectivity, thereby improving our ability to estimate the quality of regenerated bone. The percentage of healing between samples is evaluated by the bone volume BV to the total volume (TV) (Kallai et al., 2011). The porosity of the scaffolds as well as the harvested bone with implants site was analysed by Micro-CT for the 3D visualisation of the bone in relation to the implant surface. The imaging was performed using (SCANCO Medical µCT 40, Switzerland) with a 70 kV tube voltage and 114 µA beam intensity.

Mechanical Property Evaluation by Compressive Strength Measurements The hydrothermally converted scaffolds both tricalcium phosphate-derived and calcium carbonate- derived ones (n = 12) were fabricated in the form of cylinders (2 cm height and 1 cm diameter) as per ASTM D 882-97 procedure. The compressive strength was analysed using Universal Testing Machine (Instron Corporation Series IX Automated Materials Testing System) at a crosshead speed of 1 mm / min and full

scale load range of 5 kN. Mean and standard deviation of stress at maximum was measured and expressed in megapascal (MPa). Compressive strength testing is done to measure the maximum amount of compressive load a material can bear before fracturing. The test material is usually in the form of a cube, prism, or cylinder, which is compressed between the platens of a compression-testing machine (Universal testing machine) by a gradually applied load.

In vitro bioactivity studies in Simulated Body Fluid (SBF)

The *in vitro* behaviour of the developed materials were evaluated in simulated body fluid as per Kokubo's recipe which is a solution having the ionic concentrations and pH almost equal to those of human blood plasma (Kokubo and Takadama, 2006) by dissolving reagent-grade chemicals (Sigma Aldrich, Germany) as listed in Table 1, into deionized water and buffered at pH 7.4 with tris hydroxymethyl aminomethane (Tris) and 1 M HCl at 37 °C. The dissolution behaviour was estimated by comparing the ionic concentration of SBF and the bioactivity was confirmed by the transformation of the surface layer by the apatite phase.

Order	Reagent	Weight (g)	Ion	Ions in 1L of SBF (mM)
1	NaCl	8.035	Na^+	142
2	$NaHCO_3$	0.355	HCO_3^-	4.2
3	KCl	0.255	K^+	5.0
4	K_2HPO_4	0.1759	HPO_4^{2-}	1.0
5	$MgCl_2.6H_2O$	0.311	Mg^{2+}	1.5
6	1M HCl	39 ml	Ca^{2+}	2.5
7	$CaCl_2.2H_2O$	0.3713	SO_4^{2-}	0.5
8	Na_2SO_4	0.072	Cl^-	147.8
9	Tris	6.118		
10	1M-HCl (pH=7.4)	0-5 ml		

Table 1. Order, reagent, weight (g), ion and ion concentration (mM) used for preparing 1 L of SBF

Procedure: The scaffolds were soaked in 20 mL of SBF taken in polypropylene vials and is maintained at 37±1 °C. Estimation of bioactivity was done after 1, 3, 7, and 14 days by evaluating the carbonated apatite deposition on the materials in terms of weight differences. Inductively coupled plasma-optical emission spectroscopy (ICP-OES, Perkin Elmer 5300DV, USA) was used to determine the elemental composition of SBF initially and thereafter the change in the ionic concentration during the study was also noted. For this, the samples were treated using 5% HNO_3 and analysed for calcium and phosphorous ions to confirm the apatite deposition or dissolution over the scaffolds. The experiments were done in triplicate with a calibration plot for better clarity of the results.

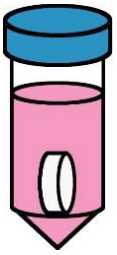

Figure 3.4. Schematic of the samples immersed SBF for bioactivity evaluation

Weight differences before and after immersion in SBF was estimated to obtain weight gain/loss of the material. The obtained weight gain or loss was assessed by calculating the percentage with respect initial weight and the final weight of the sample using the equation:

$$\left[\frac{\text{Weight gain or loss after soaking in SBF}}{\text{Initial weight of coating}}\right]\times 100\%$$

The samples were examined for the patterned growth morphology of apatite and compared with the original morphology of the scaffolds by ESEM.

In vitro degradation studies in Phosphate buffered solution (PBS)

The developed materials were characterized for *in vitro* degradation studies as per ISO standard 10993-13. Real-time degradation test (incubation temperature = 37 °C) were conducted for the TCP-derived as well as calcium carbonate-derived apatite scaffolds. The materials in triplicate were immersed in 5 ml phosphate buffered saline (PBS) and incubated at 37 °C and for 60 days. The materials were then examined for their weight differences before and after the experiment. The PBS solutions were collected every three days and supplemented with fresh PBS (5 ml) till the end of the study period. The PBS collected was then analysed for the release of calcium and phosphate ions by quantitative method using ICP-OES spectroscopy technique. With respect to the obtained result the dissolution rate of the developed materials was arrived. The reagents used for the preparation of the phosphate buffer is described in Table 2 below:

Reagent	**Quantity**
Sodium Chloride (NaCl)	8 g
Potassium Chloride (KCl)	0.2 g
Disodium hydrogen phosphate (Na_2HPO_4)	1.44 g
Potassium di hydrogen phosphate (KH_2PO_4)	0.24
Deionised water	1000 ml
1M HCl for adjusting pH to 7.4	(1-5 ml)

Table 2. Phosphate Buffered Saline (PBS) preparation

The reagents listed in table 2 are first dissolved in 800 ml of deionised water with stirring in the order as given in the table. During the addition of the reagents the pH of the solution is adjusted to 7.4 using the 1 M HCl. Finally, the solution is made up to 1 L with the remaining deionised water. This buffer prepared is sterilised by autoclaving before use for the intended studies.

Cytotoxicity Evaluation (MTT Assay)

The cytotoxicity evaluation on the developed materials were done using L929 mouse fibroblast cell line provided by National Centre for Cell Sciences (NCCS), Pune, India. Extract was prepared by incubating 0.2 g of test materials in 1 ml culture medium containing serum at 37±1 °C for 24 ± 2 h. L-929 mouse fibroblast cells is a well-established and characterized mammalian cell line used for the tests. Cells cultured in normal medium were considered as cell control. Equal volume (100 µl) of various dilution of test samples, extract of negative control, cell control and positive control were placed on the confluent sub confluent monolayer of L-929 mouse fibroblast cells. After incubation of cells with various concentrations of test samples and controls at 37±1 °C for 24 ± 2 h, extract and control medium was replaced with 50 µl MTT solution covered with aluminium foil and further incubated at 37±2 °C for 2 h. The MTT was then discarded and 100 µl of isopropanol was added to the wells. The colour developed was quantified by measuring the absorbance at 570 nm using a spectrophotometer. The metabolic activity of viable cells to reduce yellow coloured tetrazolium salt 3-(4, 5 dimethyl thiazol -2yl)- 2,5- diphenyltetrazolium bromide to purple coloured formazan was measured.

Cell Proliferation Study (Cell Titer Blue / Alamar Assay)

The presence of viable cells in the material was evaluated by seeding the material with human mesenchymal stem cell (MSC) cell lines and incubating the cell seeded material in serum supplemented medium for 14 days along with 1 ml/sample of cell titer blue reagent. The reagent was collected every day and its UV absorbance was used to evaluate the presence of viable cells by measuring the absorbance at 570 nm using 600 nm as a reference wavelength.

Isolation and Culture of Adipose derived mesenchymal stem cells (ADMSC)

ADMSC's were isolated from the adipose tissue of rabbits which was collected at the autopsy of the carcass animal. The mesenchymal origin of the isolated cells was determined through CD 90/ Thy 1marker (thymocyte differentiation antigen 1) which is a positive marker for mesenchymal stem cells. These cells were used for the cell material interaction study by scanning electron microscopy and confocal laser scanning microscopy.

Isolation of cells

Adipose tissue from New Zealand white rabbits were collected at the time of autopsy as per the guidelines of Animal Ethics Committee (IAEC) and committee for the purpose of control and supervision of experiments on animals (CPCSEA). Tissue was excised from the subcutaneous site of the animal and collected in phosphate buffered saline (PBS) with antibiotic. It was then washed 3 to 4 times in phosphate buffed saline and minced thoroughly. The minced slices were then digested in 1%

type 1 collagenase (Sigma Aldrich, St. Louis MO) in a shaking incubator at 37 °C. Enzymatic activity was neutralised with an equal volume of α-MEM (minimum essential medium) containing 10% FBS and 1% antibiotic (penicillin/streptomycin (P/S)). It was then filtered to remove the cellular debris and centrifuged at 3000 rpm to obtain the cell pellet. The cells were seeded in 25 cm^2 (T25 flask) containing 10 ml of serum containing medium and incubated at 37 °C in 5% CO2 maintaining the humidity. Medium was changed every day for the first three days and non-adherent red blood cells were removed, after this medium change was done once in two days. One-week post culture, the cells were sub cultured by treating with 25% trypsin-EDTA (Gibco, India) to remove the adherent cells. The enzymatic activity was then arrested with the addition of media, collected and centrifuged at 3000 rpm for 10 min to obtain the cell pellet. The cells at the fourth passage were used for the study and seeding density used for the samples were (1×10^5) cells/cm^2.

Immunohistochemical study

Rabbit adipose derived MSC's cultured in T25 flasks for 48 h were trypsinised with 0.25% trypsin EDTA for 5 min and centrifuged at 3000 rpm for 5 min. The cell pellet was blocked with 3% bovine serum albumin (BSA) in PBS for 30 min. It was then incubated in 1 µl FITC labelled monoclonal antibody to CD90/Thy1 at 4 °C for 1 h. The cells were then visualised in fluorescence microscope (Leica DMIL, Germany).

Cell-Material Interaction

The MSCs at the fourth passage were seeded onto the scaffolds at a seeding density of 1×10^5 cells/cm^2. The cells were supplemented with 15% serum containing media

(α-MEM) and incubated at 37 °C with 5% CO2. After 4 days of culture the cells in the material construct were fixed with 1% glutaraldehyde and processed by dehydration in a series of alcohol water dilutions and critical point dried in (Hitachi HCP-2), gold coated in an ion sputter (Hitachi E101) for viewing under scanning electron microscope (Hitachi S2400 The adherence of the cells onto the material for 2 and 4 days were evaluated.

Live dead staining by Confocal Laser Microscopy

The cells seeded on the materials were stained using fluorescein diacetate (FDA) and propidium iodide (PI) and viewed by confocal laser scanning microscopy (cLSM Carl Zeiss LSM Meta 510). After 4 days of culture the medium was removed and the combination of the two dyes (FDA and PI) were added and incubated for 5 min and viewed under the microscope. FDA (non- fluorescent) is internalised in the cells and gets converted into the green fluorescent metabolite fluorescein. The measured signal is an indicator of viable cells as it is esterase dependent, whereas PI is the nuclei staining dye and it will not pass through a viable cell membrane. PI passes through the ruptured cell membranes of dead cells, reaches the nucleus and intercalates with the DNA double helix of the cell. A depth profiling was also done to see the presence of live and dead cells inside the pores of the scaffolds. The green cells were marked live and red cells dead.

Differentiation potential by ALP activity measurements

Differentiation potential (osteogenic) of the cells seeded on the materials were evaluated by the determination of ALP activity, based on the hydrolysis of p-nitrophenyl phosphate (Sigma chemicals) to p-nitrophenol. For this, (1×10^5 cells)

human MSC cell lines were used. The cell seeded constructs were maintained in both normal medium as well as osteogenic medium for 7, 14 and 21 days supplemented with fresh medium every 2 days. The cells from the scaffolds were washed with PBS twice and lysed with TritonX-100 for 50 minutes followed by sonication for 10 minutes. The aliquot of (25 µl) was added to 125 µl of ALP reaction buffer (Sigma chemicals) containing 1mg/ml p- nitrophenyl phosphate, 1mM magnesium chloride ($MgCl_2$), 0.1M diethanolamine, 1% Triton X-100 and the mixture was incubated at 37 °C for 30 min. The enzymatic reaction is stopped by the addition of 5 M NaOH (50 µl /sample) and centrifuged at 16,000 g for 10 min. 170 µl of the supernatant was transferred to a microtiter plate and the absorbance was read at 405 nm (Erba Chem -7). A calibration line was constructed from different concentrations of p-nitrophenol. The ALP activity measured from each samples was related to the cell number in order to calculate the specific ALP activity.

The cell number was calculated by Picogreen® dsDNA Quantitation reagent (Molecular probes). The cell suspension of (50 µl) prepared above was mixed with picogreen in Tris-EDTA buffer (190 µl) for 5 min and the intensity of fluorescence was measured with a multifunction microplate reader (Infinite F200, Tecan) at an excitation and emission wavelength of 485/535 nm. Relative fluorescence units were correlated with cell number using a calibration line constructed with increasing concentration of cells.

Preparation of Osteogenic Medium

ALP activity were evaluated in normal medium and osteogenic medium for determining the effect of both the mediums on the alkaline phosphatase activity and

the expression of genes towards the osteogenic differentiation of cells in the presence of the newly developed materials.

Osteoblast differentiation was induced by culturing the cells in osteoblast differentiation medium which contains normal growth media along with10 nM dexamethasone (Sigma, Germany), 0.2 mM l-ascorbic acid (Sigma, Germany), 10 mM b-glycerophosphate (Merck), and 10 mM 1,25-dihydroxyvitamin D3 (Sigma, Germany). Differentiation medium was made fresh and replaced every 2–3 days.

Statistics

Three separate materials were used for every quantitative experiments in each group. Each parameter was expressed as mean of all values ± standard deviations. T- test was used to find out the statistical significance of the data. P-values less than 0.01 were considered significant.

Implantation studies (*in vivo*)

The resorption potential of the developed material was assessed by implanting the material as a dental extraction socket filler in rabbit model. For this the first premolar tooth of the animal was removed under anaesthesia (Procedure detailed in section **(3.7.1)**). The extraction socket was then filled with the newly developed material. Both TCP-derived apatite and carbonate-derived apatite were used as test materials along with HA granules as control. The rabbit premolar tooth has a cylindrical shape with an approximate dimension of (2.5 mm × 10 mm) diameter and length. It takes a small curvature at the root in animals above 3kg of weight and age above 3 months. In our study we have chosen animals in the age group below three months with an

average body weight between (2 and 2.7 kg) and strictly male rabbits alone to avoid any issues related to poor bone strength as seen with female animals due to hormonal imbalances and poor bone health attributed to osteoporosis.

Period of Study	Group I (THA)	Group II (CHA)	Group III (Control-HA Granule)
3 months	6 animals	6 animals	3 animals

Table 3. Experimental animal groups for dental extraction socket implantation in rabbit models

The resorption behaviour of the newly developed materials were studied for a period of 3 months to get a better understanding of the remodelling efficacy of the newly developed material. The implantable materials were fabricated according to the size and shape of the rabbit tooth which was cylindrical in shape with an approximate dimension of 2.5 mm diameter and 10 mm length. The test materials were both tricalcium phosphate-derived apatite (THA) and calcium carbonate-derived apatite (CHA) and control used was hydroxyapatite granules. The filler materials were shaped in the form of cylinders with 2.5 mm diameter and 10 mm length suitable for the socket filling. In the case of HA granules, around 0.6 g of 1 mm sized granules were effectively used to fill in the sockets.

Animal Surgical Procedure

The animals were pre-medicated with intramuscular injection of xylazine hydrochloride at 5 mg per kg body weight and ketamine hydrochloride at 50 mg per kg body weight. The animals were incubated immediately with 3mm uncuffed endotracheal tube and ventilated at 35 mm tidal volume at a rate of 30 breaths per

minute. 5 ml/kg of ringer lactate solution was administered intravenously to maintain the fluid balance in the body. Oral commissurotomy was performed on the left oral commissure to access the left mandible and the first premolar tooth of the animal. The tooth was extracted using extraction forceps ensuring the complete removal of the tooth with no damage to the alveolar bone at the time of extraction. Now the alveolar cavity was filled with the implant material, which was further shaped at the time of implantation using hand drill if needed as per the requirement. 6-7 mm portion (length wise) was inserted inside the cavity. The site was then washed with sterile PBS and the gingiva was apposed over the implant using 5/0 proline and the oral commissurotomy was closed with 3/0 silk suture. The wound was then left to heal under antibiotic and anti-inflammatory medications such as meloxicam (0.3 mg/kg) and ampiclox (10 mg/kg) dosage for 5 days and the animal was maintained under postoperative care.

The animals were sacrificed through the injection of high doses of thiopentone and 15% potassium chloride intravenously.

The left mandible with the implant site was collected in neutral buffered formalin. Radiographic and histomorphometric analysis was carried out to evaluate the healing and resorption rate of the implant materials *in vivo*. X-ray was recorded at two stages (i) post implantation (to ensure the proper filling of the graft) and (ii) after autopsy at the time of tissue collection. The collected specimens were processed for histological evaluation as per the procedure detailed below.

Procedures- Poly Methyl methacrylate (PMMA) Embedding of Tissue Sections

The bone samples were fixed in formaldehyde 10% and dehydrated in increasing ethanol concentrations (70-100%) and embedded using PMMA. After polymerisation in PMMA, thick sections (70-100 µm) were cut from the PMMA block using a linear precision saw microtome (ACCUTOME 100, Struers, Denmark). These sections were stuck to a glass slide, ground and surface was polished using a variable speed grinder polisher (ECOMET 3000, Buehler, Germany). These sections were stained with hot Stevenel's blue and Van Gieson's picrofuchsin. Stained sections were evaluated in a trinocular transmitted light microscope (Nikon E600) and photomicrographs were captured using the camera (Nikon DSRi1) attached to the microscope. From the obtained images the amount of material remaining and the amount of new bone formation is calculated.

Application of the developed material as a drug eluting ceramic material

Drug elusion studies from the developed materials were performed using CHA spherical beads of 3 mm diameter and 40% porosity with pore size from 20 to 500 microns. Drug eluting beads are effectively used to carry antibiotics and drugs to the site of infectious bone diseases such as osteomyelitis. Here the drug release was studied using a UV- Visible spectroscopic method as detailed below.

Determination of unknown concentration by UV- spectrophotometer *Procedure*:

The CHA beads prepared having weights around 0.35 g was used for the study. Drug release measurements were performed by soaking the drug loaded samples in a solution of 5 ml phosphate buffer (0.01 M, pH = 7.4) maintained at

37 °C. 5ml of the aliquots of the sample were periodically collected up to 53 days for analysis. 5ml of freshly prepared phosphate buffer were added after each sampling for further elution. The amount of gentamicin drug released was determined by a spectrophotometric method. Ultraviolet-visible spectrometer (Cary 100 Bio, Varian Inc., USA) was used to estimate the amount of drug released from the drug loaded samples.

Preparation of o- phthalaldehyde reagent: The o-phthalaldehyde reagent for the estimation of the drug was prepared to a volume of 125 ml. 0.5 g of o-phthalaldehyde ($C_8H_6O_2$, S D Fine-Chem Limited, India) was dissolved in 12.5 ml methanol (Merck Limited, India) and transferred to a brown bottle. Further 0.6 ml of 2-mercaptoethanol (Spectrochem; India) was added to this followed by the addition of 112 ml of 0.04 M disodium tetraborate solution ($Na_2B_4O_7$. 10 H $_2$O; SD Fine-Chem Limited, India). The prepared reagent is stored in dark for 24 h before use.

Preparation of solutions for colorimetric estimation: The solutions for colorimetric estimation were prepared by adding o-phthalaldehyde reagent and isopropyl alcohol in (1:4) ratio to the gentamicin solution. A standard was plotted with known concentrations of gentamicin drug and the unknown concentration was estimated with respect to the known standard values by measuring the absorbance at 333 nm using an ultraviolet-visible spectrometer.

A spectrophotometer makes use of continuously variable and monochromatic bands of light. The essential parts of spectrophotometer are a source of radiant energy, a monochromator which isolates monochromatic light with accuracy from the light source, glass or quartz cells for the solvent and solution under test, and a device to

receive or measure the beam of radiant energy passing through the solution. A standard was plotted with known concentrations of gentamicin to estimate the unknowns by measuring the absorbance log (Io/It), against the concentration. A straight line plot is obtained if Lambert Beer's law is obeyed (Mendham J, 2002).

CHAPTER - 4

HYDROTHERMAL EXCHANGE REACTIONS AND PROCESS OPTIMIZATION - PRELIMINARY STUDIES

Introduction

This chapter deals with the optimization process of reaction parameters for hydrothermal exchange reactions to obtain maximum conversion to apatite phase. The initial study was based on various precursor materials derived from both natural and synthetic sources. The naturally derived materials were heat treated to remove the organic components and the resultant powders were used as starting materials. The powders were also used to fabricate precursor bodies using poly vinyl alcohol binders and naphthalene porogen. X-ray diffraction techniques ensured phase purity of the materials before and after the reactions. It also helped to check the conversion rate to hydroxyapatite phase after the exchange process. The material so obtained was found to have inadequate strength which lead to crumbling of the preforms after the reactions and also upon the removal of binders. Hence, development of stable preform which could withstand the processing conditions associated with the hydrothermal reactions had to be sought. In light of the findings of these conversions a model system based on lower calcium phosphates were developed. The lower calcium phosphate studied was dicalcium phosphate which was fabricated in the form of small beads of 2-3 mm diameter. The details on these studies are presented below.

Conversion of Natural Material

Corbicula shells from the fresh waters were taken as the materials of natural origin and processed as detailed in section 3.1.1. The shells are composed of calcium carbonate in the naturally occurring aragonite form which was confirmed by the X-ray diffraction pattern as shown in Figure 4.1. The pattern before the conversion reaction is in congruent with the standard aragonite pattern, PDF-00-003-0405. Figure 4.2 depicts the XRD pattern of the product after the conversion reaction which is analogues to the hydroxyapatite (HA) crystal structure (PDF No. 00-009-0432) without the presence of other calcium phosphates. This complete conversion to apatite phase was observed in 24 h time. The process was optimised after various trial and error methods by changing the reaction time from 5, 8, 12, 24 h etc. It was found that 10 g of aragonite powder was completely converted to hydroxyapatite phase in 24 h of reaction in 1 M ammonium dihydrogen phosphate (AP) solution at 150 °C and 5-6 bar pressure.

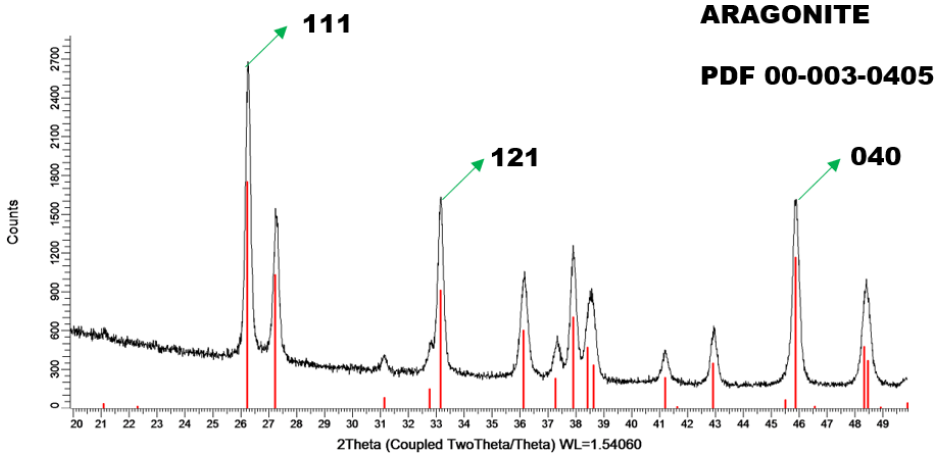

Figure 4.1. XRD pattern showing the aragonite phase of the corbicula shells.

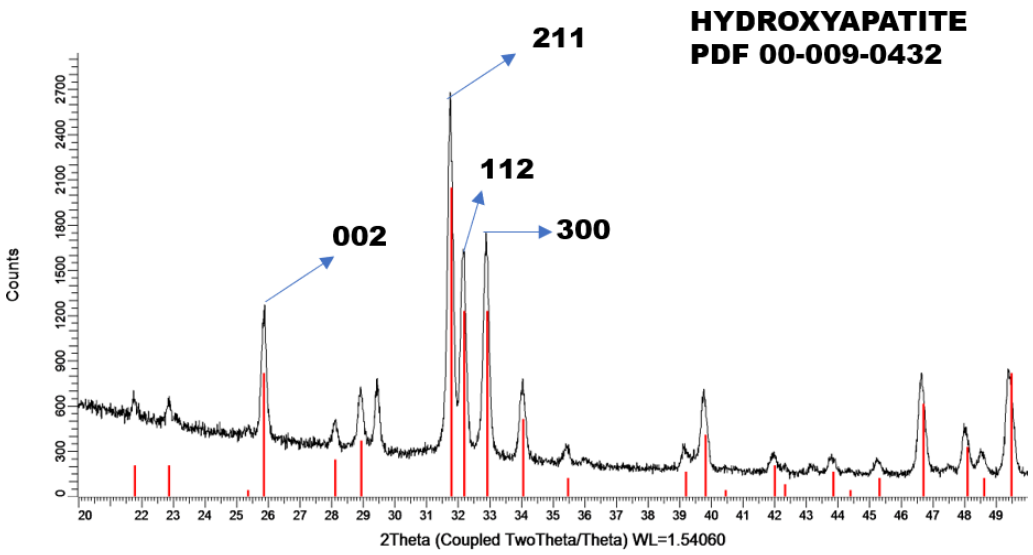

Figure 4.2. XRD pattern of hydroxyapatite formed from shells after 24 hours of reaction in AP solution.

Conversion of Synthetic Materials- Calcium Salt based materials

Conversion of Synthetic Calcium Oxide powder

To have a basic understanding of conversion process, the exchange reactions were performed using commercially available calcium oxide powders as starting materials. The pristine calcium oxide powder was having portlandite phase as confirmed by the XRD pattern indexed with the PDF No. 01-070-5492, shown in Figure 4.3. It was observed that the conversion efficiency of calcium oxide powders of portlandite phase was low. Even after 12 h under hydrothermal conditions, the portlandite phase was only partially converted to hydroxyapatite as evidenced by the XRD pattern in Figure 4.4 compared with the standard XRD pattern of hydroxyapatite (PDF No. 00-009-0432) and that of portlandite (PDF No. 01-070-5492).

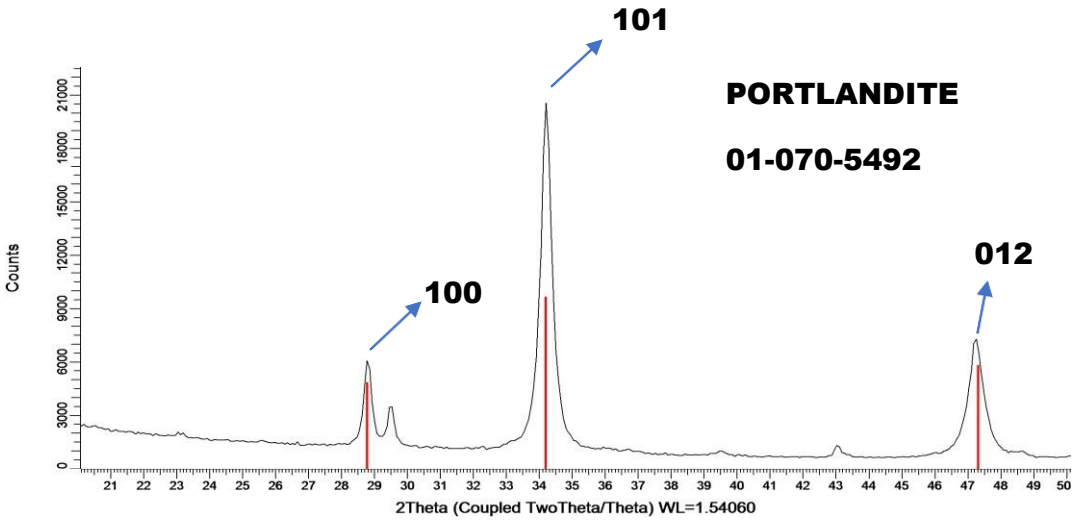

Figure 4.3. XRD pattern indexed with standard pattern of portlandite phase confirming the presence of portlandite phase of calcium oxide.

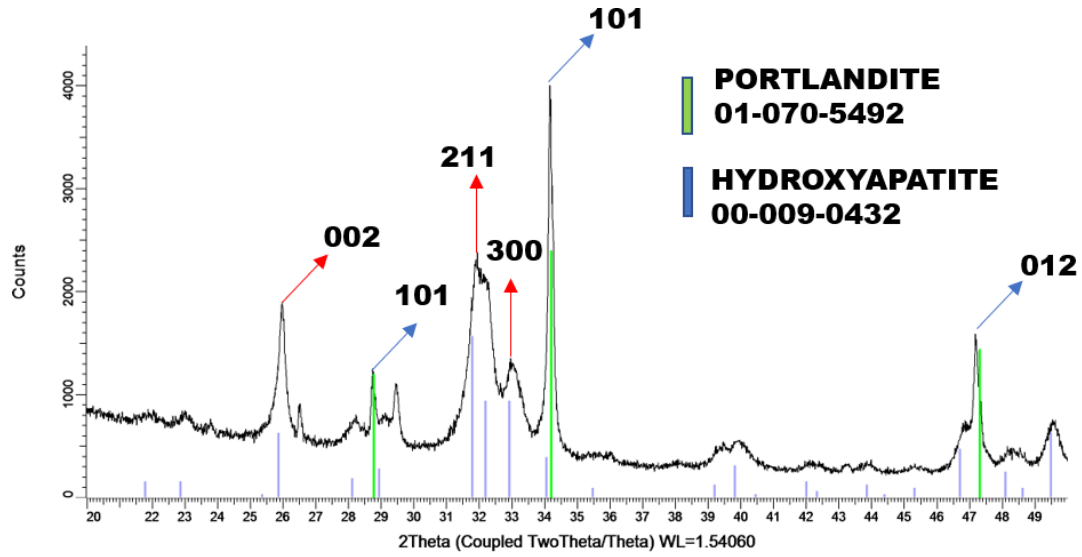

Figure 4.4. XRD pattern showing the partial transformation of portlandite phase to hydroxyapatite phase after 12 h of reaction.

During the initial 12 h period, the formation of hydroxyapatite phase was envisaged from the X-Ray Diffraction analysis showing intense peaks at 2θ values 31.7°, 32.2°, 32.9°, 25.8°, 46.7° and 49.49° which are the characteristic peaks of apatite's. Apatite

peaks are indexed with blue coloured standard pattern in the Figure 4.4. The peaks at 2θ values 28.7°, 34.4° and 47.3° shows portlandite phase as indexed with green coloured standard pattern. The reaction was continued for the next 24 h anticipating maximum conversions to apatite phase which was confirmed by the XRD pattern as depicted in Figure 4.5. From the XRD it is clear that it takes almost 24 h for the complete conversion of this phase.

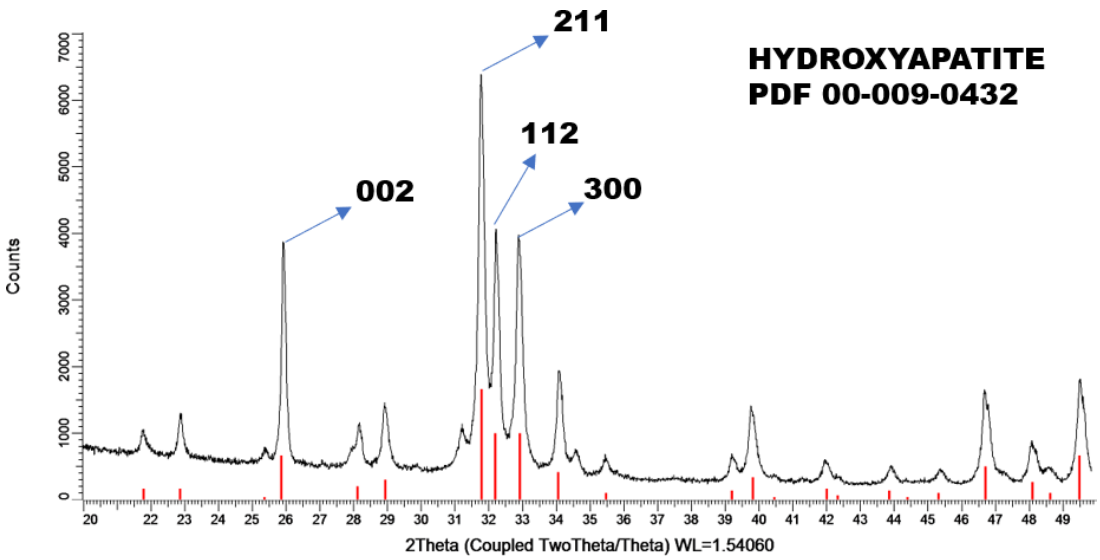

Figure 4.5. XRD pattern of hydroxyapatite formed after 24 h of reaction of portlandite phase of CaO.

Conversion of Calcium oxide-PVA based preforms

Pre-defined structures were formulated in addition to calcium oxide powders. It is worth investigating the efficiency of conversion process within the bulk of materials. Hence, various preforms were fabricated and subjected to hydrothermal reactions. The calcium oxide powders were mixed with poly vinyl alcohol as a binder in 2:1 ratio and moulded to form spheres of 10 mm diameter and discs of 13

mm diameter and 5 mm thickness. Fig 4.6 shows the optical images of the calcium oxide and PVA based preforms fabricated.

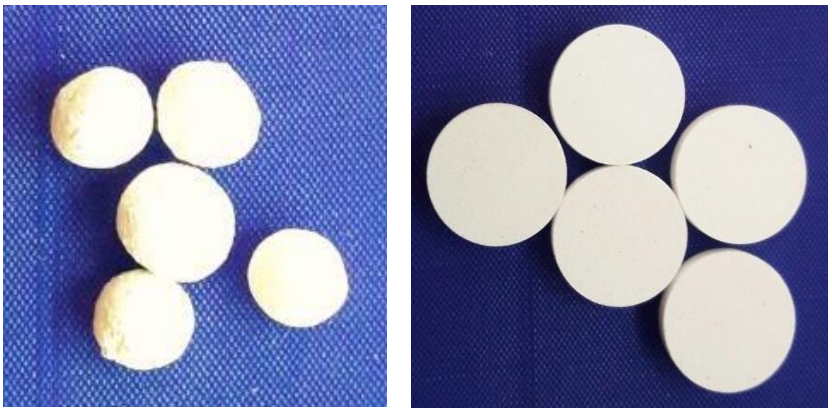

Figure 4.6. Optical images of CaO-PVA spheres and pellets

These preforms were then hydrothermally treated using 1 M ammonium dihydrogen phosphate (AP) solution. Initial studies were conducted for lower time period starting from 1 h, 3 h, 10 h, 12 h and the phase changes were evaluated based on X-ray diffraction patterns from both the interior and exterior surfaces separately in order to understand the progress of conversion. It was observed that after 12 h of reaction at 150 °C and 5-6 bars of pressure, the phase obtained was monetite as identified from the XRD pattern shown in Figure 4.7. Additional peaks of PVA were also observed along with monetite. The binder was removed by heating in an open hearth furnace at 600 °C. It was again subjected to hydrothermal process at the same reaction conditions of temperature, pressure and pH for 6 h. Finally, the monetite phase was completely converted to hydroxyapatite phase which was confirmed using X-ray diffraction pattern in Figure 4.8.

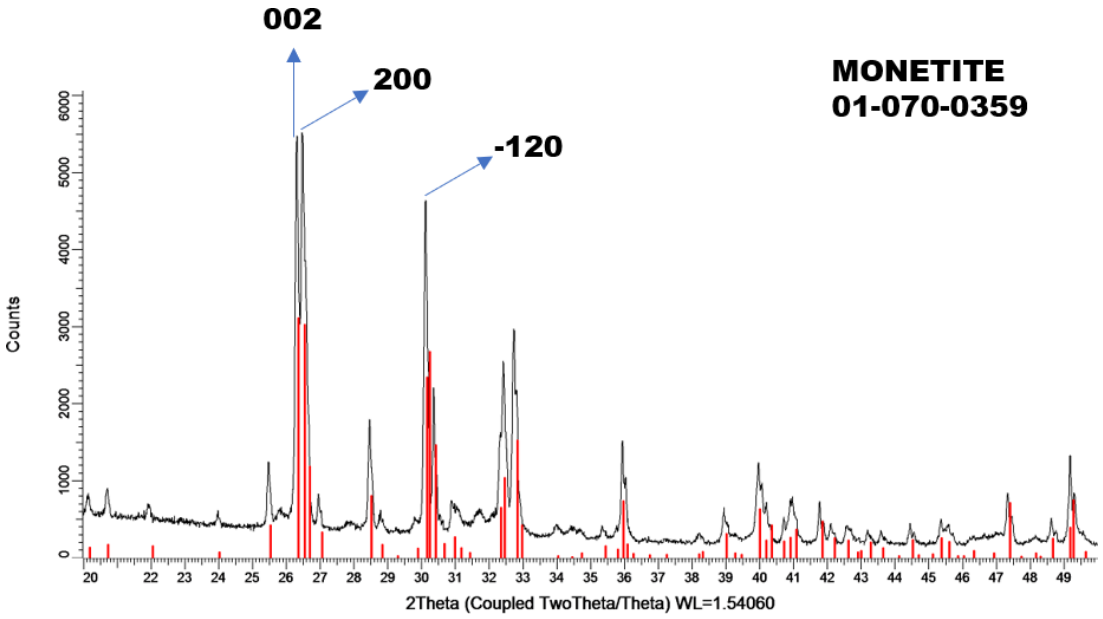

Figure 4.7. XRD pattern showing the conversion of portlandite phase to monetite phase in 12 h. The pattern is compared with standard PDF No. 01-070-0359 of monetite phase.

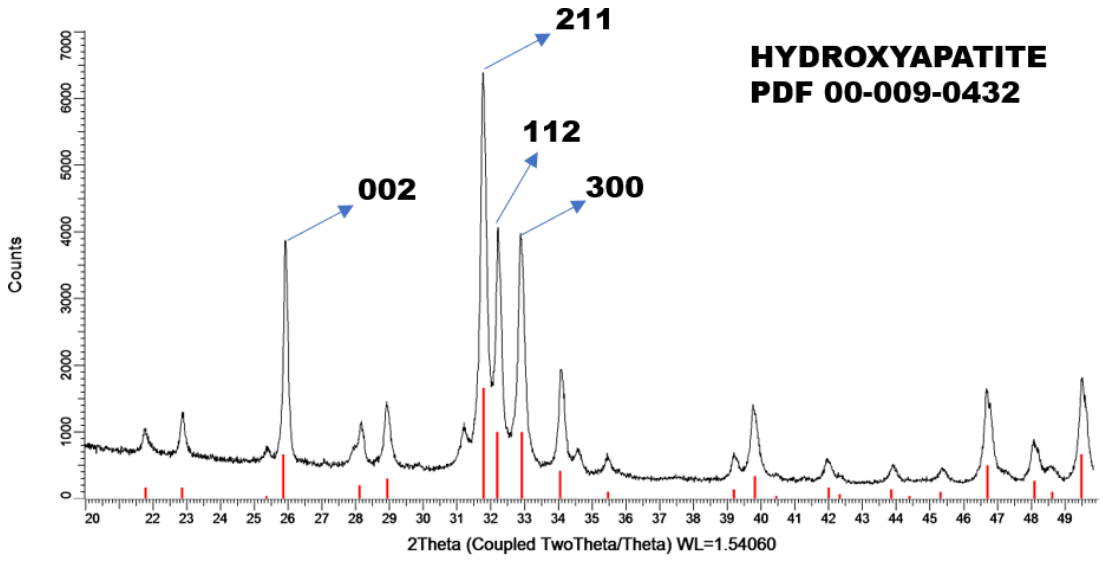

Figure 4.8. XRD pattern confirms the conversion of monetite phase to hydroxyapatite phase in 6h by indexing with the standard PDF No. 00-009-0432 of hydroxyapatite.

The FTIR spectra of the calcium oxide materials were recorded before and after the conversion reactions to detect the presence of functional groups (Figure 4.9 and 4.10). FTIR spectra of the fabricated precursor show (Figure 4.9) peaks characteristic of CaO and PVA. Peaks in the range 3100-3500cm^{-1} are due to –OH stretching (both free –OH and hydrogen bonded –OH) from PVA, 2875-2900 cm^{-1} correspond to the –CH stretching also from PVA. The peak at 710-715 cm^{-1} is indicative of Ca-O bond. Peaks at ~1417 cm^{-1} and ~866 cm^{-1} were ascribed to C-O bond. After the reaction too there is the presence of PVA but there is an increase in the phosphate content as identified by the peaks centred around 1080 cm^{-1} and 630 cm^{-1}, and a decrease in the carbonate content attributed to the transformation to the apatite phase.

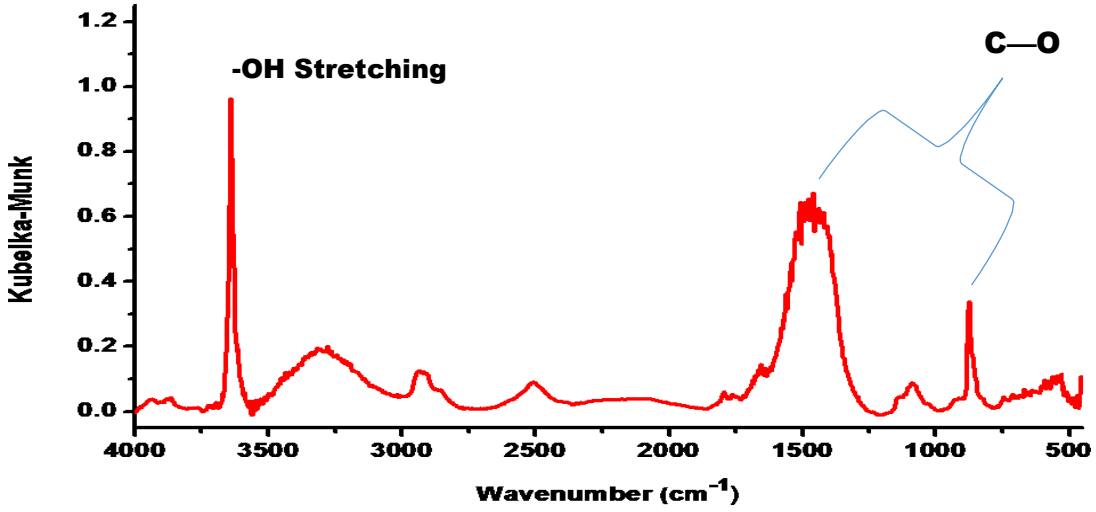

Figure 4.9. FTIR Spectra of Calcium oxide sample before hydrothermal exchange reactions.

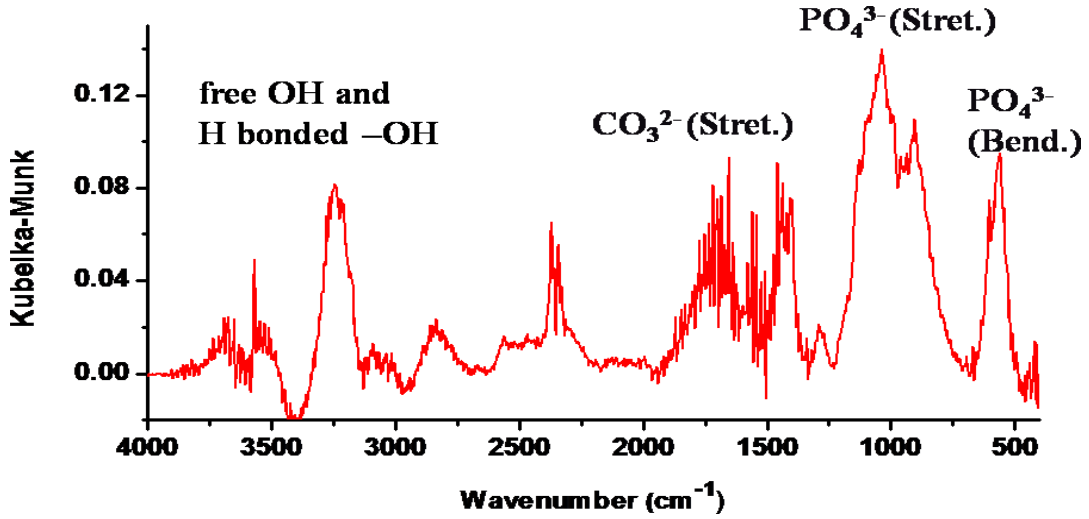

Figure 4.10. FTIR Spectra of Calcium oxide sample after 18 h under hydrothermal exchange reactions.

The morphology of the materials was observed by scanning electron microscopy. It was seen that the calcium oxide material showed non-uniform amorphous morphology before the conversion reactions, which eventually transformed to structures consisting of clusters of crystals post hydrothermal treatment. Typically, the crystals formed appeared to have two different morphologies; one showing long feathery flake-like morphology of apatite randomly distributed over the surface and another appeared as stacked plates. ESEM images of the material before hydrothermal treatment are shown in Figure 4.11 and that of the transformed material reflecting the crystal growth patterns in Figure 4.12.

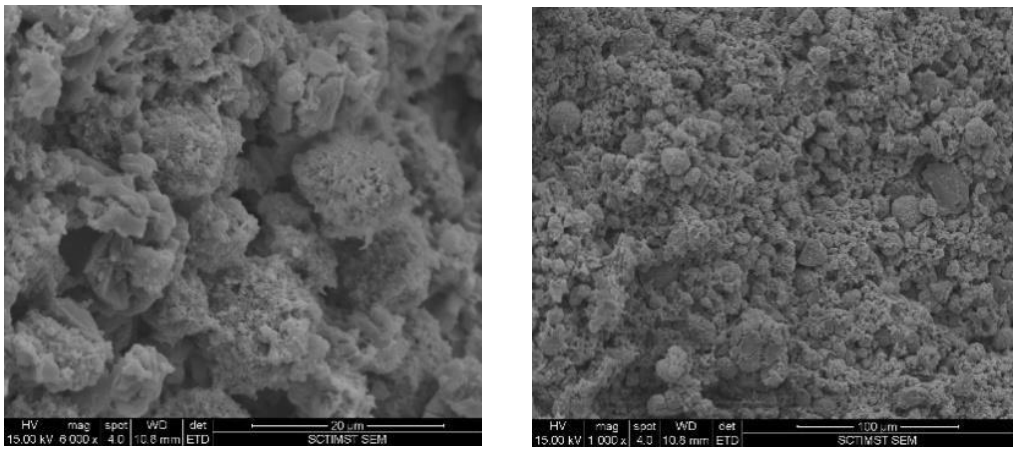

Figure 4.11. ESEM image of the calcium oxide precursor material

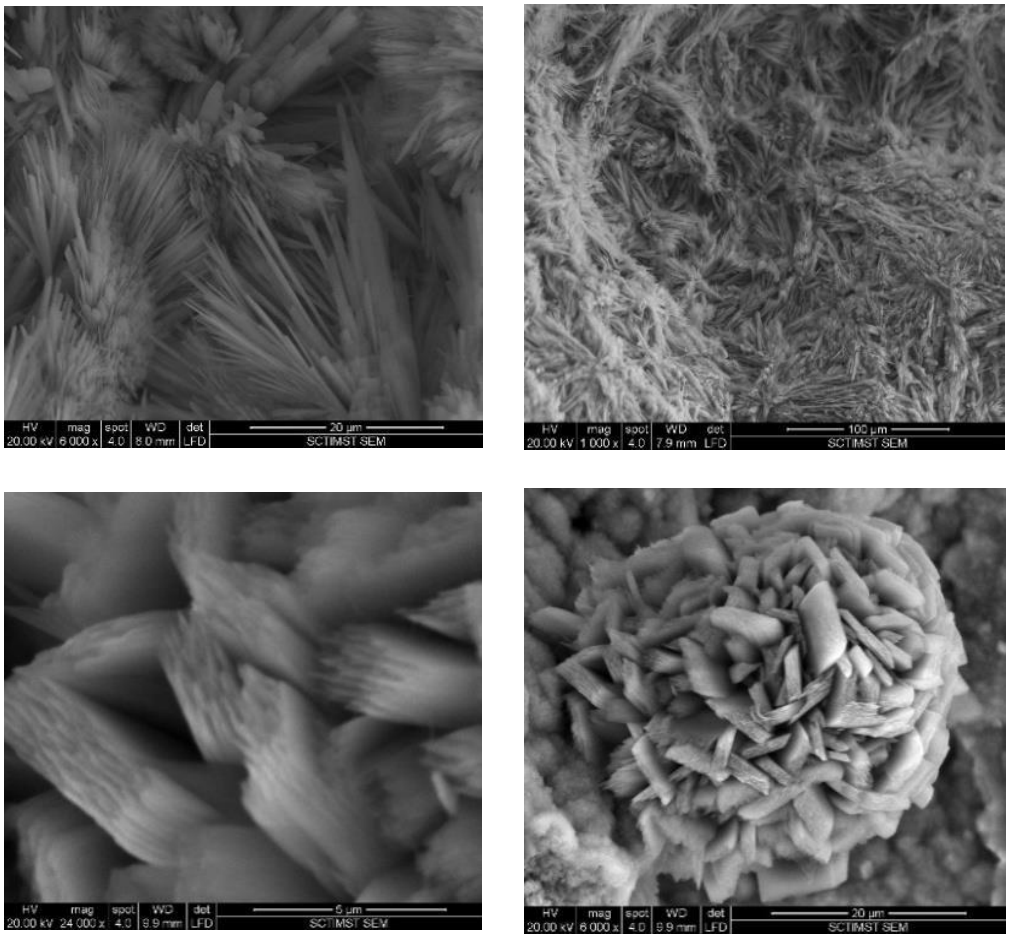

Figure 4.12. ESEM images of different hydroxyapatite crystal morphologies derived from calcium oxide precursors 18 h post hydrothermal treatment.

From the analysis of the materials prepared, it is evident that the hydrothermal process is effective in transforming oxides of calcium to calcium phosphate, ie. apatite phase. However, the converted material lost its strength as a result of the dissolution of PVA and also while heat treatment is applied at 300 °C after the reaction, to burn out the porogen. Hence, this method of preparation of CaO precursor in the bulk form requires additional consideration.

Conversion of Dicalcium phosphate based preforms

Dicalcium phosphate (DCP) powders were used as starting materials for the preparation of DCP beads. The powders were prepared by the precipitation routes and were analysed for the phase purity using X-ray diffraction techniques. These powders were then mixed with the binders and drop casted onto hydrophobic bed to form the beads. These beads are shown in Figure 4.13. The XRD pattern of the synthesized beads are shown in Figure 4.14. X-ray diffraction analysis shows that the conversion of DCP precursor originally in the monetite phase to hydroxyapatite is via an intermediate pyrophosphate upon heating at 900 °C. The thermal treatment is given to improve the precursor stability. The stabilised beads were then hydrothermally converted to hydroxyapatite phase in calcium hydroxide solution of 1 M concentration having a pH of 12, and a duration of 12 h.

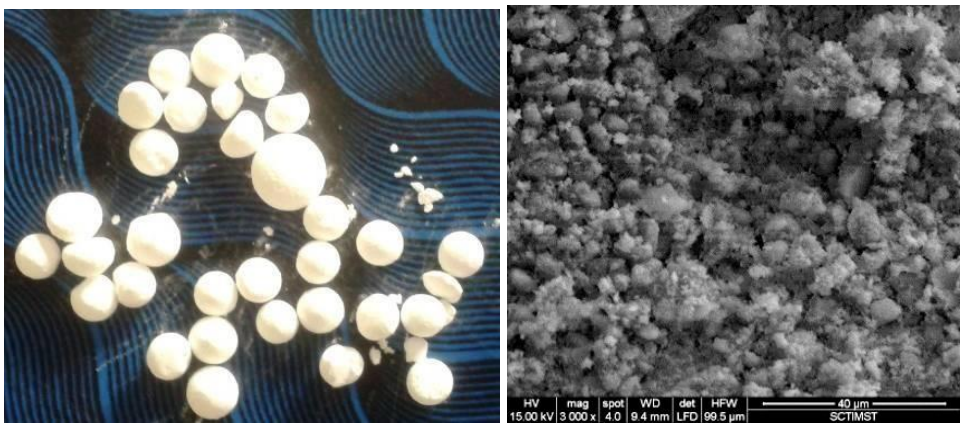

Figure 4.13. Photograph of the DCP beads prepared (left) and ESEM image of precursor bead showing the morphology (right).

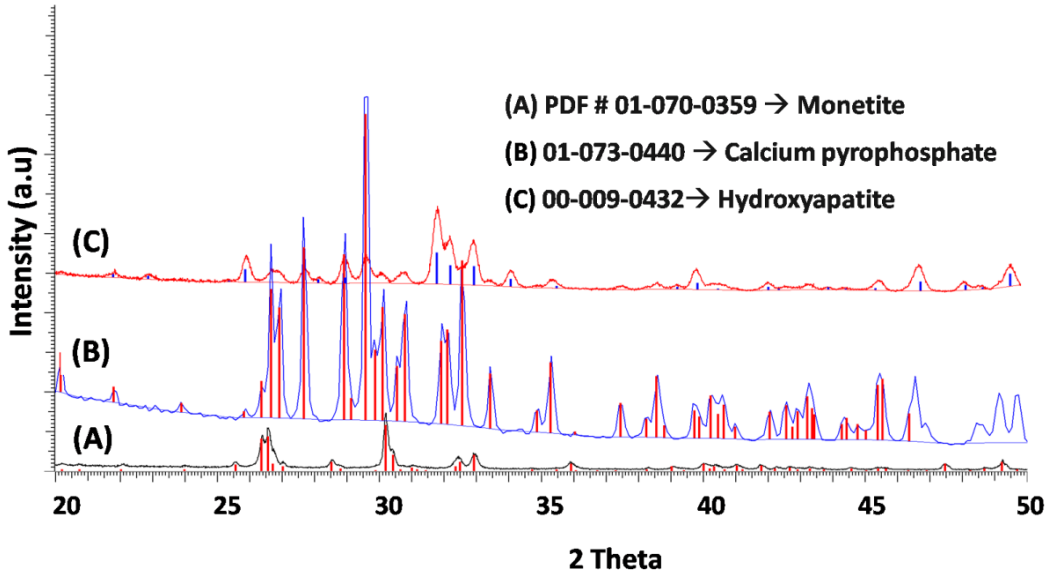

Figure 4.14. XRD pattern depicting the transformation of monetite phase (A) to pyrocalcium phosphate (B) which finally transformed to hydroxyapatite phase (C) in 12 h.

FTIR spectral information shown in Figure 4.15 also supports the transformation of DCP to hydroxyapatite under hydrothermal conditions. The phosphate group peaks are refined and –OH group is well identified at ~3500 cm^{-1} as a result of the formation of crystalline hydroxyapatite.

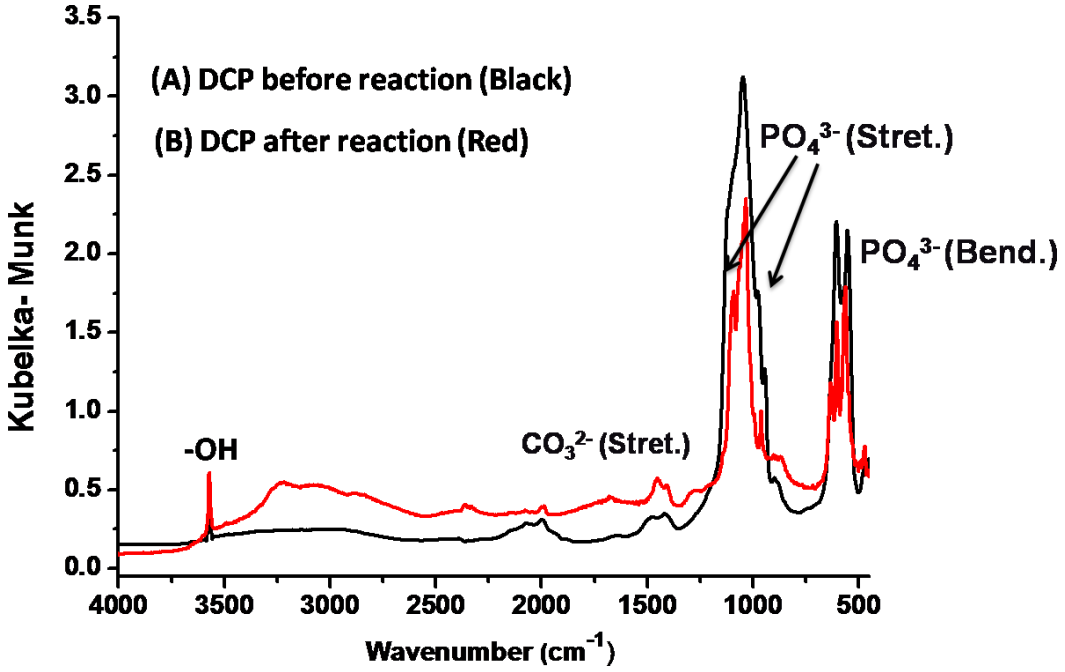

Figure 4.15. FTIR spectra of DCP beads before (A) and after hydrothermal treatment (B) in calcium hydroxide solution.

It was observed that the structural features of the precursor DCP forms were drastically changed from a shallow globular pattern to a tubular / semi tubular morphology as shown in Figure 4.16. These crystals were formed from the basic structural features present in the materials. These crystalline morphology was thought to be a reason for the increased crystallinity observed after the hydrothermal conversion reactions.

Although the required conversion of DCP to HA phase was achieved in this process, the developed materials showed poor strength and handleability after the hydrothermal reactions and hence further studies were limited in this form. Dicalcium phosphate materials are still under study incorporating several modifications to improve precursor stability for further studies.

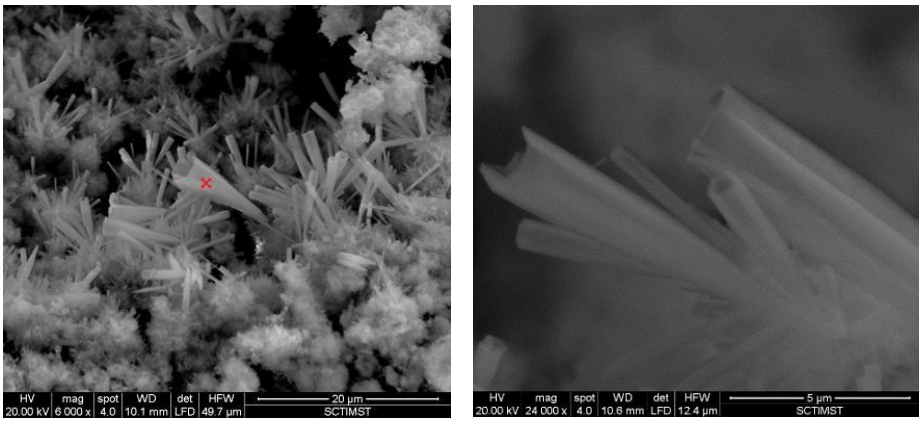

Figure 4.16. ESEM image of DCP bead after 12 h of hydrothermal treatment in calcium hydroxide solution.

Conversion of Bioactive glass systems

Bioactive glass (BG) materials were prepared as a synthetic precursor for hydrothermal reactions. The aim was to obtain a crystalline bioactive glass system which is a new concept in bioceramic material preparation. The BG precursor systems were fabricated from the powders of BG prepared through sol-gel method. The powders were then consolidated to form discs of 13 mm diameter and 5 mm thickness. BG systems were sintered to 1230 °C to obtain a stable precursor for the exchange reactions. The hydrothermal reactions were conducted in basic ammonium phosphate solution of 1 M concentration and pH 10 for various time period to obtain transformations of the material to a more crystalline matrix. The XRD patterns presented in Figure 4.17 reflects the transformation of the glass-ceramic matrix to a more crystalline apatite phase. The amorphous glass-crystalline ceramic nature of bioactive glass composition is evident from the X-ray diffraction analysis. The patterns show that the overall composition is composed of phosphates and silicates of

calcium in the form of wollastonite (PDF No. 00-002-689), whitlockite (PDF No. 01-076-8364) and hydroxyapatite (PDF No. 00-009-0432) as major phases. The major peaks of wollastonite were observed at 2θ values of 23°, 25.3°, 26.9°, 30.06° and 39.6°. The whitlockite peaks appear at 2θ values of 17°, 28.8°, 31.2° and 34.6°. The presence of HA phase is identified by the presence of peaks at 2 θ values 25.8°, 31.7°, 32.1°, 32.9°, and 49.4°. After the hydrothermal reactions, over time, it was observed that all the phases initially present in the system was retained. However, there is a gradual increase in the crystallinity of the material and especially the apatite phase during the progress of reaction when compared to the wollastonite and whitlockite phases. This indicates that there is an increase in the crystallinity of apatite phase and hence by transforming to a new crystal morphology which is further observed through SEM.

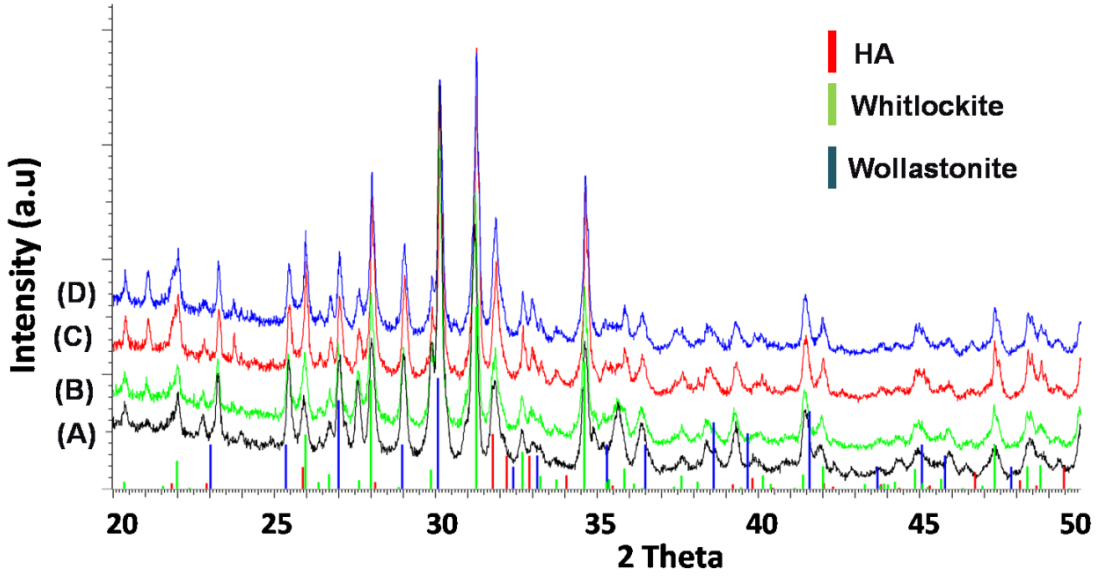

Figure 4.17. XRD pattern - (A) Bioactive glass scaffold before hydrothermal treatment (B) Bioactive glass scaffold after 1 h hydrothermal treatment in AP solution (C) after 4 h and (D) after 8 h.

The functional group analysis was performed by FTIR technique. FTIR spectra of the material before and after the conversion in Figure 4.18 represents the bioactive glass scaffold at different time periods in ammonium phosphate solution. The major vibrations are due to silicate, phosphate and hydroxyl groups. The IR active groups are Si-O, CO_3^{2-}, $-PO_4^{3-}$ groups, and –OH present as free –OH and H-bonded –OH. It is seen that the phosphate and hydroxyl peaks increase substantially with increase of reaction time which indicates an increase in the hydroxyapatite content with increased crystallinity.

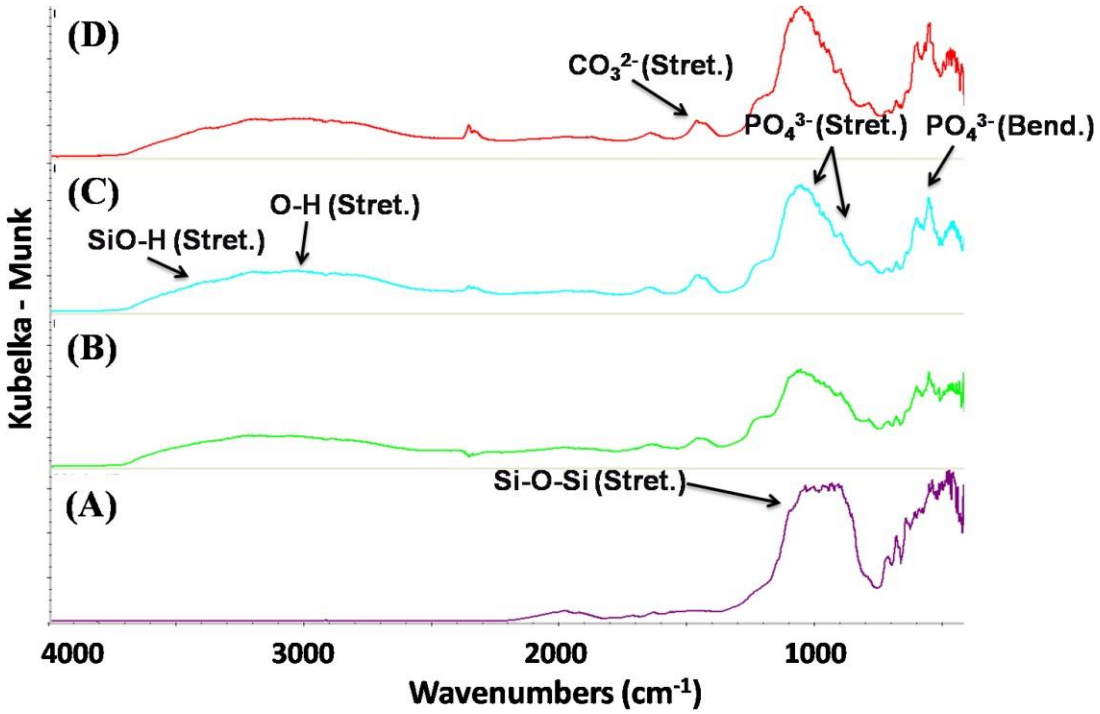

Figure 4.18. FTIR spectra - (A) BG before hydrothermal reaction (B) BG after 1 h (C) BG after 4h, BG after 8h of hydrothermal reaction in 1M ammonium phosphate solution.

The transformation of the surface morphological features of the BG material before and after conversion reactions was evidenced from the ESEM images in

Figure 4.19. The initial morphology of the bioactive glass system consists of particles in a slightly coalesced manner without showing a peculiar structural difference, pattern or orientation. After hydrothermal process, the structural features are entirely different as observed in Figure 4.19 C, D.

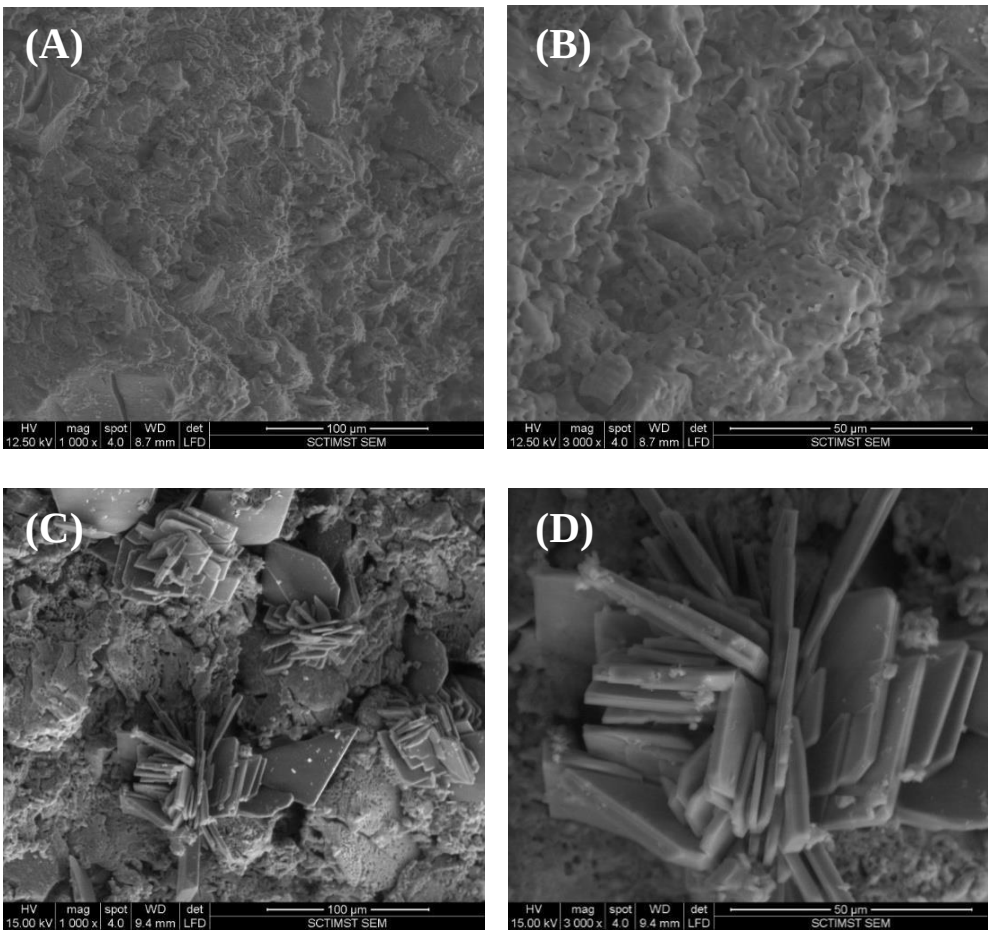

Figure 4.19. ESEM representing bioactive glass materials before (A) and (B) and after the conversion (C) and (D).

The hydrothermally treated sample shows plate-like crystals are grown out from the basic morphology observed in the precursor. This indicates that the apatite phase already present is now transformed to a very distinct crystalline morphology in a matrix of other phases such as the wollastonite and whitlockite.

These converted materials are expected to be of much interest in near future as it contains both the crystalline HA phase and the amorphous phosphate phases in a single matrix. The amorphous phosphor-silicates in this bioactive system can contribute to the early regeneration and healing process, while the oriented HA crystals can contribute to long term integrity of the materials.

Conversion of Synthetic Materials - Calcium carbonate preforms Commercially available calcite powders were converted to apatite by hydrothermal exchange reactions in basic ammonium dihydrogen phosphate solution of 1 M concentration which is used to supplement phosphate ions to the material. It was seen that after 12 h of reaction 5 g of calcite powders were completely converted to hydroxyapatite phase. The XRD pattern shown in Figure 4.20 depicts the conversion of calcite powders to hydroxyapatite phase in 12 h.

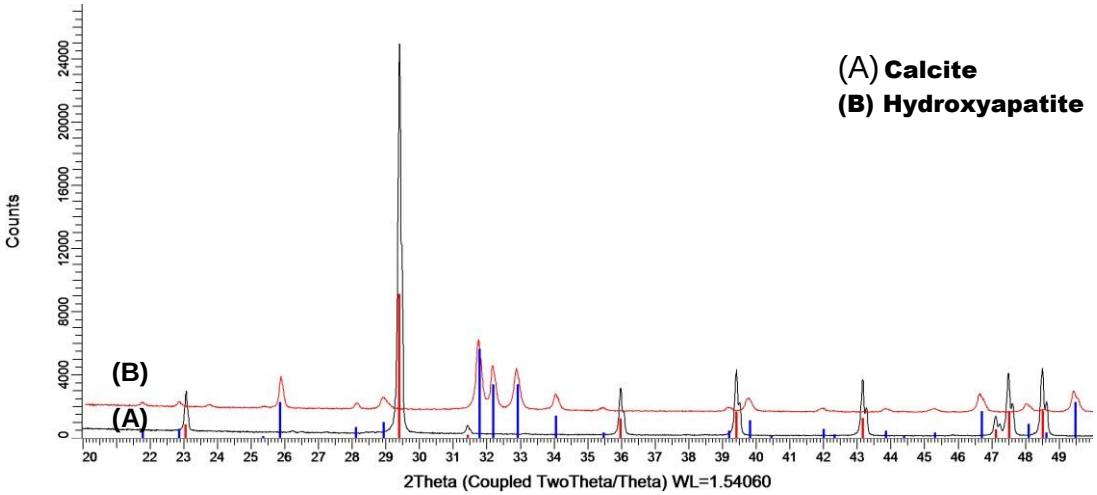

Figure 4.20. XRD pattern of (A) pristine calcite and the converted product (B) showing the transformation to apatite phase in 12 h.

The preforms fabricated with calcium carbonate and PVA failed with the removal of binders. Hence the process was further modified to develop porous

precursors without PVA binder. The improvisation of the material lead to the development of stable calcite preforms using an inorganic binder source. The preparation and processing of this material is detailed in chapter 5.

Summary

Hydrothermal reactions were carried out using natural and synthetic materials to identify precursor stability, reaction parameters, conversion efficiency and suitability to obtain maximum conversions within the limitations of the process. Materials were initially used in the powder form and then scaffolds/preforms prepared out of the powder were subjected to hydrothermal process. It was found that the conversion process was optimal in suitable reagents, such as ammonium phosphate and calcium hydroxide solutions. The choice of reaction medium depends on the ions to be exchanged with the precursor, for an effective phase conversion. However, the conversion of pre-fabricated body originally in one phase to another phase while retaining the structural integrity may not be always effective as that of the powder counterparts. Hence, preparation of large scaffolds and its effective conversion is a challenging task. Various trials were attempted to fabricate precursor ceramics with the aid of binders such as PVA. Even though the conversion process is effective, the structural integrity was not retained after the removal of the binder and do not have the required handleability. In the case of precursors of dicalcium phosphate, a heat treatment method was adopted for preform stabilisation. This lead to the development of pyro calcium phosphate which eventually transformed to crystalline apatite after conversion process, but the fate was same with regard to the structural integrity. In case of bioactive glass composition, the structural integrity was

maintained after the reaction, and the product after conversion was composed of hydroxyapatite crystals along with the presence of the glass phases of wollastonite and whitlockite. Since this process requires high temperature for the initial precursor formation and retains the amorphous phases in the final product also, it was found to nullify the advantages offered by the hydrothermal process. Hence, it is noteworthy to modify these conversion processes and to investigate alternate precursor fabrication-conversion methods as discussed in chapter 5 and chapter 6.

CHAPTER - 5

PREPARATION OF HYDROXYAPATITE FROM CALCITE PREFORMS VIA HYDROTHERMAL EXCHANGE REACTIONS

Calcium carbonate derived hydroxyapatite- CHA

Introduction

Surfactant free hydrothermal method was employed for the preparation of large blocks of hydroxyapatite scaffolds. Calcite, the most abundant polymorph of calcium carbonate was used as the starting material for the preparation of precursor bodies. Calcite was mixed with an inorganic setting solution containing phosphoric acid and sodium hydroxide to form the porous precursor body with pore size 20-700 microns. These preforms were then hydrothermally converted to hydroxyapatite scaffolds when treated in basic phosphate solution of pH 10.5 at 150 °C and 15 bar pressure in hydrothermal pressure vessel. The resultant product retained the structural stability and integrity after the conversion process. X-ray diffraction and Fourier transform infrared spectroscopy confirmed that the developed material consist of single phase crystalline hydroxyapatite. Surface morphology and microstructures were studied using scanning electron microscopy and porosity was evaluated by micro CT analysis. The cell material interactions evaluated by cell viability assays and live cell staining methods confirmed the cell material compatibility. The drug release study at physiological pH (7.2) implied that the developed materials could be a promising

scaffold material with long term sustained release of the incorporated drug. The results obtained shows that the hydrothermal conversion of synthetic inorganic coral like precursor is effective to produce large hydroxyapatite scaffolds for bone regeneration applications. It can also be used as drug delivery vehicles for the treatment of infectious bone diseases such as osteomyelitis.

Hydroxyapatite is accepted in various forms such as rods, blocks, beads, implant coatings, etc. for various applications over the years in the field of orthopaedics and dentistry (Acharya et al., 2010, Kawachi et al., 2010). Designing of porous materials for bone repair is critical such that it should favour cell ingrowth along with the adsorption of protein moieties, and at the same time it should provide the appropriate mechanical strength suitable to act as tissue engineering scaffolds for bone regeneration (Hannink and Arts, 2011). In order to undergo effective remodelling process the scaffold should get resorbed on par with *de novo* bone formation and get osteointegrated as healing progresses with time. Effective bone regeneration requires a porous structure since it supports osteoconduction and direct osteogenesis into the porous matrix (Kuboki et al., 1998). Porosity in ceramics is normally created by introducing organic binders, templates or by adding inorganic pore - formers like naphthalene or camphor which is later removed while heating and sintering. Sintering of ceramics leads to shrinkage, crystallisation and phase transformation making it difficult to retain the porosity and structural integrity (Denry and Kuhn, 2016). Preparation of ceramics through a non-sintered route is considered to be an effective strategy in the preparation of bioceramic scaffolds for non-load bearing applications.

Hydrothermal synthesis is one of the best alternative methods to synthesise hydroxyapatite ceramics with crystallinity, homogeneity and phase purity without the agglomeration of particles. It is also an effective method to produce unique crystal microstructures such as whiskers, plates, tubes etc. which cannot be achieved by other processing methods easily. The morphology of the crystals formed during hydrothermal exchange reactions is influenced by the reaction parameters such as pH, temperature, concentration of the reaction medium and the choice of precursor materials.

Coral in its aragonitic form is one of the widely studied natural precursor material for hydrothermal exchange reactions because of its interconnected porosity and optimal strength (Hu et al., 2000). Coralline HA as both converted and non-converted is reported as a biocompatible, osteoconductive and osteogenic bone graft ceramic of bone remodelling and bone ingrowth (Vago et al., 2002). However, considering the hazards of harvesting corals from the sea and also due to heavy metal contamination associated with this natural substance, we have devised a viable alternative from a coral like precursor material of calcite mineral. This new material developed has the desired porosity and strength which can effectively be converted to hydroxyapatite via hydrothermal exchange reactions. This biomimetic scaffold is comprised of oriented crystals along the a-axis mimicking plate-like morphology of nacre. The developed materials were characterised using X-ray diffraction (XRD), Fourier transform infrared spectroscopy (FTIR), environmental scanning electron microscopy (ESEM), and Micro CT analysis. The scaffolds were also shaped to beads for use in drug delivery applications. The precursor materials were prepared in various shapes and dimensions such as spheres, cones, cylinders, pellets, and blocks

in order to suit for various physico-chemical and biological evaluation. Proposed reactions of calcite under aqueous conditions are as follows in a solution of ammonium dihydrogen phosphate:

$$10CaCO_3 + 6NH_4H_2PO_4 + 2H_2O \rightarrow Ca_{10}(PO_4)_6(OH)_2 + 3(NH_4)_2CO_3 + 7H_2CO_3$$

Figure 5.1. Optical micrographs of the calcite preforms for various applications in the study.

Physicochemical Characterizations of the Materials

Physicochemical characterisations of the materials was carried out to ensure phase purity, crystallinity, elemental composition, and morphology.

X-Ray Diffraction Analysis

The phase analysis for the calcium carbonate powder was done by the X-ray diffraction technique before the precursor fabrication. The calcium carbonate powder used for preparing precursor body showed single phase calcite as observed by the

XRD pattern in Figure 5.2. The pattern was found to be in agreement with standard data for the rhombohedral calcite phase (ICDD PDF No. 01-071-3699).

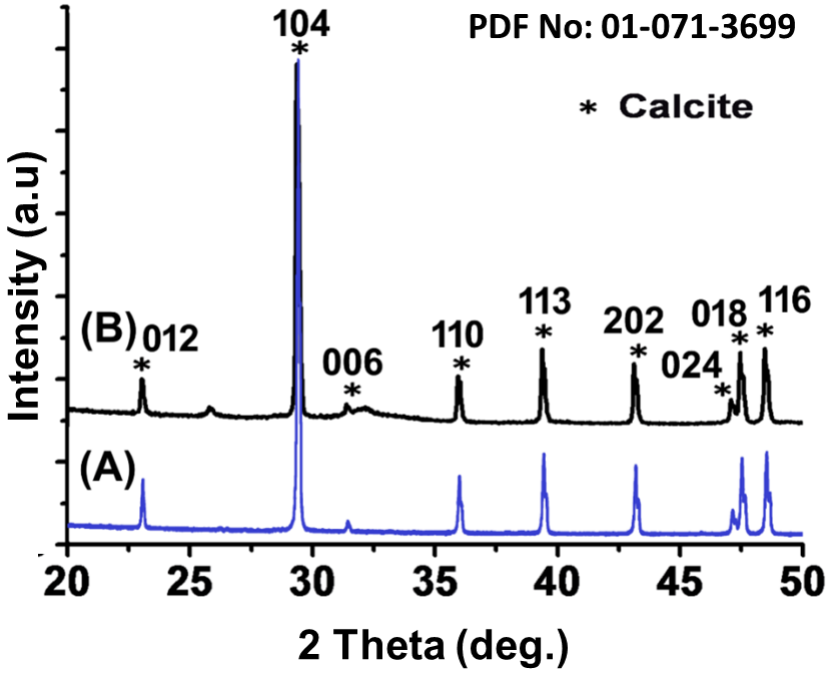

Figure 5.2. XRD pattern of (A) pristine calcite powder which shows single phase and (B) fabricated precursor which shows major calcite phase and minor hydroxyapatite phase.

Major peaks of calcite appear at 2θ- 29.3° with maximum intensity corresponding to 104 plane, other minor peaks appear at 2θ-23° (012 plane), 2θ- 35.9° (110 plane), 2θ-39.3° (113 plane), 2θ-43.1° (202 plane), 2θ-47.4° (018 plane), and 2θ- 48.4° (116 plane). Upon mixing with the setting solution, a rigid body was formed within 10 minutes as a result of transformation of calcium carbonate to an intermediate sodium incorporated hydroxyapatite as minor phase and calcium carbonate as major phase. XRD pattern shown in Figure 5.2 (B) confirms that the precursor obtained did not change much and composed of calcite (major) and apatite (very minor) phases. The apatite growth can be observed as a very minimal growth of peaks at 2θ -31.7° (211),

32.1° (112) and 32.9° (300) when compared with standard pattern (ICDD: PDF No. 00-009-0432). The exothermic reaction in the formation of apatite with the evolution of CO_2 is thought to be the driving force for the setting reaction which finally leads to more stable porous body. The complete conversion to apatite phase was achieved in 8 h of reaction under a temperature of 150 °C and a pressure of 15 bars which was confirmed by analysing XRD pattern of samples reacted for 1, 4, and 8h (Figure 5.3).

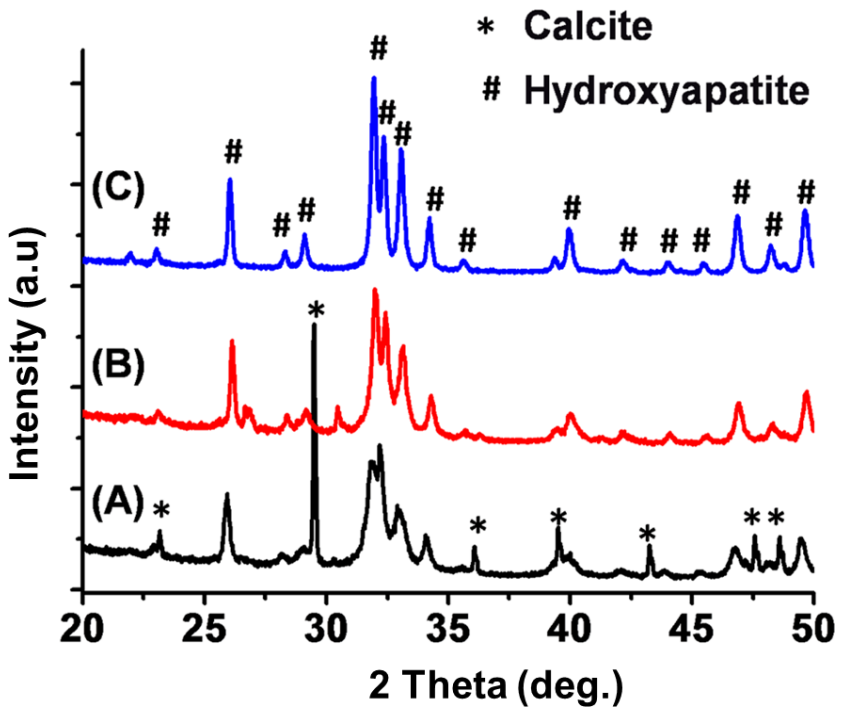

Figure 5.3. XRD patterns of the scaffolds after hydrothermal reactions in $NH_4H_2PO_4$ solution for 1 h (A), 4 h (B) and 8 h (C).

The crystals of apatite formed after 8 hours were isolated by mild sonication and analysed in XRD to study the orientation effects of the formed crystals (Figure 5.4 A). It was seen that the major peaks of hydroxyapatite were at 2θ- 31.7° with (100%) intensity corresponding to 211 planes. The peak at 2θ- 32.1° corresponding to 112

plane showed 61.85% intensity, 2θ- 32.9° corresponding to 300 plane showed 68% intensity and the peak at 2θ - 25.8° corresponding to (002) showed 65.9 % intensity. Other minor peaks of lesser intensity were seen at 2θ- 34.04° (27.62%) corresponding to 202 plane, 2θ-46.7° (23.73%) corresponding to 222 plane, 2θ-28.9° (23.34%) corresponding to (210) plane.

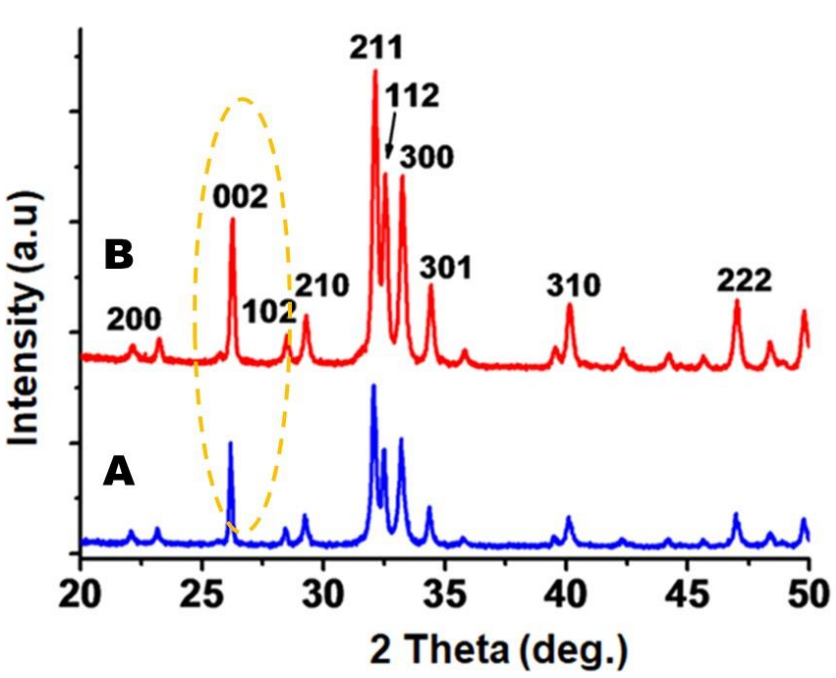

Figure 5.4. XRD patterns of preferred orientation of crystals obtained after hydrothermal conversion in AP solution for 8 h. (A) XRD pattern of the isolated crystals and (B) XRD pattern of the crystals after removing orientation by crushing the crystals.

The crystals were then crushed to remove the orientation effect and X-ray diffraction analysis was performed again (Figure 5.4B). It was seen that the intensity of 002 plane decreased to 51.7% from 65.9 %, when removing the orientation effects. This shows that the crystals have a positive orientation in the c-plane i.e. the crystals have an inclination towards a-axis but the major peak is seen to be the same at 211 plane

with 100% intensity. Orientation degree of c-plane was calculated from intensity measurements (I=intensity) using the equation;

$$\text{Degree of orientation} = [I_{002} / (I_{002} + I_{211} + I_{300})] \times 100\%$$

Orientation along the c-plane was found to be 28.17% in the case of individual crystals, whereas in a non-oriented lattice this value approaches 20%. The growth of the apatite crystals into plate-like structures along the radial direction may be attributed to the presence of carbonate ion substitution in the lattice which prevents the axial growth (Okazaki, 1993, Sampath Kumar et al., 2000).

Evaluation of Calcium to Phosphorus ratio in the materials

The Calcium to Phosphorus ratio in the materials before and after conversion reactions were evaluated ICP-OES studies. It was found that the material showed a Ca/P ratio of 1.827 before hydrothermal reaction which indicates a higher percentage of calcium ion in the lattice. The phosphate ion content is due to the reaction between the sodium hydrogen phosphate in the setting solution mentioned in section [3.1.4] and calcite powders which results in the formation of minor amounts of hydroxyapatite as a result of the setting reaction. These porous bodies upon hydrothermal exchange reactions in ammonium phosphate solutions lead to the formation of hydroxyapatite materials with Ca/P ratio of 1.562 confirmed by ICP-OES measurements.

Functional Groups Identification Studies

The FTIR spectra of the scaffolds were recorded before and after the conversion reactions to identify the changes in carbonate, hydroxyl and phosphate functional

groups as the reaction proceeds to completion (Figure. 5.5(A), (B)). FTIR spectrum of initial phase of calcite (Figure 5.5 (A)) was characterized by the main asymmetric ν_3 CO_3 band (at ~1410 cm^{-1}), ν_2 asymmetric (at ~ 875 cm^{-1}) and a ν_4 symmetric vibration at ~725 cm^{-1}. In addition to these bands, poorly ordered amorphous and crystalline polymorphs gave rise to ν_1 symmetric vibrations at 1090 cm^{-1} and (ν_1 + ν_4) symmetric vibrations at 1805 cm^{-1}.

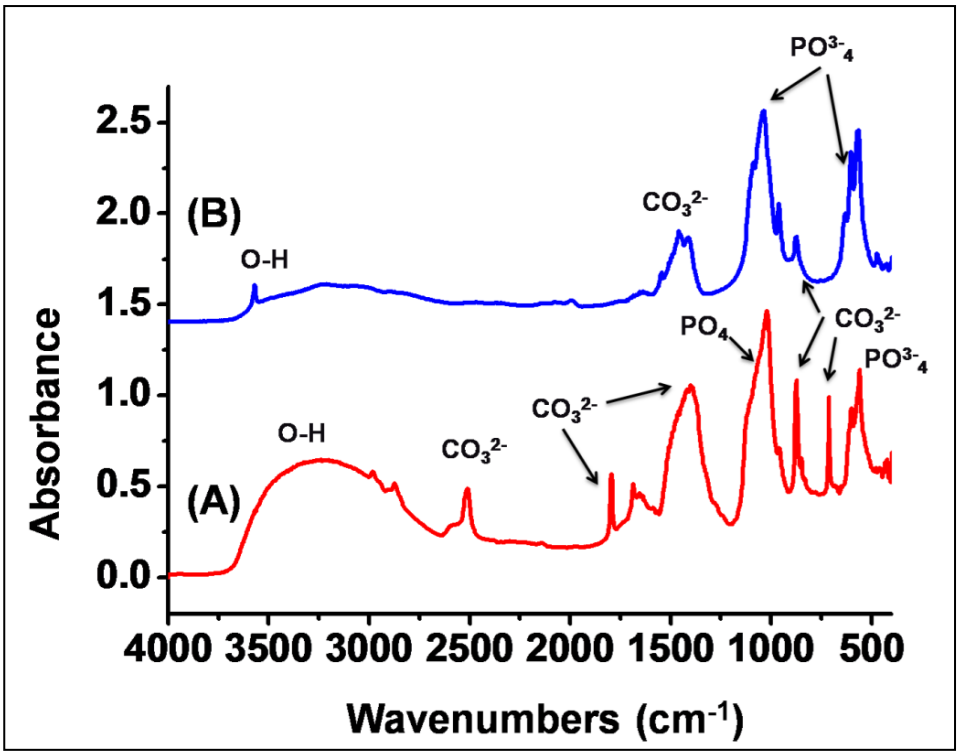

Figure 5.5. FTIR spectra of synthesized scaffolds (A) before and (B) after the conversion reactions.

The carbonate groups in the calcite on reaction with basic phosphate solution, both carbonate and a phosphate of calcium co-exists in the solid mass. As the reaction results in the generation of gaseous CO_2 which escapes during the course of reaction, the resulting porous body would have lower carbonate content compared to the starting calcite powder. This was further confirmed by the decreased IR vibrations

from carbonate and increased vibrations from phosphates as reaction proceeds to completion. Figure 5.5 (A), and (B) respectively shows the FTIR spectra of the scaffolds before and after hydrothermal exchange reactions and confirms the transformation of calcite to carbonated hydroxyapatite.

After the exchange reactions, the transformation of the material to carbonated apatite is evidenced by the characteristic bands for phosphate, carbonate and hydroxyl groups. PO_4^{-3} vibrations were observed at ~470(ν_2), 560 - 600 (ν_4), 960 (ν_1), and 1030 - 1104 (ν_3) cm^{-1}. The peaks at 632 cm^{-1} and 3560 cm^{-1} correspond to the structural –OH bands in apatite. The broad absorption bands in the range 3425-1635 cm^{-1} were attributed to the –OH vibrations from adsorbed water. The weak bands between 1410–1550 cm^{-1} region and the peak at ~ 870 cm^{-1} are characteristic of carbonate groups which results from the substitution of phosphate ion, to form B-type HA (Meejoo et al., 2006). Among the two types of carbonate substitution observed in HA, A-site (hydroxyl ion site) and B-site (phosphate ion site); B-site substitution PO_4^{-3} groups is replaced by CO_3–OH tetrahedron and causes –OH groups simultaneously to exist at two sites. Hence vibration of –OH group was disturbed by the substitution of CO_3–OH which causes reduction of intensity in –OH band. The structural –OH bands are weakened and the characteristic A-site substitution is totally absent confirming a typical B-site substitution.

Surface Analysis - Scanning Electron Microscopy

The ESEM analysis shows the morphological transformations of the carbonate materials to crystalline hydroxyapatite scaffolds with reaction in progress. ESEM images Figure 5.6 A and B shows the 3D surface morphology of precursor scaffold

formed as a result of setting reaction of calcium carbonate with phosphate solution. The morphology of the precursor scaffold, clearly indicates the amorphous calcite scaffolds without much consolidation of the powders. The structure seems to have developed intergranular space required for efficient hydrothermal exchange reactions through solvent penetration. The porous morphology is a result of the controlled evolution of CO_2 gas during the setting reaction, which prevent the coalescence of particles even if there is conversion reaction to form amorphous calcium phosphate.

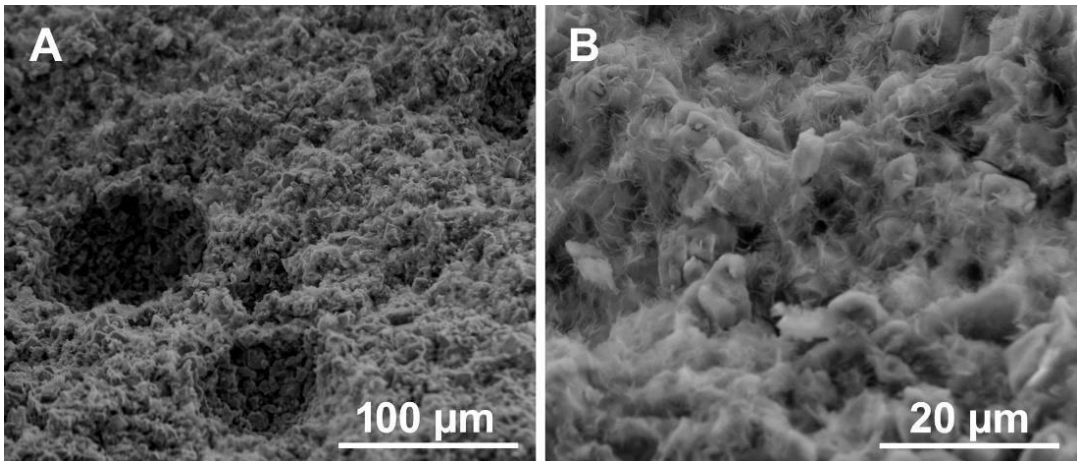

Figure 5.6. ESEM images of the amorphous and porous morphology of the precursor scaffold

The changes in the surface features after hydrothermal exchange reactions as a result of the phase transformation of the precursor calcite matrix can be seen as flowery growth of calcium phosphate in one hour (Figure 5.7 A, B) with protruding petal-like structures of dimensions 20-30 microns in length and 2-5-micron width. The flowery pattern changes to a plate-like apatite growth during the next four hours of reaction. The crystals are now grown to an approximate dimension of 15 (length): 10 (breadth): 3 (thickness) shown in (Figure 5.7 C, D). The reaction is further continued for another 4 hours in order to obtain maximum phase conversions to apatite phase.

During the last four hours the crystals grow to around 50 microns in length, 2 microns in width and 1 micron in thickness shown in (Figure 5.7 E, F).

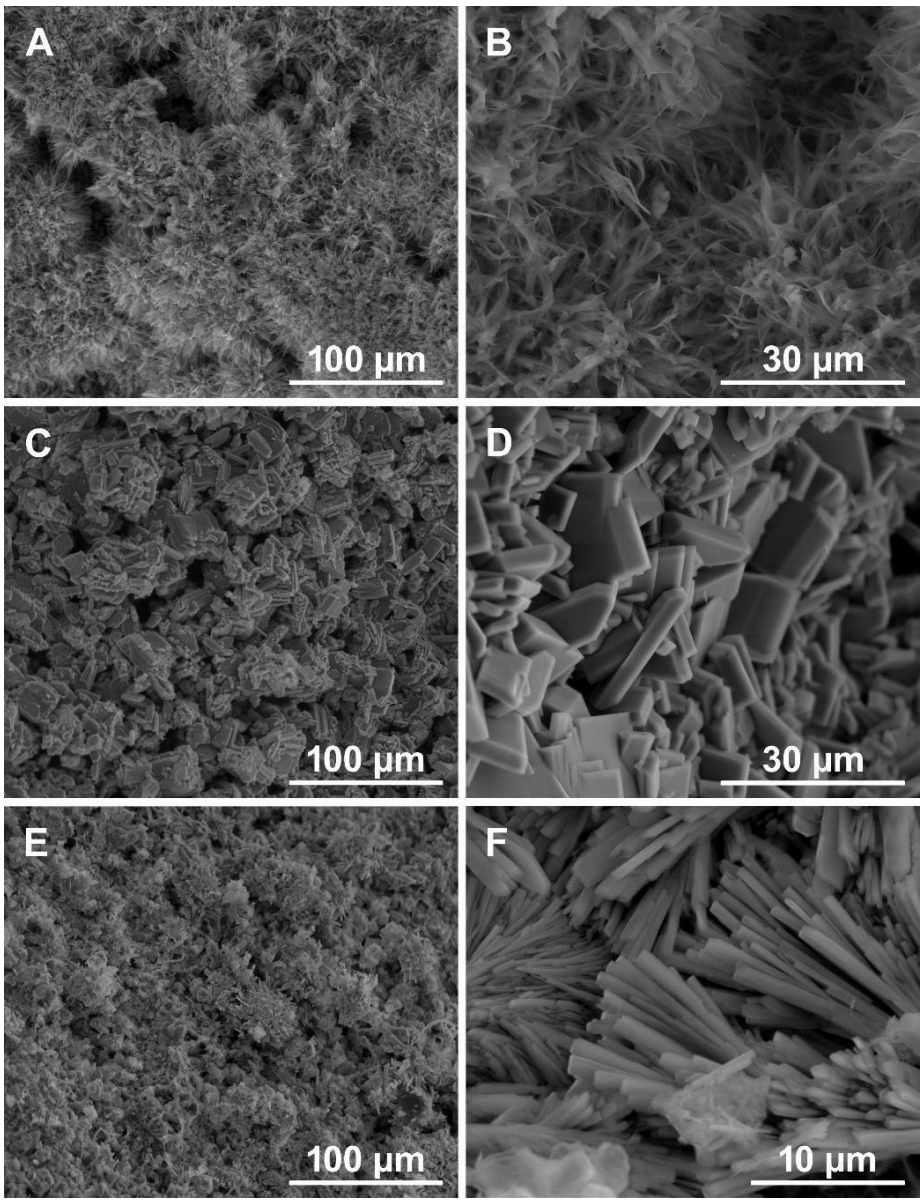

Figure 5.7. ESEM image of the scaffolds (A, B) after 1 h of hydrothermal reaction, (C, D) after 4 h reaction and (E, F) after 8 h of reaction.

The morphology changes with time which is also accompanied by the phase transformation to calcite to hydroxyapatite, evident from the XRD patterns. The arrangement of these uniform crystal plates produced after 8 hours of reaction were

in the form of stacked arrays as seen in nacre microstructures. Nacre is known for its exceptional mechanical properties and its ability to self-assemble to produce hierarchical structures. In nacre, the tablets of aragonite crystals are glued in between with polymer and polysaccharide which is thought to act as ceramic plywood to resist crack, provide toughness and impact resistance. Here a similar structure was *in situ* generated after 8 h of reaction with bundles of stacked crystals which can provide enough strength suitable for a synthetic scaffold. The higher surface area of the crystals and the porous nature of the scaffolds acts as active sites for the incorporation of therapeutic molecules like drugs, or biologic moieties like BMPs or siRNA like genetic materials (Cartwright and Checa, 2007, Yourdkhani et al., 2011).

In vitro bioactivity studies in Simulated Body Fluid (SBF)

The developed CHA scaffolds were subjected to *in vitro* bioactivity studies by immersing them in simulated body fluid for different time period such as 3,7 and 14 days to visualise the apatite deposition over the materials. The difference in weight was taken from the initial to the final day to see for the effect of apatite growth. It was observed that there was considerable weight gain with time. It is represented graphically in the Figure 5.8.

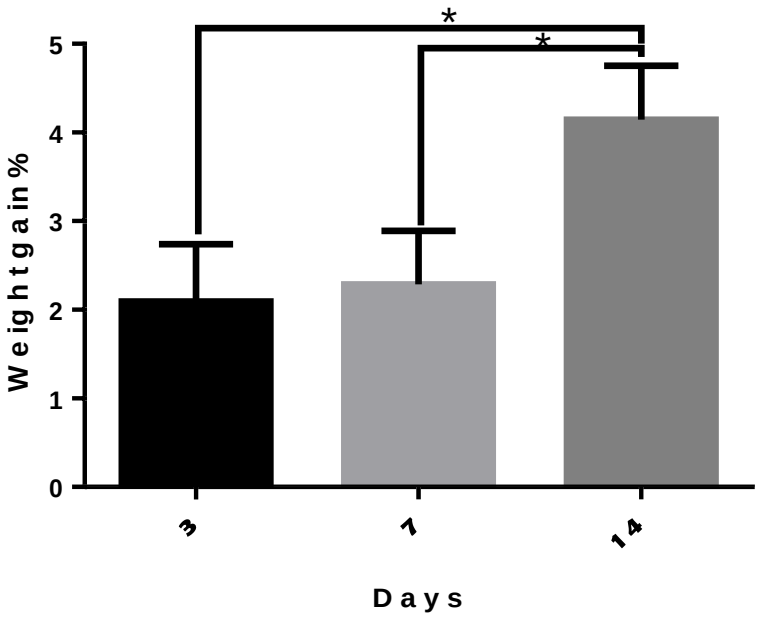

Figure 5.8. *In vitro* bioactivity studies of CHA in SBF (ICP- OES)

In vitro dissolution studies in phosphate buffered saline (PBS)

In vitro dissolution study was performed for 50 days in phosphate buffer (PBS) in order to evaluate the dissolution behaviour of hydrothermally converted calcite beads. During this period the hydrothermally prepared samples underwent a significant dissolution process with an average weight loss of 8.4 % compared to the less significant weight gain of 0.81% of sintered calcium phosphate due to the precipitation deposition at physiological pH of 7.4. The result for sintered ceramic is in agreement with reports for similar systems such as sintered hydroxyapatite based scaffolds which showed insignificant weight change and dissolution in phosphate buffer over short time periods (Guarino et al., 2009). It was seen that the calcium ion content of the material was seen to decrease during the study period whereas the phosphate ion was seen to increase in the scaffolds. The ICP-OES measurements of

the PBS shows that the Ca ion concentration increased progressively with number of days whereas the phosphate ion content decreased. The findings from ICP-OES measurements are depicted graphically in Figure 5.9 A and B.

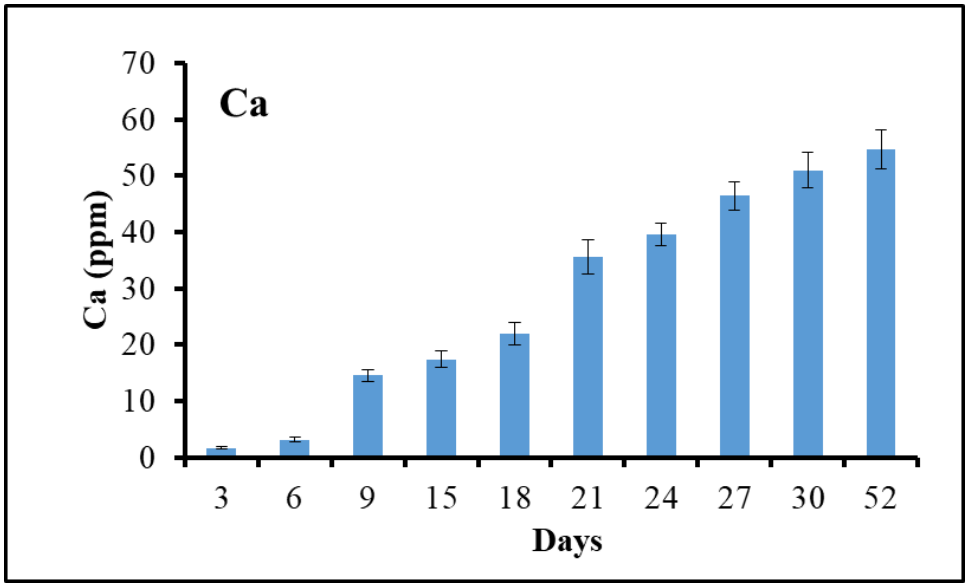

Figure 5.9 A. Graph showing the cumulative release of Ca ions from the sample to PBS

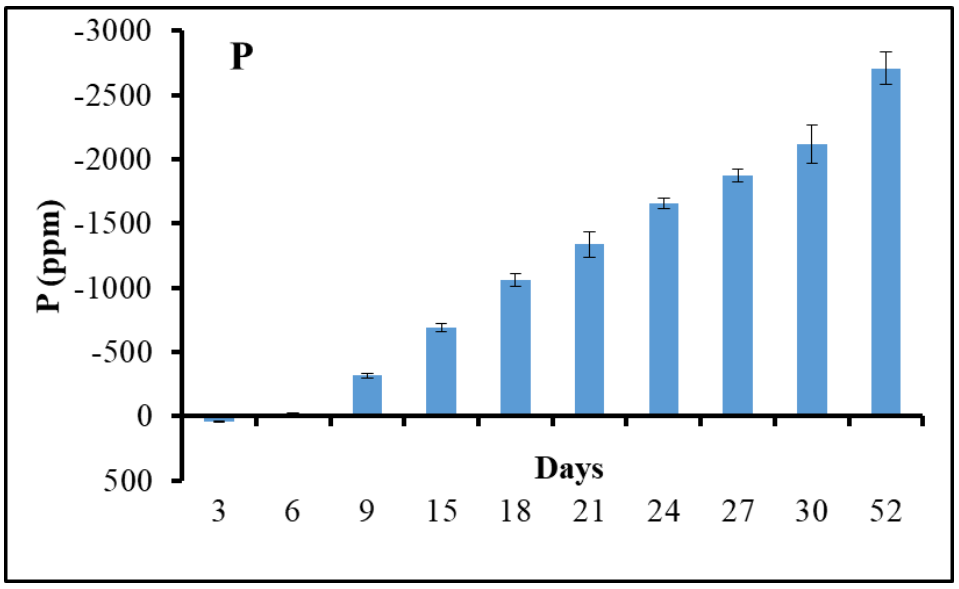

Figure 5.9 B. Graph showing the cumulative uptake of P ions from the PBS to the sample

Mechanical Property Evaluation by Compressive Strength Measurements

Mechanical properties of the samples were also analysed to ensure the suitability for further applications. The samples were having an average compressive strength of 5.9 ± 1.2 MPa without any high temperature processing shown in Figure 5.10 and confirm the mechanical stability for the intended application. These values of compressive strength for porous blocks were comparable to the compressive strength of porous hydroxyapatite scaffolds obtained by Kawachi *et al (Kawachi et al., 2010).*

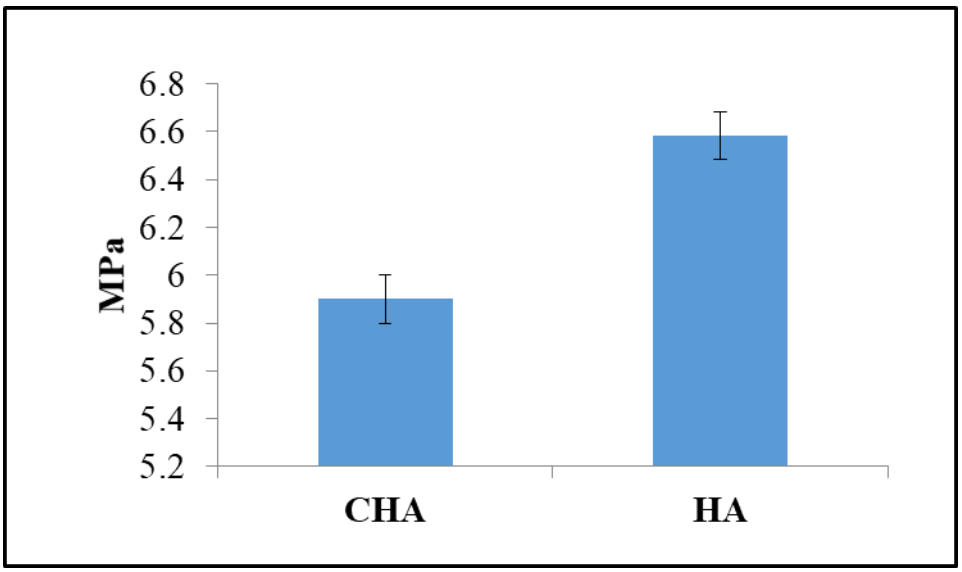

Figure 5.10. Compressive Strength measurement of CHA with respect to porous HA.

Micro CT studies for Porosity Evaluation

Micro CT analysis was found to be much effective in quantitatively identifying the pore size distribution, spacing profile as well as thickness profile of the bulk material Figure 5.11(A, B, C). The porosity of the material was also assessed by density

measurements (Archemedes' method) and shows that the materials were 40±5% porous. Figure 5.11A is the scout view of the positioned material and gives a global view at low resolution. Figure 5.11 B and C respectively shows the wall thickness and pore size distribution in the CHA spheres. The different colours represents the size of the particles as per the colour coding scale given below. Figure 5.11C shows that the material has almost uniform distribution of pores throughout the material.

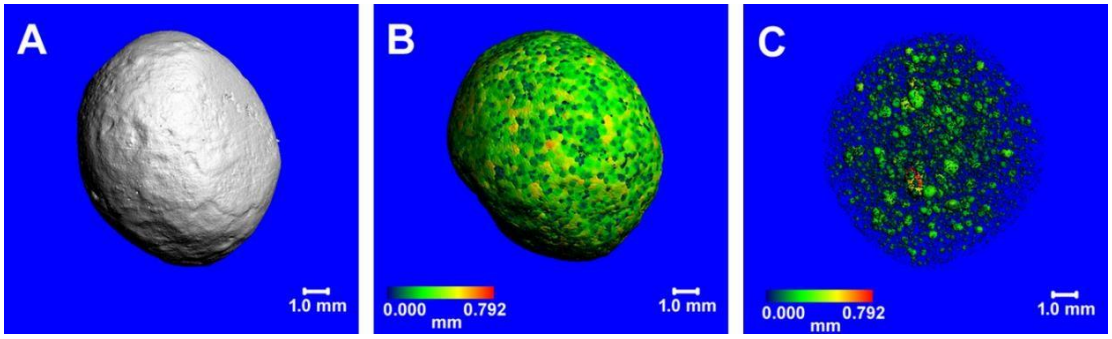

Figure 5.11. (A) Scout view (3D) of the synthesized scaffold by micro CT analysis, (B) wall thickness and (C) pore size distribution.

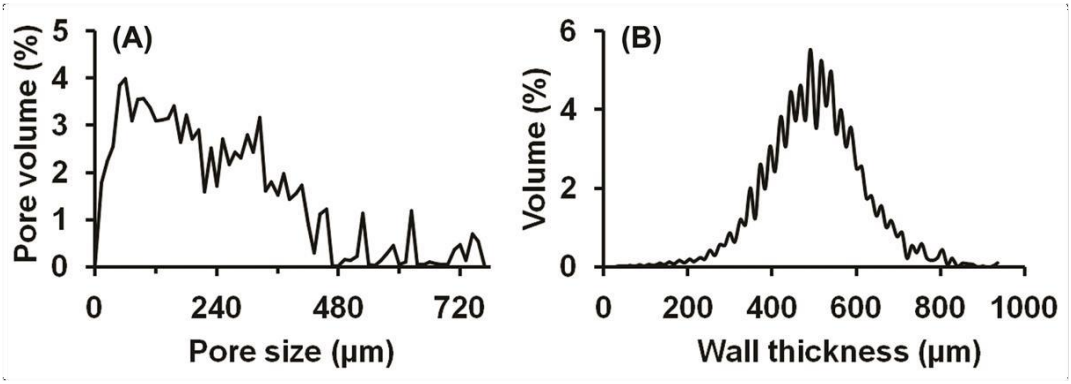

Figure 5.12. Histogram of (A) pore size distribution and (B) wall thickness of the scaffolds.

The pore size distributions and the wall thickness obtained are represented graphically in Figure 5.12 (A) and (B) respectively. The pore size distribution from the histogram obtained from the micro CT analysis shows that the pore size of the

material largly varies from 100 to 750 microns with majority of pores having dimensions from 100 to 400 microns. These pores are distributed randomly throughout the material as a result of the liberation of gaseous carbon dioxide during the setting reactions of calcite and later conversion reactions of the formed porous precursor under hydrothermal conditions. The wall thickness of the material with respect to the pore volume was observed in the range of 500 microns. Because of this wall thickness, even if the scaffold was 40% porous, it was found to maintain adequate strength.

Characterisation of MSC's Isolated

A number of markers such as CD49e, CD44, CD90, CD105, CD73, STRO-1, are used to characterize MSCs (Zhu et al., 2006). The ADMSCs isolated were characterized by the specific cell surface marker CD 90 positive staining (Figure 5.13A) and the cytoskeletal arrangement was observed by means of F-Actin staining as shown in (Figure 5.13 B). The isolated ADMSC's showed the plastic adherent nature which helped them grow with better anchorage on cell culture plates. The actin network has a major role in the mechanical properties of living cells like anchorage of cells to different substrate materials. The specific morphological characteristics confirm that the cells are of mesenchymal origin.

The mesenchymal phenotype characterised by flow cytometric analysis showed that ADMSC's were negative for hematopoietic stem cell marker CD 34, and positive for CD 44 and CD 105, seen as an increase in the fluorescent intensity when compared to unstained cells. Figure 5.14 shows the flow cytometry data of the isolated cells.

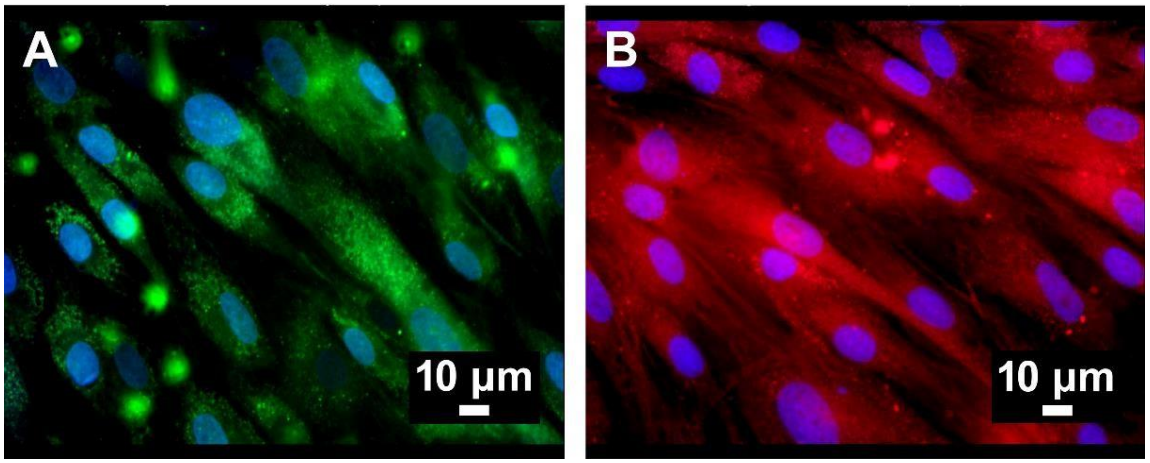

Figure 5.13. Fluorescent images of rabbit ADMSC's with spindle shaped morphology (A) staining of CD90, specific cell surface marker and (B) Actin staining showing the cytoskeletal arrangement.

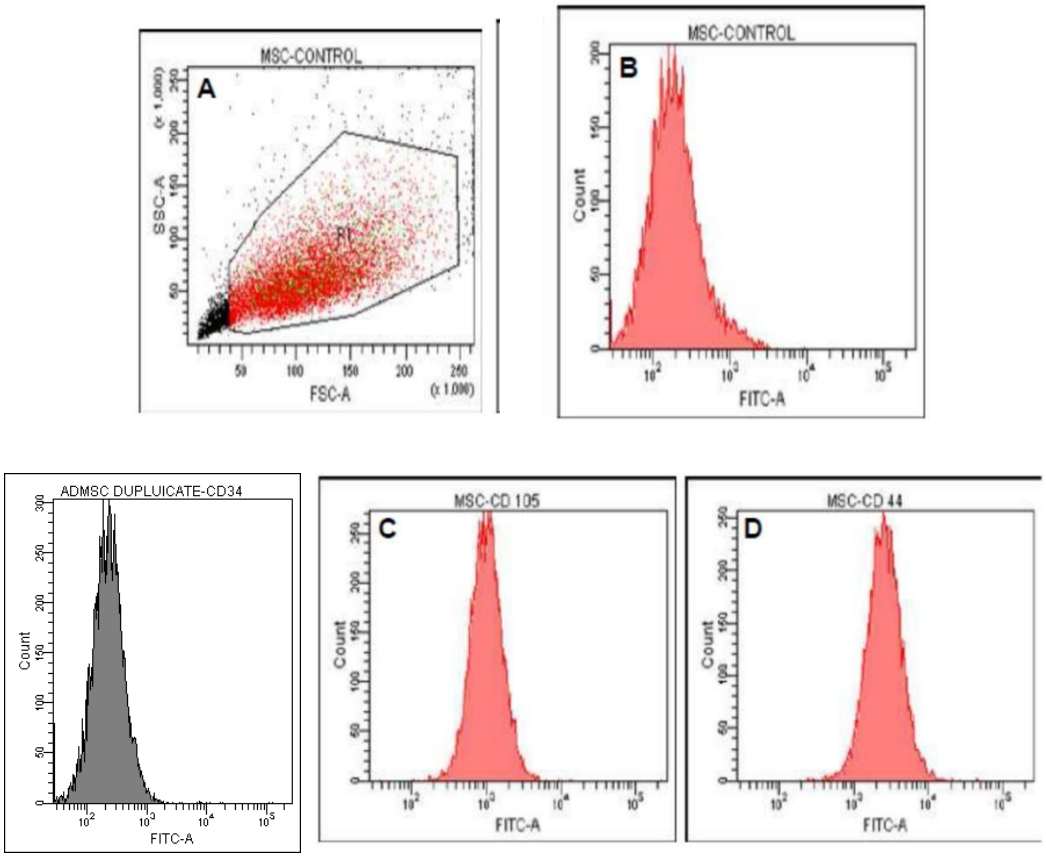

Figure 5.14. Flow cytometry analysis of the expression of MSCs Control, CD34, CD44, CD 105 on ADMSCs – 48 h. PE-A labelled CD34 (hematopoietic stem cell marker) and FITC labelled CD44 and CD 105 (mesenchymal stem cell marker) staining. Unstained ADMSCs (Control cells).

Cell-Material Interaction Studies

ESEM images depicted the cell friendly nature of ADMSCs over the scaffolds amidst newly grown hydroxyapatite crystals. After two days of culture the cells adhered well to the surface of the material (Figure 5.15 A, B). After 4 days of culture it is observed that the material surface is completely covered with cells (Figure 5.15 C, D). The cells were also seen to penetrate into the internal pores of the scaffold with excellent proliferation maintaining cell-cell contact. They grew profusely over the crystals from the surface to the bulk of the material.

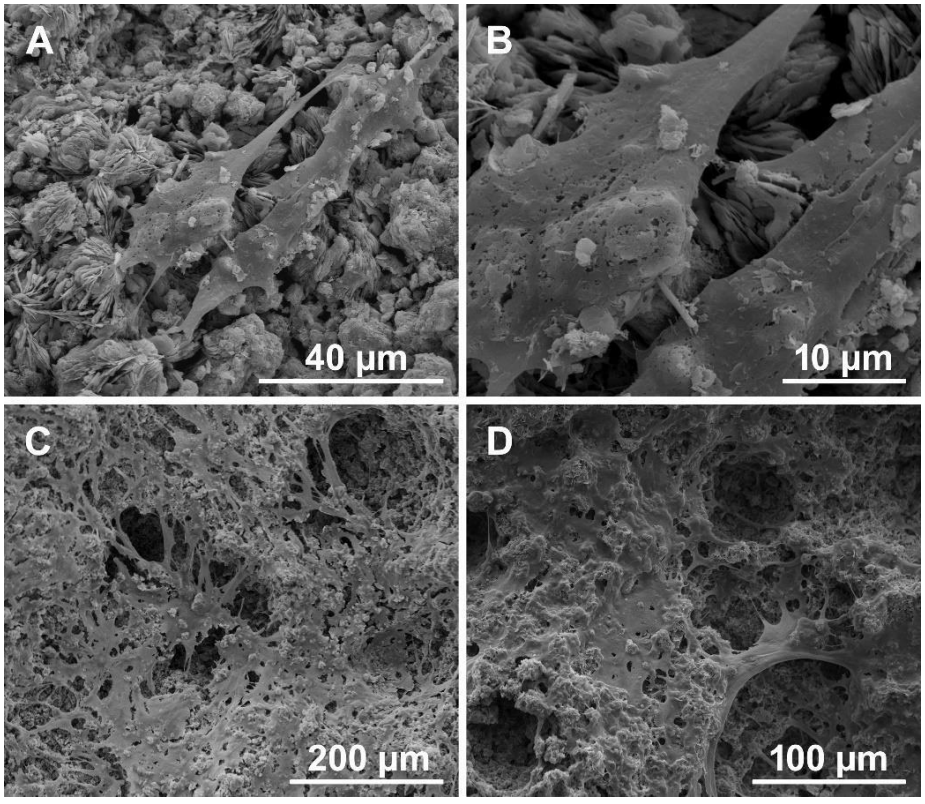

Figure 5.15. ESEM images - (A, B) the cell attachment after 2 days in cell culture and (C, D) after 4 days in cell culture.

Cell Proliferation Study (Cell TiterBlue/ Alamar Assay)

The cell titer blue assay for the material seeded with human mesenchymal cell line showed cell viability for the 14 days study period with a progressive increase in the intensity of fluorescence indicating the increased metabolic rate of the proliferating cells (Figure 5.16). The assay works on the ability of living cells to convert the redox dye resazurin into a fluorescent end product resorufin. Non-viable cells rapidly lose their metabolic activity and hence will not generate the fluorescent signal. There is a slight decrease in the peak intensity from 12 to 14 days which may be attributed to the beginning of the differentiation phase.

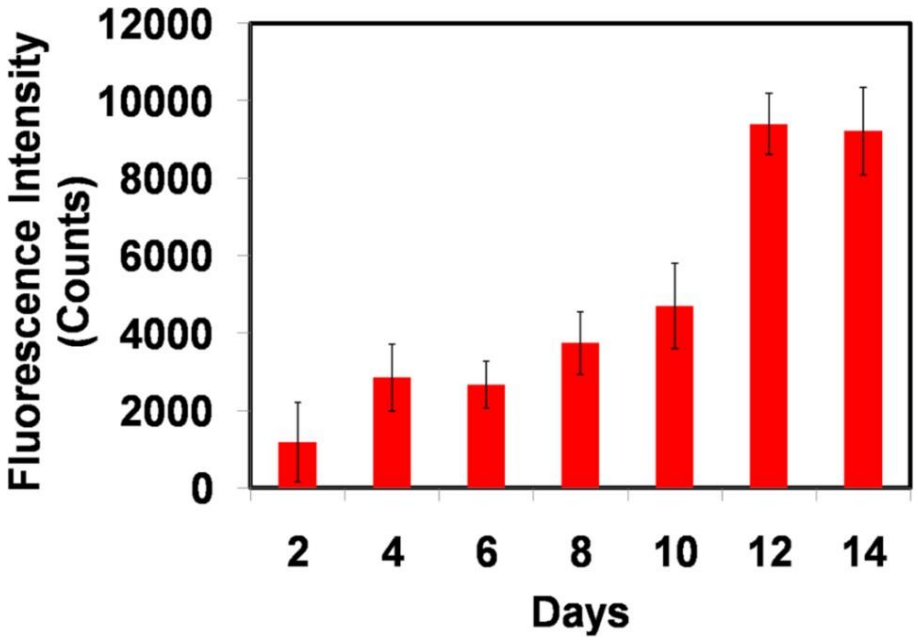

Figure 5.16. Graphical representation showing the cellular activity by cell titer blue assay.

Viability of ADMSC's on the scaffolds

Confocal laser scanning microscopy reveals the presence of live cells (shown in green) throughout the material after 2 days in cell culture (Figure 5.17). The spindle-like fibroblast morphology of stem cells were retained and the live cells attached, adhered and expanded over the material surface. Acridine orange, a vital dye stains both live and dead cells by interacting with the DNA of the living cells or RNA of acidic vacuoles such as lysosomes, endosomes, and autophagosomes emitting green (DNA) or red colour (RNA). This happens as a result of the electrostatic interactions of the acridine molecule on intercalation with nucleic acid base pairs. Ethidium bromide stains only dead cells whose activity is also by binding to the DNA of metabolically inactive cells. Live cells with intact cell membranes are stained as green and dead cells with ruptured cell membranes are stained red. The 3D image of the cell seeded scaffold clearly identified that the cells are viable even to a depth of 85 µm which shows that metabolically active cells can penetrate deep and spread into layers as the developed material offered suitable porosity for the permeation of culture media without generating any hypoxia mimicking environment (Figure 5.17 B). The emmision of green fluorescence obtained from the surface as well as bulk clearly indicated that all cells were metabolically active and viable.

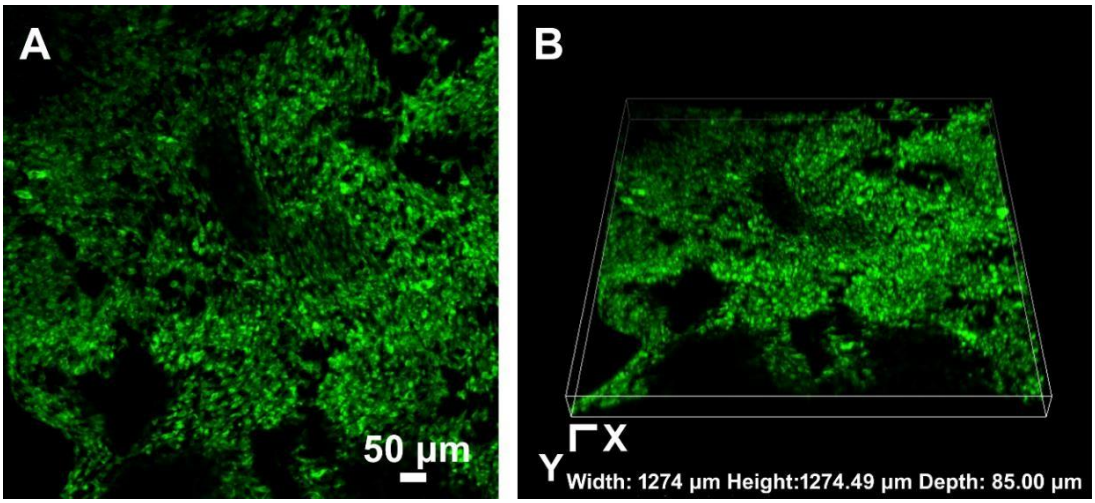

Figure 5.17. Confocal laser scanning images - (A) live dead assay of cell seeded material after 2 days in culture and (B) 3D image of the same

Evaluation of Drug Elusion from the CHA beads

UV spectro-photometric analysis was performed to study the release profile of gentamicin sulphate from gentamicin loaded beads. The drug release profile for 53 days is shown in Figure 5.18. It was observed that about 25% of the drug was released during the first 24 h indicating an initial burst release. During the next 5 days a linear elution was observed with a release of 50% of total loaded drug. From 5 to 20 days, 45 % of the drug was eluted, showing a sustained release of the drug. From the elusion profile it is clear that 5% of the drug still remains after 20 days and gets gradually released in detectable amounts upto 53 days. Prolonged local antibiotic delivery for a month at the infected site is highly critical and essential for infections like osteomyelitis. With the sustained release of the drug for more than 30 days, the carbonate derived hydroxyapatite beads (CHA) are prospective materials for drug carriers.

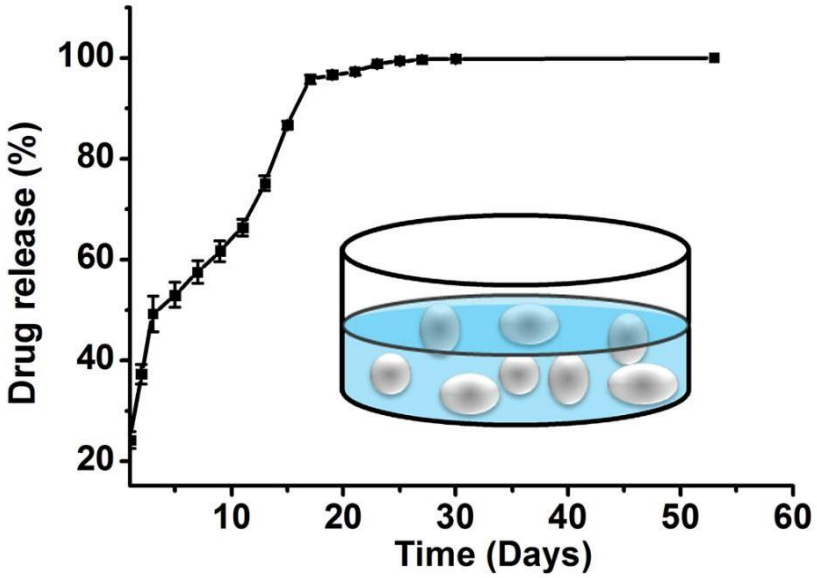

Figure 5.18. *In vitro* drug elution study: cumulative release of gentamicin drug from the scaffold up to 53 days. The inserted scheme shows beads immersed for drug loading.

Summary

Hydroxyapatite scaffolds prepared from calcium carbonate (calcite) precursors CHA mimics the natural nacre like microstructure. The developed materials were non-cytotoxic and cell friendly. CHA supported the healthy growth and proliferation of MSC's for 14 days as evidenced from the alamar blue assay. CHA material also proved to be a promising scaffold and drug carrier. The drug release potential was observed for 53 days making it useful as drug carriers for the treatment of infectious bone diseases such as osteomyelitis.

CHAPTER - 6

PREPARATION OF HYDROXYAPATITE FROM LOWER CALCIUM PHOSPHATE (TCP) PREFORMS VIA HYDROTHERMAL EXCHANGE REACTIONS

Tricalcium phosphate derived hydroxyapatite - THA

Introduction

Hydroxyapatite scaffolds with oriented crystal morphologies were fabricated through hydrothermal exchange reactions of tricalcium phosphate porous precursors in different reaction mediums. The novel scaffolds having unique clusters of hydroxyapatite crystal with a preferred orientation were prepared by hydrothermal exchange reactions. These crystals depicted micro and nano dimensional structures resembling fibres, rods, tubes and flowers. The growth of the apatite crystals was observed to be along the a(b)- plane of the hydroxyapatite lattice oriented along the c-axis. The synthesised scaffolds were subjected to *in vitro* bioactivity evaluation in simulated body fluid (SBF) and degradation studies in phosphate buffered solution (PBS). Physicochemical characterization of the materials was performed by X-ray diffraction, Scanning Electron Microscopy, Transmission Electron Microscopy, Micro CT and Fourier transform infrared spectroscopy. Transformation of a lower calcium phosphate material to a faster resorbing hydroxyapatite scaffold with a preferred orientation along the c-axis and a higher aspect ratio of crystals could be achieved from the study. The prepared material is intended for use in the field of

dentistry and orthopaedics as a scaffold for tissue regeneration and for bone filling applications.

Preparation and Physicochemical Characterisations of the developed materials

TCP preforms fabricated in various shapes such as spheres, pellets, blocks, cylinders etc. were formulated for various studies. Porosity was introduced into the precursors with the use of naphthalene as pore former.

(13 mm × 5 mm) discs

(10 mm dia spheres)

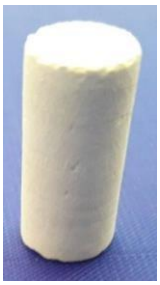

(8 mm × 16 mm) cylinders

(4 mm × 10 mm) cones

Figure 6.1. Optical Micrographs of the preforms developed for hydrothermal conversions.

Pellets of 13 mm diameter and 5 mm thickness were used for the *in vitro* studies. Each of the pellets weighed around 0.4 g. These materials were heated to 900 °C to obtain precursor stability. The pellets so obtained were hydrothermally converted in three different reaction mediums such as:

(1) basic ammonium phosphate **(AP)**-1 M concentration (500 ml), pH = 10.5

(2) calcium nitrate made basic using ammonium hydroxide solution- (**CN)** 1 M concentration (500 ml), pH = 9 and

(3) calcium hydroxide – **(CH)** 1 M concentration (500 ml), pH = 12

The hydrothermal exchange reactions were carried out at a temperature of 150 °C and with the indigenously developed pressure during the reaction which varied between (5-8) bars. Maximum conversion efficiency was optimised by conducting the reactions at different time periods. Material characterisations were performed to ensure phase purity, microstructural changes, crystallinity, and functional group identification of materials before and after the hydrothermal reactions. The proposed reaction for the conversion reaction is based on a dissolution and reprecipitation mechanism as shown below (Eq.1 and Eq.2) proposed for the reactions under aqueous conditions (Liu et al., 2011):

$$10Ca_3(PO_4)_2 \xrightarrow{H_2O} 3Ca_9(PO_4)_6 + 3Ca^{2+} + 2(PO_4)^{3-} \quad \text{(Eq.1)}$$

$$3Ca_9(PO_4)_6 + 3Ca^{2+} + 2(PO_4)^{3-} \xrightarrow{6H_2O} 3Ca_{10}(PO_4)_6(OH)_2 + 2H_2PO_4 + 2H^+ \quad \text{(Eq.2)}$$

Equation (1) represents the dissolution of the material in an aqueous medium. As per the above mechanism it is clear that TCP under aqueous environment dissociates into

three posner clusters ($Ca_9(PO_4)_6$) along with three calcium ions and two phosphate ions. A Posner cluster is the building block in apatite nucleation, it is an amorphous calcium phosphate with a central Ca^{2+} ion surrounded by six phosphate PO_4^{3-} anions which in turn are surrounded by eight further calcium ions (Kanzaki et al., 2001). Appropriate reaction mediums for hydrothermal exchange process were selected in such a way as to supplement the calcium and phosphate ions to the material for aiding the conversion process. The ions present in the three reaction mediums such as phosphate ions from ammonium dihydrogen phosphate solution, calcium ions from calcium nitrate, calcium and hydroxide ions from calcium hydroxide along with the hydroxide ions from the solvent water, helps in the rearrangement of the lattice structures and the formation of hydroxyapatite phase. The reaction mechanism proceeds via a dissolution precipitation mechanism.

Evaluation of calcium to phosphorus ratio in THA

The materials converted were analysed via ICP-OES method to find out the calcium to phosphorus ratio in each of the three systems and it was found that the material before hydrothermal treatment had a calcium to phosphorus ratio of 1.47 which was correlating to the mineral content of tri calcium phosphate. After hydrothermal treatment of 8 h complete conversion of the materials was observed in the three reaction mediums. The materials converted in ammonium phosphate and calcium nitrate showed the formation of a calcium deficient pseudo apatite. This effect was more pronounced in the materials converted in ammonium phosphate with a Ca/P ratio of 1.37. Since calcium nitrate solution supplemented the calcium ions, this ratio

improved to 1.56. But due to the presence of acidic nitrate ions a stoichiometric apatite formation was hindered. In the case of calcium hydroxide medium, the basicity and the presence of calcium and hydroxide ions have favoured the formation of a more stoichiometric calcium rich apatite having a Ca/P ratio of 1.68. Owing to the chemical composition, this material was chosen for further studies and it was named tricalcium phosphate derived hydroxyapatite or (THA).

Material	**Ca/P ratio**
TCP	**1.47**
TCP (**A**mmonium **P**hosphate)- **AP**	**1.3707**
TCP (**C**alcium **N**itrate)- **CN**	**1.5683**
TCP (**C**alcium **H**ydroxide)- **CH**	**1.6843**

Table 4. ICP-OES analysis of the materials before and after the exchange reactions

X-Ray Diffraction Analysis

The materials were characterised for their phase purity before and after the reactions. It was seen from the XRD pattern that complete conversion of the material was observed after 8 hrs of reaction. Figure 6.2 shows the XRD pattern of the materials before and after the reaction in the three different reaction mediums. Figure 2 (A)

denotes the TCP phase before the conversion reaction and Figure 2 (B), (C) and (D) represents the formation of apatite phase in AP, CN and CH solutions respectively.

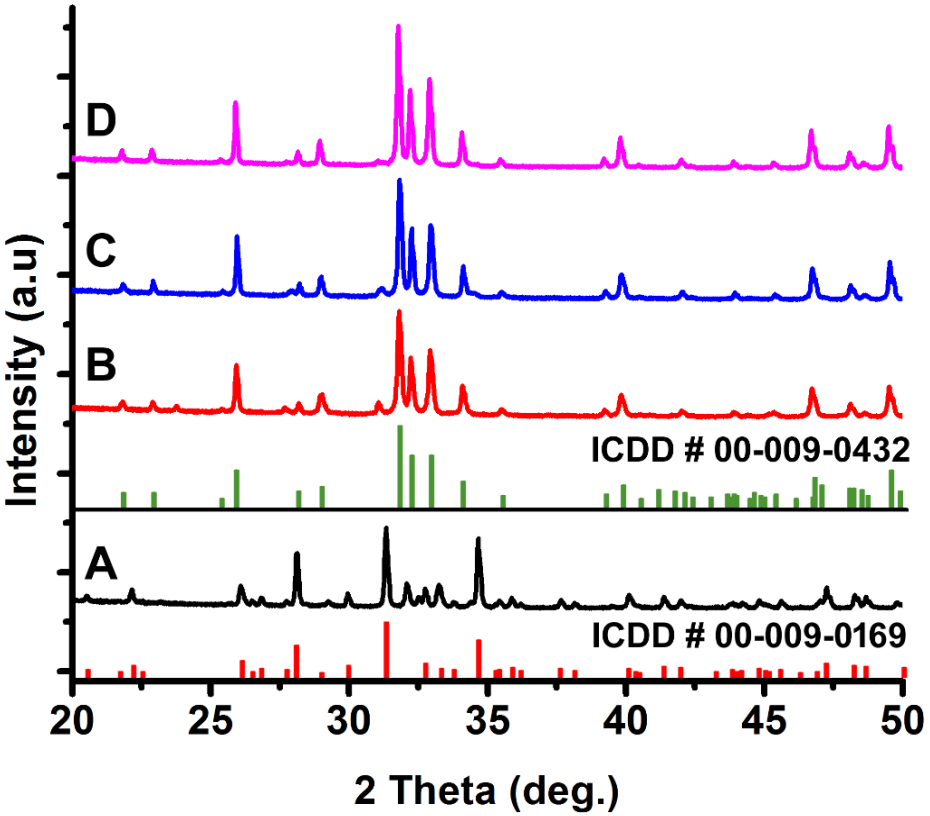

Figure 6.2. XRD patterns of synthesised precursor material (A) with the standard data of β-TCP (ICDD No. 00-009-0169) as reference, **after hydrothermal conversion in ammonium phosphate (B), calcium nitrate (C) and in calcium hydroxide solution (D)** with reference to hydroxyapatite (ICDD PDF No. 00-009-0432).

The increased peak intensities observed in comparison to the precursor β-TCP indicates relatively higher crystallinity achieved after the conversion process. Irrespective of the solutions used in exchange reactions, the major phase obtained after the exchange reactions are of apatite. However, depending on the pH and mediums, the formed apatite phase was seen to be more crystalline in basic solutions of CH than CN or AP. Complete conversion to apatite phase was achieved in calcium

hydroxide medium when compared to the other two reaction mediums. The scaffolds were further analysed to see the effects of preferred orientation in the crystals formed. It was seen that the newly formed apatite crystals on the surface of the scaffolds showed different morphologies under ESEM observation. These crystals were isolated by minimal sonication without disturbing their structures and prepared for X-ray diffraction analysis. Figure 6.3 shows the XRD pattern of the isolated crystals, from which it is surprising to see that the diffraction pattern is different from the classical standard pattern of hydroxyapatite (PDF No. 00-009-0432).

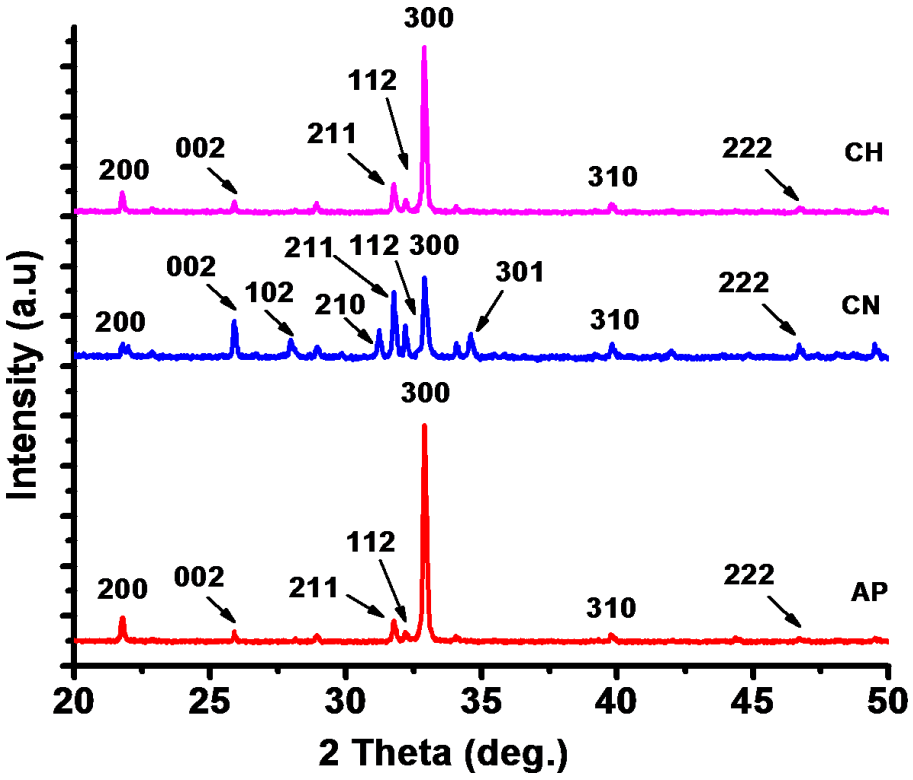

Figure 6.3. XRD patterns indicating preferred orientation of crystals obtained after hydrothermal conversion in ammonium phosphate (AP), calcium nitrate (CN) and calcium hydroxide solutions (CH) identified with reflection planes reference to standard hydroxyapatite (ICDD PDF No. 00-009-0432).

There is a significant observation from the XRD pattern that the hydroxyapatite crystals had a preferred orientation in the c- axis which is indicated by the growth of

a- plane (300 and 200) at 2θ value of 32.9° and 21.8°. The maximum intense peak is observed at 2θ value 32.9° in all the converted samples in preference to the standard hydroxyapatite which gives the maximum intense peak at 2θ value 31.8° corresponding to (211) plane. The (200) a- plane has shown an increase in intensity in all the samples but significantly higher in samples converted in calcium nitrate (CN, pH=4) solution compared to those in ammonium phosphate (AP, pH=10) and calcium hydroxide (CH, pH=12) solution. Suppression in the intensity of the main peaks of hydroxyapatite at 2θ values of 31.7° and 32.1° (211 and 112 planes) is noted as a major change in scaffolds converted in AP and CH solutions whereas this is slightly less in those from CN solution. It can be due to the difference in pH of these solutions which also affects the conversion rate and morphology of the developed materials. Other significant changes in the suppression of peak intensities can be observed at 2θ values 46.7° and 49.4° corresponding to (222) and (213) planes. The peak at 2θ value of 25.8° corresponding to (002) plane (c- plane) has significantly reduced in samples derived from AP and CH solutions, but it has grown high in CN solution. This shows that the c- plane growth corresponding to a- axis is higher in scaffold converted in CN which is at the lower pH. Hence the preferred orientation effect towards c-axis is slightly less in these scaffolds in comparison to the other two groups.

The effect of the three solutions on orientation degree of a-plane of each ceramic was compared on the basis of the intensities (I) of (300), (211) and (002) reflections according to Eq. 3 (Zhuang et al., 2012). The orientation degree of a-plane for scaffolds converted from ammonium phosphate, calcium nitrate and calcium hydroxide respectively are 83.96%, 42.51% and 80.81%.

Orientation degree of a- plane = {I(300)/[I(300) + I(211) + I(002)]}×100% (Eq. 3)

The analysed crystals were then powdered in agate mortar and pestle to remove the natural orientation effects of the hydroxyapatite crystals which was analysed by X-ray diffraction studies whose pattern is same as in Figure 6.2. All the three samples shows the conversion of β-TCP phase with ICDD- PDF no. 00-009- 0169 to single phase hydroxyapatite (ICDD PDF No. 00 009-0432) with maximum intense peak at 2θ value of 31.8° corresponding to the (211) plane of HA followed by the minor peaks at 2θ values of 32.2°, 32.9° and 25.8° respectively from (112), (300) and (002) planes.

In order to study the bioactivity and remineralization, the scaffolds were immersed in simulated body fluid. After immersion in SBF, the scaffolds were shown to have carbonated apatite growth which was characterised by FTIR and ESEM. The XRD pattern of all the hydrothermally treated samples after immersion in SBF was similar in nature. XRD pattern of the TCP scaffold before and after hydrothermal conversion in each of the solutions with different soaking duration in SBF is depicted in Fig. 6.4-6.7. The untreated scaffolds showed the major phase of TCP even after 14 days of immersion in SBF. The observation of apatite growth having spheroidal morphology was seen in the surface of the scaffolds. But this has not been reflected much in the phase change of the surface.

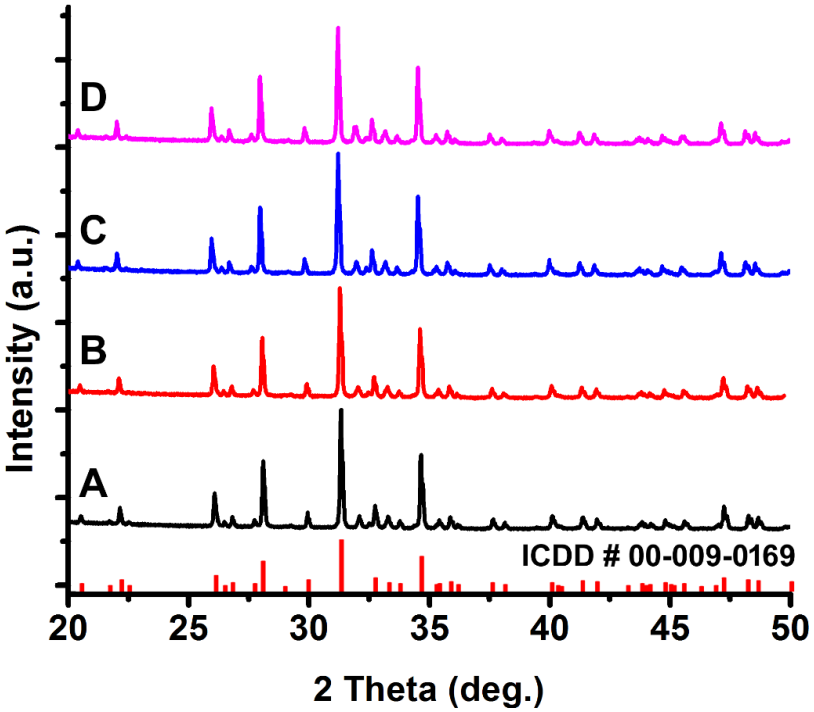

Figure 6.4. XRD pattern of β-TCP preform immersed in SBF for (A) 1 day, (B) 3 days, (C) 7 days and (D) 14 days, indexed with standard pattern of TCP (ICDD No. 00-009-0169).

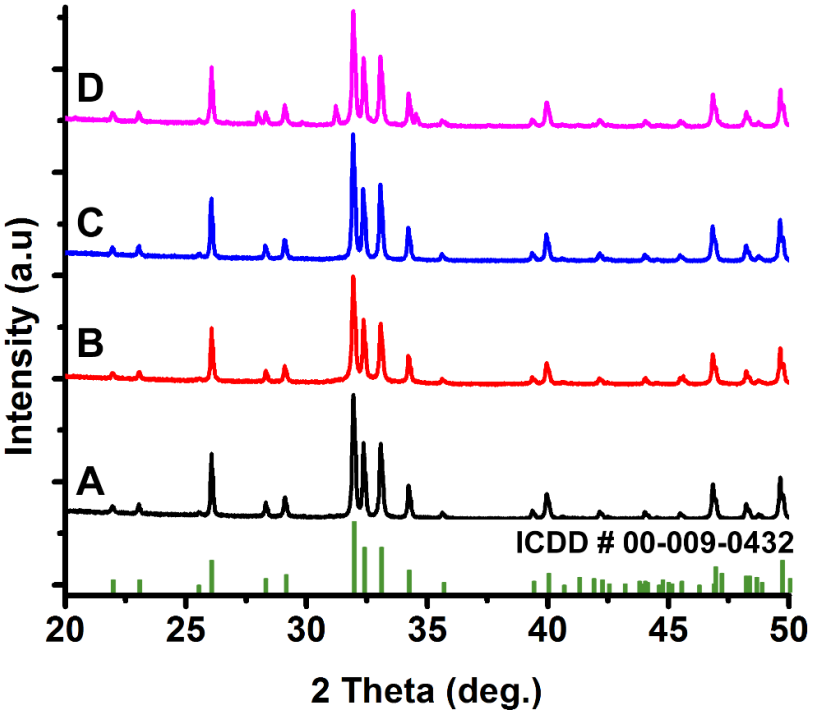

Figure 6.5. XRD patterns showing influence of SBF over hydrothermally converted scaffolds in calcium hydroxide (CH) for (A) 1 day, (B) 3 day, (C) 7 and (D) 14 days. The phase confirmation of hydroxyapatite is indicated by the reference (ICDD No. 00-009-0432).

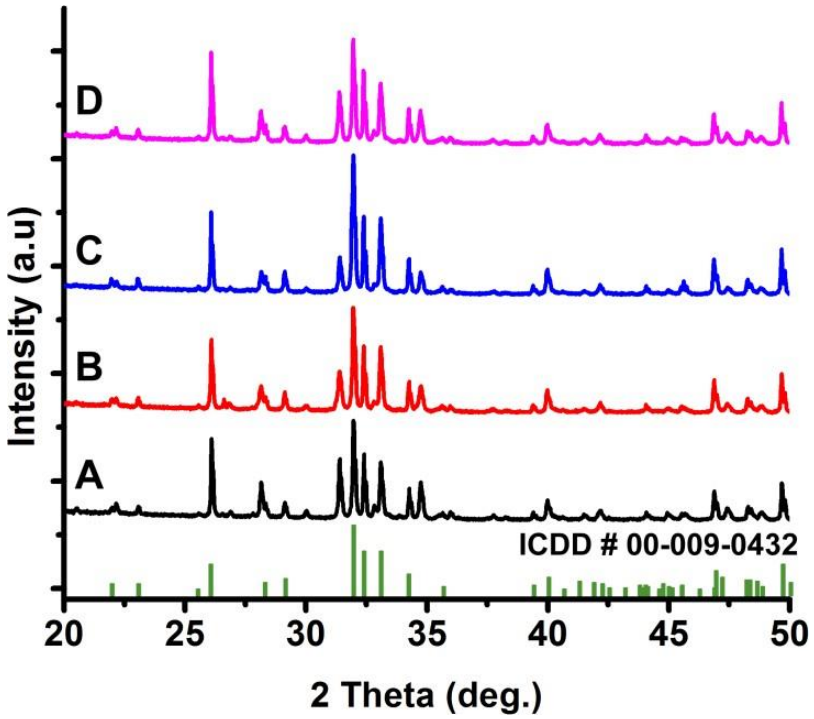

Figure 6.6. XRD patterns showing influence of SBF over hydrothermally converted β-TCP scaffolds in Ammonium Phosphate (AP) for (A) 1 day, (B) 3 day, (C) 7 and (D) 14 day. The phase confirmation of hydroxyapatite is indicated by the reference (ICDD No. 00-009-0432).

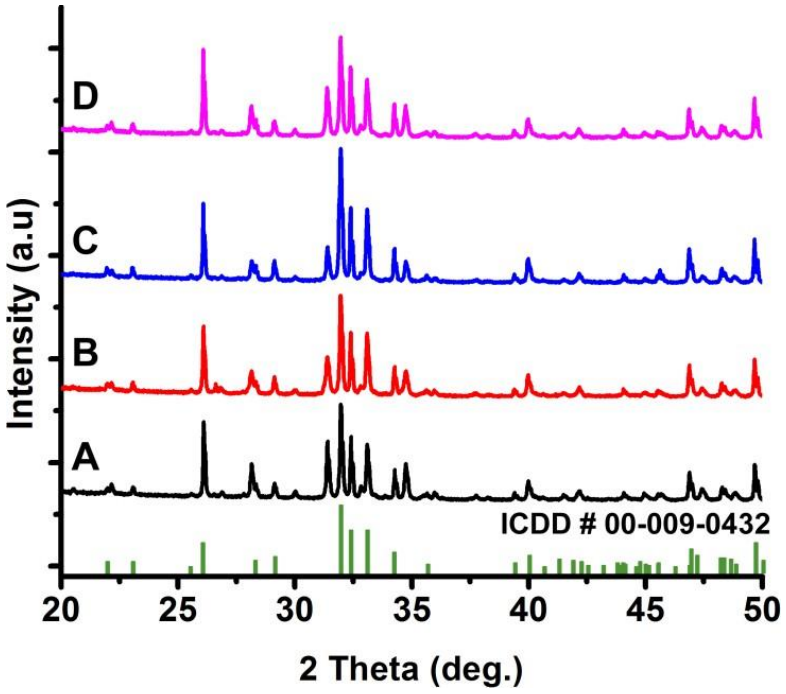

Figure 6.7. XRD patterns showing influence of SBF over hydrothermally converted β-TCP scaffolds in Calcium Nitrate (CN) for (A) 1 day, (B) 3 day, (C) 7 and (D) 14 day. The phase confirmation of hydroxyapatite is indicated by the reference (ICDD No. 00-009-0432).

The pattern shows that the deposited apatites over the exotic crystal morphologies were highly crystalline in nature which is clearly observable by the sharp, distinct and more intense peaks than the hydrothermally derived apatite. As the soaking time in SBF progresses, the peaks get intensified as observed in Figure 6.5-6.7. This observation is very much different from the conventional amorphous pattern observed as growth in SBF.

Functional Group Identification in the developed materials – Fourier Transform Infrared Spectroscopy (FTIR)

FTIR spectra of the samples after hydrothermal treatment show (Figure 6.8 B-D) the formation of hydroxyapatite. Characteristic bands for PO_4^{3-} groups can be observed at 472 (ν2), 566 (ν4), 605 (ν4), 960 (ν1), 1030 (ν3), and 1104 (ν3) cm^{-1}. The peaks at 632 (νL) and 3560 (νs) cm^{-1} correspond to the structural -OH bands in the apatite while this is almost absent in the β-TCP precursor (Figure 6.8A).

The broad absorption bands around 3425 and 1635 cm^{-1} were attributed to the adsorbed water in all the samples after hydrothermal process. The weak bands between 1410–1550 cm^{-1} region and the peak at 872 cm^{-1} were attributed to carbonate groups. Two types of carbonate substitution can be observed in HA, A-site (hydroxyl ion site) and B-site (phosphate ion site). In B-site substitution PO_4^{3-} groups is replaced by CO_3-OH^- tetrahedron and causes -OH groups simultaneously exist at two sites. Hence vibration of -OH groups was disturbed by the substitution of CO_3^- OH^- which causes reduction of intensity in -OH band.

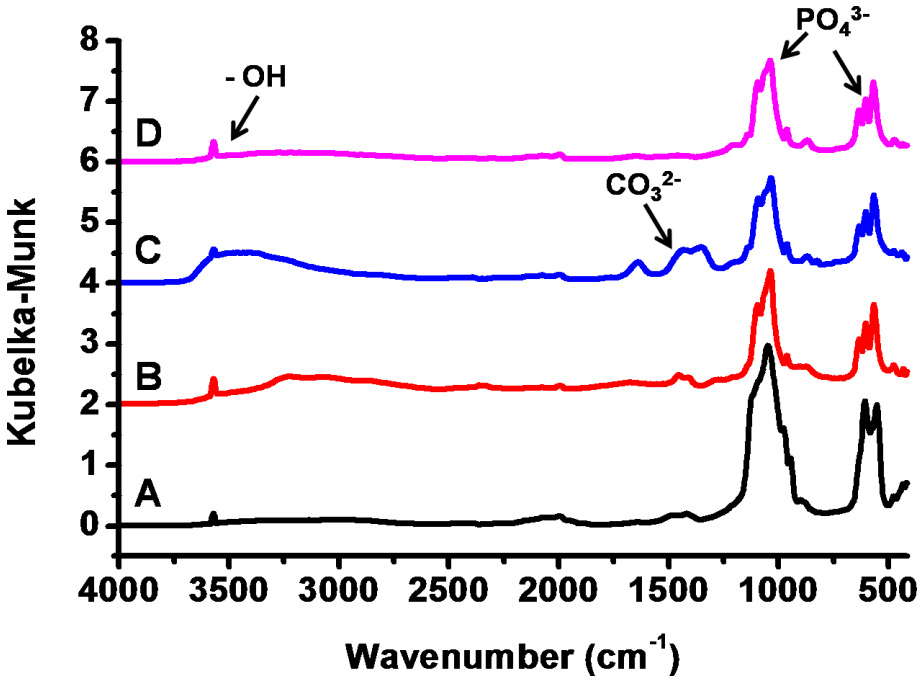

Figure 6.8. FTIR spectra of synthesised precursor β-TCP material (A), after hydrothermal conversion in ammonium phosphate (B), calcium nitrate (C) and calcium hydroxide solutions (D).

The structural -OH bands are weakened and the characteristic A- site substitution is totally absent confirming a typical B-site substitution in scaffolds converted in ammonium phosphate and calcium nitrate (Zhuang et al., 2012, Koutsopoulos, 2002, Nelson and Featherstone, 1982, Elliott et al., 1985, Chickerur et al., 1980, Binder and Troll, 1989, Panda et al., 2003). Carbonate substitution is almost negligible in scaffolds obtained from calcium hydroxide solution (Figure 6.8D). The FTIR results combined with the XRD data confirms the presence of carbonated apatite formation in ammonium phosphate and calcium nitrate derived materials whereas this substitution is absent in calcium hydroxide derived one.

After immersion in SBF, the scaffolds in AP and CN shows dissolution of carbonate whereas deposition of carbonate is seen in CH derived materials. The scaffolds incorporated more carbonate and hydroxyl ions on higher pH derived samples

(Arends et al., 1987). The FTIR spectra of the scaffolds immersed in SBF are shown in Figure 6.9-6.11.

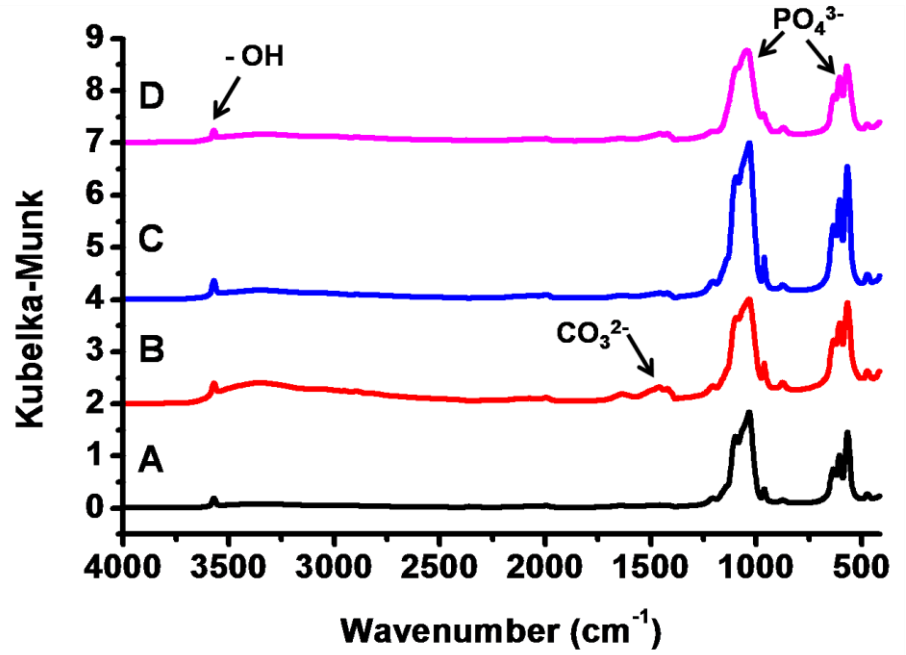

Figure 6.9. FTIR spectra of THA scaffold reacted in calcium hydroxide (CH) after immersion in SBF for (A) 1 day, (B) 3 day, (C) 7 and (D) 14 days.

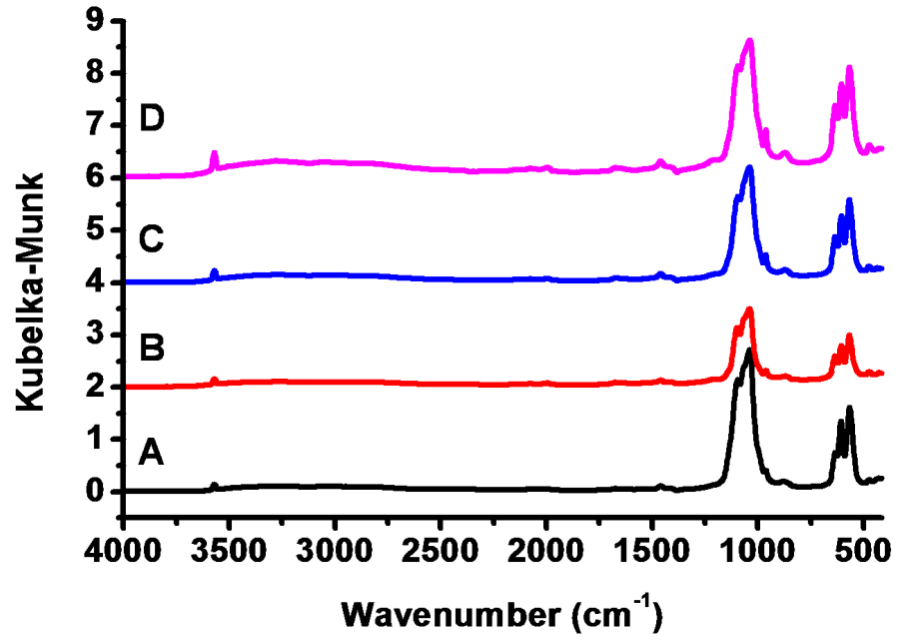

Figure 6.10. FTIR spectra showing influence of SBF over hydrothermally converted β-TCP scaffolds in ammonium phosphate for (A) 1 day, (B) 3 day, (C) 7 and (D) 14 day.

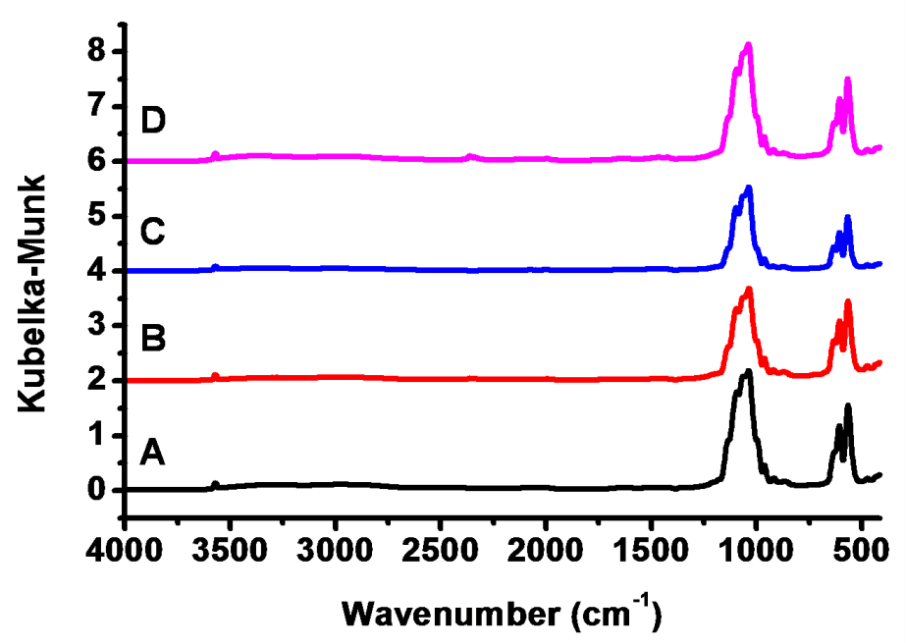

Figure 6.11. FTIR spectra showing influence of SBF over hydrothermally converted β-TCP scaffolds in calcium nitrate for (A) 1 day, (B) 3 day, (C) 7 and (D) 14 day.

Surface Characterization of THA- SEM

Optical image of the scaffold is shown in Figure 6.12 (A). These represents β- TCP discs of dimensions 13 mm diameter × 5 mm thickness. The morphology of precursor TCP ceramic before hydrothermal treatment is shown by ESEM in Figure 6.12 (B) and (C). The amorphous porous nature of the surface of the scaffold can be seen here too.

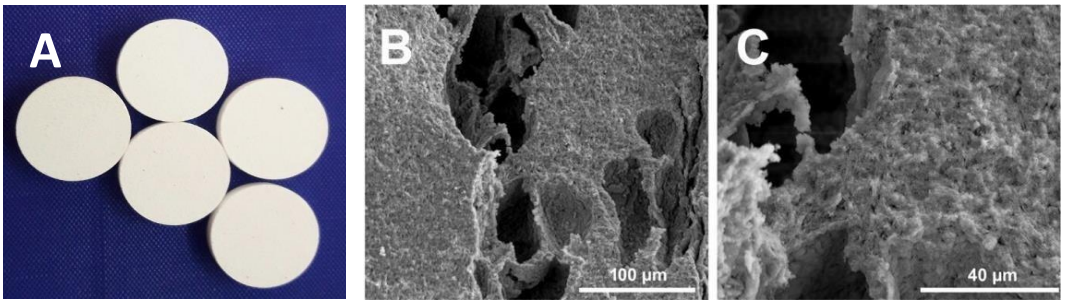

Figure 6.12. Optical images of the bulk THA scaffold (A) and scanning electron micrographs of β-TCP scaffold (B and C) before hydrothermal treatment.

The materials under hydrothermal exchange reactions showed lattice transformations and conversion to hydroxyapatite phase. Morphologies of hydrothermally converted scaffolds show crystal structures (Figure 6.13) resembling fibres, rods, flakes, flowery chrysanthemums, etc. which later transformed to morphologies resembling banana-like inflorescence, heaped hay- like bundles, and hollow tubular orientation of the crystals as a result of depositional apatite from simulated body fluid (Figure 6.10-6.12). HA fibrous rods with lengths about 15 μm and diameters around 1 μm can be observed in phosphate solution (Figure 6.13 A,B) whereas smaller dimensions of length 4 μm and diameter of 500 nm were seen in samples converted with calcium hydroxide solution (Figure 6.13 E,F). Clusters of chrysanthemum-like HA micro flowers were composed of HA nano- and micro rods with diameters of approximately 10 μm could be seen in samples converted in calcium nitrate solution (Figure 6.13 C,D). The possible impact of pH and specific ions of the solutions can be considered as the reason for the different crystal morphologies (Arends et al., 1987, Shen et al., 2015). As the reaction time increases, HA crystal structures gradually shift from chrysanthemum to plate-like by combination of the petals.

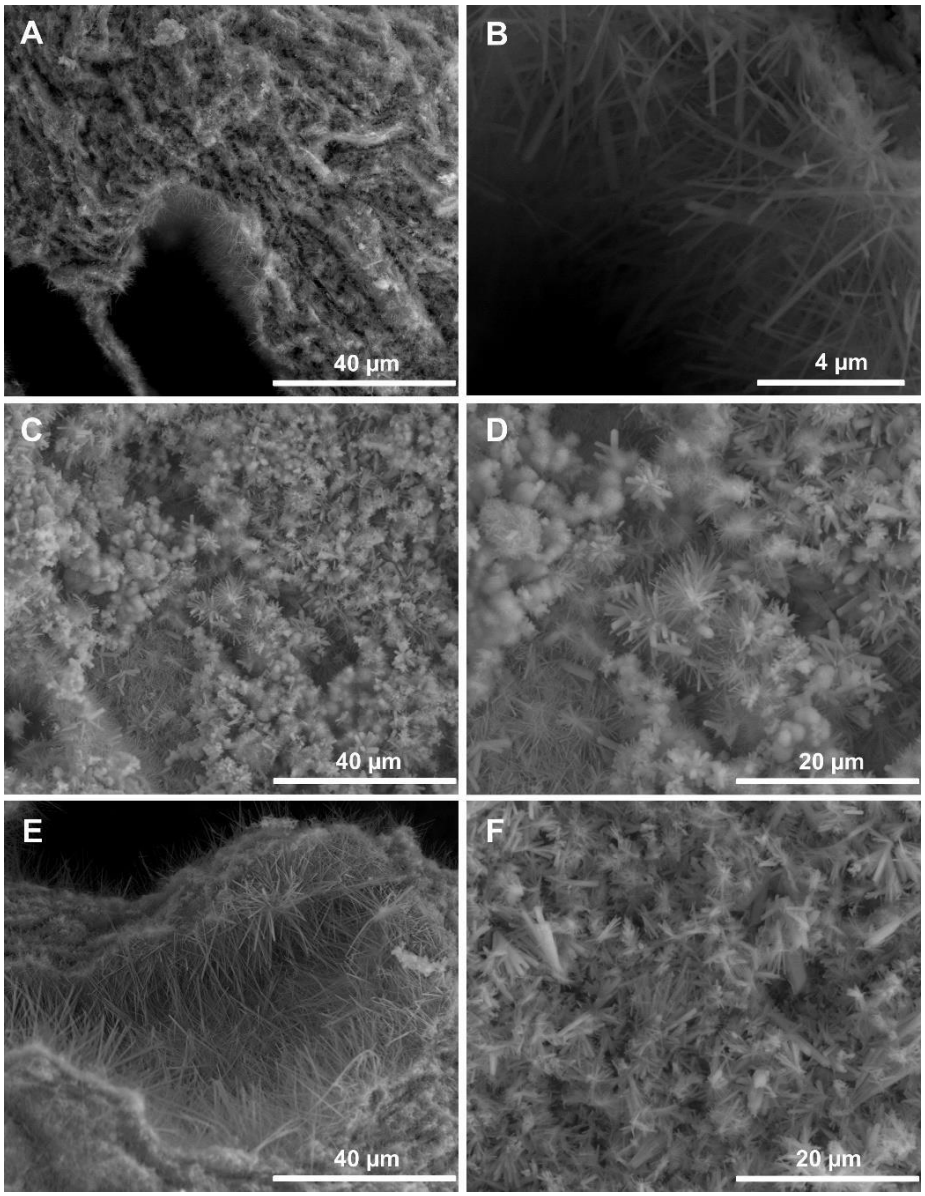

Figure 6.13. ESEM images of β-TCP scaffolds converted in ammonium phosphate (A, B), calcium nitrate (C, D) and calcium hydroxide (E, F).

In vitro bioactivity studies in simulated body fluid (SBF)

On immersion in simulated body fluid, the surface of the untreated scaffold was converted into spheroid morphology as a result of soaking in SBF for 14 days as shown in Figure 6.14. This change was observed as spheroids throughout the scaffold surface with dimension 0.5-1 µm. Even though varied surface morphology is

observed for β-TCP in about 14 days in SBF, the major phase is still TCP, which is confirmed by XRD (Figure 6.4).

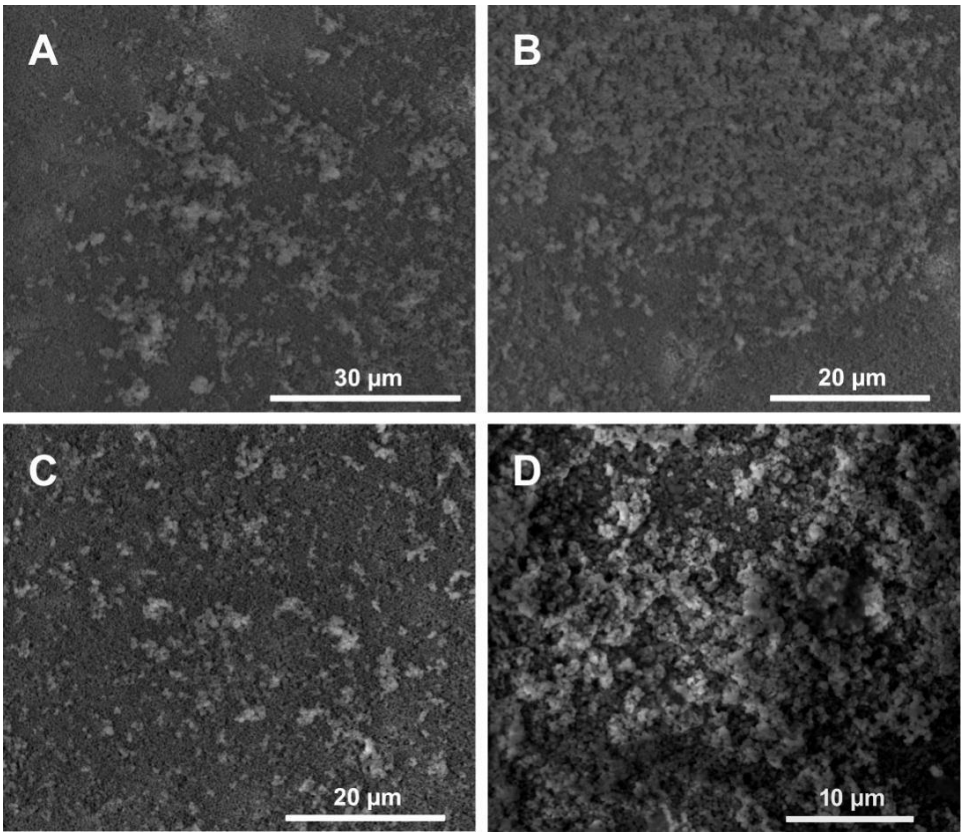

Figure 6.14. ESEM image of β-TCP precursor soaked in SBF for (A) 1 day, (B) 3 days, (C) 7 days and (D) 14 days

In the case of hydrothermally converted scaffolds, the crystal morphologies were further modified after soaking in SBF. Biomimetic deposition over the converted scaffolds for 1, 3, 7 and 14 days in various solutions show a variety of other microstructures differing from the conventional spheroid carbonated apatite growths from simulated body fluid. TCP samples converted in phosphate solution shows orientational modifications on the crystals from the third day (Figure 6.15 B) which then transforms to web-like structures and micro wells of 5 micron diameter on the

7th day (Figure 6.15 C,D). These structures, eventually turns to heaped hay-like bundles of apatitic calcium phosphates on the 14th day as in (Figure 6.15 E,F).

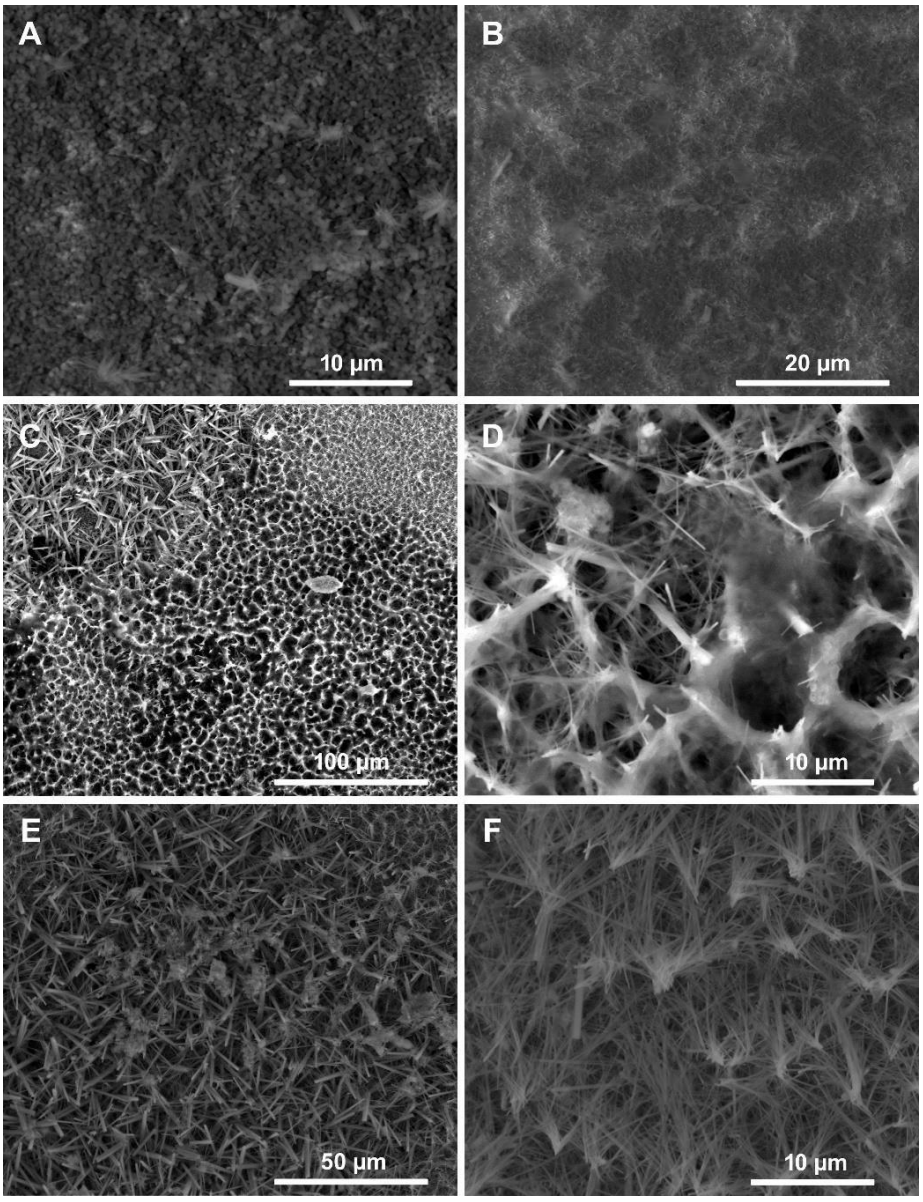

Figure 6.15. ESEM images showing effect of SBF over hydrothermally converted β-TCP scaffolds in ammonium phosphate for (A) 1 day, (B) 3 day, (C, D) 7 and (E, F) 14 days.

For samples converted in calcium nitrate solutions, during the first three days in SBF, the flowery chrysanthemums are just about to be oriented to enamel like structures and hay like clusters which is clearly seen on day 7 (Figure 6.16 C,D)

which later reorients itself to a tent-like nano array of crystal arrangements in about 14 days (Figure 6.16 E,F).

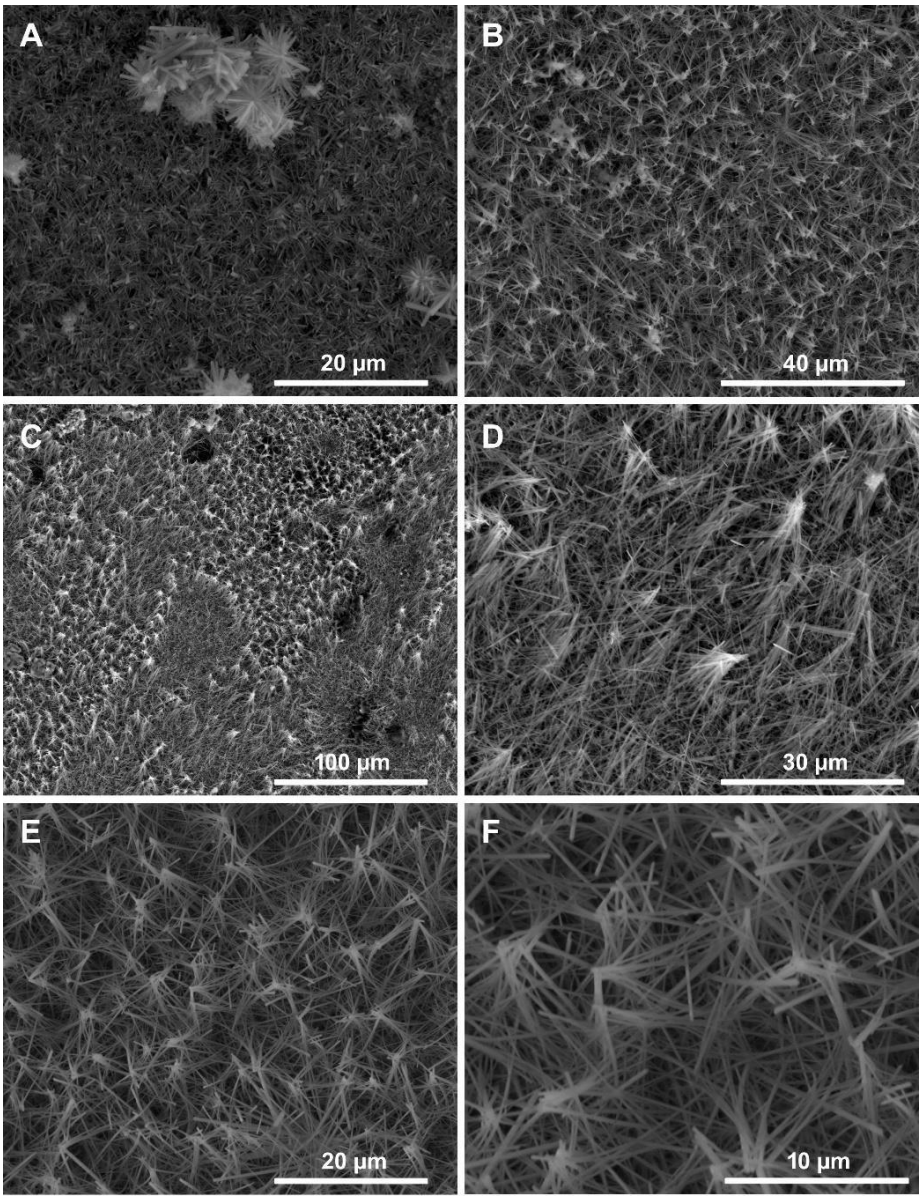

Figure 6.16. ESEM images showing effect of SBF over hydrothermally converted β-TCP scaffolds in calcium nitrate for (A) 1 day, (B) 3 day, (C, D) 7 and (E, F) 14 days.

Scaffolds converted in basic calcium hydroxide solutions forms tubular outgrowths of carbonated apatite from the existing crystals which grows from 1-10µm from day one to three (Figure 6.17 A,B) which eventually forms banana-like inflorescence of

arrays (Figure 6.17 C,D) on the 7th day. Here crystals take tubular as well as rod-like morphologies along a single strand growing in either sides of it. Finally, they exist as flowery growths of hollow tubes and nano rods of apatite all over the material on day 14 (Figure 6.17 E, F).

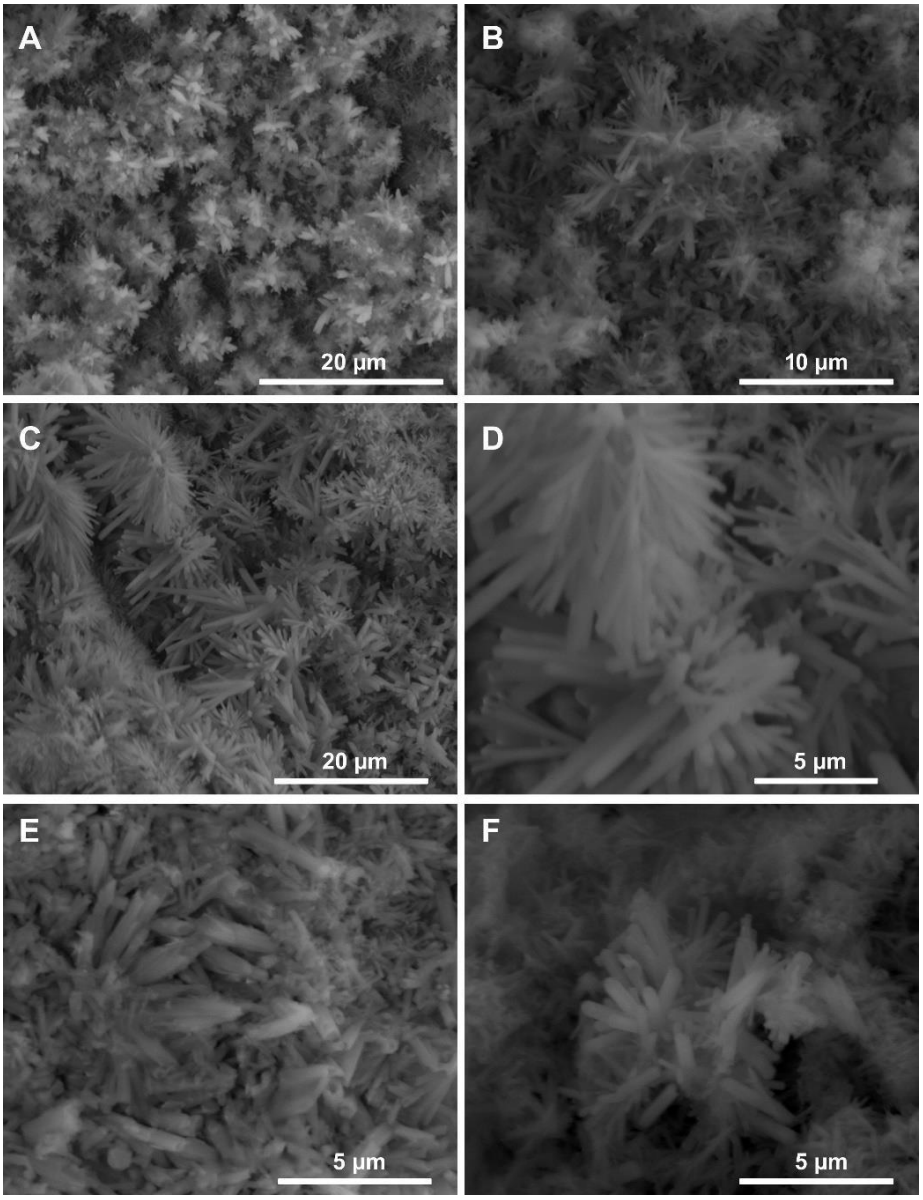

Figure 6.17. ESEM images of the effect of SBF over hydrothermally converted β-TCP scaffolds in calcium hydroxide for (A) 1 day, (B) 3 day, (C, D) 7 and (E, F) 14 days.

Evaluation of Weight Gain after immersion of the scaffolds in Simulated Body Fluid (SBF)

The scaffolds prepared by hydrothermal process when subjected to *in vitro* bioactivity analysis using SBF, taking β-TCP as the control which shows a gradual increase in weight as a result of interaction with the simulated body fluid (Figure 6.18).

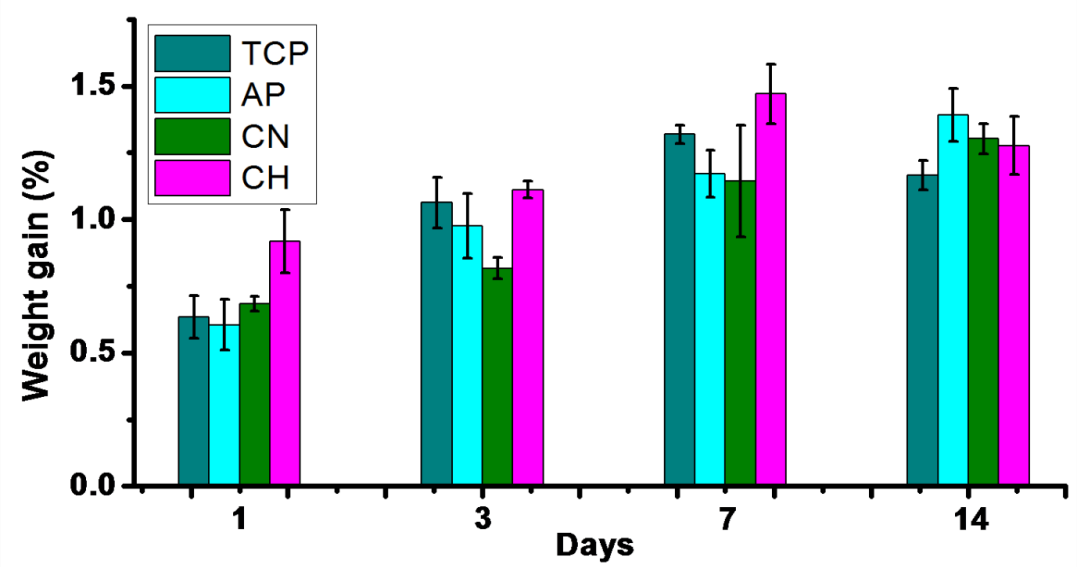

Figure 6.18. Graph depicting weight gain in scaffolds after soaking in SBF (TCP-control β-TCP, AP-Scaffold prepared using ammonium phosphate, CN-Scaffold prepared using calcium nitrate and CH-Scaffold prepared using calcium hydroxide.

In the case of scaffolds converted in ammonium phosphate, it is seen that the material shows a rapid growth and conversion to apatite from day one onwards. From ICP analysis, (Figure 6.19) it is evident that the Ca and P ion concentration of SBF drastically changed in 24 h, compared to the standard SBF.

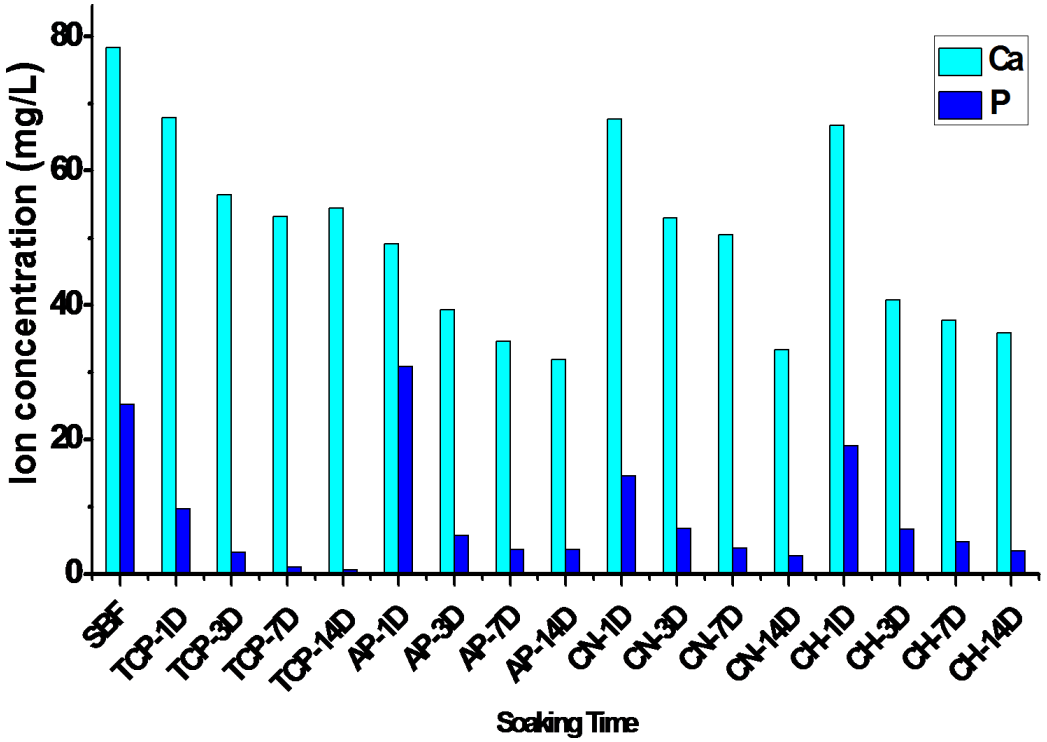

Figure 6.19. Calcium and phosphorous ion concentrations of SBF solutions after soaking: control β-TCP (TCP-1D to TCP-14D), (AP-1D to AP-14D), CN-1D to CN 14 D) and (CH-1D to CH-14D). The ion concentrations were compared with the freshly prepared SBF.

AP-Scaffold prepared using ammonium phosphate, CN-Scaffold prepared using calcium nitrate and CH-Scaffold prepared using calcium hydroxide

This difference in ion concentration is responsible for the gain in weight. During the first 24 h, the P ion concentration is increased in SBF while that of Ca is decreased. This indicates P ion is released to SBF from sample, while on the other hand Ca ions from SBF are taken by the sample. These exchange processes result in transformation of the lower calcium phosphate material to a more Ca rich (Phosphorus deficient) apatite compared to the starting material. There is no loss in weight during this period, but only change in ion concentration is observed. After 3 days, the decrease in both Ca and P ions shows similar trend, and these ions account

for the steady increase in weight gain without any abnormal behaviour till the 14th day. From ESEM images these differences can be observed as transformation of HA whiskers to an amorphous nature having less crystallinity on the first day which eventually shows a patterning of surface from the third day and leads to the deposition of Ca rich apatite with micro well formations on day seven and finally into bundles of micro and nano crystals packed together (Figure 6.15). In calcium nitrate solution, there is weight gain after soaking in SBF, but is less compared to that reacted in ammonium phosphate solution. The corresponding decrease in the Ca/P ion can also be observed. The Ca/P ion concentration ratio of SBF remain constant indicate that there is no preferential intake or accumulation of individual ion by the sample. Thus it is evident that a stoichiometric apatite growth is taking place for the sample prepared in calcium nitrate solution after SBF soaking. As the soaking duration is increased, the percentage of weight gain also increased. This stoichiometric deposition of apatite from SBF is seen in ESEM images as transformation of flowery chrysanthemums to random crystals on day one, to aligned and stacked bundles on days three to seven which then forms tented micro crystal orientations on day 14 (Figure 6.16).

For scaffolds converted in calcium hydroxide solution, even though conversion to apatite calcium phosphate is evident by XRD, SEM, etc. studies, the general behaviour in SBF looks similar to that of the control material (TCP) after 14 days. But there is considerable difference in the weight gain after 3rd day. This gain is found to be more for the sample treated in hydroxide solution than the control. The change in Ca/P ion is gradual in one day for the control, while similar change is observed only at 3rd day in the converted sample. The steady ion concentration from

3-14 days indicates the maximum conversion/deposition of apatite during this time. A slight decrease in weight gain is observed during 7-14 days may be due to the re-dissolution of calcium phosphate which is again evident by the small increase in ion concentration. This dissolution or exchange process can be considered as a mechanism towards attaining most stable phase of apatite in the simulated condition. ESEM images showed that HA nano fibres were transformed to tubular conical sprouts of crystals on the initial day which grows as number of days in SBF increases and transforms to the inflorescence-like structures aligned along a strand on day 7 (Figure 6.17). But as a result of the redissolution of Ca and P ions these structures get modified to the hollow cones of HA with phase stability and integrity. Also, it can be seen that the carbonate ions already present in the materials converted in ammonium phosphate and calcium nitrate are released to SBF but there is no reprecipitation of carbonate to the material even after 14 days of contact with SBF. Whereas in the case of materials converted in calcium hydroxide solution initially there is no carbonate substitution but after treatment with SBF, carbonate substitution is evident. This increase in carbonated apatite growth over crystals maybe due to the higher pH used in synthesis of the material. Hence the effect of pH and the difference in carbonate ion substitution can be stated as the main reasons for the morphological change from the conventional SBF deposition patterns. Materials derived from CH solution is seen to have more aspect ratio of carbonated apatite crystals forming thin elongated fibre-like structures and a higher apatite growth in SBF making it a better scaffold among the group.

Crystal morphology evaluation- TEM

The crystal morphology and dimensions were critically evaluated using high resolution transmission electron microscopy. TEM data Figure 6.20 shows that the material contains approximately 5 µm length and 0.1 µm thickness. The qualitative data for the Calcium to Phosphorus ratio was obtained from the EDAX Figure 6.21 which shows that the Ca/P ratio matches with the hydroxyapatite 1.67 confirming the elemental composition of the developed crystals.

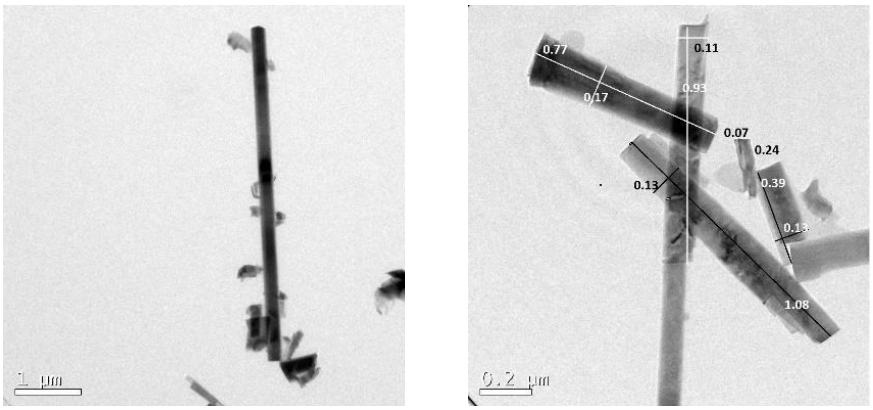

Figure 6.20. TEM images of isolated crystals of THA a) low magnification and b) high magnification.

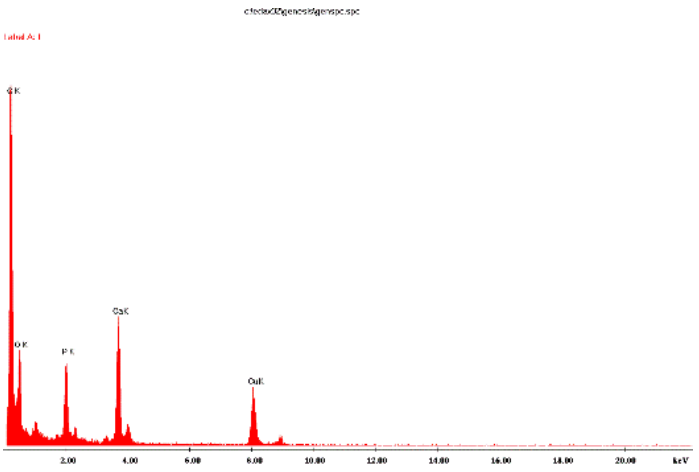

Figure 6.21. EDAX showing the Ca to P ratio of 1.67 in the isolated crystals from THA.

In vitro degradation studies in Phosphate Buffered Saline (PBS)

The degradation studies on the developed material was performed to evaluate the resorption behaviour of the developed materials. The cumulative release of Calcium and Phosphorus ions were estimated for 52 days by ICP-OES measurements. It was seen that there was a progressive release of calcium and phosphate ions with time. It is graphically represented in Figures 6.22 and 6.23. The dissolution study of the material demonstrates the resorption behaviour of the material under *in vitro* conditions. Around 20% weight reduction in the test samples were observed in the study period of 52 days indicating the dissolution of the material.

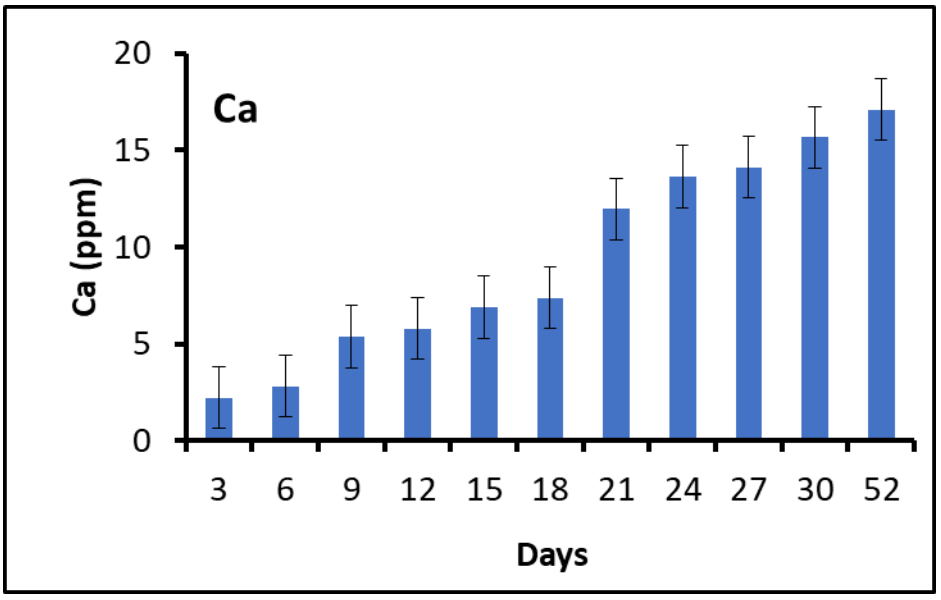

Figure 6.22. Cumulative Release of Ca ions from THA for a study period of 52 days.

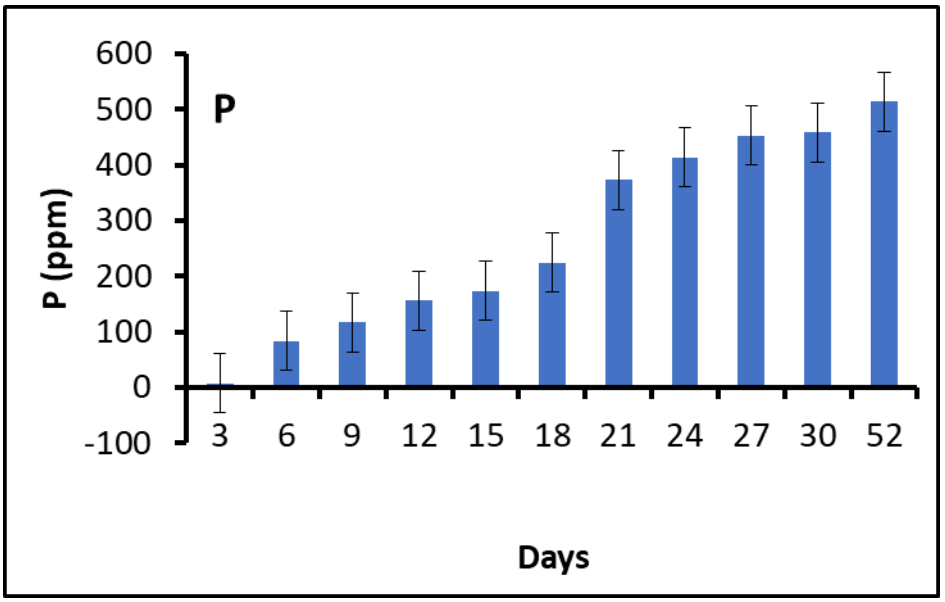

Figure 6.23. Cumulative Release of P ions from THA for a study period of 52 days.

Mechanical Property Evaluation -Compressive Strength

Mechanical strength is an essential criteria in the development of materials for bone tissue engineering applications. The materials should have sufficient mechanical strength to withstand the hydrostatic pressure and to maintain the spaces required for cell ingrowth and ECM production. Compressive testing has been successfully used in the characterization of cancellous bone and has also been adopted in the testing of porous and dense HA (Hodgskinson and Currey, 1990). Figure 6.24 shows the compressive strength evaluations of THA material with respect to porous sintered HA. Herein the compressive strength of TCP derived hydroxyapatite (THA) was 3.5 ±0.5. Compressive strength of sintered HA was 6.583 ± 1.8 MPa. These values are comparable to the compressive strength of trabecular bone of humans, which is in the range of 1.5 to 9.3 MPa, but not with load bearing sites like femur and tibia which showed a range of 90 – 215 MPa (Liebschner, 2004). Since the degree of porosity of the developed material was 25%, a compromise

between strength and porosity is always needed for the fabrication of a successful porous bone substitute.

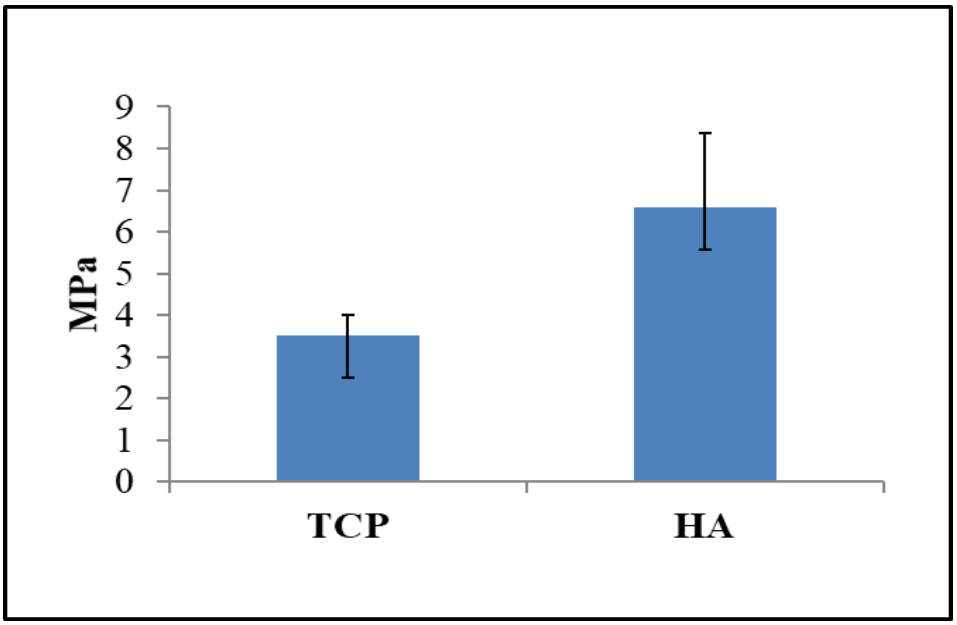

Figure 6.24. Compressive Strength of THA in comparison to porous HA.

Porosity Evaluation of the Material- Micro CT

Porosity analysis refers to the counting of empty space and characterization of their connections. Empty space is either fully surrounded by material on all sides, making it a closed pore, or if the empty space is not fully enclosed but at some point in 3D it can find a connection to the space outside of the object, it is defined as an open pore. Micro CT was used to determine the porosity of the developed material. This 3D radiographic imaging technique have a maximum spatial resolution of approximately 1 mm^3. Micro-CT is capable of achieving a spatial resolution of the order of 1μm^3 or less. Furthermore, it is an effective method for non-destructive 3D imaging of porous objects on a micrometric scale providing qualitative and quantitative information on the morphology of complex porous specimens, with high resolution at the

micrometric level. The pore network strongly affects the biological performance of the material *in vitro* and *in vivo* and have an influence on the permeability, rate of cell migration, and tissue ingrowth in biomaterials. Figure 6.25 (A) represents the 3D morphometry of the scaffold. The spacing profile of the particles in Figure 6.25 (B) clearly indicates the uniformity of particle distribution and porosity throughout the scaffold. Figure 6.25 (C) indicates the thickness profile of the particles in the scaffolds. The different colour coding given as a scale bar below represents the size of particles which are consolidated to porous discs.

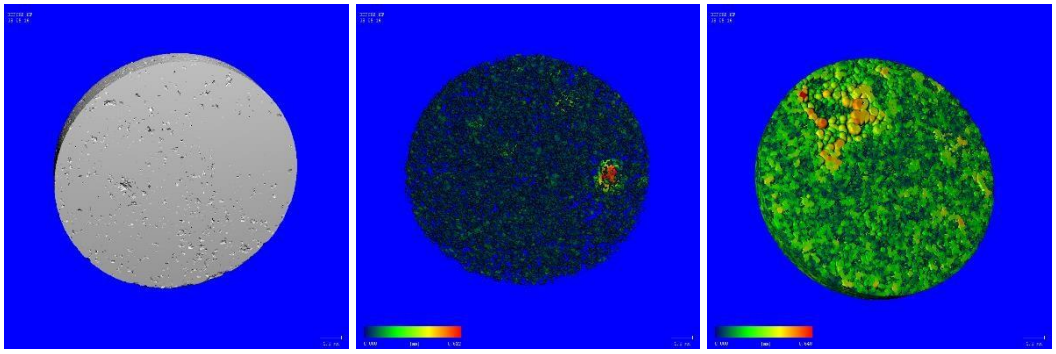

Figure 6.25. Micro CT of the 3D morphometry of the scaffold (A) Spacing Profile (B) and Thickness Profile (C).

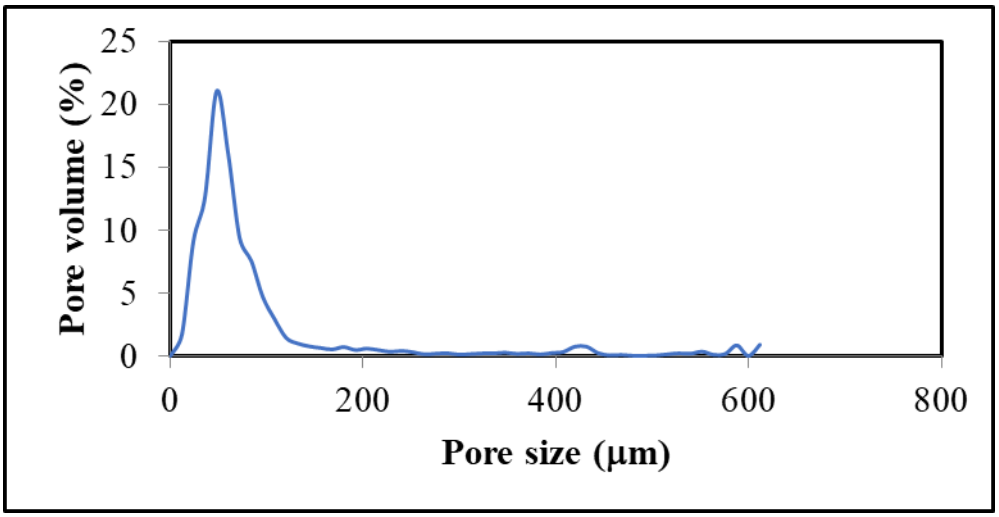

Figure 6.26. Histogram showing the pore size distribution in the developed materials.

Figure 6.26 represents the histogram showing the distribution of porosity in the material. It is observed that the THA material shows porosity in the range of (1-130 µm). From the trabecular spacing profile obtained it is clear that the material has almost uniform distributions of pores with interconnections throughout the material. By density calculations using Archimedes method it was found that THA showed 30% porosity. BV/ TV values from Micro CT studies support this finding showing 28% porosity in the scaffolds.

Cytotoxicity Evaluation by MTT Assay

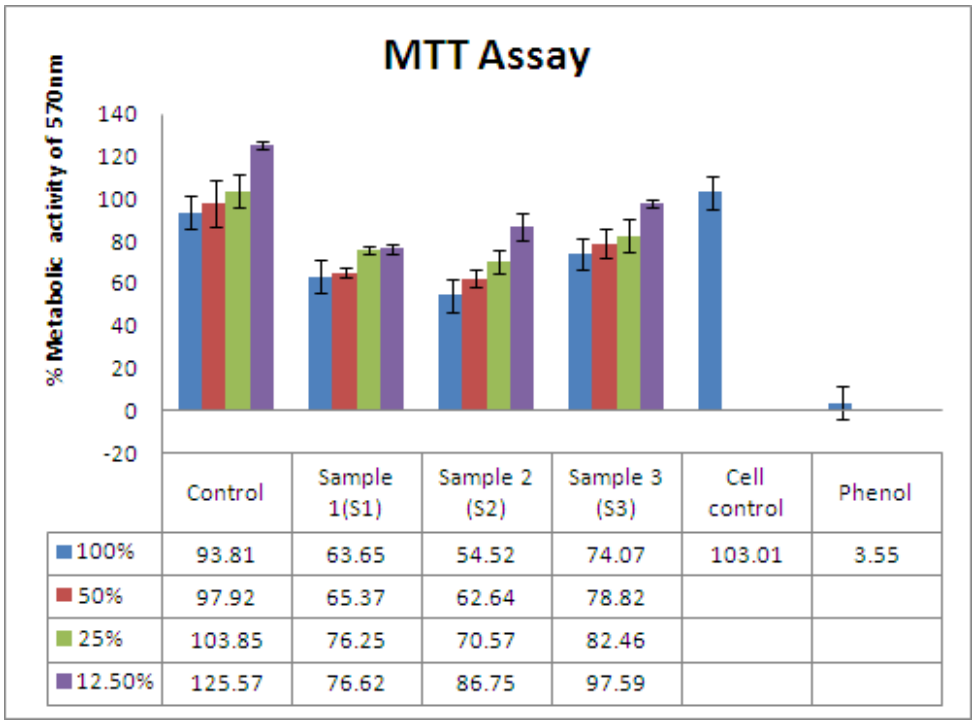

	Control	Sample 1(S1)	Sample 2 (S2)	Sample 3 (S3)	Cell control	Phenol
100%	93.81	63.65	54.52	74.07	103.01	3.55
50%	97.92	65.37	62.64	78.82		
25%	103.85	76.25	70.57	82.46		
12.50%	125.57	76.62	86.75	97.59		

Figure 6.27. MTT assay showing the non-cytotoxicity of the developed materials.

The cytotoxicity of the materials was evaluated by MTT Assay using L929 mouse fibroblast cell lines. It was seen that all the test materials were non-toxic to the cells in all the four concentrations of the materials tested namely - 12.5%, 25%, 50% and

100%. MTT assay measures the viability of cells by spectrophotometric methods. This colorimetric method measures the reduction of the yellow, water-soluble MTT (3-4,5 dimethylthiazol-2-yl) – 2,5-diphenyl tetrazolium bromide by mitochondrial succinate dehydrogenase. A minimum of four concentrations of the test material are tested. This biochemical reaction is only catalysed by living cells. Here control material is β- TCP alone, Sample 1 (S1) represents materials converted in AP, Sample 2 (S2) represents materials converted in CN, and Sample 3 (S3) represents materials converted in CH which is (THA).

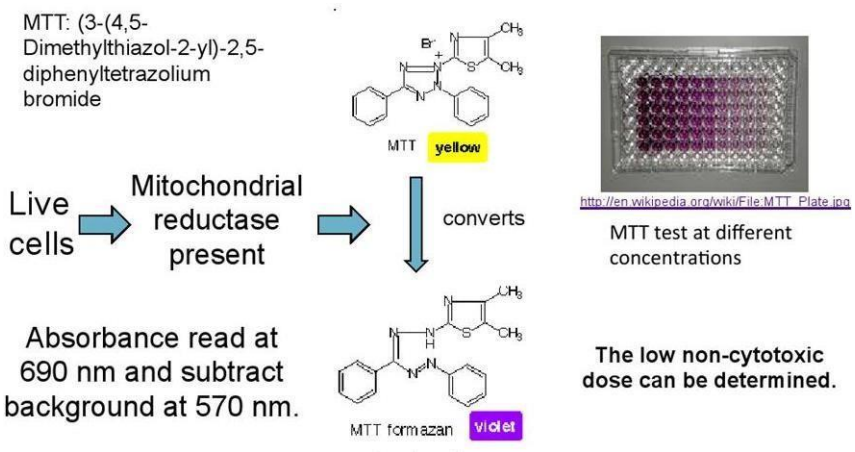

Cell Proliferation Study (Cell TiterBlue/ Alamar Assay)

Alamar blue assay was performed to evaluate the proliferation ability of the cells over the materials. In a 14-day period it was seen that the cellular activity increased progressively in the control TCP group as well as all the three converted materials. A slight decrease in the peak height was observed after 12 days in all three materials and controls. This is expected as a result of the onset of the differentiation phase which is normally seen after 14 days. Figure 6.28, 6.29, 6.30 and 6.31 shows the results from the cell proliferation studies.

Alamar blue assay quantifies the metabolic activity of the cells. If it is measured at a single time point, it can be used to determine the concentration of viable cells in a sample. If it is measured at two or more time points of the same or similar samples, the assay can be used to measure cell growth kinetics – the growth of a cell population over time. The alamar blue reagent contains non-fluorescent blue-coloured molecule resazurin, which is chemically reduced by the metabolic activity of cells into fluorescent red-coloured resorufin. Both the colour change and the change in fluorescence allow for the direct measurement of cell metabolic activity and viable cell concentration via absorbance or fluorescence measurements in a plate reader. Control Material is β-TCP, AP= materials converted in ammonium phosphate, CN= materials converted in calcium nitrate, CH= materials converted in calcium hydroxide= THA

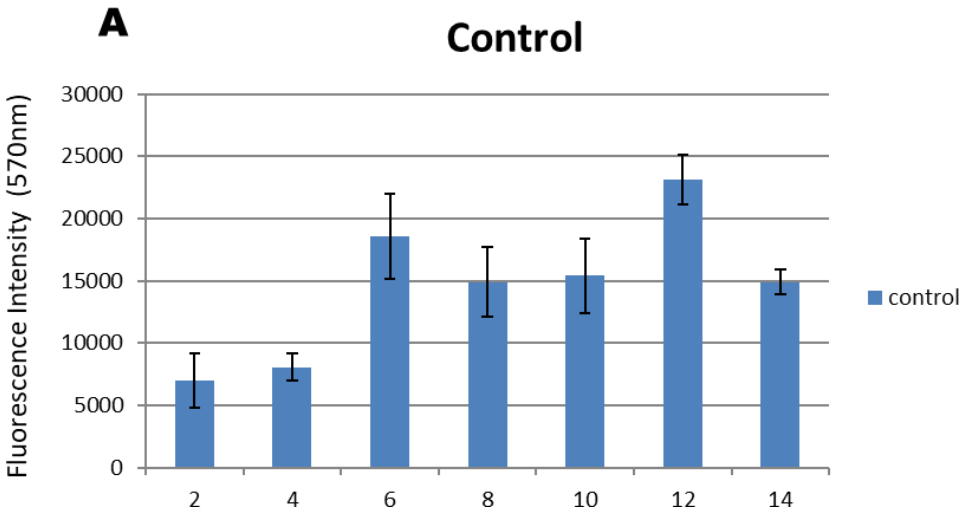

Figure 6.28. Alamar blue assay of control β-TCP materials.

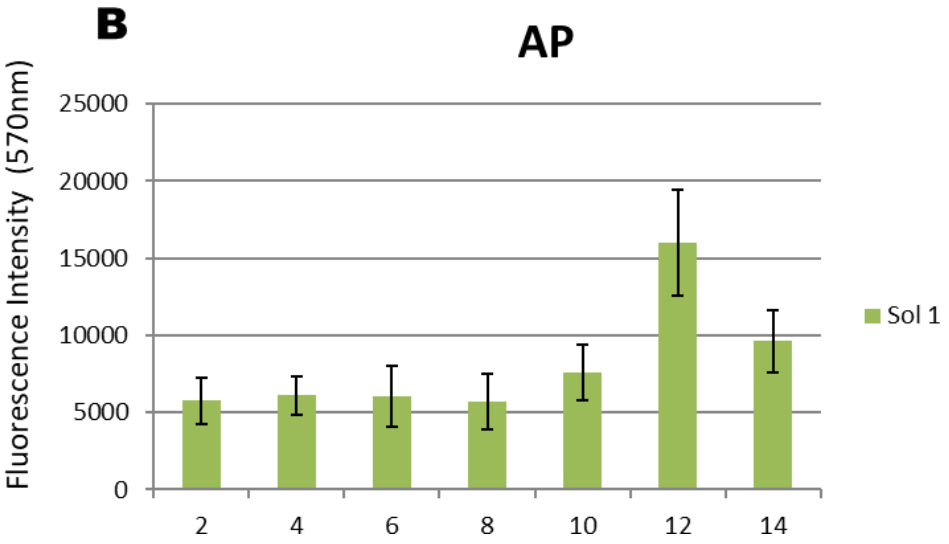

Figure 6.29. Alamar blue assay of materials converted in ammonium phosphate solution.

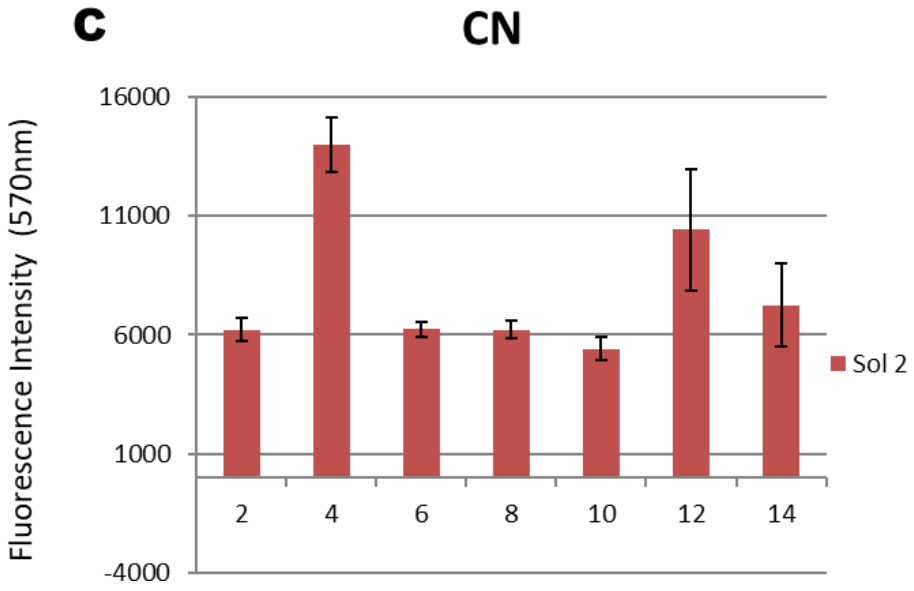

Figure 6.30. Alamar blue assay of materials converted in calcium nitrate solution.

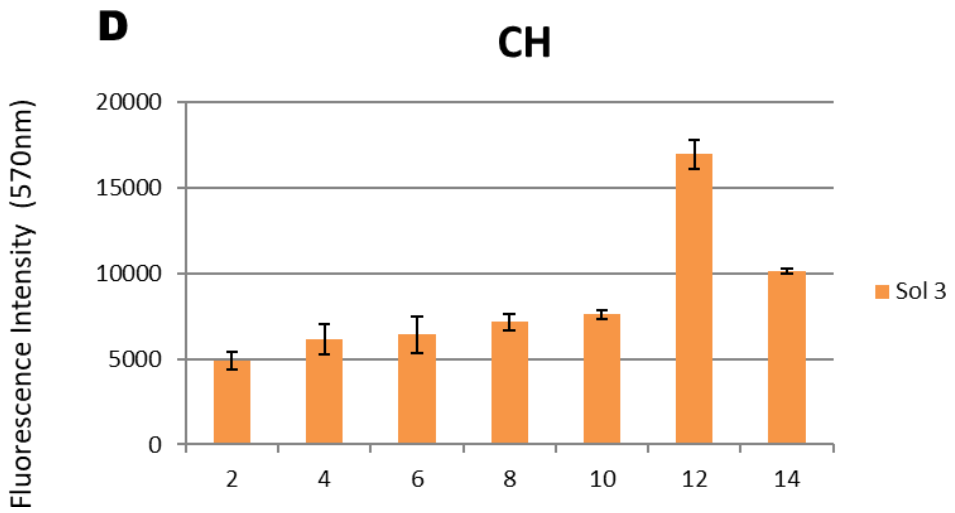

Figure 6.31. Alamar blue assay of materials converted in calcium hydroxide solution.

It was seen that the cells seeded over the scaffolds showed a proliferative growth during the study period of 14 days and a slight decrease in the cellular activity is seen from day 12 to day 14 in all the samples which may be indicative of the onset of the differentiation phase.

Phase II

Evaluation of the materials in vitro in combination with Rabbit adipose-derived primary mesenchymal stem cells (RADMSCs).

Cell-material interaction study by SEM

The cellular interactions on the developed scaffolds was evaluated by seeding RADMSs over the materials. The interaction of the cells with the HA crystals was visualized by SEM. It was observed that the scaffolds were cell friendly even as the cells expanded over the newly grown hydroxyapatite crystals.

After two days of culture the cells still adhered well to the apatite crystals. They were also seen to invade into the internal voids and interconnections of the porous scaffold, proliferated and maintained cell to cell contact with good adhesion to the substrate. The cells grew and spread all over the crystals like a canopy from the surface to the bulk of the material. Figure 6.32 shows the cell material interactions of the control TCP scaffolds with the cells. The control gives positive cell growth and proliferation as seen in the ESEM images. Figure 6.33 represents the surface of materials converted in AP medium. The interaction of ADMSCs with the c-axis oriented HA crystals, were seen to provide better anchorage and spread of the cells over the material surface. Figure 6.34 shows the interaction of the cells over the materials converted in CN medium. The apatite crystals even though of lower dimensions were seen to provide a base supportive of cell growth and proliferation. Figure 6.35 shows the cellular interactions over the hydrothermally converted samples in CH medium. Cells grew over the crystals showing their inherent proliferative ability.

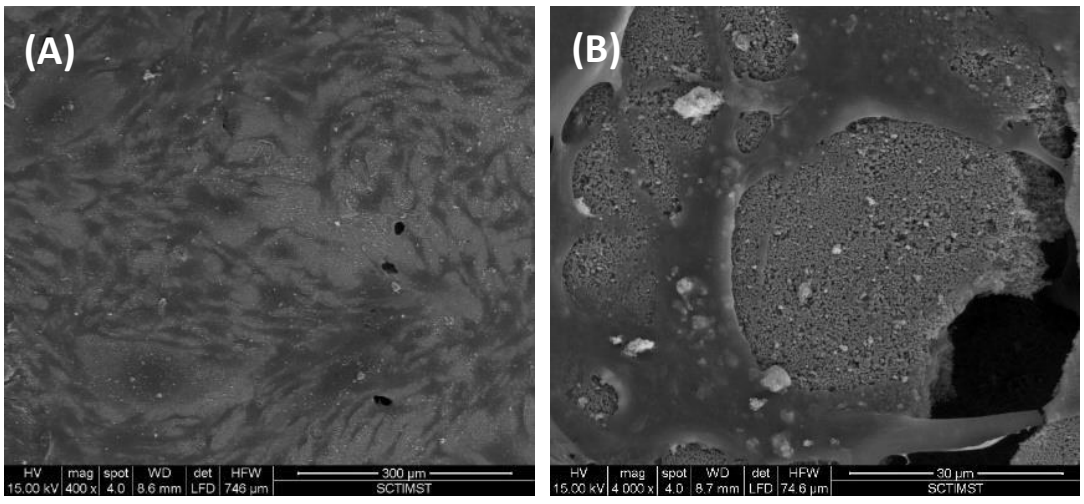

Figure 6.32. ESEM images of Control TCP - (A) and (B) showing cell attachment after 2 days in culture

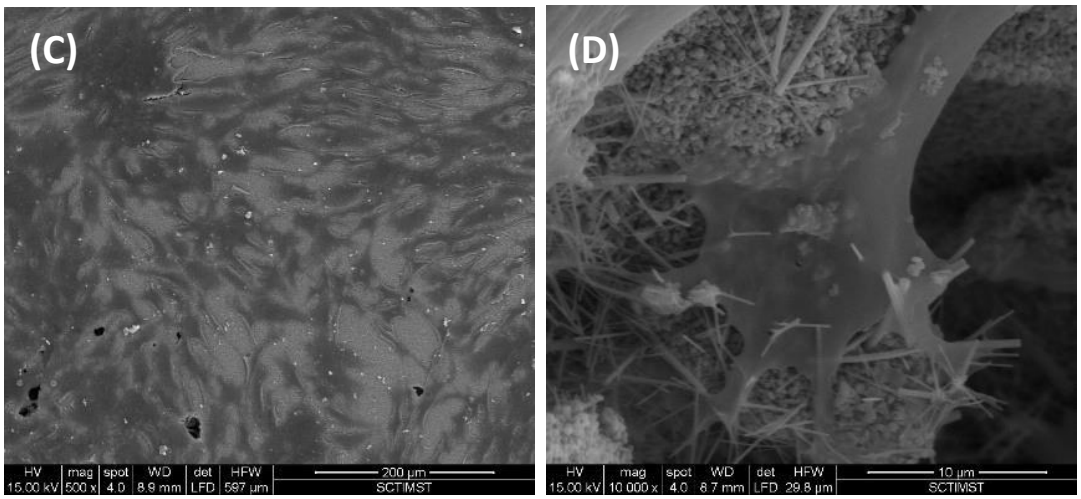

Figure 6.33. ESEM images of materials derived from AP reaction medium - (C), and (D) depicting cell attachment after 2 days in culture.

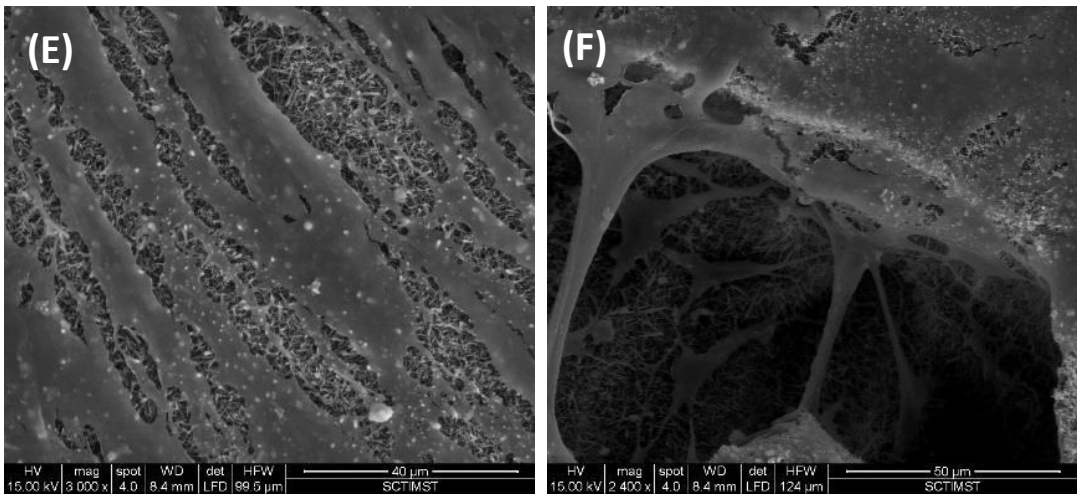

Figure 6.34. ESEM images of materials derived from CN reaction medium - (E), and (F) showing cell attachment after 2 days in culture.

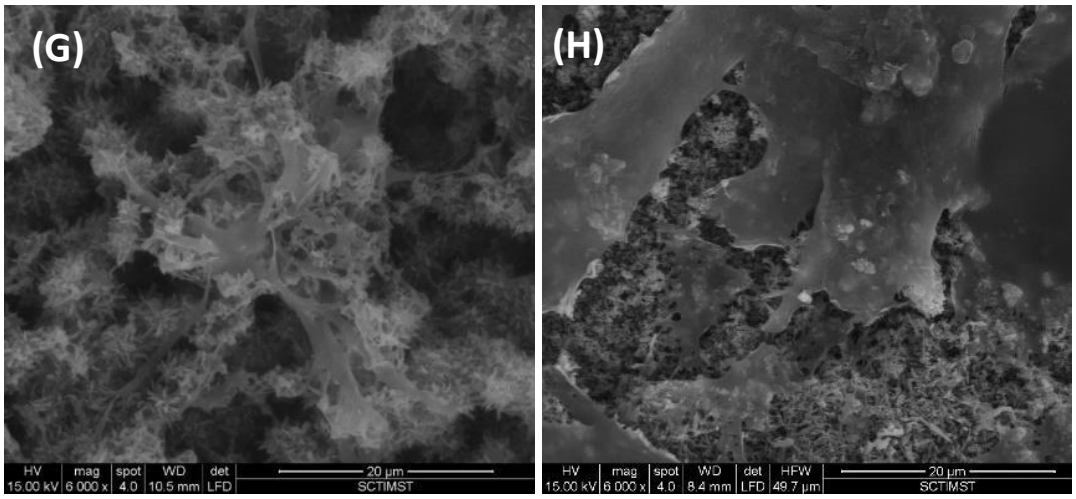

Figure 6.35. ESEM images of materials derived from CH reaction medium - (G), and (H) showing cell attachment after 2 days in cell culture.

Viability of ADMSCs on the scaffolds

Viability of cells on the scaffold was measured qualitatively by fluorescein diacetate and propidium iodide (FDA/PI) staining. Fluorescence-based live-dead assays can be used to evaluate the viability of mammalian cells. Simultaneous use of two fluorescent dyes allows a two colour discrimination of the population of living cells from the dead-cell population. FDA (non- fluorescent) is internalised in the cells and gets converted into the green fluorescent metabolite fluorescein. The measured signal is an indicator of viable cells as it is esterase dependent, whereas PI is the nuclei staining dye and it will not pass through a viable cell membrane. PI passes through the ruptured cell membranes of dead cells, reaches the nucleus and intercalates with the DNA double helix of the cell. A depth profiling was also done to see the presence of live and dead cells inside the pores of the scaffolds. The green cells were marked live and red cells dead. It was seen that the control and the test materials supported the growth on MSC's. The cells were seen to be alive on the material surface as well

as inside the pores. The samples were scanned up to 174 µm with a slice thickness of 10 µm for depth profiling.

The cells seeded scaffolds were analysed after 4 days. Figure 6.36 shows confocal images of the live dead staining of cells seeded materials - β- TCP control materials after 4 days in culture.

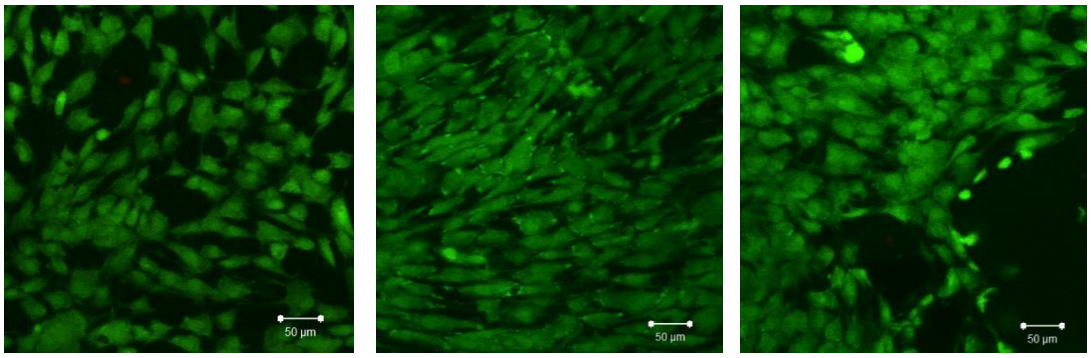

Figure 6.36. Confocal micrographs showing the presence of viable cells in the control (TCP) material after 4 days in culture.

Figure 6.37 and Figure 6.38 showed the confocal images of live stained cell seeded materials converted in AP medium. A depth profiling of the scaffolds were made up to 175 µm. Cells were seen to be alive in the pores after 4 days of culture indicating cell friendliness of the crystalline scaffolds.

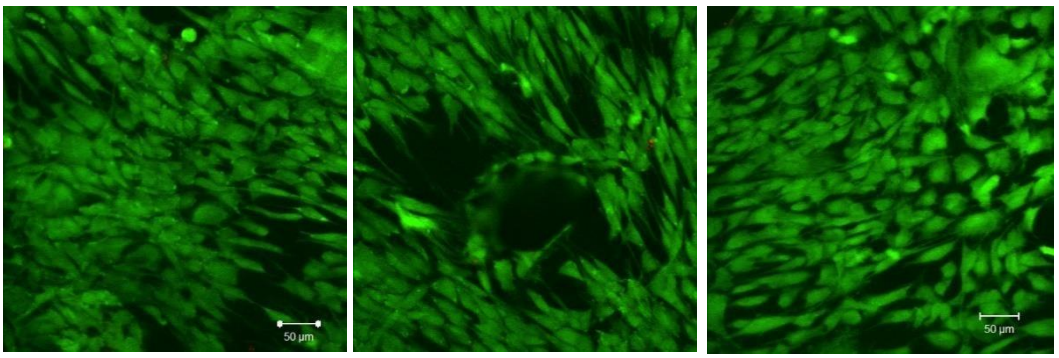

Figure 6.37. Confocal micrographs showing the presence of viable cells on the materials derived from AP medium after 4 days of culture.

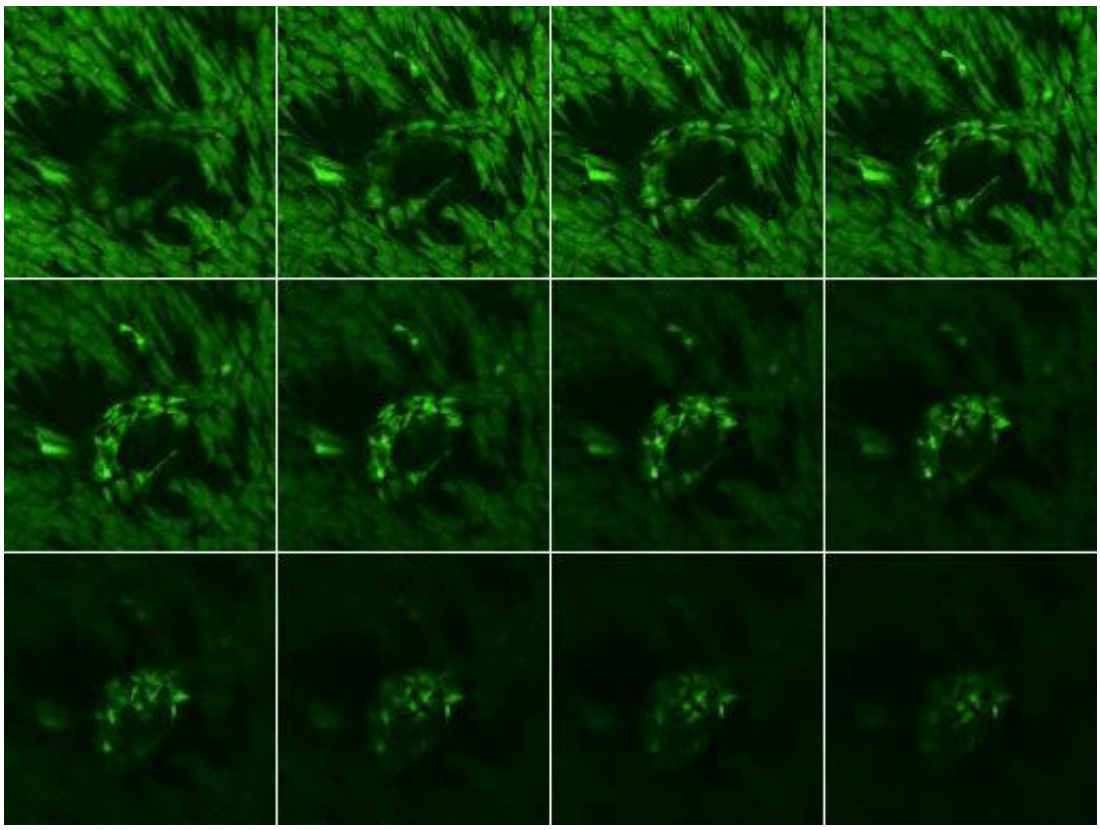

Figure 6.38. Confocal Images: Depth Profiling of a Pore showing the presence of live cells in a sample converted in AP medium (9 µm to 170 µm).

The scaffolds derived from CN medium shows the presence of live cells on the material (Figure 6.39), but the number of cells seen on the material surface are seen to be lesser in number when compared to the materials from AP and CH. However, there were no dead cells seen. This is an indication of the cytocompatibility of the material. Figure 6.40 shows a depth profiling of cells seeded scaffolds from CN medium. It is indicative of the presence of live cells visible inside the pores to a depth of 170 µm.

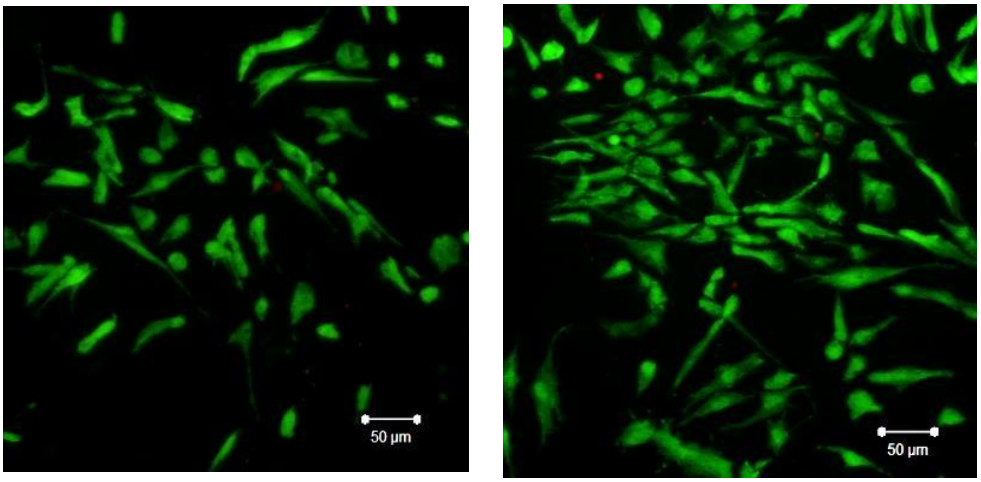

Figure 6.39. Confocal micrographs showing the presence of viable cells on the materials derived from calcium nitrate reaction medium after 4 days in culture.

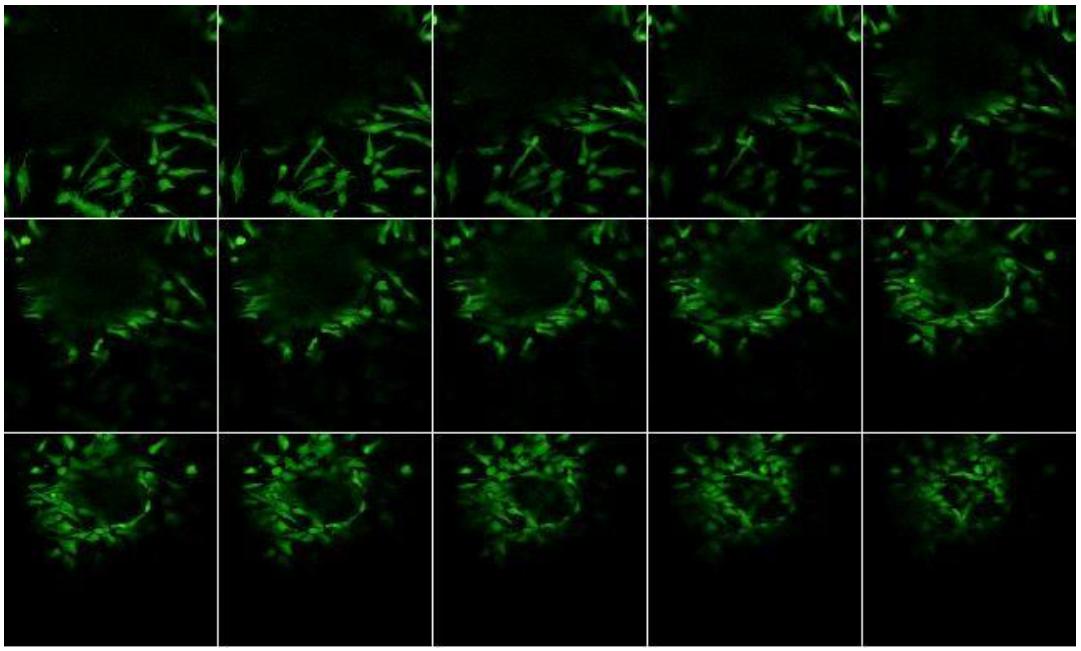

Figure 6.40. Confocal Images: Depth Profiling of a Pore showing the presence of live cells in a sample converted in $Ca(NO_3)_2 .4H_2O$ medium (9 µm to 170 µm).

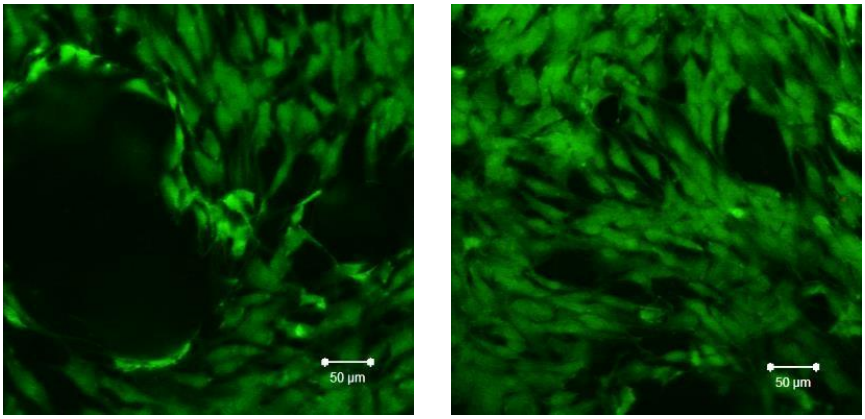

Figure 6.41. Confocal micrographs showing the presence of viable cells in the materials derived from calcium hydroxide reaction medium after 4 days of culture.

Confocal micrographs of cells seeded materials from CH are shown in Figure 6.41. The presence of live cells all over the material surface is visible. Figure 6.42 depicts a depth profiling of the cells seeded materials showing the presence of cells to a depth of 170 µm. THA proved to be cytocompatible by *in vitro* evaluations.

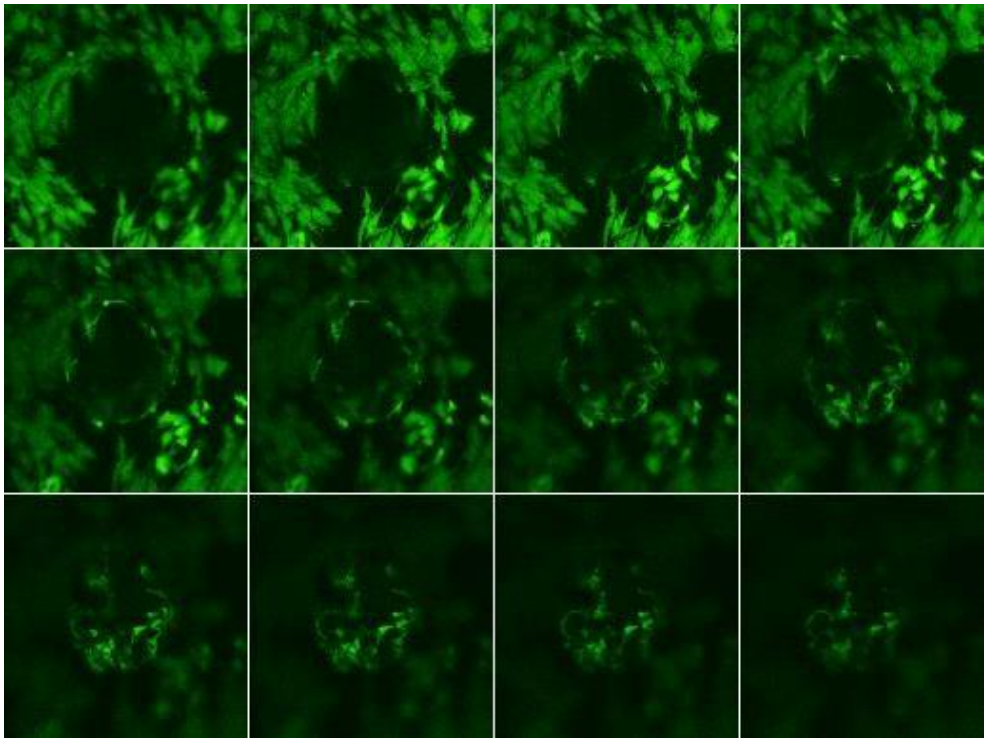

Figure 6.42. Confocal Images: Depth Profiling of a Pore showing the presence of live cells in a sample converted in $Ca(OH)_2$ medium (9 µm to 170 µm).

Alkaline Phosphatase Activity (ALP)

ALP, an essential enzyme for the deposition of minerals is present in pre-osteoblasts at an early stage of osteoblast differentiation and its level is found to be increased around the second week of culture (zur Nieden et al., 2003, Stein et al., 1990). ALP activity is a critical parameter for the bone mineralization process under *in vitro* and *in vivo* conditions. The phosphatase enzyme acts on the organic phosphate and release free phosphate ions, aiding the active transport of ions across the cell membrane. The process of formation of calcium phosphate crystals are initiated which eventually leads to mineralization of the matrix (Ciapetti et al., 2003). Addition of osteogenic supplements on ADMSC cultures upregulate the production of collagen-rich matrix and also increases the expression of non-collagenous proteins like ALP, osteocalcin etc. (Ohgushi and Caplan, 1999). The stem cell potential of the ADMSC's are reported to get accelerated using dexamethasone (dex) and β glycerophosphate (βGP) which results in the mineral matrix formation under *in vitro* conditions (Ohgushi et al., 1989). Taking a similar approach, the newly developed materials with cells were evaluated for their osteogenic differentiation on the scaffolds prior to implantation. Biochemical data (Figure 6.43) showed a gradual increase in the ALP activity during the culture period, is found to increase up to 21 days. In the calcium deficient apatite from AP, the ALP was seen to peak till the 14^{th} day and decline thereafter. Whereas in the case of CN and CH scaffolds the ALP activity was seen to gradually increase till 21 days.

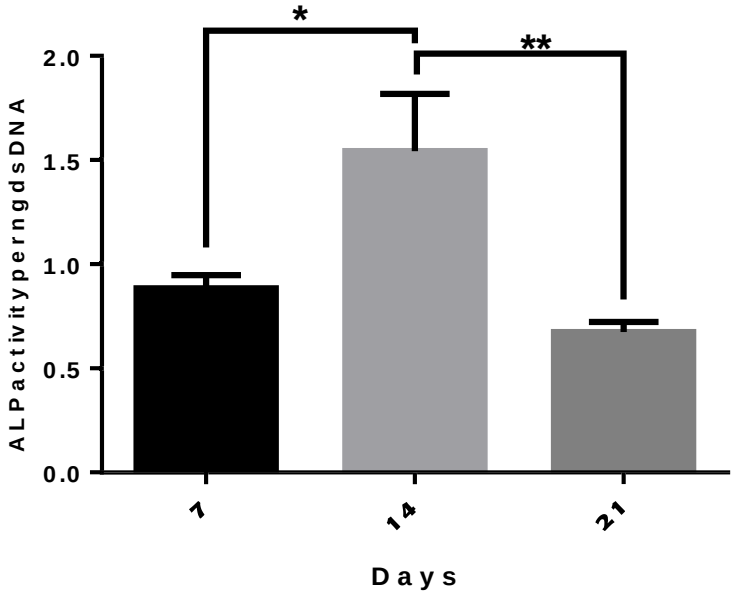

Figure 6.43. ALP activity of the cell seeded material after 7, 14, 21 days of cell culture in osteogenic media: AP- material converted in $NH_4H_2PO_4$

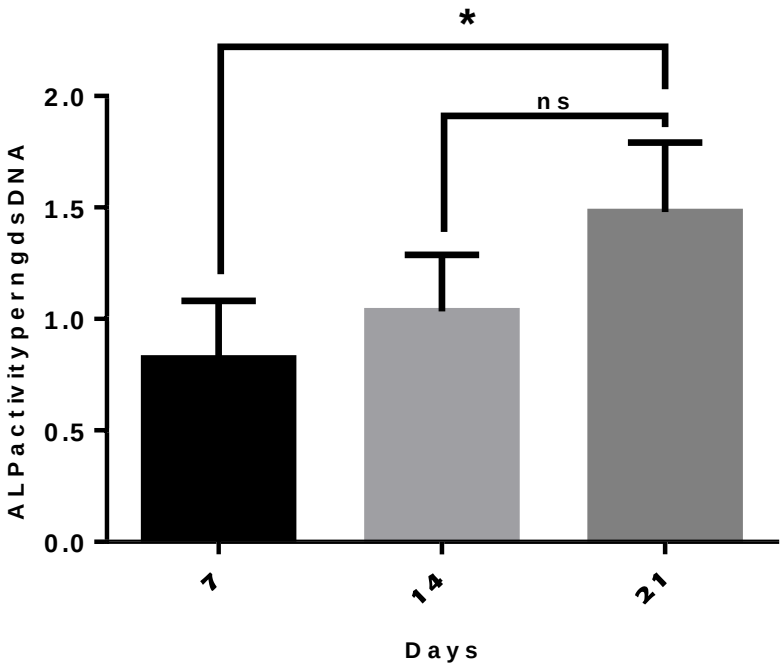

Figure 6.44. ALP activity of the cell seeded material after 7, 14, 21 days of cell culture in osteogenic media: CN- material converted in $Ca(NO_3)_2 .4H_2O$

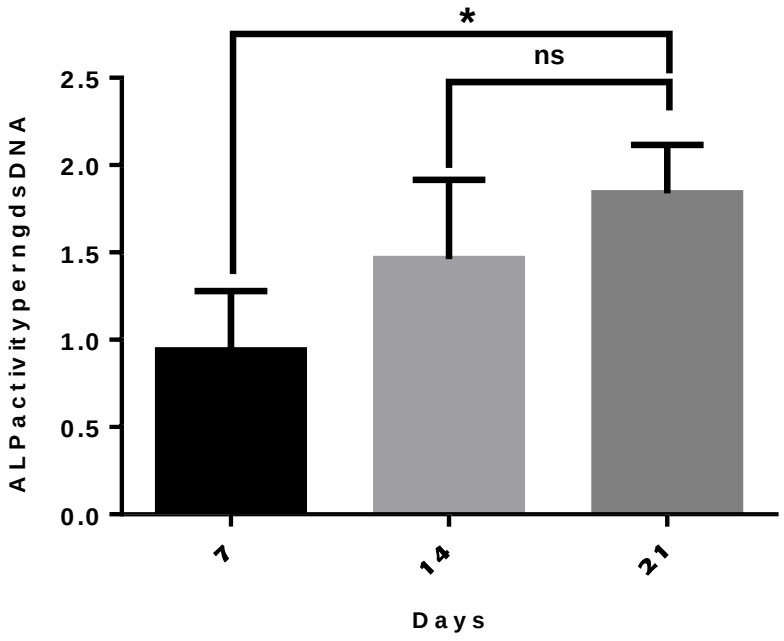

Figure 6.45. ALP activity of the cell seeded material after 7, 14, 21 days of cell culture in osteogenic media: CH material converted in $Ca(OH)_2$ = THA.

From the design and *invitro* evaluations of the TCP derived materials, it is clear that they are prospective scaffolds for tissue engineering applications. The safety and efficacy of the THA material were evaluated as dental extraction socket fillers in a rabbit dental defect model. The results obtained are presented in chapter 7.

Summary

Hydroxyapatite scaffolds were fabricated from a lower calcium phosphate precursor (TCP) by hydrothermal exchange reactions in three different reaction mediums by varying the kinetic and thermodynamic parameters to obtain maximum conversions. THA material (from CH medium) was selected from the group based on the calcium to ratio of the scaffolds. C-axis oriented crystal growth pattern was observed in THA materials. Upon *in vitro* bioactivity studies in simulated body fluid these crystals

transformed to surface patterning with the formation of bimodular structures with micro and macro features. This growth pattern in SBF was entirely different from the amorphous calcium phosphate deposition usually formed over sintered ceramics. Further the materials were non-cytotoxic and cell friendly which was confirmed by MTT assay, viability assays and cell material interaction studies. The ALP activity measurements shows that the material has a good performance as a tissue engineering scaffold for orthopaedic applications.

CHAPTER -7

EVALUATION OF THE HYDROTHERMALLY DERIVED MATERIALS AS A DENTAL EXTRACTION SOCKET FILLER

Introduction

Tooth extraction is a common procedure usually done when a tooth suffers from decay, abscess, gum disease or injury. From the time a tooth is removed, the surrounding bone namely the alveolar ridge bone decrease in volume and undergoes degenerative changes. This bone loss is possible to occur in two dimensions. One is loss of horizontal width caused by the collapse of the bone surrounding the socket making the remaining ridge narrower than when the tooth was present. Another is loss of vertical height which makes the remaining bone less tall (Figure 7.1). This process is faster in areas where you wear a partial or complete denture [online available from https://www.drwdcampbell.com/procedures/socket-preservation, (accessed on 24-03-2019)]. These changes are usually clinically significant and can make placement of a conventional bridge or an implant-supported crown difficult. A significant resorption of the underlying bone causes the placement of a dental implant extremely challenging.

In a typical clinical study, it was seen that post extraction of tooth followed by no bone filling resulted in decrease of alveolar bone volume. In a 12 month study of post extraction of the tooth it was seen that the width of the alveolar ridge decreased

50% (from 12 mm to 5.9 mm, on average), and two-thirds of the reduction within the first 3 months (Dimova et al., 2014).

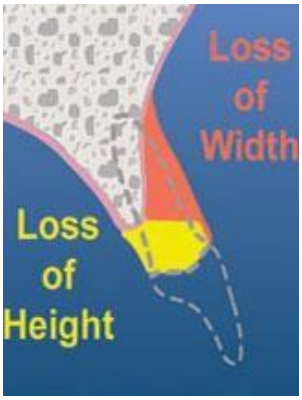

Figure 7.1. Pictorial representation of bone loss after tooth removal

The percentage reduction was larger in the molar compared with the premolar region. The level of bone regenerated in the extraction socket never reached the coronal level of bone attached to the tooth surfaces distal and mesial to the extraction site. The bone surface becomes curved apically. Pictorially these changes are seen as in the following images 7.2 (A) and 7.2 (B) (Irinakis, 2006). These changes in the degeneration of the underlying bone makes the restorative procedures difficult.

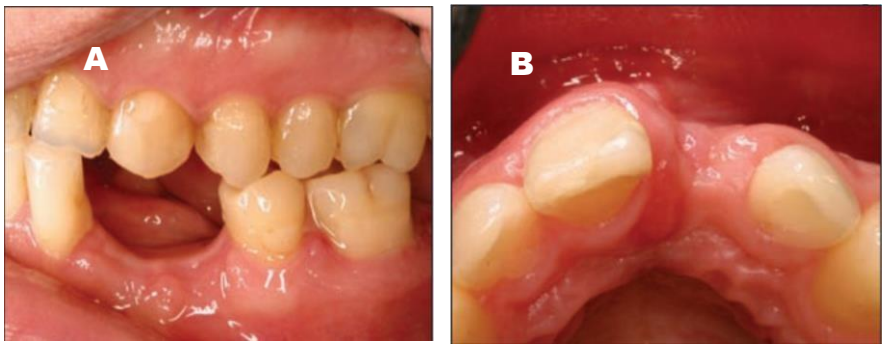

Figure 7.2. Clinical Study showing the loss of bone mass after tooth removal;

(A) Reduced height of alveolar ridge following extraction of the lower left canine and first premolar; (B) Collapse of buccal socket wall two months after extraction of the upper left central incisor.

Importance of Alveolar Ridge Preservation

Replacement of an extracted tooth has several options available in the market. All the available choices rely on the available bone support and bone contour for the best function and aesthetics. One of the major choice for the replacement of tooth is by placing dental implants. Dental implants are root-shaped supports that hold our replacement tooth. Depending on the bone support available stronger implant replacements are possible. If the alveolar bone degrades /resorbs to a point where implant fixation is not possible, complex bone grafting procedures are required to create the necessary support. Obviously, preventing bone loss is much easier than recreating the bone later. Another choice would be to replace the tooth with a fixed bridge. This restoration method is supported by the adjacent tooth to the missing tooth space. The replacement tooth (pontic) spans across a space and if the bone is deficient, there will be an unsight area under the pontic that can trap food and also affect our speech. Other alternatives include removable partial or full dentures which perform better with more supporting bone.

Maximum care is taken by dentists while extracting a tooth so as to preserve the bone in the best possible way. Placement of bone replacement/graft materials to the extraction socket is another alternative. Once the tooth is extracted, the socket will be packed with a bone-like material and covered with a small absorbable plug or suture. The grafting material will support the tissue surrounding the socket, and in time gets replaced by new alveolar bone. This bone will be an excellent support to place a dental implant-supported replacement tooth later. Placement of dental implants four to twelve months after the extraction and socket grafting will provide the best long-

lasting support for preserving the alveolar bone and allows functioning as before. The treatment procedure in the application of bone fillers and the placement of dental implants with artificial tooth are illustrated in Figure 3(A), 3(B) and 3(C) given below.

Figure 7.3. (A) Cross section showing the extraction socket marked in blue and the surrounding alveolar bone marked in red, (B). A typical bone graft filling, (C) Implant fixation and artificial tooth placement.

Dental Extraction Socket filling is one of the major areas where ceramic materials are used in the shape of tooth roots and such implants are known as 'root form implants' (Denissen and de Groot, 1979). Cone shaped materials usually in (30 × 10 × 10) mm size are used for this purpose. The synthetic roots are placed 2mm below the crest and the influence of lower and upper teeth is also checked to avoid failure due to mechanical loading. Root cones requires very low flexural and torsional strength. The post clinical evaluation is done two years after the implantation procedure is done. Evaluation of the healing process and the tissue binding to the material is performed using radiographic analysis for a qualitative data interpretation. Usually no clinical rejection of inflammation, formation of fistulae, ulceration or pain is observed in case reports and it is seen that the experiments have high success rate. Commercially available extraction socket filler Osteo Gen® Plug (Figure 7.4) in the shape of root forms are available in two different dimensions.

Figure 7.4. Commercially available root form filler OsteoGen® Plug

OsteoGen® Plug is a bioactive, resorbable crystalline hydroxyapatite bone graft similar to the composition and chemistry of human bone. The crystal clusters of HA in OsteoGen® are proven to be safe, reliable and clinically effective for use with implants for over 30 years. The product is available in various sizes – 10 mm in Diameter × 20 mm in Length, or Slim: 6 mm Diameter × 25 mm in length. Collagen derived from bovine source is used as a carrier material in the graft. Type I collagen acts as a wound dressing to stabilize the clot and to absorb and deliver blood flow to the slowly resorbing graft. This helps in the initiation of bone formation and early angiogenesis. It also provides an environment for keratinized tissue to develop over the grafted site.

Various grafting materials have been used to preserve the socket or augment the lateral ridge before implant placement. Literature justifies the use of bone grafting materials in freshly extracted sockets. When demineralized freeze-dried bone allograft (DFDBA) was used as a filler material the width of the alveolar ridge decreased from 9.2 mm to 8.0 mm, while in the naturally healed ones the decrease was from 9.1 mm to 6.4 mm on average. When placing xenografts or DFDBA in fresh extraction sockets, Becker et al (Becker et al., 1998) found that there was

minimal vital bone-to-implant contact (BIC). In such studies the histology of the samples were taken within 3–6 months of extraction and it is common to wait 6–9 months to place implants when using these materials. Bioactive glass fillers was reported for longer healing time for even a small amount of new bone to be incorporated into the graft (Norton and Wilson, 2002).

Experimental Procedure

The resorption potential of the developed materials CHA and THA were assessed by implanting the material as a dental extraction socket filler in rabbit models. The animals were incubated with 3mm uncuffed endotracheal tube and ventilated at 35mm tidal volume at a rate of 30 breaths per minute as shown in Figure 7.5A. Oral commissurotomy was performed on the left oral commissure to access the left mandible and the first premolar tooth of the animal, Figure 7.5 B and 7.5 C. The tooth extraction was performed using forceps and the extracted tooth is shown in Figure 7.5 D. The socket filling is done using the fabricated CHA and THA filler cones as test materials and HA granules as control. Figure 7.5 E shows the filling of the extraction site. The site was then washed with sterile PBS and the gingiva was apposed over the implant using 5/0 proline suture and the oral commissurotomy was closed with 3/0 silk suture shown in Figure 7.5 F.

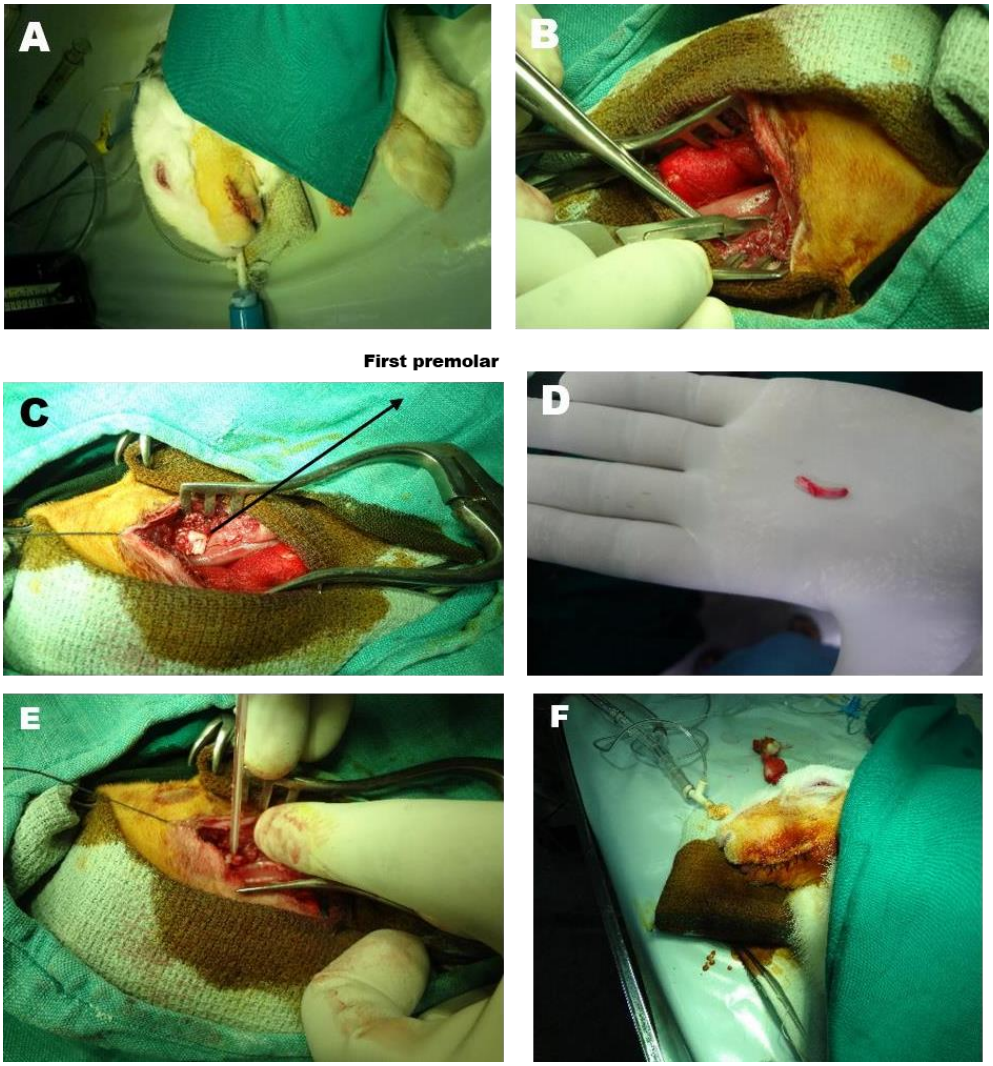

Figıre 7.5. (A) Incubation & Anaesthesia (B) Oral Commissurotomy (C) Premolar identification (D) Tooth removed, Socket filling (E) Site closure (F).

Radiographic Evaluation post-surgery

Radiographic analysis was performed after the surgical procedure before the animal was moved to the critical care area. This was to confirm the optimum filling in the dental socket area with the material and also to ensure that there is no fracture in the mandibular area as a result of the tooth extraction performed. It was seen that the dental socket filling was intact and no fracture has occurred during the tooth

extraction in all the three cases: two test materials and one control material. Figure 7.6 (A) and 7.6 (B) shows the radiographic images of the socket filling with CHA material. 7.6 (C) and (D) shows the socket filling with THA material and 7.6 (E) and (F) shows the socket filling of HA control material post-surgery.

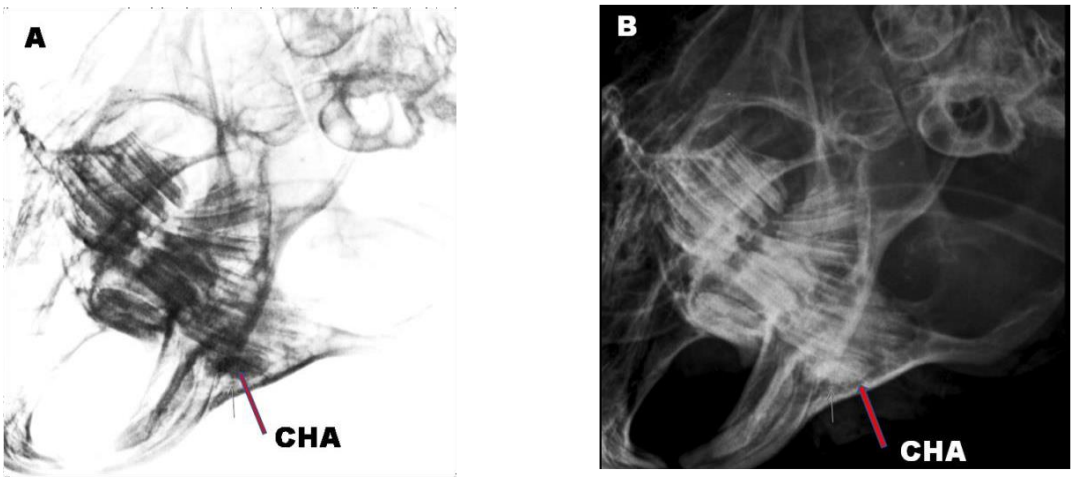

Figure 7.6A and 7.6B shows the radiographic images of the filling of dental sockets post-surgery with CHA material.

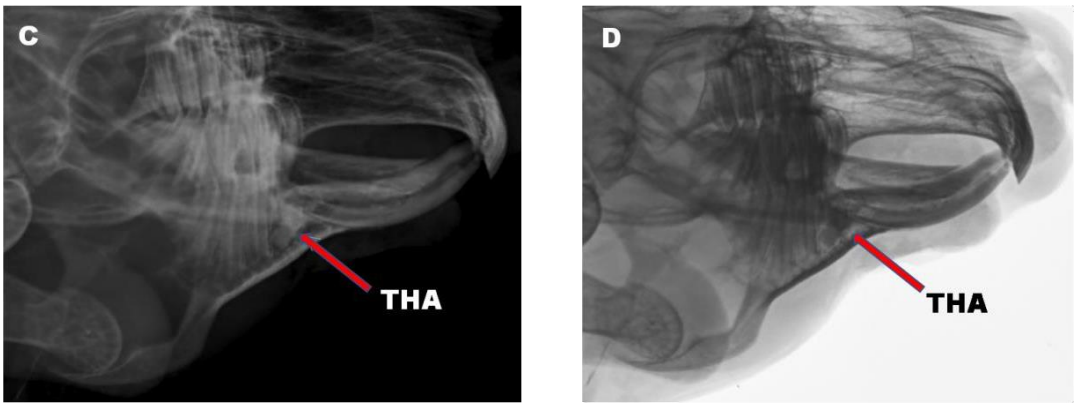

Figure 7.6C and 7.6D shows the radiographic images of the filling of dental sockets post-surgery with THA material.

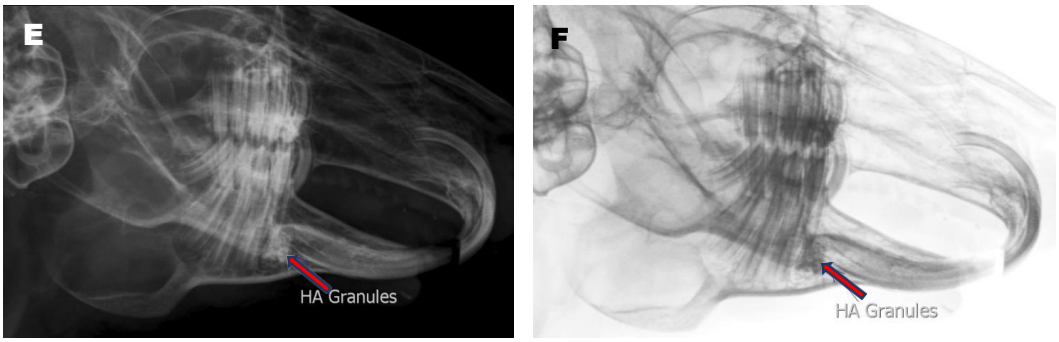

Figure 7.6E and 7.6F shows the radiographic images of the filling of dental sockets post-surgery with HA granule control material.

Post- Explanation Evaluation

Gross Evaluation

All animals were euthanized by excess dose of anaesthetics – Thiopentone (100 mg/kg), Pancuronium Bromide (0.08 mg/kg) and 35 ml of 7.5% w/v of Potassium chloride intravenously, post 3 months of implantation. Left mandible was dissected out and fixed in 10% neutral buffered formalin (NBF). Healing was uneventful, no signs of inflammation nor infection at the surgical site was seen prior to humane killing of animals post 3 months' implantation.

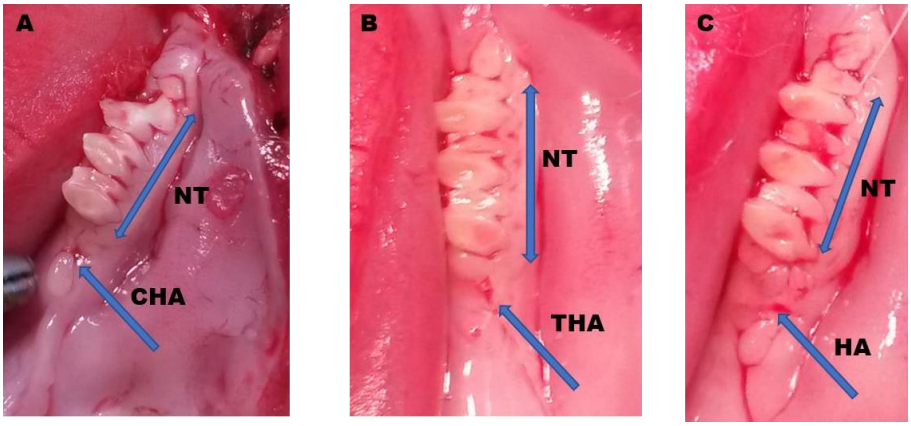

Figure 7.7. Gross image showing the site of implantation at autopsy (A) depicts CHA material site, (B) depicts THA material site and (C) depicts HA material site.

Figure 7.7 A represents the implanted site of the CHA material and NT denotes the neighbouring tooth. Figure 7.7 B represents the implanted site of THA material and Figure 7.7 C represents the implanted site of the HA material. From the gross images it can be seen that there has not been any adverse effects or immune rejections at the implanted site due to the material properties.

Radiographic Evaluation post autopsy

Radiographs were recorded after autopsy procedures to evaluate the healing process. The zones of healing and the material remaining were pictured to understand the resorption of the test materials and the control materials – CHA, THA, and HA granules.

It was seen that CHA shows resorption in the central region as well as in the periphery. Significant degenerative effect was seen as the material was changed to granular form in these regions. No inflammatory reactions were observed at the implant site. Figure 7.8 (A) and 7.8 (B) shows the radiographic images of the CHA material after 3 months (12 weeks). THA material showed similar results comparable to CHA. Significant resorption was observed from the central and periphery regions of the material. No inflammation was observed at the site. Figure 7.8 (C) and 7.8 (D) represent the radiographic images of the THA material 3 weeks after the implantation. HA granule (control) showed very negligible resorption when compared to the test materials. The central, periphery and the upper regions showed almost no significant changes after the study period of 3 months. Figure 7.8 (E) and 7.8 (F) shows the radiographic image of the control HA material 3 months after implantation.

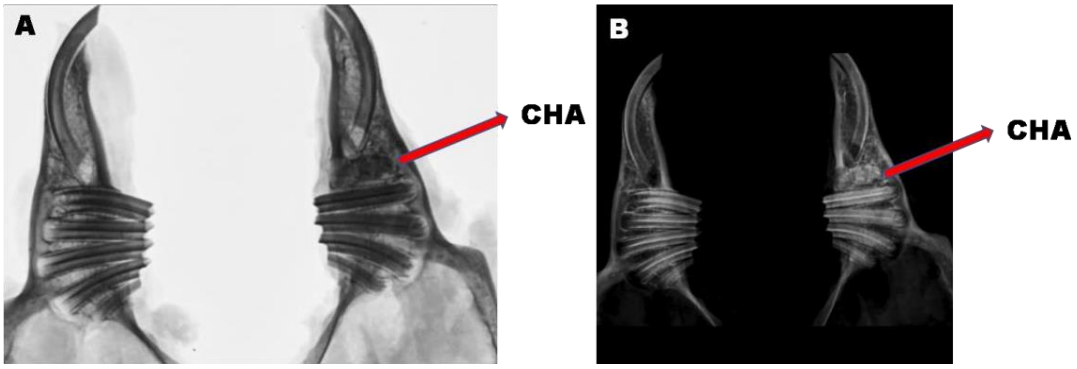

Figure 7.8 A and 7.8 B Radiographic image showing healing of CHA after 12 weeks of implantation

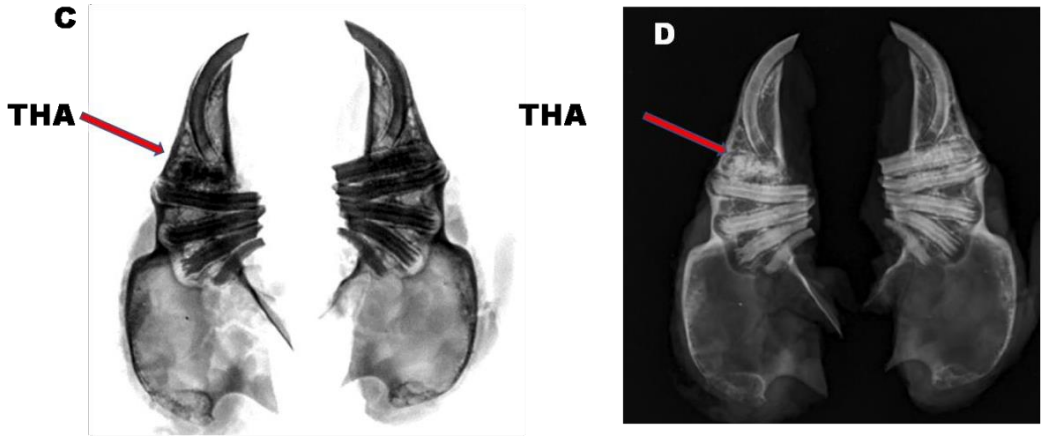

Figure 7.8 C and 7.8 D Radiographic image showing healing of THA after 12 weeks of implantation.

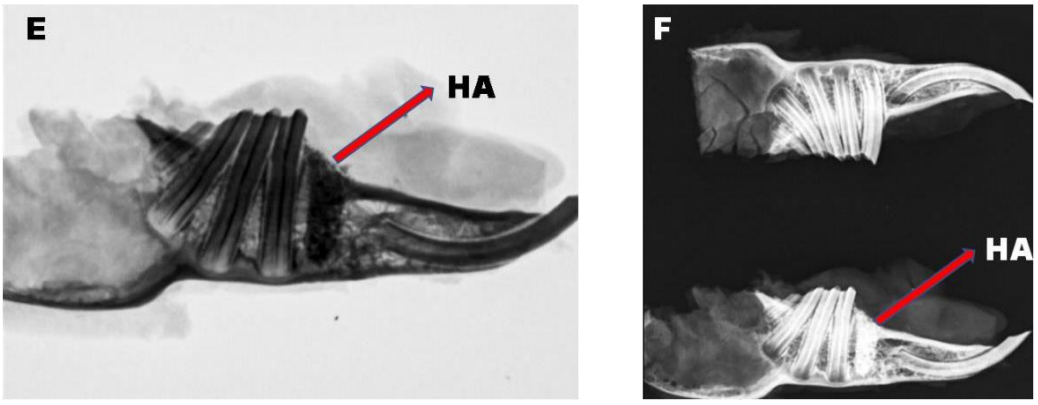

Figure 7.8 E and 7.8 F Radiographic image showing healing of HA granule after 12 weeks of implantation.

Mineralisation Studies

The newly formed bone undergoes mineralization which was verified through the density distribution graph plotted from 2D micro-CT images 12 weeks post implantation (Figure 7.9 (A) represents CHA; 7.9 (B) THA; and 7.9 (C) HA. The density of CHA was observed to be in the range of 980.3 mg HA /ccm which was on par with the material density. THA was 800 mg HA /ccm and Control HA showed 560 mg HA/ccm. It was seen that CHA materials showed higher mineralisation when compared to THA material and HA control. Both the test materials show better mineralisation on comparison with the control HA granule. Micro-CT imaging is an efficient, non-destructive tool to measure the amount and distribution of mineralised matrix throughout 3D constructs *in vitro* and *in vivo* as reported by Cartmell S et al., 2004. In the histograms shown below AB represents the density of the surrounding alveolar bone. The material remaining is denoted as M, neighbouring tooth NT, and the new bone formation is represented as NB. The inset image shows the retrieved tissues from the implanted site.

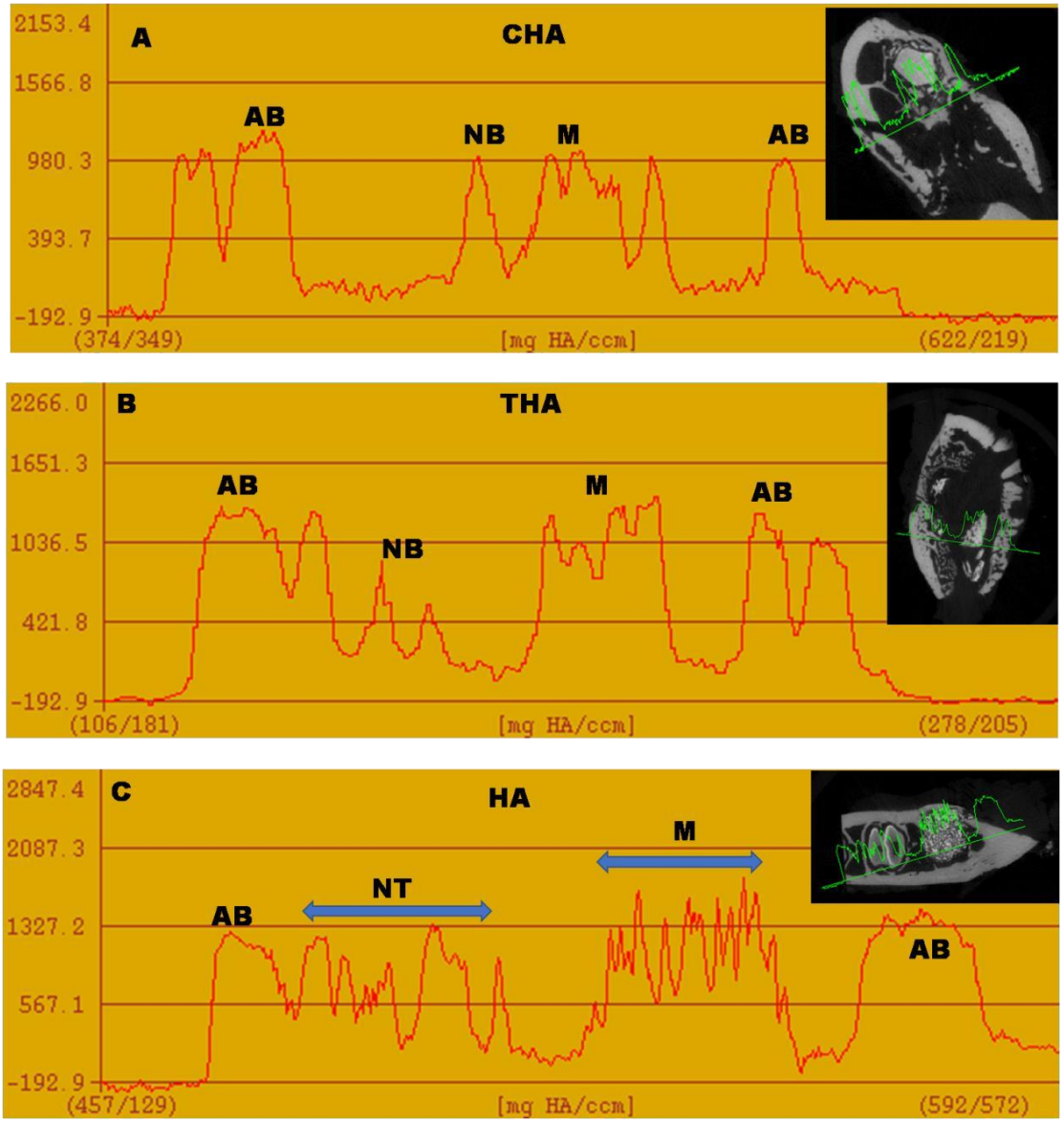

Figure 7.9. Density distribution graphs showing mineralization of newly formed bone (A) CHA material; (B) THA material; and (C) HA material 12 weeks post implantation. The graphs were plotted from 2D micro CT image, mg HA / ccm denotes milligram of hydroxyapatite per cubic centimetre. The inset image shows the retrieved tissues from the implanted site.

Evaluation of neo-osteogenesis and resorption of the material

Neo-osteogenesis was evaluated through histology (Stevenal's blue and van Gieson's picrofuchsin staining), histomorphometry and micro-CT analysis.

Micro Commuted Tomography shows the scout view of the site in Figure 7.10 A which is the region of interest. CHA material having resorption in the periphery as well as central regions can be visualized. Figure 7.10 B shows the 3D morphometry of the dental socket filling. The surrounding alveolar bone and the filling is clearly visible here which is denoted as AB.

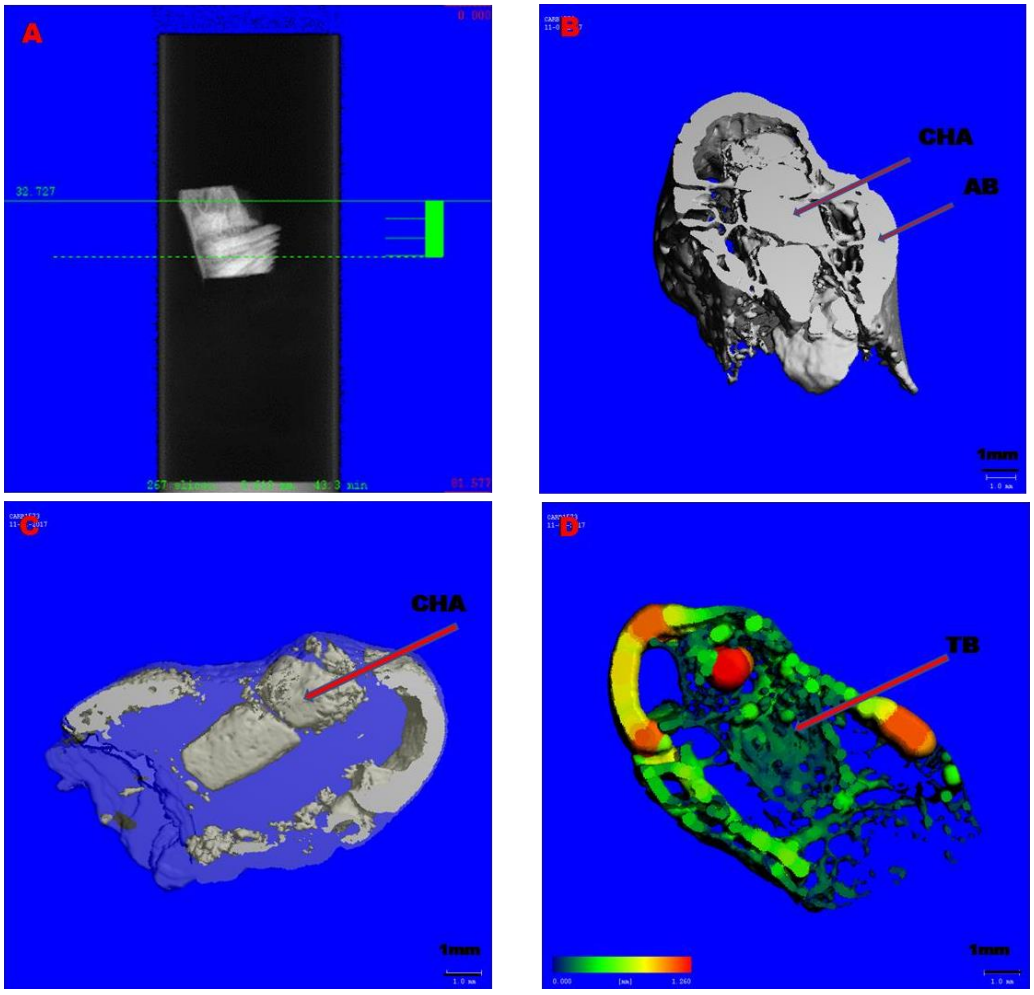

Figure 7.10. A shows the scout view of the CHA implanted site; B shows the 3D morphometry of the CHA implanted region in the extraction socket; C shows the transparent profile of the CHA implanted site; D shows the trabecular thickness profile in the CHA implanted region.

Figure 7.10 C shows the transparent profile of the implanted site. The implant site is made opaque which is marked as CHA and the surrounding regions are made transparent for the better visibility of the site. The surrounding alveolar bone with the same mineral density of the material is also visible here. It is seen that the CHA material shows better trabecular bone formation all over the implanted area. The trabecular bone thickness can be observed in Figure 7.10 D; the green colouration indicates the newly mineralised areas and the yellow to red areas denotes highly mineralised areas which are observed mostly at the alveolar bone region. The upper proximal end shows a higher degree of mineralisation which is denoted by the red colour.

Scout view of the THA implanted site is depicted in Figure 7.11 A. Material shows resorption from the central and peripheral areas. The neighbouring tooth can also be seen in the picture which is denoted as NT. Figure 7.11 B shows the 3D morphometry of the implanted region. The remnant material with the surrounding alveolar bone is visible, denoted as AB. The trabecular structural formation in and around the material is also visible here indicating the newly formed tissues. The transparent profile of the implanted region in Figure 7.11 C clearly shows the material and the neo- tissue formations which had a weaker radiodensity when compared to the adjacent cortical bone with higher radiodensity. These areas are made transparent and the areas of weaker radiodensity are made opaque for better clarity observation. Figure 7.11 D shows the trabecular thickness of the bone formed around the implanted area. Trabecular thickness increases from green to red as per the colour coding scale. Here it is observed that the trabecular formations are in the

initial phase. Most of the surrounding implanted regions show green colouration in the study period of 12 weeks.

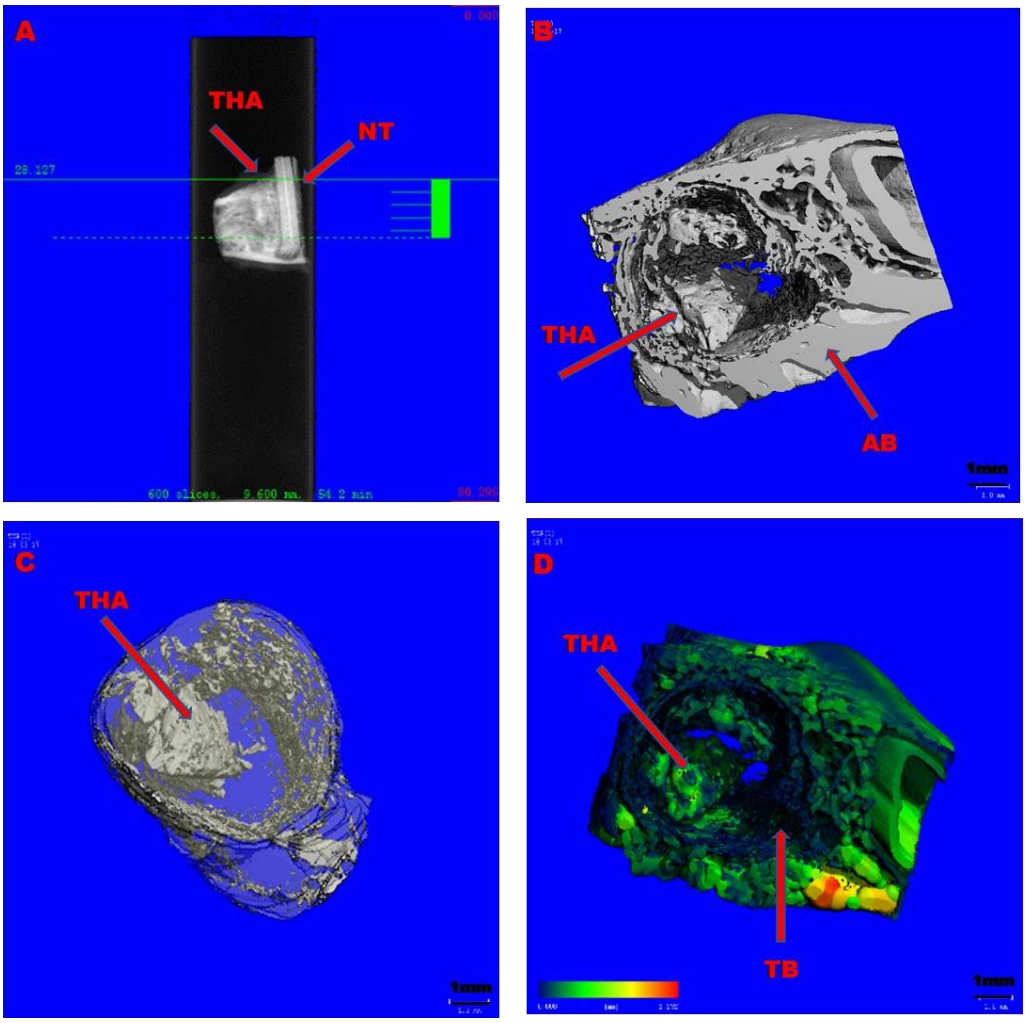

Figure 7.11. A shows the scout view of the THA implanted site, B shows the 3D morphometry of the THA implanted region in the extraction socket, C shows the transparent profile of the THA implanted site, D shows the trabecular thickness profile in the THA implanted region: Alveolar bone is represented as AB and trabecular thickness denoted as TB.

In the case of control group where 1 mm sized granule of hydroxyapatite was used as the filler material it was seen that the filler material showed negligible resorption during the study period of 12 weeks. Figure 7.12A shows the scout view of the

implantation site where the presence of the material along with the adjacent tooth is visible. Figure 7.12 B shows the 3D morphometry of the socket filling. The surrounding support from the existing alveolar bone is also visible here. Figure 7.12 C represents the transparent proofing of the implanted region. Here the filling alone is clearly visible and its radiodensity is very much varied with respect to the surrounding tissues. Hence the surrounding areas are observed to be transparent and the filling alone is made visible.

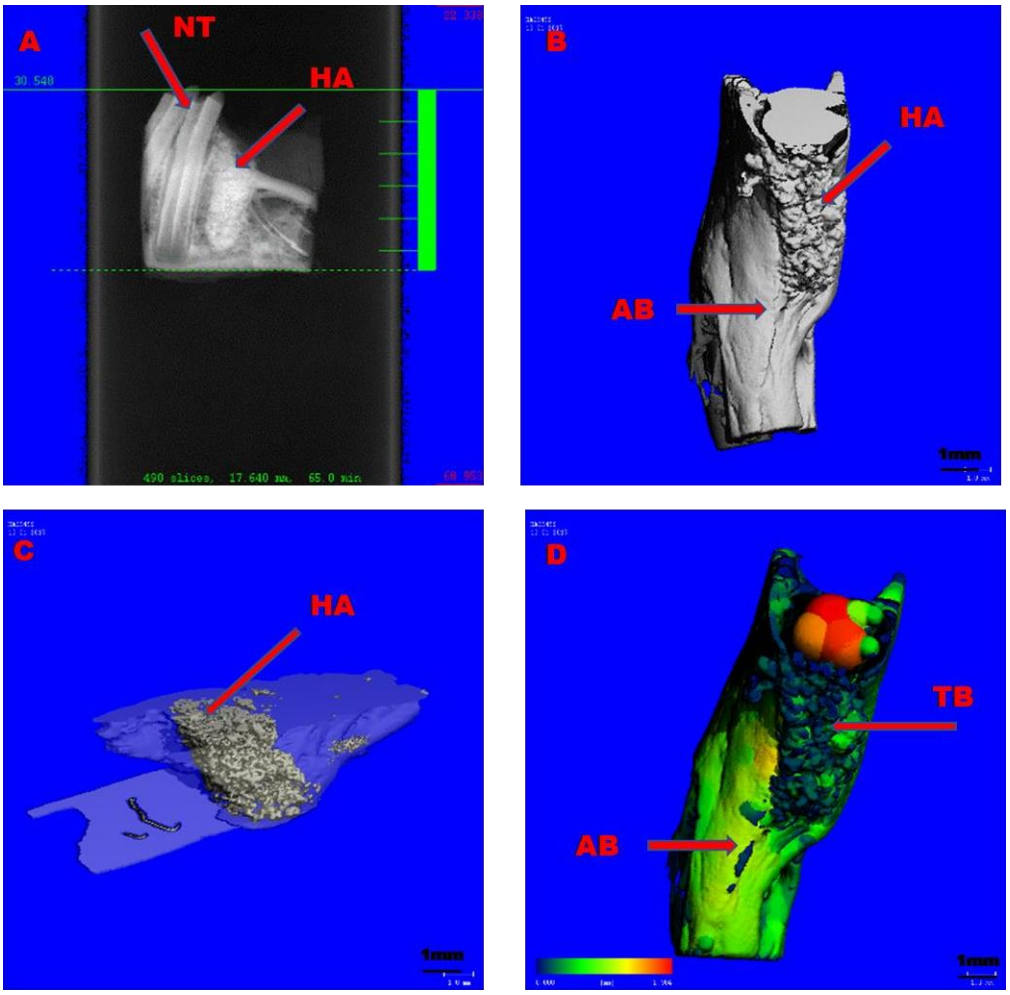

Figure 7.12.A -Scout view of the HA granule implanted site; B-3D morphometry of the HA implanted region in the extraction socket; C- transparent profile of the HA implanted site; D -trabecular thickness profile in the HA implanted region: Alveolar bone is represented as AB and trabecular thickness denoted as TB.

Figure 7.12 D shows the trabecular thickness in the defect area. It is seen that the trabecular bone formation is in the initial stages. The green colouration shows the development of trabeculae. Greater trabeculae formation is visible in the upper proximal end depicting a higher mineralised area, observed as orangish red in appearance as per the colour coding scale.

Further quantification of bone formation was done by evaluating the bone parameters like trabecular number (Tb.N.) and trabecular separation (Tb.Sp) and trabecular bone volume fraction (BV/TV). In micro CT evaluation, CHA implanted animals have more trabecular number formation compared to the THA implanted animals indicating a higher mineralisation in CHA implanted materials. The trabecular number (Tb.N) was 1.2452 1/mm in CHA while THA materials showed lesser value of 0.8105 1/mm. However the control group showed a Tb.N value of 0.9189 which was higher than the trabecular number of THA. The trabecular separation/spacing was observed to be 0.5104 mm for CHA while THA depicted a spacing of 0.6970 mm. But control HA group showed a lesser trabecular separation of 0.4675 mm. However the bone mineral density profile of the samples showed that CHA materials showed a higher degree of mineralisation when compared to THA and control HA granules On comparing the BV/TV values of the material alone (CHA and THA) before implantation to the BV/TV values of the materials retrieved after implantation shows that there is a significant increase of about 72% bone volume of CHA samples whereas THA showed only 54% increase in bone volume after implantation.

(BS/BV) is a measure for the bone surface per given bone volume. In bone biology, this is used to measure the number of bone lining cells over a given volume of bone.

It was seen that (BS/BV) of CHA, THA and HA granules were found to be 3.6127 1/mm, 3.7261 1/mm, and 3.2223 1/mm. The activity of bone forming cells/osteoblasts was higher in the test materials when compared to control HA indicating a positive cellular response of the CHA and THA materials.

Histomorphometry Analysis

Histomorphometry analysis of the implanted CHA, THA and HA granules were done to evaluate the process of tissue healing. The PMMA embedded sections were stained with Stevenal's blue and van Gieson's picrofuchsin dyes. The stained sections under microscopic evaluation showed that the test materials CHA and THA showed better resorption when compared to the control HA granules. Stevenal's blue stained the osteoblast-like cells blue in colour and van Gieson's picrofuchsin stained the osteoid matrix yellow. Figure 7.13 A shows the implanted site of CHA material and the neighbouring tooth is marked as NT. It was seen that the mucosal epithelium of the implanted site showed distorted morphological appearance in comparison to the normal mucosal epithelium. This is an indication of a healing process, probably of tissue formation in the vicinity. The remnant material is denoted as M which is seen in black colour. The yellowish brown areas represent the new bone formation and the cellular activity is seen in blue colour. New bone formation was observed around the periphery as well as at the central portion mainly concentrated at the ridges between the resorbing material. The resorbing material area shown in Figure 7.13 C and 7.13 D clearly shows that the density of the material is decreased around the regions of degradation marked as RM denoted as resorbing material. The bone

formed around the region of RM is slightly more matured than the bone formed near the M area. This shows that as the material progresses with degradation the new bone formation around the area is matured and this can be seen as a colour change from golden yellow to brown. The cellular infiltrations around the material shows the presence of osteoblast like cells marked in blue colour. Few number of osteoclasts were also observed around the implant area which shows that there is a good turnover of material degradation and neo tissue formation. Centres of ossification (osteoid formations) are seen in ring like appearances marked as OS in Figure 7.13 B. Overall it is seen that the material has an excellent degradation profile of around 60%, during the study period of 12 weeks. However, this degradation rate is quite high since it is not on par with the new bone formation. New bone formation and the material remaining was quantified using Image analysis software (Image J) and it is seen that CHA showed around 72% resorption. Remnant material was 28% and the new bone formation was around 42%.

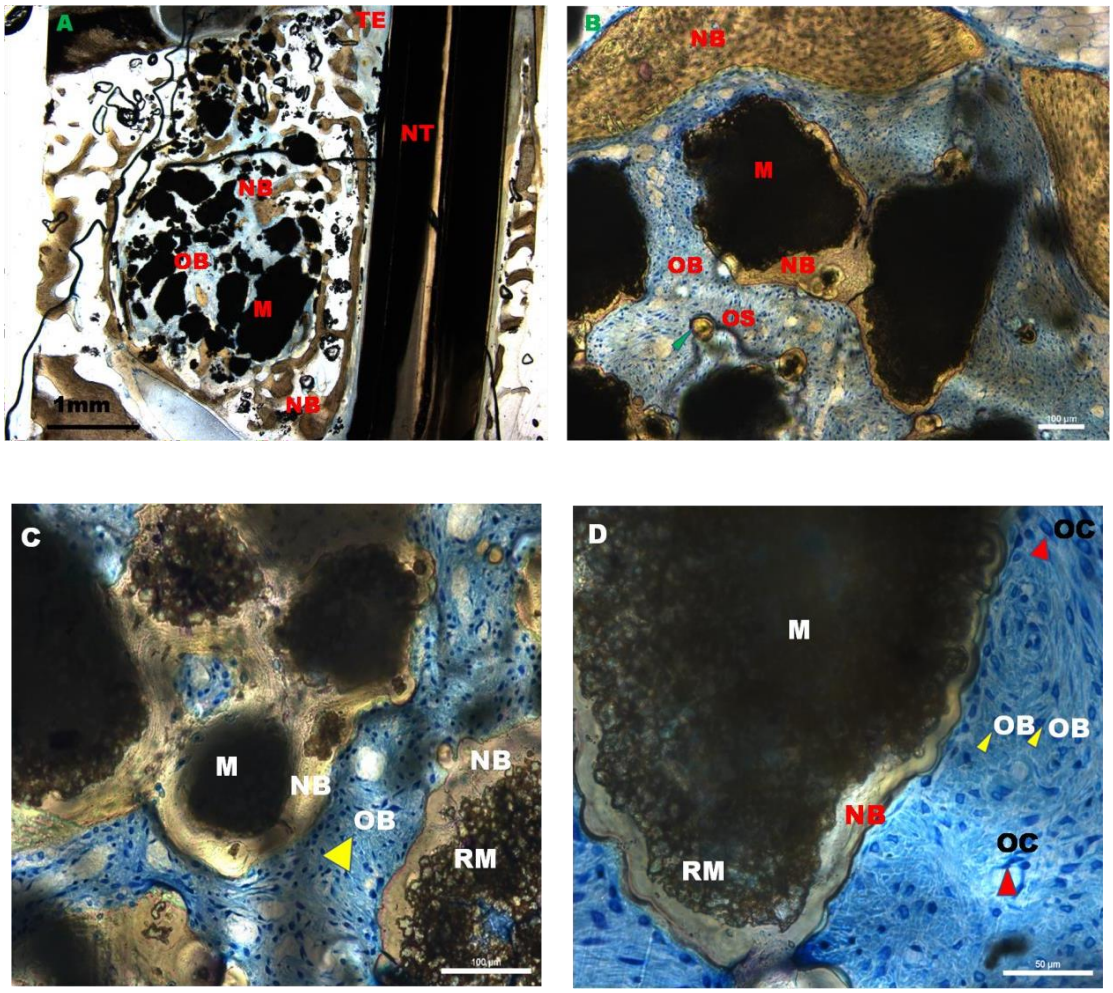

Figure 7.13. Light micrographs of PMMA sections of implanted CHA material stained with Stevenal's blue (osteoblast-like cells - blue) and van Gieson's picrofuchsin (osteoid matrix – yellow) staining.

CHA material:7.13 (A) - the implanted region at 4X magnification. Material remnants, new bone formation and osteoblasts are seen at the site along with the neighbouring tooth; 7.13 (B) and 7.13 (C) - shows the implant and new bone formation around the material, ossification centres are visible here 10X magnification; 7.13 (D) - The osteoblast-like cells (oval shape) are seen around the new bone area - 20 X magnification.

Abbreviations and symbols used: M denotes material remnants, osteoid formation denoted as OS, Osteoblast-like cells marked as OB with yellow pointers, Osteoclast-like cells marked as OC with red pointers New bone formation is seen around the material denoted as NB, Neighbouring tooth denoted as NT, Resorbing material area is shown as RM, Mucosal epithelium lining the defect area and the neighbouring tooth is denoted as E.

THA implanted materials showed better resorption in comparison to control HA granule. However, the degradation was less the CHA material. Here also the mucosal epithelium had a distorted morphology which shows that the adjacent tissue is undergoing a repair process. From the Figure 7.14 A we can observe that the material can undergone degradation from the peripheral portions and the central areas remain intact. Also significant new bone formations are observed along the peripheral ridge and the upper proximal end. The onset of new bone formation is clearly visible in Figure 7.14 B and 7.14 C marked as NB. In the surrounding area prominent osteoblasts activity were also seen. Figure 7.14 D shows the region of material resorption marked as RM. Adjacent to this area, lies a zone of osteoclasts activity is observed marked with yellow pointer, and the number of osteoclasts are high which may be recruited to digest the degrading material. Osteoblasts are also seen in the picture which are prospective for mineral deposition. Overall it is seen that the material has an excellent degradation profile of around 40%, during the study period of 12 weeks but less when compared to CHA material. New bone formation and the remnant material was quantified using Image analysis software (Image J) which showed around 38 % resorption for THA, remnant material 62% and new bone formation around 22%.

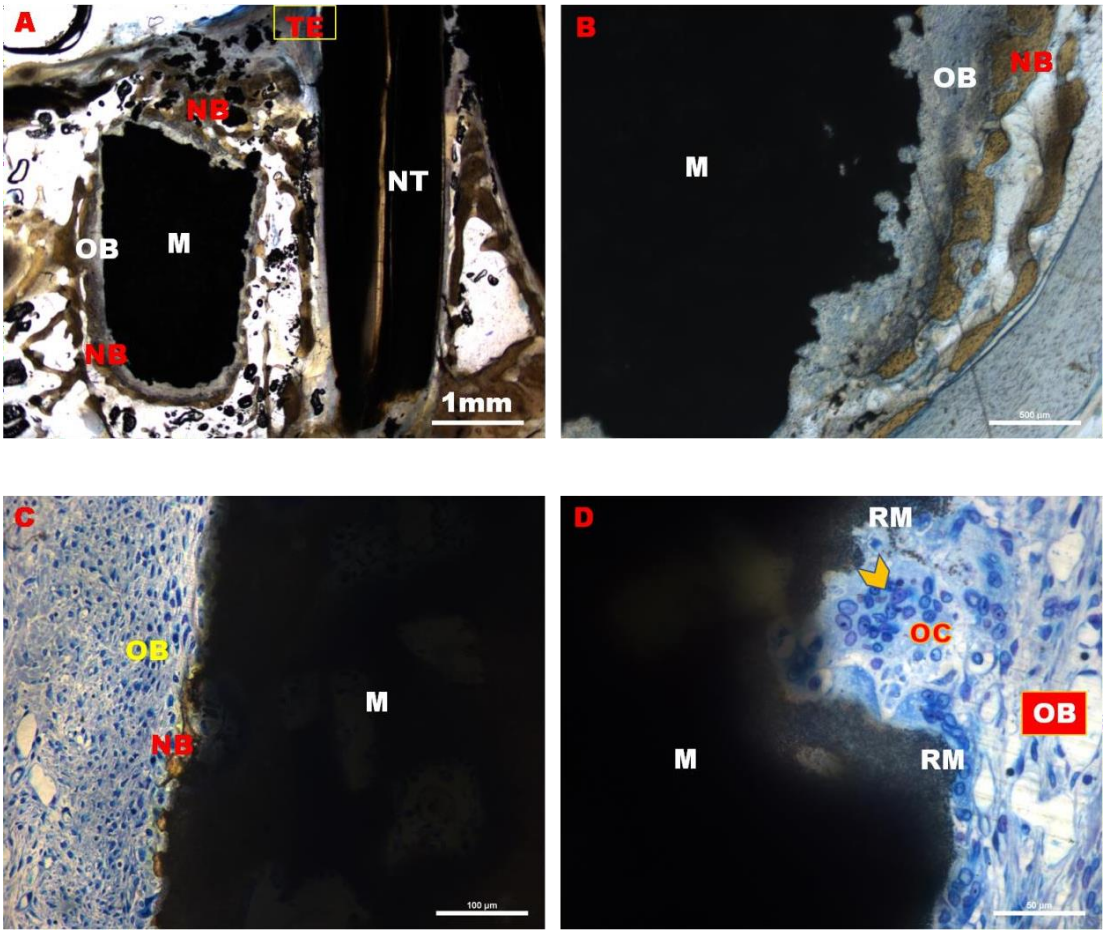

Figure 7.14. Light micrographs of PMMA sections of implanted THA material stained with Stevenal's blue (osteoblast-like cells - blue) and van Gieson's picrofuchsin (osteoid matrix – yellow) staining.

Figure 7.14 (A) - THA implanted region at 4× magnification. Material remnants, new bone formation and osteoblasts are seen at the site along with the neighbouring tooth; 7.14 (B) and 7.4 (C) - the appositional bone growth along the length of the implant indicating good material bone interaction 10× magnification; 7.14 (D) - Cellular infiltration at material interface d 20× magnification.

Abbreviations and symbols used: M denotes material remnants, Osteoblast like cells as OB, zone of Osteoclastic activity d as OC with yellow pointer, New bone formation is seen around the material denoted as NB, Neighbouring tooth denoted as NT, Resorbing material area as RM, Mucosal epithelium lining the defect area and the neighbouring tooth is denoted as E.

In a closer examination we could observe that the c-axis oriented crystals present in THA was seen to be very stable even after all the tissue processing steps. The crystals were seen dispersed from the material along the resorbing ridges and also in the osteoblastic activity areas around the material. This was a very interesting finding and a prospective data supporting the stability of such morphologies of hydroxyapatite generated via hydrothermal exchange process. Figure 7.14 E shows this observation: the regions marked in yellow shows the areas where the crystals are found.

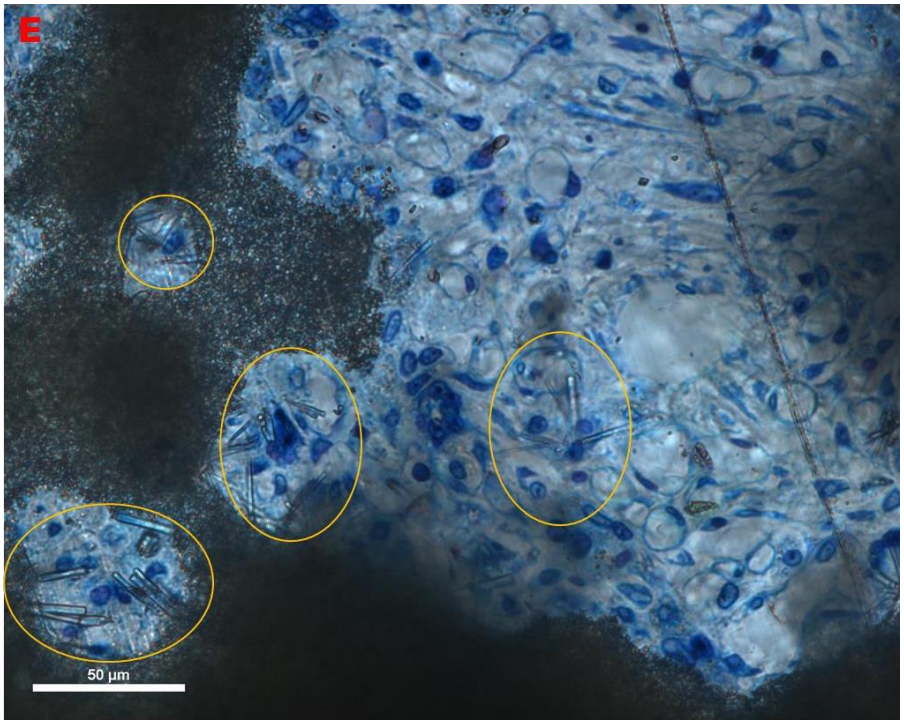

Figure 7.14 E. - Presence of c-axis oriented crystals from the THA at the resorption site.

In the case of control HA granules, the resorption of the material was found to be the least. Figure 7.15 A shows the defect site with the remaining material and the neighbouring tooth marked NT. Almost 90% of the filler was left without any

degradation. New bone formation was seen mostly in the lower proximal end invading into the intergranular spaces. Figure 7.15 B and 7.15 C shows the presence of osteoblastic activity marked as OB. New bone formation and the resorbing material are also seen here. It is evident that remnants of material is more in comparison to the test materials CHA and THA. On a closer examination we could observe that even though the new bone formation was less, the maturity of the new tissue was very obvious. The development of haversian systems (fundamental unit of compact bone) is observed and marked as HS in Figure 7.15 D and mature osteocytes (bone tissue maintaining cells) are visualised as entrapped within the bony tissue. This difference in the maturity of the newly formed tissue may be due to the inherent osteoconductive behaviour of sintered hydroxyapatite. Here the resorption process is slow and thereby the turnover of the bone tissue is also less. The osteoclastic activity is observed to be less than THA and CHA which clearly indicates the decrease in the degradation rate of the material which slows down the deposition but simultaneously hastens the maturation of new bone. On a quantitative evaluation it was observed that the amount of remnant material was 86% and new bone formation was 9.5% signifying a lower degradation of 14% for sintered hydroxyapatite ceramics compared to the test materials CHA and THA.

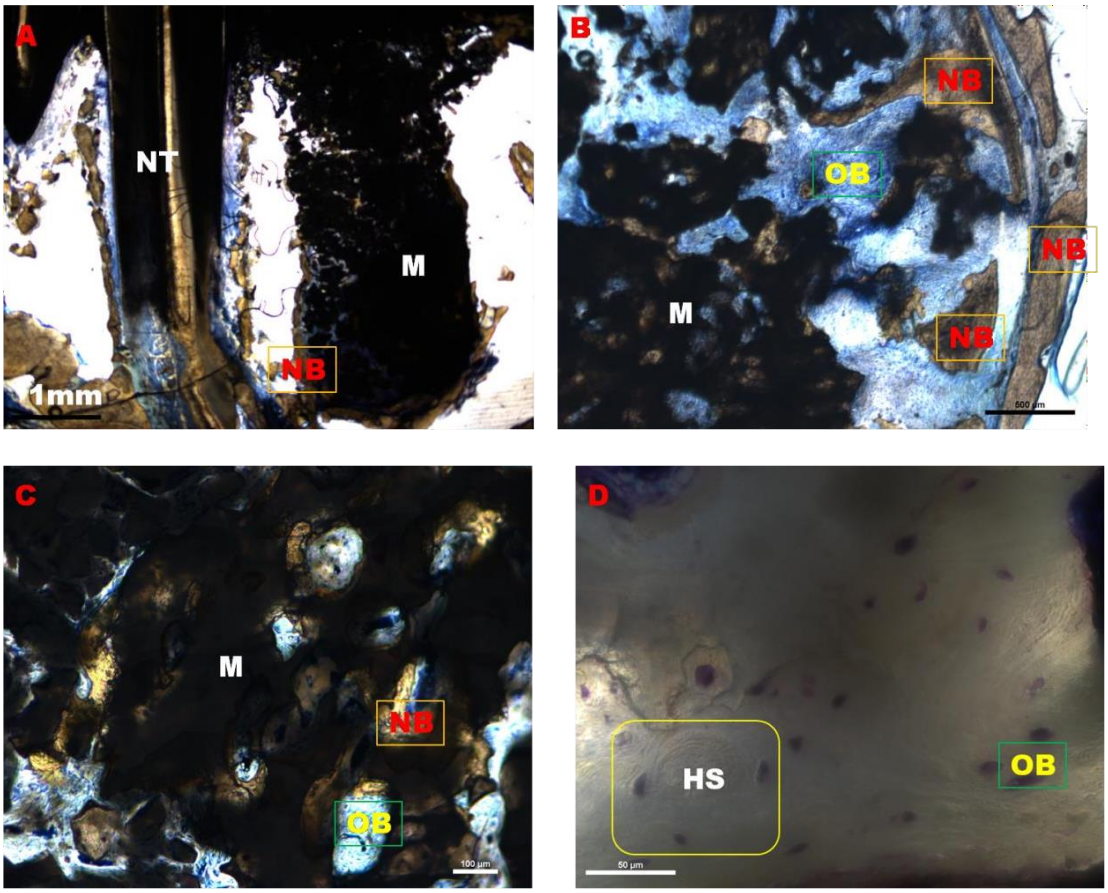

Figure 7.15 Light micrographs of PMMA sections of implanted HA material stained with Stevenal's blue (osteoblast-like cells - blue) and van Gieson's picrofuchsin (osteoid matrix – yellow) staining.

Figure 7.15 (A) - HA implanted region at 4× magnification. Remnants of material, new bone formation are observed in the vicinity of the neighbouring tooth; 7.15 (B) and 7.15 (C) shows *de novo* bone formation along the sides of the implant and bone islands in the intergranular spaces - 10× magnification; 7.15 (D) Formation of harversian systems and presence of osteocytes observed - 20× magnification.

Abbreviations and symbols used: M denotes material remaining, Osteoblast like cells marked as OB, New bone formation is seen around the material denoted as NB, Neighbouring tooth denoted as NT, Harversian system: HS, Osteocytes OC.

Evaluation of biodistribution of calcium and phosphorus ions in the test animals

The vital organs of the animals namely heart, lungs, liver, spleen, kidney were collected and the tissue digestion procedure was done as per the protocol given in section (3.3.5.1). The digested tissues were analysed by ICP-OES method to find the level of calcium and phosphorus ions in those tissues. It was seen that the Ca ions levels were found to be below the detection level of the instrument and the phosphate ion levels were in the range of 40 – 60 ppm. This phosphate content is expected to be from the blood serum of the animal which is normal and not alarming. These values shows that the material has got no toxic effects in the implanted system proving it biologically safe for use.

Summary

The success of osseointegrated dental implants depends on whether there is a sufficient volume of healthy bone at the recipient site at the time of implant placement. Placement of an implant at the extraction site could result in a significant buccal dehiscence. Despite the reasons for socket preservation, there is always a consensus that sufficient alveolar bone volume and favourable architecture of the alveolar ridge are essential to achieve ideal functional and aesthetic prosthetic reconstruction following implant therapy. Preserving or reconstructing the extraction socket of a failed tooth according to the principles of guided bone regeneration enhances our ability to provide aesthetically pleasing restorations to the patients.

Here our objective was to develop a faster resorbing ceramic filler material which can be used as a dental extraction socket filler to prevent the alveolar bone loss after tooth extraction. The study proves to be successful. There was no reduction in height of alveolar ridge or collapse of buccal socket during the study period of 12 weeks in the test and control materials. The rate of new bone formation and the degradation of the material was found to be higher for CHA in comparison to THA. Both the test materials excelled the performance of the control sintered HA granule in terms of bone formation and material degradation. Hydrothermal method can be suggested as a reliable and effective method for the synthesis of fast resorbing ceramic materials for orthopaedic and dental applications in Health Care.

DISCUSSION

Hydroxyapatite scaffolds prepared from calcium carbonate (calcite) precursors mimics the natural nacreous microstructures. The calcite powders were casted into different moulds using a setting solution of phosphoric acid and sodium hydroxide to form porous precursors bodies. They were then chemically transformed to hydroxyapatite via hydrothermal exchange reactions. The phase conversion was confirmed by the XRD analysis of the precursor and the newly synthesised material. The developed material exhibited highly crystalline morphologies consisting of micro pores within the crystallites of high surface area. The material was prepared without the sintering process and is expected to resorb faster than the sintered calcium phosphate scaffolds. *In vitro* cell culture studies showed excellent cell compatibility for the developed material. The *in situ* developed pores within the material can help to act as a drug-carrying moiety which can be further used for the treatment of diseases like osteomyelitis. It can also be useful a prospective scaffold for tissue engineering applications.

Hydroxyapatite scaffolds were also synthesised from lower calcium phosphate precursor (TCP) by hydrothermal exchange reactions in three different reaction mediums by varying the kinetic and thermodynamic parameters to obtain maximum conversions. Surfactant free hydrothermal reactions led to the formation of exotic crystal morphologies based on a cluster growth nucleation model. The converted scaffolds are seen to have different crystal morphologies with structures with nano and micro dimensional features of fibres, rods, tubes, and flowers depending on the pH and the mediums used for the exchange reactions. The hydroxyapatite crystals so

formed showed preferred orientation effects mimicking biological apatites with significant growth of a-planes (300 and 200) in the hexagonal lattice of hydroxyapatite. The *in vitro* bioactivity evaluation showed profound influence on the microstructure and stoichiometry of the apatites. The crystals were re-oriented in SBF to form stacked arrays, banana like inflorescence, tented and micro well like structures which is attributed to the different mediums. High temperature sintering processes are avoided to restrict grain growth in the ceramic, which can eventually help in improving the dissolution of the material *in vivo*. The novel materials can be used as fast resorbing bioactive scaffolds for the repair and replacement of hard tissues or as fillers in dental applications. The developed materials were named CHA (calcium carbonate derived hydroxyapatite) and THA (tri calcium phosphate derived hydroxyapatite). The phase purity and the structural features were studied using X-Ray Diffraction Techniques. The composition of the materials was evaluated by ICP-OES methods to determine the Ca/P ratios of the material. The surface morphological evaluations were done using ESEM. Mechanical property evaluation of the materials by compressive strength testing proved that the materials were suitable as bone fillers. The materials also showed good bioactivity in simulated body fluid. CHA and THA materials were proved to be biocompatible and cell friendly with MSCs. The osteogenic differentiation potential of the materials was evaluated by ALP activity screening which showed that the materials supported osteogenesis by the increase in the levels of alkaline phosphatase activity.

The *in vivo* efficacy testing of the developed materials were carried out as dental extraction socket fillers in rabbit models. Bone Fillers are materials that are capable of bringing about cancellous bone in growth. CHA and THA proved that their

degradation and resorption rates excelled the sintered HA granule control material. New bone formation was also higher in CHA and THA in comparison to HA granules.

Granular bone fillers show biological action in several phases. First phase is hyperhydration which occurs one month after implantation where the granules changes its intimate form to interconnected structures of augmented granules. This change of spacial arrangement is known as condensation. Two months after this process a hyperdense state is formed as a result of biological action *in vivo.* This biologically mediated arrangement is known as consolidation. Once the new tissue is formed by the action of mechanical loading and biochemical turn over, the next stage is the construction of the definitive tissue called compaction where remodelling and mineralisation takes place (A. Ravaglioli, 1992). It was seen that the developed materials excelled the performance of the sintered granules in promoting higher percentage of bone formation. However, the maturation phase of the mineralised tissue is still in the remodelling phase.

A major role in the bone tissue formation is played by osteoblasts (bone forming cells) which causes mineralisation. Osteoblast activity is enhanced in the presence of alkaline ions in the surroundings. The first stage of osteoblast migration consists of the production of an extracellular matrix inside which a fibrin/fibronectin clot develops providing a three dimensional scaffolding through which the cells migrate and other matrix components during wound healing processes are secreted. Fibrin clot is usually invaded by fibroblasts which secretes collagen to form fibrous callus.

Subsequently this fibrous tissue undergoes osteogenesis and is replaced by newly formed bone.

Osteoclasts perform the opposite function by controlling the resorption of the bone by controlling the dissolution of the materials like bone (hydroxyapatite) *via* the action of local acidic environment created by the secretions of these cells. For a prosthetic adaptation osteoclast activity is necessary as it eliminates the dead bone during the initial stages of implantation. On the implant surface direct formation of new bone takes place with the establishment of a firm bond with the surrounding bone by an interfacial calcium phosphate bond. The implant gets slowly resorbed depending on the nature of calcium phosphate compound and porosity of the implanted material and subsequently gets replaced by the newly formed bone. Sintered ceramic undergoes resorption in two phases, first phase consists of release of particles from the ceramic through the solubilisation of grain boundary and second phase is the ingestion or intracellular digestion phase aided by the osteoclasts. However, calcium phosphate ceramics undergo complete resorption in six months to two years' time or sometimes even higher in the case of sintered hydroxyapatite. Pure hydroxyapatite has poor degradation but has the best bone bonding properties among calcium phosphate ceramics. Various studies have proved that TCP is a faster resorbing material than HA. This is mainly due to the difference in solubility of the various calcium phosphates.

This work proves that the hydrothermal technique of ceramic synthesis can be a very effective method for the preparation of large porous ceramic bodies having better resorption in comparison to the sintered ceramic. These materials are prospective

scaffolds, fillers and drug delivery matrices which can be used for dental as well as orthopaedic applications.

CHAPTER-8

SUMMARY AND CONCLUSION

- Hydrothermal synthesis was employed to synthesize fast resorbing ceramic materials (large scaffolds) from a calcite and a tricalcium phosphate precursor source to form the new materials namely - CHA & THA. The ceramic processing to make these structures were purely through a non-sintered route.

- Hydroxyapatite scaffolds prepared from calcium carbonate (calcite) precursors namely CHA mimics the natural nacre microstructure with stacked plate like morphological features showing a more pronounced growth of 002 plane (c-plane) along the a-axial direction.

- Hydroxyapatite scaffolds prepared from lower calcium phosphate (TCP) precursor by hydrothermal exchange reactions were studied in three different reaction mediums by varying the kinetic and thermodynamic parameters to obtain maximum conversion efficiency. Among the developed materials, THA was formulated and chosen with respect to its calcium to phosphorus ratio of the material and it was further studied.

- C-axis oriented crystal growth was observed in THA materials with a preferred orientation in 300 plane. These materials upon bioactivity tests in simulated body fluid transformed the material surface to bimodal structures with features of microwells, tented arrays and stacked structures with

crystallinity. These growth patterns were very much different from the amorphous calcium phosphate deposition of carbonated apatite in SBF.

- The developed nano and micro structured CHA & THA showed excellent cytocompatibility and promoted proliferation and growth of MSCs. The osteogenic differentiation of the cell seeded materials (THA) were evaluated by measuring the ALP activity. The study proved that the materials promoted osteogenesis and were prospective scaffolds for tissue engineering applications.

- CHA scaffolds were promising materials as scaffolds and drug carrier vehicles. Sustained release of antibiotics (gentamicin) was observed for 56 days from the material.

- The *in vivo* efficacy testing of the CHA and THA was evaluated as dental extraction socket fillers in rabbit models for a study period of 12 weeks. It was seen that CHA depicted faster biodegradation compared to THA in the *in vivo* system. This data is supported with radiographs, micro CT and histology. Sintered hydroxyapatite showed negligible resorption and very less bone formation compared to CHA and THA during the study period of 12 weeks.

- Hydrothermal method can be employed as an effective synthesis route for the preparation of large porous bodies of hydroxyapatite with large crystals, high surface area and faster dissolution excelling the performance of sintered ceramics under *in vivo* conditions.

Future Investigations

- Hydrothermally developed materials showed excellent resorption behaviour. But it was seen that the new bone formation process is ongoing. More time is required for the formation of cortical bone structures which can be evidenced by the formation of harversian systems. For this the *in vivo* study has to be extended to a longer duration of 6 months to 1 year. Depending on the outcome of the results the degradation rates of the materials if needed has to be tailored for aiding the complete remodelling process of the bone.
- The material property can be enhanced by the incorporation of ions such as strontium to improve the radioopacity.
- Incorporation of growth factors such as BMP's, VEGF etc to the materials can be done to functionalise them as hybrid scaffolds for Tissue Engineering Applications.
- The study of crystal growth mechanisms, the kinetics and thermodynamics of the growing crystals can be very effective in improving the quality of the material synthesis.
- Development of biphasic systems of bioactive glass/ceramic composites via hydrothermal route can be effective to synthesise hybrid scaffolds having better bone bonding and faster resorption.

References

A. ALEX JAHANGIR, R. M. N., SAMIR MEHTA, ALOK SHARAN, AND THE WASHINGTON HEALTH POLICY FELLOWS 2008. Bone-graft substitutes in orthopaedic surgery. *AAOS*.

A. K. CHEETHAM, P. D. 1987. Solid State Chemistry – Techniques. Clarendon, Oxford.

A. RAVAGLIOLI, A. K. 1992. *Bioceramics : Materials, Properties, Applications*, Chapman and Hall Publishing.

ACHARYA, N. K., MAHAJAN, C. V., KUMAR, R. J., VARMA, H. K. & MENON, V. K. 2010. Can iliac crest reconstruction reduce donor site morbidity?: a study using degradable hydroxyapatite-bioactive glass ceramic composite. *J Spinal Disord Tech,* 23**,** 266-71.

ALBEE, F. H. 1920. Studies in Bone Growth: Triple Calcium Phosphate as a Stimulus to Osteogenesis. *Ann Surg,* 71**,** 32-9.

ALIVISATOS, A. P. 2000. Naturally Aligned Nanocrystals. *Science,* 289**,** 736.

ANATOMY AND PHYSIOLOGY, R. U. *Anatomy and Physiology, Rice University*, Rice University.

AOKI, H. 1991. *Science and Medical Applications of Hydroxyapatite* Tokyo, Takayama Press.

ARCE, H., MONTERO, M. L., SÁENZ, A. & CASTAÑO, V. M. 2004. Effect of pH and temperature on the formation of hydroxyapatite at low temperatures by decomposition of a Ca-EDTA complex. *Polyhedron,* 23**,** 1897-1901.

ARENDS, J., CHRISTOFFERSEN, J., CHRISTOFFERSEN, M. R., ECKERT, H., FOWLER, B. O., HEUGHEBAERT, J. C., NANCOLLAS, G. H., YESINOWSKI, J. P. & ZAWACKI, S. J. 1987. A Calcium Hydroxyapatite Precipitated from an Aqueous-Solution - an International Multimethod Analysis. *Journal of Crystal Growth,* 84**,** 515-532.

BAUER, T. W. & MUSCHLER, G. F. 2000. Bone graft materials. An overview of the basic science. *Clin Orthop Relat Res***,** 10-27.

BECKER, W., CLOKIE, C., SENNERBY, L., URIST, M. R. & BECKER, B. E. 1998. Histologic findings after implantation and evaluation of different grafting materials and titanium micro screws into extraction sockets: case reports. *J Periodontol,* 69**,** 414-21.

BHATT, R. A. & ROZENTAL, T. D. 2012. Bone graft substitutes. *Hand Clin,* 28**,** 457-68.

BINDER, G. & TROLL, G. 1989. Coupled Anion Substitution in Natural Carbon-Bearing Apatites. *Contributions to Mineralogy and Petrology,* 101**,** 394-401.

BOIVIN, G. 2007. The hydroxyapatite crystal: a closer look *Medicographia,* 29**,** 126-132.

BOYCE, T., EDWARDS, J. & SCARBOROUGH, N. 1999. Allograft bone. The influence of processing on safety and performance. *Orthop Clin North Am,* 30**,** 571-81.

BROWN, W. E. 1983. A new calcium phosphate setting cement. *J Dent Res,* 63**,** 672.

BUCHANAN, F. J. 2008. *Degradation Rate of Bioresorbable Materials: Prediction and Evaluation*, Elsevier.

BUDDY D. RATNER, A. S. H., FREDERICK J. SCHOEN 2004. *Biomaterials Science: An Introduction to Materials in Medicine*, Elsevier.

BURTRAND LEE, S. K. 2005. *Chemical Processing of Ceramics*, CRC Press

C. SCHWARTZ, R. B. 2005. Biphasic phospho-calcium ceramics used as bone substitutes are efficient in the management of severe acetabular bone loss in revision total hip arthroplasties. *Eur. J. Orthop. Surg. Traumatol. ,* 15**,** 191-196.

CARLISLE, E. M. 1980. Biochemical and morphological changes associated with long bone abnormalities in silicon deficiency. *J Nutr,* 110**,** 1046-56.

CARSON, J. S. & BOSTROM, M. P. 2007. Synthetic bone scaffolds and fracture repair. *Injury,* 38 Suppl 1**,** S33-7.

CARTWRIGHT, J. H. & CHECA, A. G. 2007. The dynamics of nacre self-assembly. *J R Soc Interface,* 4**,** 491-504.

CASTAÑO, V. M. 2012. *Water, Air, & Soil Pollution* 223 5707-5717.

CATROS, S., GUILLEMOT, F., LEBRAUD, E., CHANSEAU, C., PEREZ, S., BAREILLE, R., AMEDEE, J. & FRICAIN, J. C. 2010. Physico-chemical and biological properties of a nano-hydroxyapatite powder synthesized at room temperature. *Irbm,* 31**,** 226-233.

CHEN, J., WEN, Z., ZHONG, S., WANG, Z., WU, J. & ZHANG, Q. 2015a. Synthesis of hydroxyapatite nanorods from abalone shells via hydrothermal solid-state conversion. *Materials & Design,* 87**,** 445-449.

CHEN, Y., WANG, J., ZHU, X. D., TANG, Z. R., YANG, X., TAN, Y. F., FAN, Y. J. & ZHANG, X. D. 2015b. Enhanced effect of β-tricalcium phosphate phase on neovascularization of porous calcium phosphate ceramics: In vitro and in vivo evidence. *Acta Biomaterialia,* 11**,** 435-448.

CHIARELLO, E., CADOSSI, M., TEDESCO, G., CAPRA, P., CALAMELLI, C., SHEHU, A. & GIANNINI, S. 2013. Autograft, allograft and bone substitutes in reconstructive orthopedic surgery. *Aging Clin Exp Res,* 25 Suppl 1**,** S101-3.

CHICKERUR, N. S., TUNG, M. S. & BROWN, W. E. 1980. A mechanism for incorporation of carbonate into apatite. *Calcif Tissue Int,* 32**,** 55-62.

CIAPETTI, G., AMBROSIO, L., SAVARINO, L., GRANCHI, D., CENNI, E., BALDINI, N., PAGANI, S., GUIZZARDI, S., CAUSA, F. & GIUNTI, A. 2003. Osteoblast growth and function in porous poly epsilon -caprolactone matrices for bone repair: a preliminary study. *Biomaterials,* 24**,** 3815-24.

CULLITY, B. 1956. *Elements of X-ray Diffraction*, Addison-Wesley Publishing USA.

DA, C. 1972. The ultra structure of bone. *In:* GH, B. (ed.) *The biochemistry and physiology of bone.* New York: Academic Press.

DACULSI, G., MENANTEAU, J., KEREBEL, L. M. & MITRE, D. 1984. Length and shape of enamel crystals. *Calcif Tissue Int,* 36**,** 550-5.

DE GROOT, K. 1993. Clinical applications of calcium phosphate biomaterials: A review. *Ceramics International,* 19**,** 363-366.

DENISSEN, H. W. & DE GROOT, K. 1979. Immediate dental root implants from synthetic dense calcium hydroxylapatite. *J Prosthet Dent,* 42**,** 551-6.

DENISSEN, H. W. & GROOT, K. D. 1979. Immediate dental root implants from synthetic dense calcium hydroxylapatite. *The Journal of Prosthetic Dentistry,* 42**,** 551-556.

DENRY, I. & KUHN, L. T. 2016. Design and characterization of calcium phosphate ceramic scaffolds for bone tissue engineering. *Dent Mater,* 32**,** 43-53.

DIMITRIOU, R., JONES, E., MCGONAGLE, D. & GIANNOUDIS, P. V. 2011. Bone regeneration: current concepts and future directions. *BMC Med,* 9**,** 66.

DIMOVA, C., PAPAKOCA, K. & PAPAKOCA, V. 2014. Alveolar Bone Augmentation. *Key Engineering Materials,* 614**,** 89-94.

DU, X., CHU, Y., XING, S. & DONG, L. 2009. Hydrothermal synthesis of calcium hydroxyapatite nanorods in the presence of PVP. *Journal of Materials Science,* 44**,** 6273-6279.

E. HAYEK, H. N. 1963. Pentacalcium Hydroxyorthophosphate *Inorganic Syntheses, McGraw-Hill, Inc.,* vol. VII**,** 63-65.

EGGLI, P. S., MULLER, W. & SCHENK, R. K. 1988. Porous hydroxyapatite and tricalcium phosphate cylinders with two different pore size ranges implanted in the cancellous bone of rabbits. A comparative histomorphometric and histologic study of bony ingrowth and implant substitution. *Clin Orthop Relat Res***,** 127-38.

ELLIOTT, J. C., HOLCOMB, D. W. & YOUNG, R. A. 1985. Infrared determination of the degree of substitution of hydroxyl by carbonate ions in human dental enamel. *Calcif Tissue Int,* 37**,** 372-5.

ELSINGER, E. C. & LEAL, L. 1996. Coralline hydroxyapatite bone graft substitutes. *J Foot Ankle Surg,* 35**,** 396-9.

FINKEMEIER, C. G. 2002. Bone-grafting and bone-graft substitutes. *J Bone Joint Surg Am,* 84-A**,** 454-64.

FOUNTOS, G., YASUMURA, S. & GLAROS, D. 1997. The skeletal calcium/phosphorus ratio: a new in vivo method of determination. *Med Phys,* 24**,** 1303-10.

FURUTA, S., KATSUKI, H. & KOMARNENI, S. 1998. Porous hydroxyapatite monoliths from gypsum waste. *Journal of Materials Chemistry,* 8**,** 2803-2806.

GAASBEEK, R. D. A., TOONEN, H. G., VAN HEERWAARDEN, R. J. & BUMA, P. 2005. Mechanism of bone incorporation of β-TCP bone substitute in open wedge tibial osteotomy in patients. *Biomaterials,* 26**,** 6713-6719.

GE, H., ZHAO, B., LAI, Y., HU, X., ZHANG, D. & HU, K. 2010. From crabshell to chitosan-hydroxyapatite composite material via a biomorphic mineralization synthesis method. *J Mater Sci Mater Med,* 21**,** 1781-7.

GERSTEN, B., LENCKA, M. & RIMAN, R. 2002. Engineered Low Temperature Hydrothermal Synthesis of Phase-Pure Lead-Based Perovskites Using Ethylenediamine Tetra-acetic Acid Complexation. *Chemistry of Materials,* 14**,** 1950-1960.

GITELIS, S. & COLE, B. J. 2002. The use of allografts in orthopaedic surgery. *Instr Course Lect,* 51**,** 507-20.

GOTO T, K. M., KIM I Y, OHTSUKI C 2011. Effects of ethanol addition on formation of hydroxyapatite through hydrothermal treatment of dicalcium phosphate dihydrate. *IOP Conference Series: Materials Science and Engineering,* 18**,** pp. 192015.

GUARINO, V., TADDEI, P., DI FOGGIA, M., FAGNANO, C., CIAPETTI, G. & AMBROSIO, L. 2009. The influence of hydroxyapatite particles on in vitro degradation behavior of poly epsilon-caprolactone-based composite scaffolds. *Tissue Eng Part A,* 15**,** 3655-68.

HANKE, L. D. 2001. *Handbook of analytical methods for materials*, Materials evaluation and engineering, Inc. USA.

HANNINK, G. & ARTS, J. J. 2011. Bioresorbability, porosity and mechanical strength of bone substitutes: what is optimal for bone regeneration? *Injury,* 42 Suppl 2**,** S22-5.

HENCH, L. L. & PASCHALL, H. A. 1973. Direct chemical bond of bioactive glass-ceramic materials to bone and muscle. *Journal of Biomedical Materials Research,* 7**,** 25-42.

HENCH, L. L., SPLINTER, R. J., ALLEN, W. C. & GREENLEE, T. K. 1971. Bonding mechanisms at the interface of ceramic prosthetic materials. *Journal of Biomedical Materials Research,* 5**,** 117-141.

HENCH, L. L. A. W., JUNE 1993. *An Introduction to Bioceramics*.

HILDEBRAND, T., LAIB, A., MULLER, R., DEQUEKER, J. & RUEGSEGGER, P. 1999. Direct three-dimensional morphometric analysis of human cancellous bone: microstructural data from spine, femur, iliac crest, and calcaneus. *J Bone Miner Res,* 14**,** 1167-74.

HODGSKINSON, R. & CURREY, J. D. 1990. The effect of variation in structure on the Young's modulus of cancellous bone: a comparison of human and non-human material. *Proc Inst Mech Eng H,* 204**,** 115-21.

HOLMES, R., MOONEY, V., BUCHOLZ, R. & TENCER, A. 1984. A coralline hydroxyapatite bone graft substitute. Preliminary report. *Clin Orthop Relat Res***,** 252-62.

HU, J., FRASER, R., RUSSELL, J. J., BEN-NISSAN, B. & VAGO, R. 2000. Australian coral as a biomaterial: Characteristics. *Journal of Materials Science & Technology,* 16**,** 591-595.

HULBERT, S. F., MORRISON, S. J. & KLAWITTER, J. J. 1972. Tissue reaction to three ceramics of porous and non-porous structures. *J Biomed Mater Res,* 6**,** 347-74.

IRINAKIS, T. 2006. Rationale for socket preservation after extraction of a single-rooted tooth when planning for future implant placement. *J Can Dent Assoc,* 72**,** 917-22.

ISHIKAWA, K. 2010. Bone Substitute Fabrication Based on Dissolution-Precipitation Reactions. *Materials,* 3**,** 1138-1155.

ISHIKAWA, K. & EANES, E. D. 1993. The hydrolysis of anhydrous dicalcium phosphate into hydroxyapatite. *J Dent Res,* 72**,** 474-80.

J.B. GOODENOUGH, J. A. K., J.M. LONGO 1972. *Preparative Methods in Solid State Chemistry,* New York Academic Press.

JANSEN, J. A., VEHOF, J. W., RUHE, P. Q., KROEZE-DEUTMAN, H., KUBOKI, Y., TAKITA, H., HEDBERG, E. L. & MIKOS, A. G. 2005. Growth factor-loaded scaffolds for bone engineering. *J Control Release,* 101**,** 127-36.

JINAWATH, S., POLCHAI, D. & YOSHIMURA, M. 2002a. Low-temperature, hydrothermal transformation of aragonite to hydroxyapatite. *Materials Science and Engineering: C,* 22**,** 35-39.

JINAWATH, S., PONGKAO, D. & YOSHIMURA, M. 2002b. Hydrothermal synthesis of hydroxyapatite from natural source. *J Mater Sci Mater Med,* 13**,** 491-4.

JM., F. 2011. Fracture Repair and Bone Grafting *In:* ROSEMONT, I. (ed.) *OKU 10: Orthopaedic Knowledge Update.* American Academy of Orthopaedic Surgeons.

JOON PARK, R. S. L. 2007. *Biomaterials, an introduction*, Springer-Verlag New York.

K BYRAPPA, M. Y. 2001. *Handbook of Hydrothermal Technology* William Andrew Inc.

KALLAI, I., MIZRAHI, O., TAWACKOLI, W., GAZIT, Z., PELLED, G. & GAZIT, D. 2011. Microcomputed tomography-based structural analysis of various bone tissue regeneration models. *Nat Protoc,* 6**,** 105-10.

KANZAKI, N., TREBOUX, G., ONUMA, K., TSUTSUMI, S. & ITO, A. 2001. Calcium phosphate clusters. *Biomaterials,* 22**,** 2921-9.

KATTIMANI, V. S., KONDAKA, S. & LINGAMANENI, K. P. 2016. Hydroxyapatite–-Past, Present, and Future in Bone Regeneration. *Bone and Tissue Regeneration Insights,* 7**,** BTRI.S36138.

KAWACHI, G., MISUMI, H., FUJIMORI, H., GOTO, S., OHTSUKI, C., KAMITAKAHARA, M. & IOKU, K. 2010. Fabrication of porous blocks of calcium phosphate through hydrothermal processing under glycine coexistence. *Journal of the Ceramic Society of Japan,* 118**,** 559-563.

KIM, B. S., KIM, J. S., SUNG, H. M., YOU, H. K. & LEE, J. 2012. Cellular attachment and osteoblast differentiation of mesenchymal stem cells on natural cuttlefish bone. *J Biomed Mater Res A,* 100**,** 1673-9.

KIM, D. W., CHO, I. S., KIM, J. Y., JANG, H. L., HAN, G. S., RYU, H. S., SHIN, H., JUNG, H. S., KIM, H. & HONG, K. S. 2010. Simple large-scale synthesis of hydroxyapatite nanoparticles: in situ observation of crystallization process. *Langmuir,* 26**,** 384-8.

KIM, I.-Y. K. K. O. C. 2012. Formation of Oriented Hydroxyapatite Rods by Hydrothermal Treatment of Calcite Single Crystal. *Korean Journal of Materials Research,* 22**,** 397-402.

KLAWITTER, J. J. & HULBERT, S. F. 1971. Application of porous ceramics for the attachment of load bearing internal orthopedic applications. *Journal of Biomedical Materials Research,* 5**,** 161-229.

KLAWITTER, J. J. & WEINSTEIN, A. M. 1974. The status of porous materials to obtain direct skeletal attachment by tissue ingrowth. *Acta Orthop Belg,* 40**,** 755-65.

KOKUBO, T. & TAKADAMA, H. 2006. How useful is SBF in predicting in vivo bone bioactivity? *Biomaterials,* 27**,** 2907-2915.

KOUTSOPOULOS, S. 2002. Synthesis and characterization of hydroxyapatite crystals: A review study on the analytical methods. *Journal of Biomedical Materials Research,* 62**,** 600-612.

KUBOKI, Y., TAKITA, H., KOBAYASHI, D., TSURUGA, E., INOUE, M., MURATA, M., NAGAI, N., DOHI, Y. & OHGUSHI, H. 1998. BMP-induced osteogenesis on the surface of hydroxyapatite with geometrically feasible and nonfeasible structures: topology of osteogenesis. *J Biomed Mater Res,* 39**,** 190-9.

LE HUEC, J. C., SCHAEVERBEKE, T., CLEMENT, D., FABER, J. & LE REBELLER, A. 1995. Influence of porosity on the mechanical resistance of hydroxyapatite ceramics under compressive stress. *Biomaterials,* 16**,** 113-8.

LIEBSCHNER, M. A. 2004. Biomechanical considerations of animal models used in tissue engineering of bone. *Biomaterials,* 25**,** 1697-714.

LIU, X. G., LIN, K. L. & CHANG, J. A. 2011. Modulation of hydroxyapatite crystals formed from alpha-tricalcium phosphate by surfactant-free hydrothermal exchange. *Crystengcomm,* 13**,** 1959-1965.

MALHOTRA, A. & HABIBOVIC, P. 2016. Calcium Phosphates and Angiogenesis: Implications and Advances for Bone Regeneration. *Trends in Biotechnology,* 34**,** 983-992.

MARTINOLICH, A. J. & NEILSON, J. R. 2017. Toward Reaction-by-Design: Achieving Kinetic Control of Solid State Chemistry with Metathesis. *Chemistry of Materials,* 29**,** 479-489.

MASAHIRO OKADA, T. M. 2015. Synthesis and modification of apatite nanoparticles for use in dental and medical applications. *Japanese Dental Science Review* 51**,** 85-95.

MEEJOO, S., MANEEPRAKORN, W. & WINOTAI, P. 2006. Phase and thermal stability of nanocrystalline hydroxyapatite prepared via microwave heating. *Thermochimica Acta,* 447**,** 115-120.

MENDHAM J, D. R., BARNER JD, THOMAS M 2002. *Vogel's quantitative chemical analysis*, Pearson Education Ltd.

.

MERCER, D. C. 2004. *www.healio.com/orthopedics* [Online]. [Accessed 24-03-2019 2019].

MOHAN, N., PALANGADAN, R. & VARMA, H. 2016. Hydroxyapatite scaffolds constituting highly oriented crystals derived from synthetic precursors by hydrothermal reactions. *Ceramics International,* 42**,** 17259-17268.

NELSON, D. G. & FEATHERSTONE, J. D. 1982. Preparation, analysis, and characterization of carbonated apatites. *Calcif Tissue Int,* 34 Suppl 2**,** S69-81.

NEO, M., NAKAMURA, T., OHTSUKI, C., KASAI, R., KOKUBO, T. & YAMAMURO, T. 1994. Ultrastructural study of the A-W GC-bone interface after long-term implantation in rat and human bone. *Journal of Biomedical Materials Research,* 28**,** 365-372.

NICH, C. & SEDEL, L. 2006. Bone substitution in revision hip replacement. *Int Orthop,* 30**,** 525-31.

NORTON, M. R. & WILSON, J. 2002. Dental implants placed in extraction sites implanted with bioactive glass: human histology and clinical outcome. *Int J Oral Maxillofac Implants,* 17**,** 249-57.

OHGUSHI, H. & CAPLAN, A. I. 1999. Stem cell technology and bioceramics: from cell to gene engineering. *J Biomed Mater Res,* 48**,** 913-27.

OHGUSHI, H., GOLDBERG, V. M. & CAPLAN, A. I. 1989. Repair of bone defects with marrow cells and porous ceramic. Experiments in rats. *Acta Orthop Scand,* 60**,** 334-9.

OKAZAKI, M. 1993. Crystallographic Morphology of Heterogeneous Fluoridated Carbonate Apatites. *Journal of Dental Research,* 72**,** 1285-1290.

OLSZTA, M. J., CHENG, X., JEE, S. S., KUMAR, R., KIM, Y.-Y., KAUFMAN, M. J., DOUGLAS, E. P. & GOWER, L. B. 2007. Bone structure and formation: A new perspective. *Materials Science and Engineering: R: Reports,* 58**,** 77-116.

OMORI, Y., OKADA, M., TAKEDA, S. & MATSUMOTO, N. 2014. Fabrication of dispersible calcium phosphate nanocrystals via a modified Pechini method under non-stoichiometric conditions. *Mater Sci Eng C Mater Biol Appl,* 42**,** 562-8.

ONODA, H. & YAMAZAKI, S. 2016. Homogenous hydrothermal synthesis of calcium phosphate with calcium carbonate and corbicula shells. *Journal of Asian Ceramic Societies,* 4**,** 403-406.

ONUMA, K. 2006. Recent research on pseudobiological hydroxyapatite crystal growth and phase transition mechanisms. *Progress in Crystal Growth and Characterization of Materials,* 52**,** 223-245.

OONISHI, H., IWAKI, Y., KIN, N., KUSHITANI, S., MURATA, N., WAKITANI, S. & IMOTO, K. 1997. Hydroxyapatite in revision of total hip replacements with massive acetabular defects: 4- to 10-year clinical results. *J Bone Joint Surg Br,* 79**,** 87-92.

OSHIMURA M, S. W., BYRAPPA K 2000. Soft Solution Processing: A Strategy for One-Step Processing of Advanced Inorganic Materials. *MRS Bulletin,* 25**,** 17-25.

PANDA, R. N., HSIEH, M. F., CHUNG, R. J. & CHIN, T. S. 2003. FTIR, XRD, SEM and solid state NMR investigations of carbonate-containing hydroxyapatite nano-particles synthesized by hydroxide-gel technique. *Journal of Physics and Chemistry of Solids,* 64**,** 193-199.

PAVEL FEJDI, A. H. 2001. Relationship between crystal morphology and preferred orientation in polycrystalline specimens for diffraction *Materials Structure,* 8**,** 22-24.

POSNER A.S, B. N. C., BETTS F 1984. *Chemistry and Structure of Precipitated Hydroxyapatites.,* Berlin, Heidelberg, Springer.

POSNER, A. S., PERLOFF, A. & DIORIO, A. F. 1958. Refinement of the hydroxyapatite structure. *Acta Crystallographica,* 11**,** 308-309.

PRAMANIK, S., AGARWAL, A. K., RAI, K. N. & GARG, A. 2007. Development of high strength hydroxyapatite by solid-state-sintering process. *Ceramics International,* 33**,** 419-426.

QIZHI CHEN, G. T. 2018. *Biomaterials: A Basic Introduction*, CRC Press

R. E. RIMAN, W. L. S., M. M. LENCKA 2002. Hydrothermal crystallization of ceramics. *Ann. Chim. Sci. Mat.,* 27**,** 15-36.

RECUM, A. F. V. 1998. *Handbook Of Biomaterials Evaluation: Scientific, Technical And Clinical Testing Of Implant Materials*, CRC Press

REFFITT, D. M., OGSTON, N., JUGDAOHSINGH, R., CHEUNG, H. F., EVANS, B. A., THOMPSON, R. P., POWELL, J. J. & HAMPSON, G. N. 2003. Orthosilicic acid stimulates collagen

type 1 synthesis and osteoblastic differentiation in human osteoblast-like cells in vitro. *Bone,* 32**,** 127-35.

RIMAN, R. E. 1993. *High Performance Ceramics: Surface Chemistry in Processing Technology* U.S.A., Marcel-Dekker

ROBERTS, T. T. & ROSENBAUM, A. J. 2012. Bone grafts, bone substitutes and orthobiologics: the bridge between basic science and clinical advancements in fracture healing. *Organogenesis,* 8**,** 114-24.

ROY, D. M. & LINNEHAN, S. K. 1974. Hydroxyapatite formed from coral skeletal carbonate by hydrothermal exchange. *Nature,* 247**,** 220-2.

ROY, R. 1994. Accelerating the Kinetics of Low-Temperature Inorganic Syntheses. *Journal of Solid State Chemistry,* 111**,** 11-17.

S. MANAFI, M. R. R., B. YAZDANI, S. K. SADRNEZHAAD, M. H. AMIN 2008. Hydrothermal synthesis of alingned hydroxyapatite nanorods with ultra high crystallinity. *IJE Transactions B: Applications* 21**,** 109-116.

SALGADO, A. J., COUTINHO, O. P. & REIS, R. L. 2004. Bone tissue engineering: state of the art and future trends. *Macromol Biosci,* 4**,** 743-65.

SAMPATH KUMAR, T. S., MANJUBALA, I. & GUNASEKARAN, J. 2000. Synthesis of carbonated calcium phosphate ceramics using microwave irradiation. *Biomaterials,* 21**,** 1623-1629.

SCHEER, J. H. & ADOLFSSON, L. E. 2009. Tricalcium phosphate bone substitute in corrective osteotomy of the distal radius. *Injury,* 40**,** 262-7.

SHANDILYA, M., RAI, R. & SINGH, J. 2016. Review: hydrothermal technology for smart materials. *Advances in Applied Ceramics,* 115**,** 354-376.

SHEN, J., JIN, B., HU, Y. M. & JIANG, Q. Y. 2015. An effective route to the synthesis of carbonated apatite crystals with controllable morphologies and their growth mechanism. *Crystengcomm,* 17**,** 5422-5430.

SIVAKUMAR, M., KUMAR, T. S. S., SHANTHA, K. L. & RAO, K. P. 1996. Development of hydroxyapatite derived from Indian coral. *Biomaterials,* 17**,** 1709-1714.

STEIN, G. S., LIAN, J. B. & OWEN, T. A. 1990. Relationship of cell growth to the regulation of tissue-specific gene expression during osteoblast differentiation. *FASEB J,* 4**,** 3111-23.

STEVENSON, S. 1987. The immune response to osteochondral allografts in dogs. *J Bone Joint Surg Am,* 69**,** 573-82.

STEVENSON, S. & HOROWITZ, M. 1992. The response to bone allografts. *J Bone Joint Surg Am,* 74**,** 939-50.

STEVENSON, S., LI, X. Q. & MARTIN, B. 1991. The fate of cancellous and cortical bone after transplantation of fresh and frozen tissue-antigen-matched and mismatched osteochondral allografts in dogs. *J Bone Joint Surg Am,* 73**,** 1143-56.

SUCHANEK, W., YASHIMA, M., KAKIHANA, M. & YOSHIMURA, M. 1996. Processing and mechanical properties of hydroxyapatite reinforced with hydroxyapatite whiskers. *Biomaterials,* 17**,** 1715-23.

SUCHANEK, W. L., LENCKA, M., MCCANDLISH, L., PFEFFER, R. L., OLEDZKA, M., MIKULKA-BOLEN, K., ROSSETTI, G. A. & RIMAN, R. E. 2005. Hydrothermal Deposition of 〈 001 〉 Oriented Epitaxial Pb(Zr,Ti)O3 Films under Varying Hydrodynamic Conditions. *Crystal Growth & Design,* 5**,** 1715-1727.

SUCHANEK, W. Y., M. 1998. Processing and properties of hydroxyapatite-based biomaterials for use as hard tissue replacement implants. *Journal of Materials Research, Cambridge University Press,* 13**,** 94–117.

SUNARSO , A. N., S. KASIM, R. OTHMAN, I. ANA AND K. ISHIKAWA 2013. Synthesis of Biphasic Calcium Phosphate by Hydrothermal Route and Conversion to Porous Sintered Scaffold. *Journal of Biomaterials and Nanobiotechnology,* 4**,** 273-278.

SUNOUCHI, K., TSURU, K., MARUTA, M., KAWACHI, G., MATSUYA, S., TERADA, Y. & ISHIKAWA, K. 2012. Fabrication of solid and hollow carbonate apatite microspheres as bone substitutes using calcite microspheres as a precursor. *Dent Mater J,* 31**,** 549-57.

SUZUKI, O., KAMAKURA, S., KATAGIRI, T., NAKAMURA, M., ZHAO, B., HONDA, Y. & KAMIJO, R. 2006. Bone formation enhanced by implanted octacalcium phosphate involving conversion into Ca-deficient hydroxyapatite. *Biomaterials,* 27**,** 2671-81.

TANAKA Y, K. Y. 2008. *Fabrication processes for bioceramics*.

TANG, R., WANG, L., ORME, C. A., BONSTEIN, T., BUSH, P. J. & NANCOLLAS, G. H. 2004. Dissolution at the Nanoscale: Self-Preservation of Biominerals. *Angewandte Chemie,* 116**,** 2751-2755.

TZAPHLIDOU, M. & ZAICHICK, V. 2003. Calcium, phosphorus, calcium-phosphorus ratio in rib bone of healthy humans. *Biol Trace Elem Res,* 93**,** 63-74.

V.M. GOLDBERG, S. A. 2005. Biology of bone grafts. *In:* J.R. LIEBERMAN, G. E. F. (ed.) *Bone Regeneration and Repair.* Springer.

VACANTI, R. L. R. L. J. 2013. *Principles of Tissue Engineering*, Elsevier Academic Press.

VAGO, R., PLOTQUIN, D., BUNIN, A., SINELNIKOV, I., ATAR, D. & ITZHAK, D. 2002. Hard tissue remodeling using biofabricated coralline biomaterials. *Journal of Biochemical and Biophysical Methods,* 50**,** 253-259.

VÄLIMÄKI, V.-V. & ARO, H. T. 2006. Molecular Basis for Action of Bioactive Glasses as Bone Graft Substitute. *Scandinavian Journal of Surgery,* 95**,** 95-102.

VECCHIO, K. S., ZHANG, X., MASSIE, J. B., WANG, M. & KIM, C. W. 2007. Conversion of sea urchin spines to Mg-substituted tricalcium phosphate for bone implants. *Acta Biomater,* 3**,** 785-93.

VEHOF, J. W., HAUS, M. T., DE RUIJTER, A. E., SPAUWEN, P. H. & JANSEN, J. A. 2002. Bone formation in transforming growth factor beta-I-loaded titanium fiber mesh implants. *Clin Oral Implants Res,* 13**,** 94-102.

VERRON, E., PISSONNIER, M.-L., LESOEUR, J., SCHNITZLER, V., FELLAH, B. H., PASCAL-MOUSSELLARD, H., PILET, P., GAUTHIER, O. & BOULER, J.-M. 2014. Vertebroplasty using bisphosphonate-loaded calcium phosphate cement in a standardized vertebral body bone defect in an osteoporotic sheep model. *Acta Biomaterialia,* 10**,** 4887-4895.

VIOUX, A. 1997. Nonhydrolytic Sol−Gel Routes to Oxides. *Chemistry of Materials,* 9**,** 2292-2299.

W. DAVID KINGERY, H. K. B., DONALD R. UHLMANN 1976. *Introduction to Ceramics*, Wiley.

W. L. SUCHANEK, M. M. L., R. E. RIMAN 2004. Hydrothermal synthesis of ceramic materials *In:* D. A. PALMER, R. F.-P., A. H. HARVEY (ed.) *Aqueous Systems at Elevated Temperatures and Pressures: Physical Chemistry in Water, Steam, and Hydrothermal Solutions.* 1 ed.: Elsevier.

W. RATHJE, Z. K. 1939. de phosphate: I. uber hydroxyapatite, Bodenk analysis using L929 fibroblast cells provided clear evidences. *Pflernah* 12**,** 121–128.

WANG, M. 2003. Developing bioactive composite materials for tissue replacement. *Biomaterials,* 24**,** 2133-51.

WANG, W. & YEUNG, K. W. K. 2017. Bone grafts and biomaterials substitutes for bone defect repair: A review. *Bioact Mater,* 2**,** 224-247.

WEINER, S. & WAGNER, H. D. 1998. THE MATERIAL BONE: Structure-Mechanical Function Relations. *Annual Review of Materials Science,* 28**,** 271-298.

WENISCH, S., STAHL, J. P., HORAS, U., HEISS, C., KILIAN, O., TRINKAUS, K., HILD, A. & SCHNETTLER, R. 2003. In vivo mechanisms of hydroxyapatite ceramic degradation by osteoclasts: fine structural microscopy. *J Biomed Mater Res A,* 67**,** 713-8.

WEST, A. R. 2003. *Solid State Chemistry and Its Applications*, Wiley.

WILLIAMS, D. F. 2008. On the mechanisms of biocompatibility. *Biomaterials,* 29**,** 2941-53.

WILLIARD, M., DEAN, SETTLE 1986. *Instrumental methods of analysis*, CBS Publishers & Distributors, Delhi.

WONG, J. Y. & BRONZINO, J. D. 2007. *Biomaterials*, CRC Press.

XIA, L., LIN, K., JIANG, X., XU, Y., ZHANG, M., CHANG, J. & ZHANG, Z. 2013. Enhanced osteogenesis through nano-structured surface design of macroporous hydroxyapatite bioceramic scaffolds via activation of ERK and p38 MAPK signaling pathways. *Journal of Materials Chemistry B,* 1**,** 5403-5416.

YOSHIMURA, M. & SUCHANEK, W. 1997. In situ fabrication of morphology-controlled advanced ceramic materials by Soft Solution Processing. *Solid State Ionics,* 98**,** 197-208.

YOSHIYUKI YOKOGAWA, F. N. Year. Hydrothermal Synthesis of Hydroxyapatite – Polymer Composite Materials *In:* 14th International Conference on the Properties of Water and Steam, Kyoto.

YOURDKHANI, M., PASINI, D. & BARTHELAT, F. 2011. Multiscale Mechanics and Optimization of Gastropod Shells. *Journal of Bionic Engineering,* 8**,** 357-368.

ZARYANOV, A. V., PARK, D. K., KHALIL, J. G., BAKER, K. C. & FISCHGRUND, J. S. 2014. Cement augmentation in vertebral burst fractures. *Neurosurgical focus,* 37**,** E5.

ZHANG, X. & VECCHIO, K. S. 2006. Creation of dense hydroxyapatite (synthetic bone) by hydrothermal conversion of seashells. *Materials Science and Engineering: C,* 26**,** 1445-1450.

ZHU, L., LIU, W., CUI, L. & CAO, Y. 2006. Tissue-engineered bone repair of goat-femur defects with osteogenically induced bone marrow stromal cells. *Tissue Eng,* 12**,** 423-33.

ZHUANG, Z., MIKI, T., YUMOTO, M., KONISHI, T. & AIZAWA, M. 2012. Ultrastructural Observation of Hydroxyapatite Ceramics with Preferred Orientation to a-plane Using High-resolution Transmission Electron Microscopy. *Iumrs International Conference in Asia 2011,* 36**,** 121-127.

ZUR NIEDEN, N. I., KEMPKA, G. & AHR, H. J. 2003. In vitro differentiation of embryonic stem cells into mineralized osteoblasts. *Differentiation,* 71**,** 18-27.

ZWINGENBERGER, S., NICH, C., VALLADARES, R. D., YAO, Z., STIEHLER, M. & GOODMAN, S. B. 2012. Recommendations and considerations for the use of biologics in orthopedic surgery. *BioDrugs,* 26**,** 245-56.

PATENT

1. NEW GENERATION OF CALCIUM PHOSPHATE BASED BIOCERAMIC SCAFFOLDS FROM SYNTHETIC INORGANIC PRECURSORS AND A PROCESS FOR THE PREPARATION THEREOF: Number: **4362/CHE/15**

LIST OF PUBLICATIONS

1. Hydroxyapatite scaffolds constituting highly oriented crystals derived from synthetic precursors by hydrothermal reactions: *Ceramics International* 42 (2016) 17259–17268. Nimmy Mohan, Rajesh Palangadan, Harikrishna Varma* (Impact Factor- 3.057)

2. Preparation of hydroxyapatite porous scaffold from a 'coral-like' synthetic inorganic precursor for use as a bone substitute and a drug delivery vehicle: *Materials Science & Engineering C* 92 (2018) 329–337. Nimmy Mohan, Rajesh Palangadan, Francis Bonafice Fernandez, Harikrishna Varma* (Impact Factor- 5.080)

3. Pulsed laser deposition of hydroxyapatite on nanostructured titanium towards drug eluting implants: *Materials Science and Engineering C* 33 (2013) 2899–2904, Rajesh P, Nimmy Mohan, Y. Yokogawa, Harikrishna Varma. (Impact Factor- 5.080)

PAPER PRESENTATIONS AND CONFERENCE PROCEEDINGS

- **IUMRS-ICA 2013** at Indian Institute of Science Bangalore

  -Hydrothermally generated porous hydroxyapatite scaffolds with enhanced cellular activity: Nimmy Mohan, Rajesh P, Gayathri V, Mohanan P.V, Harikrishna Varma*

  -Drug Eluting Titanium Implant Having TiO_2 Nanotube Reservoirs and Their *In Vitro* Behaviour: Rajesh P, Nimmy Mohan, Harikrishna Varma*.

- **World Biomaterials Congress: WBC 2016** at Palais des congrès, Montreal Canada

  -New Generation of Hydroxyapatite Bone Grafts from 'coral like' synthetic inorganic precursors: Nimmy Mohan, Harikrishna Varma*

Curriculum Vitae

Nimmy Mohan

Nikunjam, TC-13/2091/2,

Attara Lane, Kannamoola, Mob: +91 9446377105

Trivandrum, Kerala-695011, INDIA Email: nims86@gmail.com

Date of Birth: 22/4/1986

Academic Qualification: MSc. Applied Chemistry

Summary of Work Experience

Name of the Organization	Designation	Duration of Work
Sree Chitra Tirunal Institute for Medical Sciences and Technology (SCTIMST)	Senior Research Fellow (SRF) Indo Danish Collaborative Project	Dec 2014- Present
Sree Chitra Tirunal Institute for Medical Sciences and Technology (SCTIMST)	Junior Research Fellow (JRF) Indo Danish Collaborative Project	Sep 2011- Dec 2014

Summary of Educational Qualification

Degree/Certification	Issuing Authority	Year of Achievement or Course Duration	Score
MSc. Applied Chemistry	MG University, Kottayam	2007-2009	70%
BSc. Chemistry	Kerala University	2004-2007	70.3%
Higher Secondary Education	Higher Secondary Board, Kerala	2002- 2004	74%
SSLC	Kerala State Education Board	March 2002	88.3%

Areas of expertise gained during PhD

1. Synthesis and Characterisation of bioceramic materials for tissue engineering applications. (Hydroxyapatite, tri calcium phosphate, bioactive glass, bioactive glass ceramic composites, doping of ceramic materials)

2. Hydrothermal synthesis of fast resorbing ceramic materials

3. Synthesis of drug eluting ceramic matrices

4. Cell culture

5. Basics of Molecular Biology and Genetic Research for the treatment of Osteoporosis

Expertise with Equipment's

1. X-ray diffractometer (XRD)

2. Fourier Transform Infrared Spectrophotometer (FTIR)

3. UV- Visible Spectro Photometer.

4. Environmental Scanning Electron Microscope (ESEM)

5. Hydrothermal Reactor

Publications & Patents

- 3 Papers Published in International Journals.
- 4 Conference Papers and
- 1 Patent filed.

Publications

1. Hydroxyapatite scaffolds constituting highly oriented crystals derived from synthetic precursors by hydrothermal reactions: ***Ceramics International*** *42 (2016) 17259–17268.* Nimmy Mohan, Rajesh Palangadan, Harikrishna Varma (Impact Factor- 3.057)

2. Preparation of hydroxyapatite porous scaffold from a 'coral-like' synthetic inorganic precursor for use as a bone substitute and a drug delivery vehicle: ***Materials Science & Engineering C*** 92 (2018) 329–337. Nimmy Mohan, Rajesh Palangadan, Francis Bonafice Fernandez, Harikrishna Varma* (Impact Factor- 5.080)

3. Pulsed laser deposition of hydroxyapatite on nanostructured titanium towards drug eluting implants: ***Materials Science and Engineering C*** *33 (2013) 2899–2904*, Rajesh P, Nimmy Mohan, Y. Yokogawa, Harikrishna Varma. (Impact Factor- 5.080)

Patents filed: 1

NEW GENERATION OF CALCIUM PHOSPHATE BASED BIOCERAMIC SCAFFOLDS FROM SYNTHETIC INORGANIC PRECURSORS AND A PROCESS FOR THE PREPARATION THEREOF: **Number: 4362/CHE/15**

Conferences Attended:

- **IUMRS-ICA 2013** Venue: Indian Institute of Science Bangalore

  - Hydrothermally generated porous hydroxyapatite scaffolds with enhanced cellular activity: Nimmy Mohan, Rajesh P, Gayathri V, Mohanan P.V, Harikrishna Varma*
  - Drug Eluting Titanium Implant Having TiO_2 Nanotube Reservoirs And Their In Vitro Behaviour: Rajesh P, Nimmy Mohan, Harikrishna Varma*.

- **World Biomaterials Congress: WBC 2016** Venue: Palais des congrès, Montreal Canada:
  - New Generation of Hydroxyapatite Bone Grafts from 'coral like' synthetic inorganic precursors: Nimmy Mohan, Harikrishna Varma*

- **INCCOM 2008**
- Savitha Nair, Nimmy Mohan, C.P.Reghunadhan Nair, "Acrylic based transfer adhesives: Synthesis and Characterization" Presented in INCCOM 2008

Specific Research Training gained

- Cell Culture Training at Biozeen Lab, Bangalore (2012)

- Special training at Interdisciplinary Nanoscience Centre (iNANO), Aarhus University with Prof. Jorgen Kjems, Professor and Director) in molecular biology and genetic research.

- MSc. Project: MSc Project carried out under the guidance of Dr. C.P Reghunadhan Nair at Polymers and Special Chemicals Division, Vikram Sarabhai Space Centre (VSSC) in the development of acrylic based pressure sensitive adhesive for space applications.

Specific Areas of Interest to Work

Bioceramics, Biomaterial development, Bone tissue engineering, Drug delivery

Ceramic synthesis and characterization, Functional nanoceramic coatings, Sol-gel synthesis, Composites, Clay minerals, Nanoclays

Nimmy Mohan

APPENDIX-1

1. Stevenal's blue stain:

Methylene Blue – 1 gm in 75 ml distilled water
Potassium permanganate – 1.5 gm in 75 ml distilled water

2. Van Gieson's Picrofuchsin stain:

Acid Fuchsin – 0.1 gm in 10 ml distilled water
Saturated picric acid – 100ml